Naval Research Laboratory
Stennis Space Center, MS 39529-5004

NRL/MR/7431--97-8044

Proceedings of the Coastal Benthic Boundary Layer Key West Workshop

DAWN L. LAVOIE
MICHAEL D. RICHARDSON

Seafloor Sciences Branch
Marine Geosciences Division

June 24, 1997

REPORT DOCUMENTATION PAGE

Form Approved
OBM No. 0704-0188

1. AGENCY USE ONLY *(Leave blank)*	2. REPORT DATE	3. REPORT TYPE AND DATES COVERED
	June 24, 1997	Final

4. TITLE AND SUBTITLE

Proceedings of the Coastal Benthic Boundary Layer Key West Workshop

5. FUNDING NUMBERS

Job Order No. 574-5258-07
Program Element No. 0602435N
Project No. 03522
Task No.
Accession No.

6. AUTHOR(S)

Dawn L. Lavoie and Michael D. Richardson

7. PERFORMING ORGANIZATION NAME(S) AND ADDRESS(ES)

Naval Research Laboratory
Marine Geosciences Division
Stennis Space Center, MS 39529-5004

8. PERFORMING ORGANIZATION REPORT NUMBER

NRL/MR/7431--97-8044

9. SPONSORING/MONITORING AGENCY NAME(S) AND ADDRESS(ES)

Office of Naval Research
800 North Quincy Street
Arlington, VA 22217-5660

10. SPONSORING/MONITORING AGENCY REPORT NUMBER

11. SUPPLEMENTARY NOTES

12a. DISTRIBUTION/AVAILABILITY STATEMENT

Approved for public release; distribution unlimited.

12b. DISTRIBUTION CODE

13. ABSTRACT *(Maximum 200 words)*

The coastal benthic boundary layer (CBBL) research program is a 5-year Office of Naval Research study that addresses the physical characterization and modeling of benthic boundary layer processes and the impact of these processes on seafloor structure, properties, and behavior. The lower Florida Keys, specifically the Dry Tortugas and Marquesas Keys, were selected as experiment sites to test the CBBL hypotheses and provide data for comprehensive modeling efforts. A workshop was held to provide a forum for initial research results and to define the models that relate the controlling geologic processes and observed sediment behavior. This report contains the extended abstracts from this workshop.

14. SUBJECT TERMS

Lower Florida Keys, Dry Tortugas, Marquesas, benthic boundary layer, sediment classification diagenesis, geophysical characterization, geologic processes, geochemical, physical properties, modeling microstructure

15. NUMBER OF PAGES

225

16. PRICE CODE

17. SECURITY CLASSIFICATION OF REPORT	18. SECURITY CLASSIFICATION OF THIS PAGE	19. SECURITY CLASSIFICATION OF ABSTRACT	20. LIMITATION OF ABSTRACT
Unclassified	Unclassified	Unclassified	SAR

CONTENTS

1.0 Introduction

The Key West Workshop, held between February 4-7, 1997, had two main objectives: (1) to provide a forum for initial research results from the Key West Campaign and (2) to define the models that relate the controlling geological processes and observed sediment behavior.

The presentation of research is organized in categories from the large scale regional descriptions to the small scale microfabric and modeling efforts. The initial section "Geologic Background" includes papers by Mallinson who interprets Chirp seismic data to describe the geology of the Dry Tortugas Experiment Site, and Brunner who uses microfossils to interpret the past history of the region.

A major portion of the workshop was devoted to "Sediment Classification" issues. Using sidescan data, Wever interprets bottom morphology and sediment type based on backscatter reflectivity. Walter and others use a normal incident acoustic profiling system to interpret the subbottom layering structure and sediment type, and compare sediment physical properties values with core data. Hews and others examine the information obtained from the "Magic Carpet" seismic system to estimate shear wave velocity of bottom sediments. Tooma and Chotiros put the question of remote classification of bottom sediments into practical perspective by outlining Naval interests in the technology.

In the section "Processes which Affect Near-surface Sediment Structure and Properties," Bentley and Nittrouer use ^{210}Pb to constrain rates and relevant length and time scales for sediment accumulation and mixing. Lopez and D'Andrea present a regional comparison of benthic assemblages in the Lower Florida Keys based on feeding habits and environmental conditions. Shiller presents the pore water chemistry

and its implications for the Tortugas sediments. Furukawa and Lavoie discuss diagenetic alteration of the basic sediment constituents.

"Sediment Structure and Properties" was devoted to sediment geotechnical and physical properties Richardson and others present empirical relationships between geoacoustic and physical properties of sediments from the Dry Tortugas, Rebecca Shoals and Marquesas Keys and compare them to similar relationships for siliciclastic sediments. Orsi and Briggs, using CT- scanning techniques, analyze density variations in cores recovered from the Tortugas. Carrying this one step further, Briggs and others examine small-scale fluctuations in acoustic and physical properties measured on sediments from the Marquesas Keys and Dry Tortugas sites. Using a large number of samples (>2000), Stephens and others look at the scale-dependent variability of these same sediments. Sykora and others, using an instrumented triaxial cell, illustrate the effect of effective stress on geoacoustic properties measured during laboratory testing. Brogan and others present stress - strain behavior measured on the same sediments. D.L. Lavoie, comparing the behavior of sediments in the laboratory and in situ, explains the lack of expected trends in physical properties as a function of the sediment microfabric. Still on a very small scale, Pyrak-Nolte presents fine-scale variations in acoustic velocity using acoustic tomography on a Dry Tortugas diver core. Using the same core, D.M. Lavoie presents a description of the sediment microfabric imaged in the acoustic tomography experiment.

The modeling section is relatively short. Hollyer and others use Furukawa's images to analyze the correlation structure of the Dry Tortugas Sediments. Williams and Jackson compare model predictions of high frequency scattering from the Dry Tortugas sediment. In the final paper, Sadd discusses contact microstructure for acoustic modeling of particulate marine sediments.

The second major objective of this workshop was to develop integrated models of environmental processes and sediment structure, properties, and behavior in carbonate

sediments. Prediction of sediment structure, properties and behavior based on knowledge of environmental processes is critical to extending the research results in time and space. Models must be transportable and not restricted to one set of experiments or to a single area. Mike Richardson began the discussion with a review of the CBBL objectives (Fig 1) (Richardson, 1994) using modeling results from Eckernförde Bay efforts as an example of the type of integrated model expected for carbonate sediments (Fig 2). The participants were then divided into two groups: one lead by Dave Young and Sam Bentley, the other lead by Kevin Williams. The Young/Bentley group was primarily concerned with the integrated effects of environmental processes on sediment structure. The Williams group discussed the effects of sediment structure on sediment physical properties, sediment behavior, and remotely-sensed sediment properties. Discussion was limited to processes and sediment properties within the upper 50 cm of the sediment column. Changes in sediment properties below that depth are controlled by climatic changes which affect sea level and result in vastly different sedimentary regimes. After several hours of discussion, the participants rejoined. Group leaders provided a summary of their attempt to develop integrated models and the floor was open to discussion (Fig. 3). The following paragraphs summarize the results of those discussions. These results should be considered preliminary as this was the first time the CBBL group attempted to integrate results from the Key West Campaign (Tooma and Richardson, 1996).

Benthic fauna at the Dry Tortugas site are vertically tiered and can be divided into three functional groups: a shallow fauna, surface deposit and suspension feeders, which thoroughly mix the upper 4-5 cm in days to weeks; an intermediate fauna, carnivores/scavengers, deep deposit feeders, and head-down deposit feeders, which intensely mix sediment to depths of 15 cm over time scales of 10-20 years; and a deeper fauna, gallery creating callianassid shrimp, which only partially mix sediments. Rates and depths of sediment mixing, rates of deposition and the depth and frequency of erosion can be used to predict the preservation potential of sediment layers and structure generated by both physical and biogenic processes.

Shallow-water carbonates normally undergo extensive post depositional biogeochemical diagenesis that includes dissolution, precipitation, and subsequent cementation. Significant changes in surficial carbonate fabric result from subaerial exposure, exposure to fresh-water, micritization, bioturbation, and pore water chemical changes due to the breakdown of organic matter. Although pore waters were calculated to be supersaturated with carbonate, no significant precipitation was noted in the upper meter of sediment at the Dry Tortugas. Current thermodynamic or kinetic models are unable to explain this lack of precipitation or cementation which is common in other carbonate environments. The dominate processes is micritization, or the mechanical and chemical breakdown of carbonate particles, effectively converting sand- and silt-sized carbonate particles to clay-sized matrix material.

Benthic biological processes act in complex concert with physical processes to control sediment transport and seafloor microtopography. The benthic boundary layer at the Dry Tortugas is usually characterized by low to moderate energy with bed stresses, primarily due to tidal currents, only occasionally exceeding the threshold for sediment transport. Sediment microtopography is biologically dominated, primarily because surface algal mats bind the sediments and increase sediment critical skin friction. Thus, the Dry Tortugas site is a low energy, sediment sink with most sediments presumably being derived from erosion of the Dry Tortugas Bank just to the north. Both severe winter storms and hurricanes can redistribute sediments locally.

Sediments in the Dry Tortugas originate primarily from the breakdown and subsequent transport biogenic carbonate material from nearby reefs and other hardgrounds (allochthonous) rather than in situ (autochthonous) production. Sedimentation rates are 0.3 cm/yr. The result is a carbonate sediment (>90%) consisting primarily of aragonite plates and needles derived from the breakdown of plates of aragonitic green algae (*Halimeda*, *Penicillus*, and *Udeota)*, molluscan shells, benthic and planktonic foraminifera, echinoid spines, sponge and coral fragments, diatoms, and less than 5%

particles of siliciclastic origin (quartz and clay minerals). Microroughness (0.5 to 1.75 cm rms) is primarily biogenic in origin. Sediment are tiered with a thin (0-4 cm) high porosity, homogenous layer covering a more heterogeneous (4-15 cm) shell layer. Below 15 cm, sediments biogenic heterogeneity dominates. The vertical gradients and variability of sediment physical, geotechnical, electrical and geoacoustic properties reflect the tiered nature of these sediments. Pore water is distributed as both intra- and interparticle porosity.

The distribution of sediment characteristics is primarily controlled by the biological processes that generate carbonate skeletal material and by hydrodynamic processes that erode, fragment and redistribute those particles. Post-depositional biogeochemical processes appear to have little effect on surficial sediment physical and geoacoustic properties in the lower Florida Keys. The distribution of geoacoustic properties correlates with the areal distribution of surficial sediment physical properties including grain size, porosity and sediment bulk density. Higher wave speeds are found in more energetic environments where coarser sized particles dominate and lower values of sediment porosity and density are found. Empirical relationships between sediment physical and geoacoustic properties for these carbonate sediments are significantly different than for siliciclastic sediments. Higher shear and compressional wave speeds relate to the high percentage of interparticle porosity, the higher grain bulk modulus, and the very poorly sorted nature of these carbonate sediments compared to siliciclastic sediments. High attenuation in carbonate sediments is probably the result of increased scattering from abundant gravel- and sand-size shells rather than differences in intrinsic attenuation. Empirical relationships among porosity, density, resistivity and shear wave speed have also been established for carbonate sediments. The stiff deformation and stress responses of the sediments do not reflect cementation but may be caused by interlocking of angular particles.

High normal incidence reflection is correlated with low porosity, high density, large grain size, high shear strength, large volume heterogeneity, and high bottom roughness.

High-frequency scattering strengths decorrelate rapidly probably as a result of near-surface biological activity. Surface backscattering strengths (at 40 kHz) and bistatic scattering strengths can be reasonably well predicted from bottom roughness and surficial sediment density, velocity and attenuation. The tiered nature of the sediment has not be taken into consideration in these calculations. Future models, including gradients of seafloor properties may improve model-data comparisons. Penetration of high-frequency (15 kHz)acoustic energy into the bottom is lower than expected.

References

Richardson M.D. (1994) Investigating the coastal benthic boundary layer. EOS 75: 201-206.

Tom S.J. and Richardson M.D. (1996) The Key West campaign. Sea Technology 36:17-25.

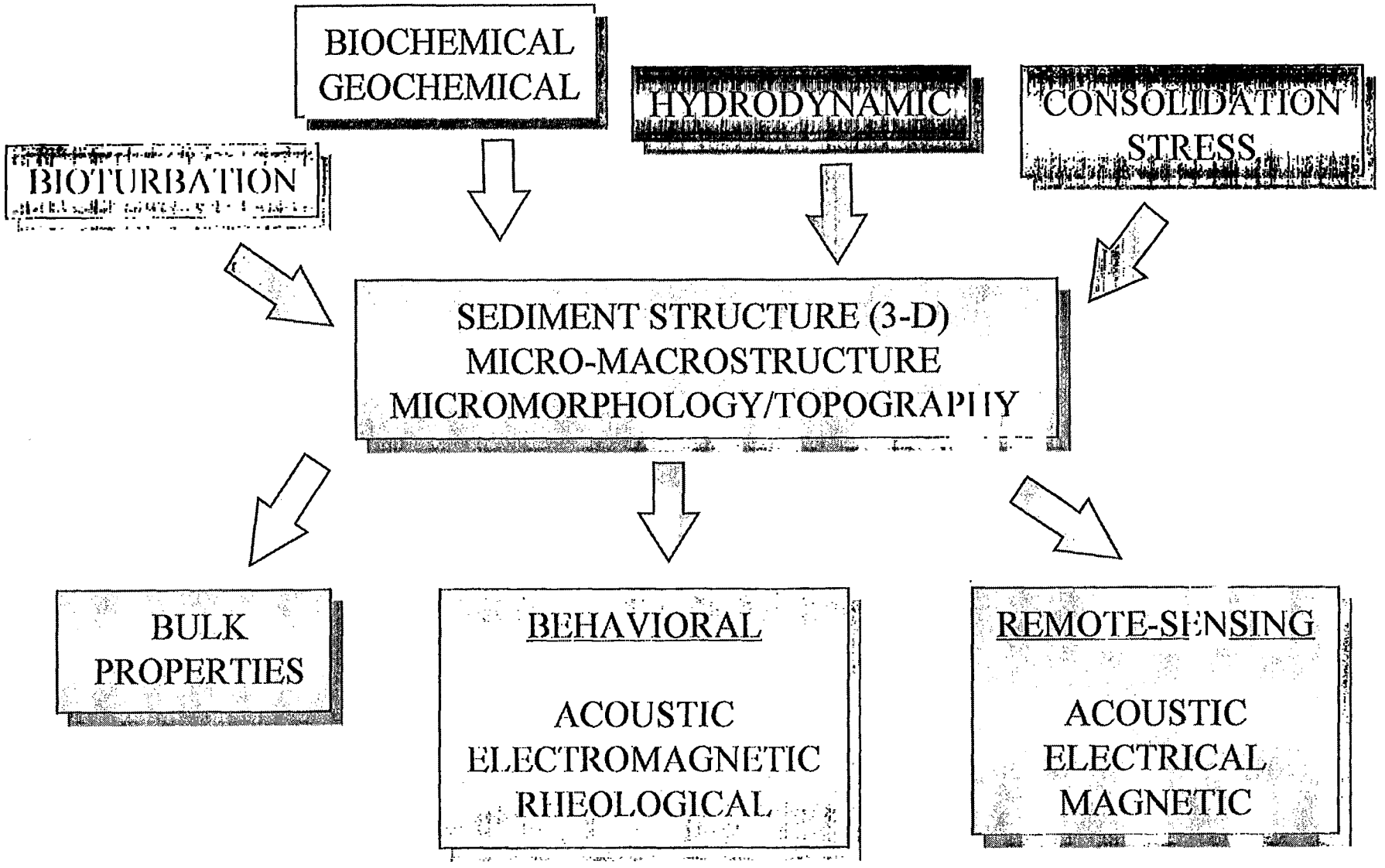

Figure 1. Multidisciplinary approach to CBBL goals.

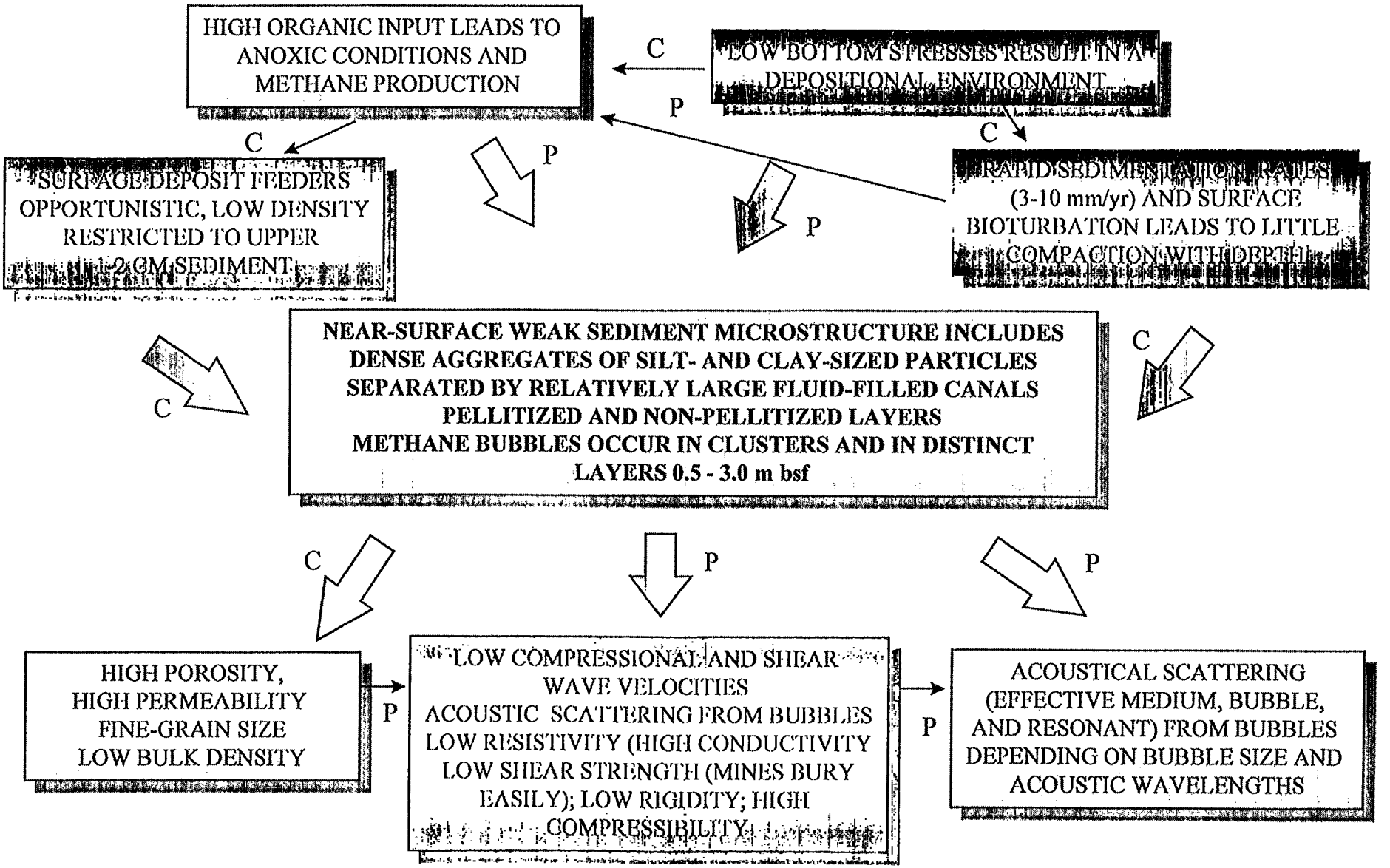

Figure 2. Eckernförde Bay: Interaction model of environmental processes and sediment structure, properties and behavior.

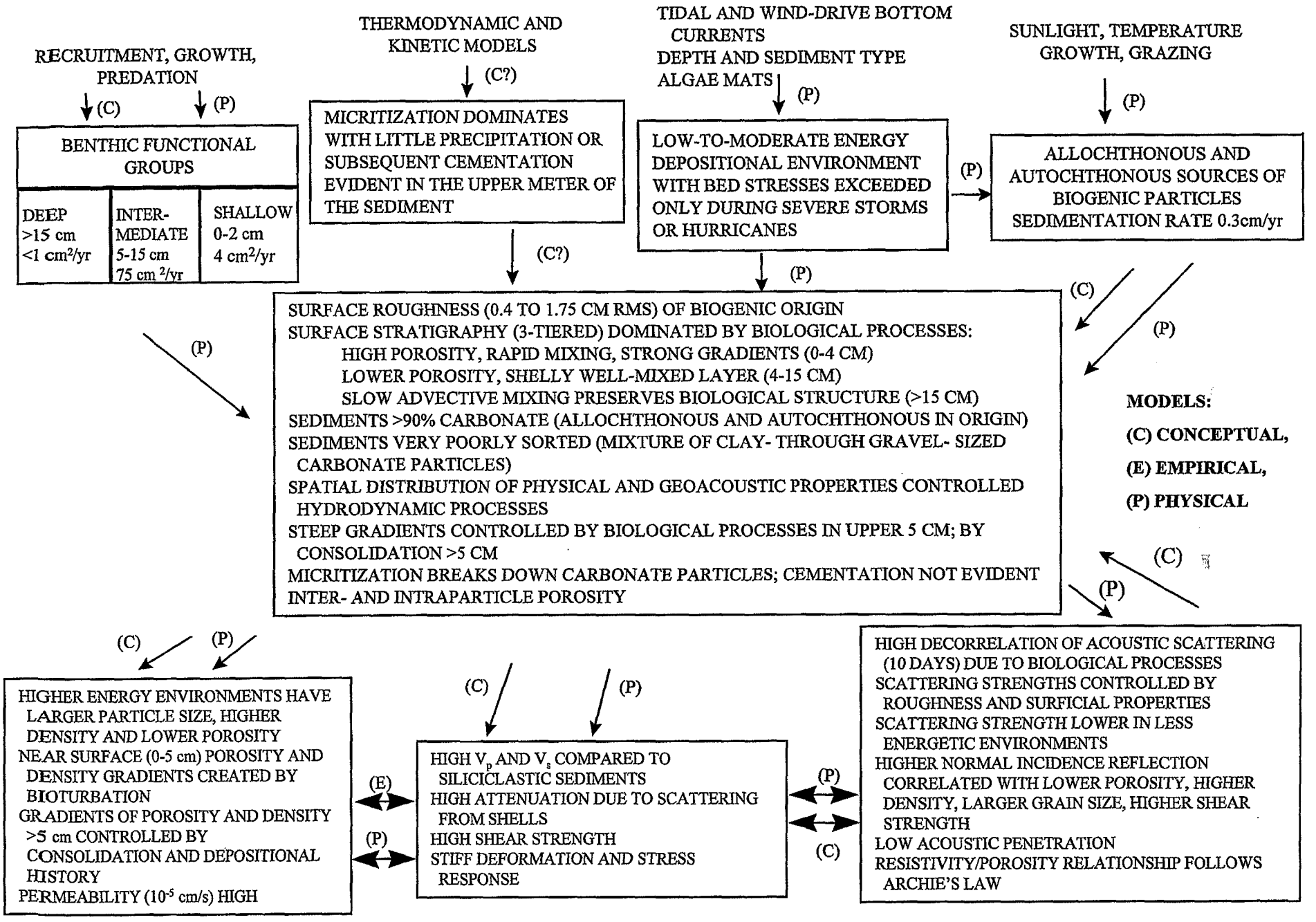

Figure 3. Dry Tortugas: summary of environmental processes and sediment structure, properties and behavior.

2.0 Geologic Background

2.1 The Shallow Subsurface Geology of the Greater Tortugas Area (D. Mallinson)

THE SHALLOW SUBSURFACE GEOLOGY OF THE GREATER TORTUGAS AREA

David Mallinson, Mark Hafen, Dave Naar, Stanley Locker, Albert Hine

Department of Marine Science, University of South Florida
St. Petersburg, FL 33701

The Dry Tortugas and associated carbonate banks on the southwest Florida margin occupy a transitional zone between the south and east facing rimmed margin (to the east) and the west facing ramp margin (to the north). The Holocene reefs which comprise the Dry Tortugas are approximately 14 meters thick, are composed of massive head corals such as *Montastrea sp.*, and are situated upon an antecedent high of the Key Largo Limestone, a stage 5e (~125 ka) reef (Shinn et al., 1977). The Dry Tortugas and adjacent reefs represent windward reef margins in regards to their orientation relative to the dominant wind and wave energies (Hine and Mullins, 1983). Tidal energy is also important in the study area with exchange occurring between the southwest Florida Shelf (Gulf of Mexico waters) to the north, and the Florida Straits to the south. Seismic data from the shelf surrounding the Dry Tortugas reveal up to six depositional sequences in the subsurface (sequences 1 through 6 in ascending stratigraphic order), bounded by high-amplitude reflectors (a, b, g, d, e, also in ascending stratigraphic order) (Fig. 1). Minor, low-amplitude, discontinuous reflectors occur in Sequence 6. Bounding reflectors appear to be unconformable surfaces based on the presence of karst, and probably represent erosion and cementation during sea-level lowstands corresponding to glacial periods. Reflector e is tentatively interpreted as a subaerial unconformity between stage 5a (~80 ka) carbonate sediments deposited in a shallow, tidal shoal setting, and Holocene sediments deposited in a forereef setting. This surface may be an extension of the paleosol surface present in the Marquesas and the Keys to the east (Shinn et al., 1990). If this interpretation is correct, then

reflector d is likely the subaerial unconformity separating stage 5a sediments from stage 5e sediments. These data indicate the importance of sea-level fluctuations in controlling carbonate production, transport, deposition, and erosion in this area.

Seismic, side-scan sonar, and chirp sonar surveys combined with ground truth data in a ~25 km^2 area southeast of Long Key and Southeast Reef reveal that significant Holocene carbonate sand and mud deposition (Sequence 6) occurs in a shallow basin at approximately 18 to 25 meters water depth, seaward of the main Holocene reef tract. The shallow basin is bordered to the south by a partially buried, NE-SW trending, stratified, linear shoal body, probably developed during oxygen isotope stage 5a (~80 ka) (Fig. 1). Holocene patch reef development occurs on the exposed portion of the shoal body. High amplitude acoustic backscatter from the shoal body (in seismic and side-scan sonar data) indicates that the surface of this feature is probably indurated with a veneer of coarse sediment and "live bottom" biota. Greatest sediment thickness (5 meters) occurs at the northern end of the basin adjacent to Southeast Channel, suggesting that much of the sediment is exported from the Holocene reefs and backreef area where carbonate production is highest. Holocene sediments are dominated by aragonite, with lesser amounts of high-Mg calcite, low-Mg calcite, and traces of dolomite. Sediments recovered by gravity core reveal three units (Units 1, 2, and 3, in ascending stratigraphic order) within the Holocene section. Chirp sonar data reveal low amplitude, subbottom reflectors in the Holocene sediments which correlate to coarse pelecypod and gastropod shell beds of Unit 2, and to lagoonal muds of Unit 1.

The three units record an evolution of depositional environments within the study area. Unit 1 indicates a very low energy sheltered environment, such as a lagoon. Such an environment is expected during lower sea level as the shoal would block significant wave energy from the south and east and the antecedent high of the Key Largo Limestone would have blocked wave energy from the north and west.

The superposition of reflector e_1 on the subaerial unconformity (e) indicates that e_1 is a marine flooding surface, or perhaps preserved lagoonal muds which may grade upward into Unit 1 identified in the cores. The occurrence of this reflector only in the northwest corner of the study area on the rim of the bedrock high may indicate mud deposition associated with a mangrove fringe, a typical environment in the Keys today.

The abrupt upward transition to much coarser sediment in Unit 2 may reflect overtopping of the outer shoal during sea-level rise and introduction of higher wave energy into the depositional area. The imbricated coarse gastropod (Turritelid) and pelecypod shell beds and interbedded fining upward sediments associated with Unit 2 indicate high energy conditions and are interpreted as storm deposits, possibly associated with hurricanes. Shinn et al. (1990) identified similar shell beds in vibracores from the Quicksands (60 km to the east), and also interpreted them as storm beds. Reflector e_2 occurs at depths corresponding to the coarse shell beds seen in the cores.

The fining upward trend in Unit 3 reflects decreasing ambient bottom energies associated with normal wave activity during sea-level rise since the early Holocene, and a change in sediment source. Much of the fining upward trend likely results from the contribution of carbonate mud from new sources as extensive Holocene reef growth began on the antecedent highs, and backreef areas were flooded allowing mud producers, such as *Halimeda* and *Penicillus*, to become more prolific.

A diagenetic profile is apparent based on microscopic analyses. SEM observations of samples from the top 20 cm of cores show little evidence of dissolution, micritization, or cementation of carbonate muds. Samples from near the base of cores show significant evidence of micritization and cementation. Aragonite overgrowths were noted on larger carbonate fragments. The diagenetic profile is most apparent in observations of coccoliths. Coccolith preservation ranges from

pristine near the sediment/water interface to highly degraded in the base of cores. Diagenesis of these grains is driven by their metastability and is accelerated by aerobic and anaerobic microbial decomposition of organic matter.

Forward modeling and impedance inversion reveal good agreement between sediment physical properties, acoustic properties measured by the electric logger, and the chirp sonar data. Reflection coefficient values appear to correspond to the mean grain size of the surface sediment as determined on core samples in the laboratory. The chirp data indicate a bottom sediment mean grain size primarily in the coarse silt size fraction. Chirp data suggest variations in the seafloor sediment grain size across the study area. The seafloor reflection coefficient in the area of core KW-205 is approximately -10 to -11 dB (0.31 to 0.28) indicating a coarse silt grain size. Grain size analyses of KW-205 indicate an average mean grain size of 15 microns (medium silt) in the top 10 cm. The seafloor reflection coefficient in the area of core KW-226, south of KW-205, is higher (-9 to -10 dB; 0.35 to 0.31) indicating coarser sediment. Surface mean grain size at KW-226 is 28.6 microns (coarse silt). Progressing south the seafloor reflection coefficient increases to -8 dB (0.40) indicating coarser sediment. Hardbottom areas are easily mapped based on a very high reflection coefficient of -2 to -4 dB. The very low reflection coefficients (-20 dB) on the seaward side of the outer reef are the product of high scattering resulting from biohermal structures at least 1 meter in relief.

Estimates of the surface sediment impedance were derived by inversion based on the reflection coefficients recorded by the chirp vertical beam sonar. The impedance (rv) may be determined using the following equation:

$$r = (\rho_1 v_1 - \rho_2 v_2)/(\rho_1 v_1 + \rho_2 v_2)$$

where r is the reflection coefficent, $\rho_1 v_1$ is the impedance of the water column, and $\rho_2 v_2$ is the impedance of the surficial sediments. This equation reduces to:

$$\rho_2 v_2 = x / 1-r$$

where $x = r(\rho_1 v_1) + \rho_1 v_1$. Density and velocity measurements of the water column were made by CTD in the Dry Tortugas area. Average seawater density and velocity was 1.025 gcm^{-3} and 1526 ms^{-1}, respectively, yielding a seawater impedance of 1.56 x 10^6 $kgm^{-2}s^{-1}$. The reflection coefficient recorded in the area of core 205 in the Dry Tortugas site is approximately 0.28 (Table 1). Inserting this r-value into the second equation above yields an impedance value of 2.78 x 10^6 $kgm^{-2}s^{-1}$. The impedance based on the electric logger ranges from 2.56 to 2.74 x 10^6 $kgm^{-2}s^{-1}$ over the top 20 centimeters, slightly less than that estimated by sonar. The reflection coefficient recorded in the area of core 226 is approximately 0.31. This r-value yields a sediment impedance of 2.97 x 10^6 $kgm^{-2}s^{-1}$, whereas the electric log data yield impedance values ranging from 2.76 to 2.95 x 10^6 $kgm^{-2}s^{-1}$ over the top 20 centimeters. These estimates indicate that the remote acoustically estimated impedance is approximately 1% to 8% higher than the directly measured impedance in the top 20 centimeters of the sediment column. These data will allow calibration refinement. It is possible that the remotely estimated value is a better measure of impedance as the core material is likely to be slightly disturbed.

Table 1. Comparison of impedance values for surficial sediments based on chirp data and ground truth data. Ground truth mean and range are determined over the top 20 cm of cores. Impedance values are in units of 10^6 $kgm^{-2}s^{-1}$.

Area	Core	Chirp	Ground truth mean	Range
DT	147	2.61-2.79	2.66	2.54-2.70
DT	205	2.78	2.64	2.43-2.74
DT	207	2.78	2.69	2.57-2.85
DT	226	2.97	2.82	2.76-2.95
DT	232	3.01	3.18	3.14-3.21

REFERENCES

Hine, A.C., and Mullins. H.T, 1983, Modern carbonate shelf-slope breaks: Society of Economic Paleontologists and Mineralogists Special Publication No. 33, p. 169-188.

Shinn, E.A., Hudson, J.H., Halley, R.B., and Lidz, B., 1977, Topographic control and accumulation rate of some Holocene coral reefs, South Florida and Dry Tortugas: Proceedings, Third International Coral Reef Symposium 2, Miami, FL, p. 1-7.

Shinn, E.A., Lidz, B.H., and Holmes, C.W., 1990, High-energy carbonate sand accumulation, the Quicksands, southwest Florida Keys: Journal of Sedimentary Petrology, v. 60, no. 6, p. 952-967.

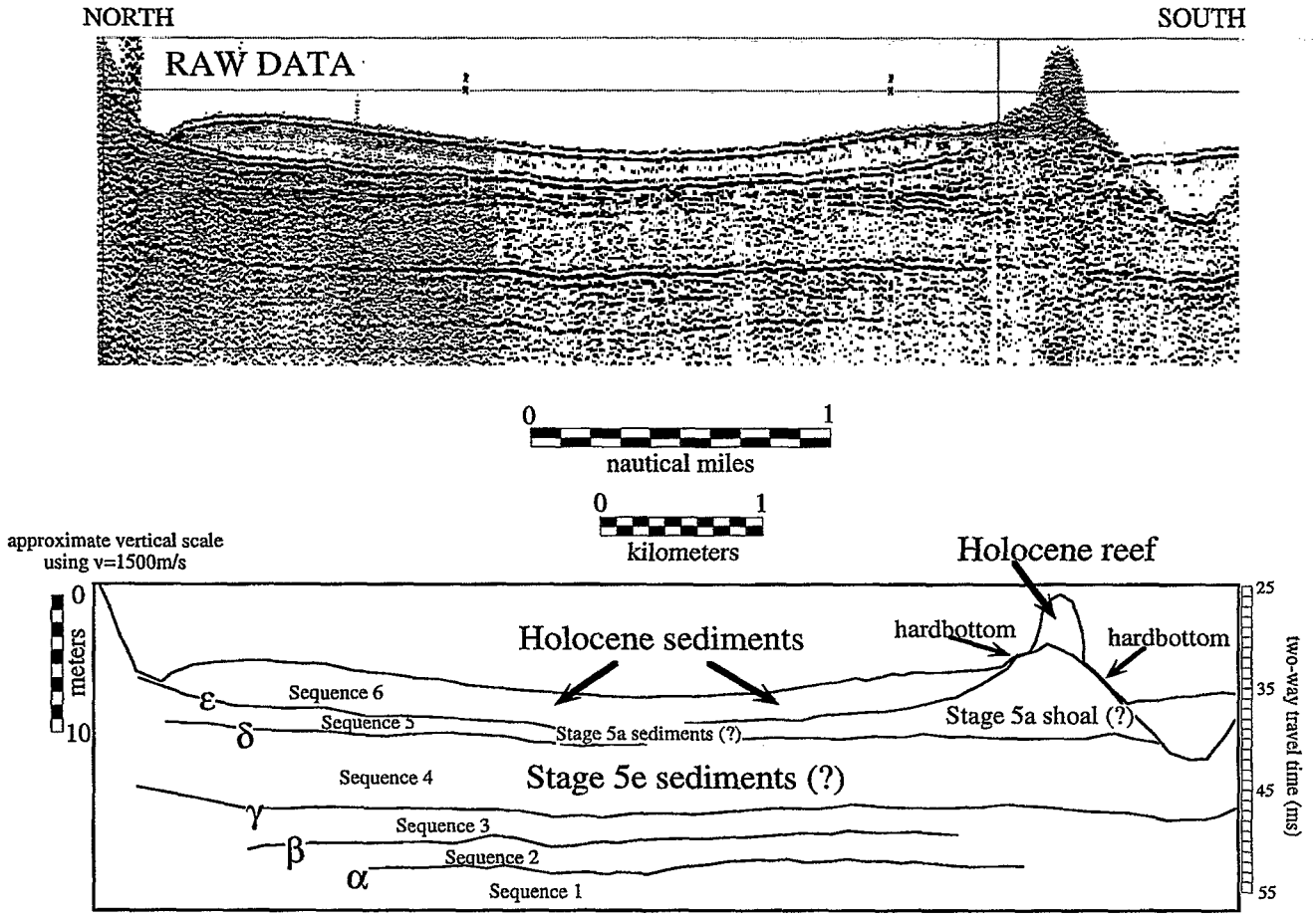

Figure 1. Seismic data and interpretation from the Dry Tortugas area showing reflectors α–ε, inferred sequence ages, and the shoal body with reef development in the south.

2.2 Backscatter Characteristics of the Seafloor Within the Dry Tortugas Research Area (T. Wever and H.M. Fiedler)

Backscatter characteristics of the seafloor within the
Dry Tortugas research area

Thomas F. Wever, Hannelore M. Fiedler

Forschungsanstalt der Bundeswehr für Wasserschall und
Geophysik (FWG), Klausdorfer Weg 2-24, 24148 Kiel, Germany.
e-mail: fwg@fwg.ki.eunet.de

During the Key West Campaign we surveyed an area of 25 km^2 (Dry Tortugas Box, DBT) with 100 kHz side scan sonar (SSS) and 3.5 kHz subbottom profiler (SBP), both mounted in one towfish. From the recordings we constructed maps of seafloor characteristics. In this paper we explain most of the acoustic remote sensing signatures.

In addition to the standard SSS and SBP data, the relative backscattering strength (BS) was measured with a digital attachment to the SSS system that was developed at FWG. The lack of absolute BS data for calibration of the system does not allow absolute BS information.

The survey consisted of a total of 34 north-south oriented profiles with a lateral distance of 150m allowing some overlap of the SSS records.

THE SSS AND SBP DATA

The SSS prints are shown in Figure 1. High backscatter produced a black signature; low backscatter regions are white. The major trend of seafloor features follows a NE-SW direction.

The SBP results were converted to depth (Figure 2) using a sediment velocity of 1500 m/s. Most sediment velocities determined in this area are in the range of 1520-1560 m/s, the calculated depths are thus minimum depths. The maximum depth error is estimated to be less than the resolution of the system.

Starting in the southeast corner of the DTB, the following SSS domains were observed and are discussed together with the SBP data:

(1) In the SE corner a small high backscatter region is mapped. In part, the high BS is produced by the rough and irregular surface of a reef where no depth penetration with the SBP was observed. The original SSS prints show some backscatter variations. SBP recordings display layering in the NW portion of this high-BS region illustrating the transition to high-BS sediments.

(2) The high-BS sediments grade into low-BS sediments. Both types of sediment outline a sediment trough 1 km wide in which layering down to 6 m depth was observed. In the NW corner this sediment trough abruptly ends at another reef.

(3) The next high-backscatter area represents again another reef with no SBP penetration into the seafloor. The BS from the reef's surface shows internal differences, possibly due to different ages of the reef. Similar to situation (1) the high-BS extends NW into a sediment basin. The transition is, however, marked here by a 4 km long and 20 m wide, slightly undulating, 'white line' of unknown origin.

(4) The average width of the sedimentary high-BS zone varies from 150 m in the SW and 250 m in the central part to >1 km in the NE. The low-BS sediments of the central and western part of the DTB cover nearly half of the investigated area and show very low backscatter. The acoustic penetration of the SBP exceeds 2 m.

Again, no depth information could be achieved with the SBP.

(5) Another region of increased backscatter is seen in the NE corner of the DTB.

The relative BS data confirm the described segmentation of the DTB. In the high-BS areas, BS is 8-10 dB higher than in the low-BS regions. The 'white line' is characterized by a 4 dB lower BS.

GROUND TRUTH DATA

We used 31 grain size analyses for interpreting the SSS records. These samples do not cover all described BS domains of the DTB. However, the distribution of grain sizes suggests a trend in which the coarser sediments cause higher BS. The finest sediments are found in the low-BS sediment troughs.

DISCUSSION

In the DTB, two observations were made with the SSS which prevented a direct correlation between BS characteristics and seafloor type: (a) sediments cause both high and low backscatter, and (b) high backscatter is caused both by sediments and reefs.

A clear identification of the seafloor type was possible only with information from the SBP because no depth penetration could be obtained from reefs.

The mechanism that controls BS from sediments is not well understood: (a) Interface scattering from seafloor roughness, and (b) volume scattering from inhomogeneities within the sediment are discussed (for a review see, e.g., Jackson et al., 1986). Clay and Medwin (1977) demonstrated that for 100 kHz systems ripples 1 cm high can produce enormous backscatter where the ripple type (gently

curved or rippled) also plays an important role. Very low backscatter is related to smooth, gently curved bottoms and high backscatter to ripples.

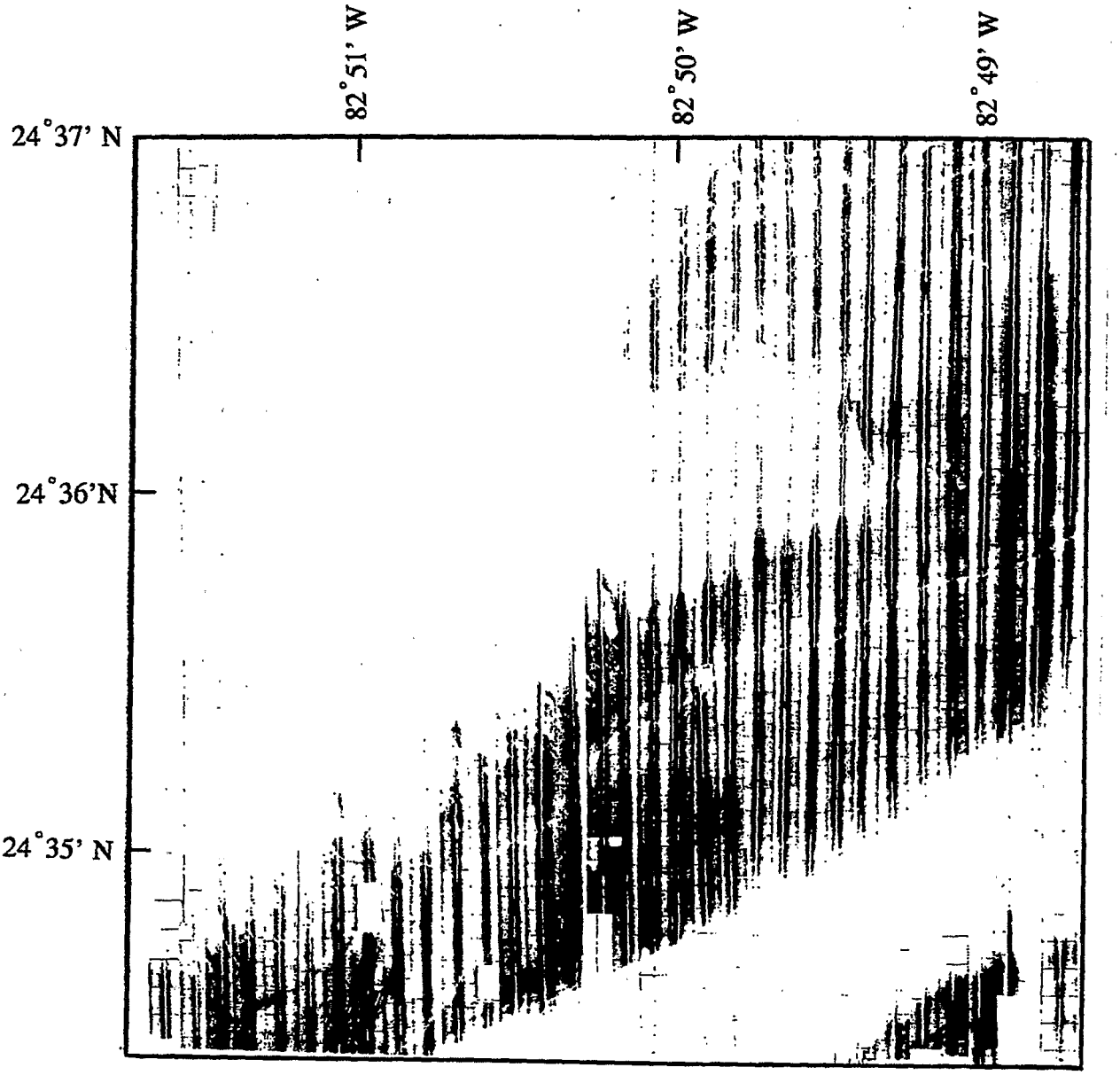

Figure 1: Map of the side scan sonar data as constructed from the original prints. Dark (white) domains represent regions of high (low) backscatter from the seafloor.

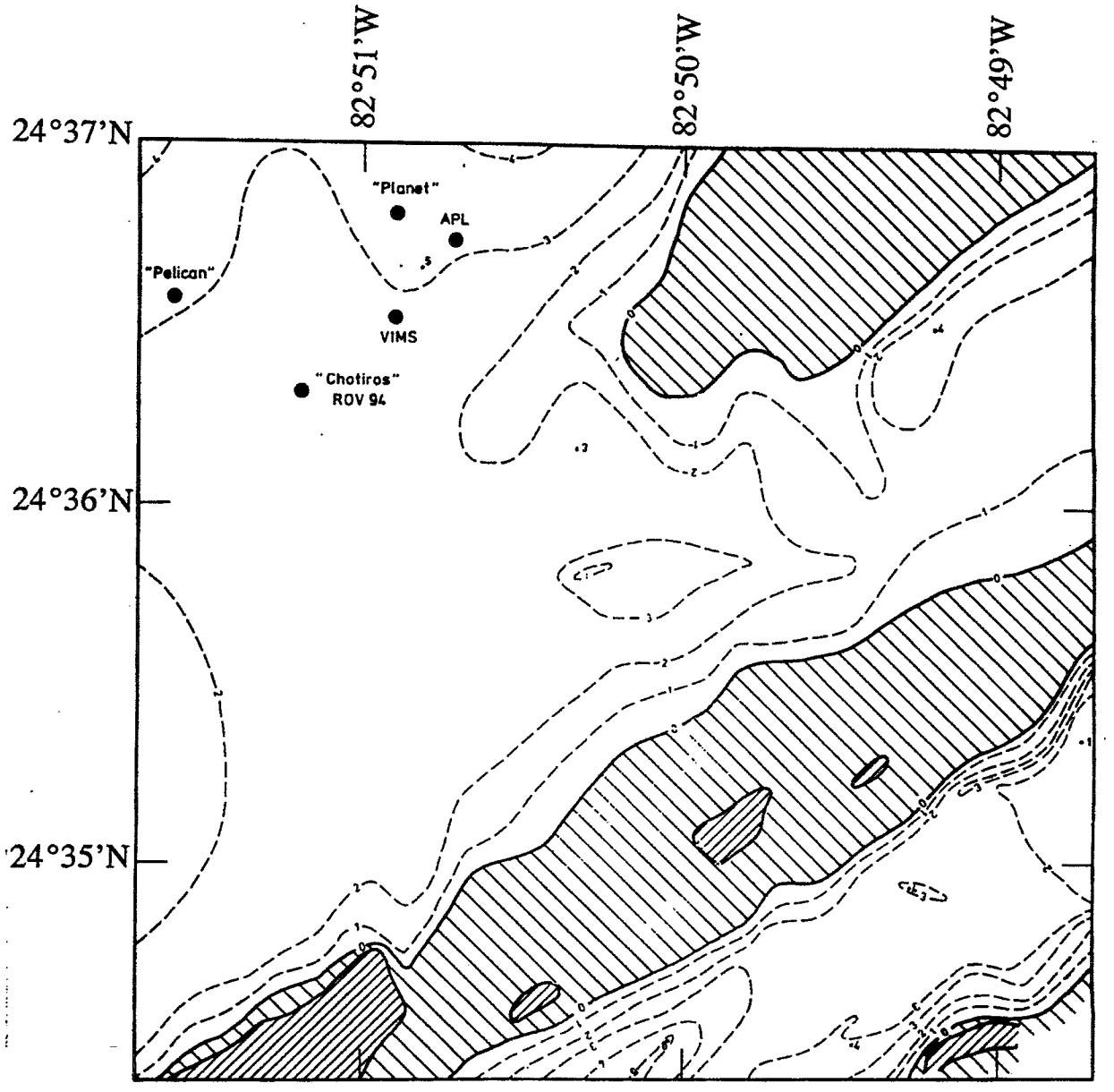

Figure 2: Depth of acoustic penetration with the 3.5 kHz subbottom profiler. Areas of no penetration (hatched) correspond to reefs (\\\\ hatching: 'new' reef, denser //// hatching: 'old' reef). The locations marked in the northwestern part were named after the first occupant and show the finally selected experimental area. The isolines give the depth of acoustic penetration.

In other attempts, BS is related to grain size. Urick (1983), for example, uses grain size as a simple rule for acoustic backscattering classification. The available sediment type data from the DTB give evidence that the high BS of sediments is caused by coarse grains.

Generally, both approaches cannot be considered independent: currents that have enough energy to form ripples at the bottom (i.e., increase the interface roughness), will erode and transport the fine sediment to more protected areas leaving the coarser grains. A 'rough' seafloor therefore is characterized by coarse material and classified as 'acoustically hard.' Little acoustic energy will be transmitted into the 'hard' seafloor (interface scattering dominates). In contrast, soft muddy bottoms will allow acoustic energy to penetrate more than a few centimeters into the seafloor and cause backscattering from volume inhomogeneities.

We interpret the differences in backscatter strength within the DTB sediments to result from different grain sizes in the surveyed area and the expected differences in surface roughness. The reef's high backscatter is caused by its irregular (rough) surface. An interesting observation is that the transition from the central reef to fine grained (low BS) sediments takes place directly towards the southeast whereas in northwest direction the transition takes place via the intercalated coarse sediments. This can be used to identify the main transport direction of reef debris towards north.

REFERENCES

Clay, C., Medwin, H. (1977). Acoustical Oceanography, Wiley, New York, 544 pp.
Jackson, D.R., Winebrenner, D., Ishimaru, A. (1986). Application of the composite roughness model to high-frequency bottom backscattering, J. Acoust. Soc. Am. 79, 1410-1422.

Urick, R. (1983). Principles of Underwater Acoustics, McGraw-Hill, New York, 423 pp.

2.3 Geophysical and Geotechnical Characterization of Carbonate Sediments (D. Huws, J. Pyrah and A. Davis)

Geophysical and Geotechnical Characterization of Carbonate Sediments

Dei Huws, James Pyrah, Angela Davis

School of Ocean Sciences, University of Wales, Bangor, UK

INTRODUCTION

The approach taken in this study is to utilize field geophysical and laboratory geotechnical test data so as to estimate the *in situ* behavior of tropical shallow-marine carbonate sediment. The ultimate goal is to predict the deformation characteristics of a range of carbonate sediments to a combination of static and cyclic loading. Until relatively recently, little was understood of the geotechnical behavior of carbonate sediments and it was not until the late 1980's that much of the research was brought together at the Engineering for Calcareous Sediments Conference (Jewell and Andrews, 1988; Jewel and Korshid, 1988). Since then, there have been sporadic publications related to the geotechnical properties of carbonate sediments (e.g. Airey and Fahey, 1991; Coop, 1990; Coop and Atkinson, 1993; Hyodo *et al.*, 1996). Geophysical field measurements such as those undertaken in this study do not appear to have been published widely.

OBJECTIVES

There are a number of objectives to set on the way to achieving the goal outlined above:

- To measure the geophysical properties (shear wave velocity, Vs, and electrical resistivity) of the material and to estimate from these the *in situ* void ratio (porosity);
- To adapt a standard micro-processor controlled triaxial apparatus for cyclic loading and to modify the end platens to incorporate shear wave bimorphs in order to enable the measurement of velocity during the testing procedures;
- To perform a series of loading tests so as to define:
  the dependency of Vs on void ratio and effective confining stress
  the critical state line for the material (in effective stress - deviator stress - Vs space)
- To investigate the response of the sediment to isotropic/anisotropic, monotonic and cyclic loading, so as to combine the field data in a meaningful manner in order to estimate *in situ* behavior.

POSITION OF SURVEY

The data presented in this study pertain to the relatively coarse carbonate sediment of the Rebecca Shoals Test Site. Figure 1 shows the position of the field survey line in relation to the Tortugas and Marquesas Test Sites.

GEOPHYSICAL CHARACTERIZATION OF THE MATERIAL

FIELD DATA:

Measurements of Vs and electrical resistivity were performed at discrete intervals along the survey line using the seafloor sled system described by Davis *et al.* (1989). Electrical resistivity data are acquired via a focused electrode 'pad' (Jackson 1976) and were initially recorded as raw voltages (figure 2) before being normalized as a series of formation factors using the formula:

$$\text{Formation Factor} = \frac{\text{Voltage recorded at measurement point}}{\text{Voltage recorded in sea water}}$$

Shear wave data were acquired in the form of refracted head waves and interpreted by simple plane horizontal-layer forward model in terms of a velocity-depth structure (see figure 3). The shear wave velocity data may, as a first approximation, be assumed to depend only upon depth (effective confining stress). Under such conditions, the best fit equation takes the form:

$$Vs = 192\ z^{-0.28},$$

where z = depth [m]. N.B. the above predicts significantly higher velocities at shallow depths than the empirical equation formulated for siliclastic sediments by Hamilton (1976) :

$$Vs = 128\ z^{-0.28}.$$

ESTIMATION OF FIELD POROSITY

In order to estimate values of *in situ* porosity, the relationship between porosity, and formation factor and Vs must be known.

The form of the relationship between porosity and formation factor is well established (Archie, 1942):

$$\text{Formation Factor} = A.\ n^{-m},$$

where A, m are constants for a particular sediment and n = porosity.

A Porosity Cell devised by Jackson (1976) (and developed by Schultheiss, 1983) allows porosity to be altered and accurately measured, whilst at the same time enabling measurement of formation factor - thus 'A' and 'm' in the above equation

may be derived for a particular sediment sample. Data for the Rebecca Shoals sand are shown in figure 4 and the following best-fit line results:

$$\text{Formation Factor} = 0.84.\ n^{-1.71} \qquad (1)$$

The form of the equivalent Vs - porosity line is not so well established, although an empirical equation formulated by Richardson *et al* (1991) appears to work well in siliclastic sediments:

$$Vs = (A/e)\ z^{B},$$

where A, B are constants e = void ratio.

Keeping the same form of the equation, and assuming a value for 'B', the Cell data may be used to tentatively derive the following inter-relationship:

$$Vs = (150/e)\ z^{0.30}. \qquad (2)$$

The velocity data are shown in figure 5. Note that, again, velocities are higher at any given porosity as compared to that normally expected for siliclastic sediments at equivalent void ratios.

Equations (1) and (2) may thus be used to estimate *in situ* values of porosity. These estimates are shown in figure 6. Two points are raised by the data:

(i) The electrical resistivity data appear to show much more variation along the line when compared to the velocity data. Indeed, some cyclicity is revealed, which appears to coincide with the wavelength of sand waves appearing on sub-bottom profiles.

(ii) The resistivity-derived porosities appear to be generally higher than their equivalent velocity-derived counterparts. This may, in part, be explained by the

fact that the former relate to the first few decimetres of sub-bottom, whereas the latter may be from up to 3 m. depth. It is known that porosity may change substantially between these depth ranges at the other Test Sites (Lavoie and Furukawa, 1996).

GEOTECHNICAL CHARACTERISATION OF THE MATERIAL

All geotechnical tests were performed upon a large grab sample collected at a point close to the geophysical survey line. Dry sieve particle size analysis yield the following data:

Median grain size	1.30 f
Mean grain size	1.18 f
Standard deviation	0.93 f
Skewness	-0.13 (towards coarse diameters)
Kurtosis	1.25 (less peaked than normal)

It can be seen that this sand is coarser than most of the Tortugas and Marquesas sediments

HARDWARE DEVELOPMENT

The hardware development objectives outlined earlier have been achieved and pilot tests performed on artificial and locally derived siliclastic sediment. Some delay in testing the Rebecca Shoals sample was experienced due to supply of defective sample membranes.

PRELIMINARY DATA

A very limited number of consolidation tests have been performed, with the initial aim of clarifying the nature of the inter-relationship between Vs, void ratio and effective confining pressure. Figure 7 shows the load/unload loop for the sample. It is noted that the sample shows low compressibility on the unload loop, confirming previous studies. This is also reflected in the shear wave velocity data (not shown). Normalized shear wave velocity is plotted versus void ratio in figure 8. On first inspection of the data, velocities are 15-20% lower than predicted by the Cell data for a given depth and void ratio, and are on the lower bounds of the *in situ* velocity-depth data. Whilst a number of reasons may be put forward to explain these data, further testing will be needed to confirm the trends observed thus far.

WORK IN PROGRESS

It is intended to investigate further the potential deformation behavior of the carbonate sediment on the premise that settlement will be dominated by liquefaction-type phenomena. Initially, the state parameter approach (Been and Jefferies, 1985) as modified by Pyrah (1996) and Robertson *et al.* (1995), will be adopted. By defining the critical state line for the material in effective confining pressure - Vs space, it becomes possible to use field velocity-depth data in order to predict the 'state' of the deposit - whether or not it is likely to be dilative or contractive in its' response to loading. It has been shown in previous offshore site investigations that bioclastic sediments tend towards contractive behavior (Semple, 1988) and are therefore more prone to failure.

Having established the variation of state *in situ*, it is intended to perform a series of isotropically and aniostropically loaded, undrained and drained monotonic tests, before progressing on to the simulation of wave loading conditions expected at the site via cyclic triaxial tests.

CONCLUSIONS

- By *in situ* measurement of Vs and electrical resistivity, combined with laboratory calibration using the Porosity Cell, it becomes possible to estimate values of void ratio, although the exact inter-relationship between Vs and void ratio will only become well defined after amalgamation of the data acquired by other workers in the CBBL project.

- Hardware has been adapted and developed so as to allow concurrent Vs measurements during cyclic triaxial loading.

- Initial triaxial data reinforce previous work, revealing an anelastic unload response during consolidation testing. The hypothesis that this is caused by fabric rearrangement is reinforced by the Vs data, which is significantly higher after loading that at the same void ratios during the loading phase. Shear wave velocity versus effective confining pressure has been defined for three samples of different packing. The *in situ* data would appear to fit on the lower end of the void ratios over which the tests have been performed.

- Further testing will define the critical state line for the sediment and will then be used with the field velocity data to predict the state of the material along the survey line.

- Cyclic loading tests shall allow the geotechnical characteristics to be further elucidated. It is intended to use the field data to predict ambient conditions on the seafloor so as to allow the simulation of the wave loading conditions as accurately as possible.

REFERENCES

Airey DW & Fahey M (1991) 'Cyclic response of calcareous soil from the North-West Shelf of Australia', Geotechnique, 41, (1), pp 101-121.

Archie GE (1942) 'The electrical resistivity log as an aid in determining some reservoir characteristics' Trans. Am. Inst. of Mining and Metallurgic Engineers, 146, pp 54-62

Been K & Jefferies MG (1985) 'A state parameter for sands' Geotechnique, 36, (2), pp 239-249.

Coop MR (1990) 'The mechanics of uncemented carbonate sands', Geotechnique, 40, (4), pp 607-626.

Coop MR & Atkinson JH (1993) 'The mechanics of cemented carbonate sands', Geotechnique, 43, (1) pp 53-67.

Davis AM, Huws DG, Bennell JD & Thomas D (1989) 'Development of a seafloor geophysical sledge' Marine Geotechnology, 1, (2), pp. 91-115.

Hyodo M, Aramaki N, Itoh M & Hyde A (1996) 'Cyclic strength deformation of crushable carbonate sand' Soil Dynamics and Earthquake Engineering, 15, pp 331-336.

Jewell RJ & Andrews DC (Eds.) (1988) Engineering for Calcareous Sediments Proceedings of the International Conf. on Calcareous Sediments, Perth, 15-18 March 1988, Volume 1.

Jewell RJ & Korshid MS (Eds.) (1988) Engineering for Calcareous Sediments Proceedings of the International Conf. on Calcareous Sediments, Perth, 15-18 March 1988, Volume 2.

Jackson PD (1976) Electric Properties of Irish Sea Sediments Ph.D. Thesis, Univ. of Wales, Bangor, unpubl.

Lavoie D & Furukawa Y (1996) 'Effects of environmental processes on shear modulus' In: Coastal Benthic Boundary Layer Research Program: A Review of the Third Year, MD Richardson (Ed.) , Naval Research Laboratories, Stennis Space Center (MS) , Report no. NRL/MR/7431 -96 - 8001, pp 117-130.

Schultheiss PJ (1983) 'The influence of packing structure and effective stress on Vs, Vp and the calculated dynamic and static moduli in sediments' In: Acoustics of the Seabed, NG Pace (Ed.), Conf. Proc. Of the Institute of Acoustics, Bath Uni. Press, pp 19-28.

Richardson MD, Muzi E, Miaschi B & Turgutcan F (1991) 'Shear wave velocity gradients in near-surface marine sediments' In: Shear Waves in Marine Sediments, JM Hovem, MD Richardson & RD Stoll (Eds), Kluwer Academic Publ., Dordrecht, pp 295-304.

Pyrah JR (1996) An Integrated Geotechnical-geophysical Procedure for the Prediction of Liquefaction in Uncemented Sands Ph.D. Thesis, Univ. of Wales, Bangor, unpubl.

Robertson PK, Sasitharan S, Cunning JC & Sego DC (1995) 'Shear wave velocity to evaluate in-situ state of Ottowa Sand ' Journal of Geotechnical Engineering, 121, (3), pp. 262-273.

Semple RM (1988) 'The mechanical properties of carbonate soils' In: RJ Jewell & DC Andrews (Eds.) Engineering for Calcareous Sediments, Proceedings of the International Conf. on Calcareous Sediments, Perth, 15-18 March 1988, Volume 1, pp. 515-530.

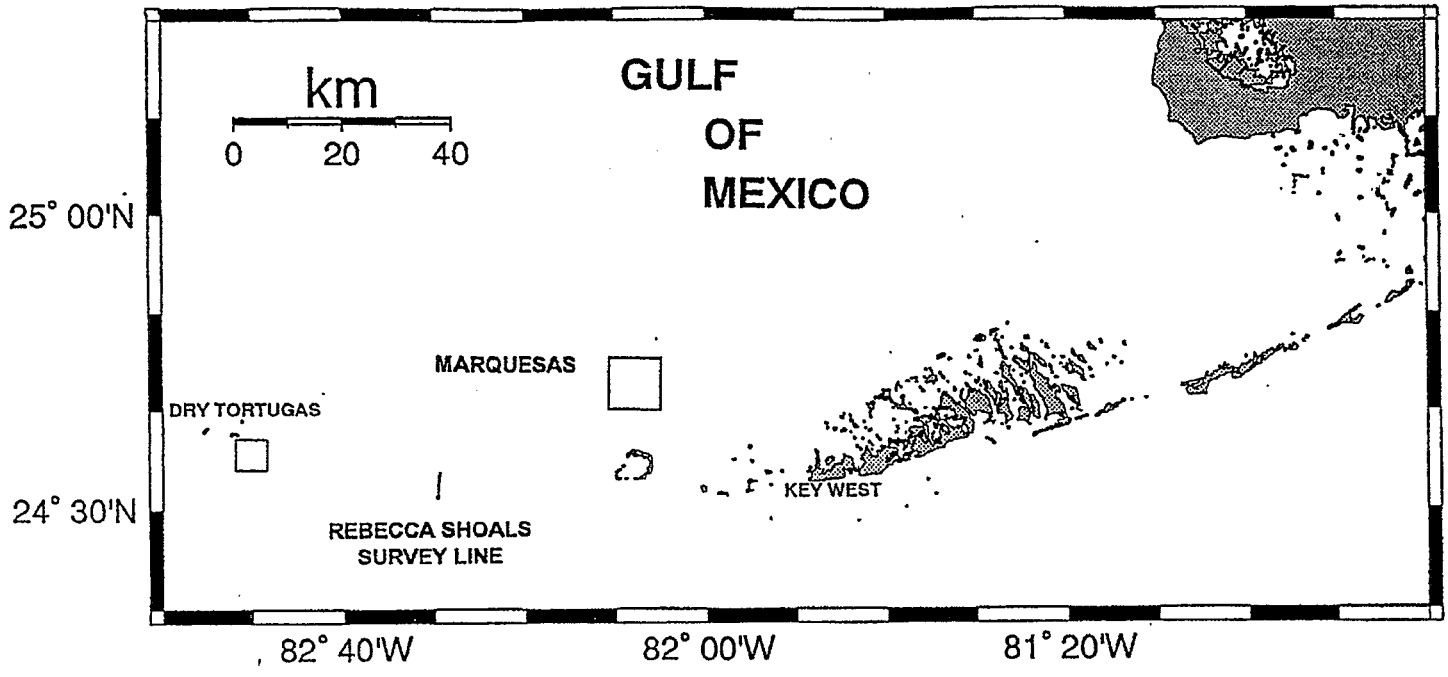

Figure 1 - Position of Rebecca Shoals survey line Relative to other Test Sites

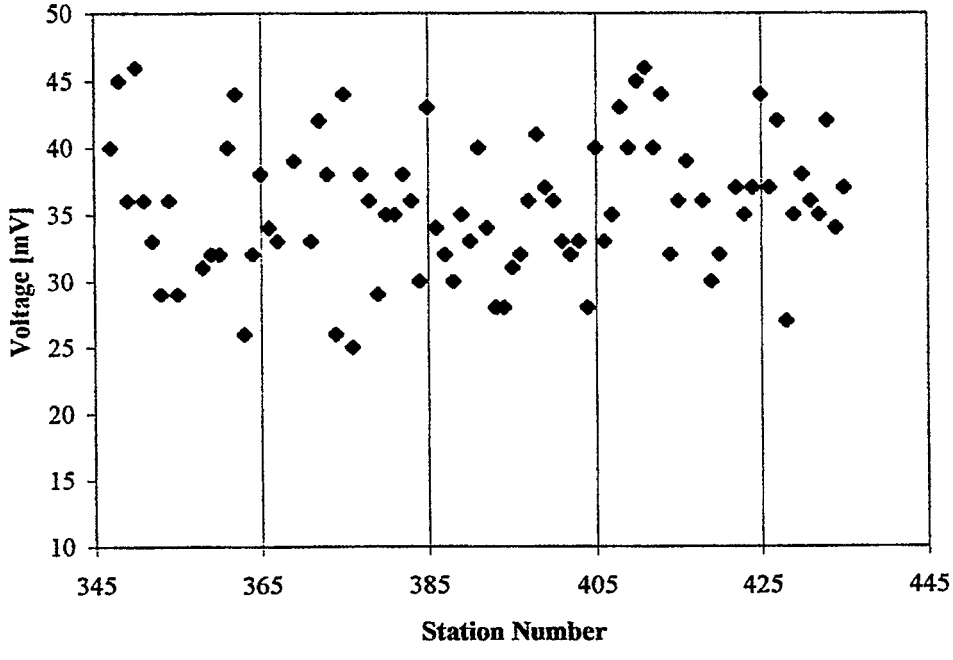

Figure 2 - Electrical reisitivity raw data

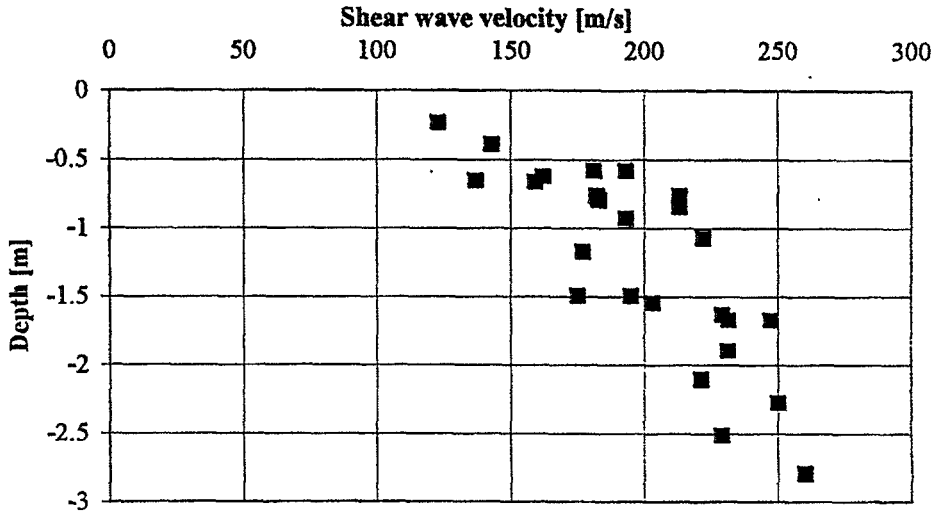

Figure 3 - Interpreted field velocity-depth data

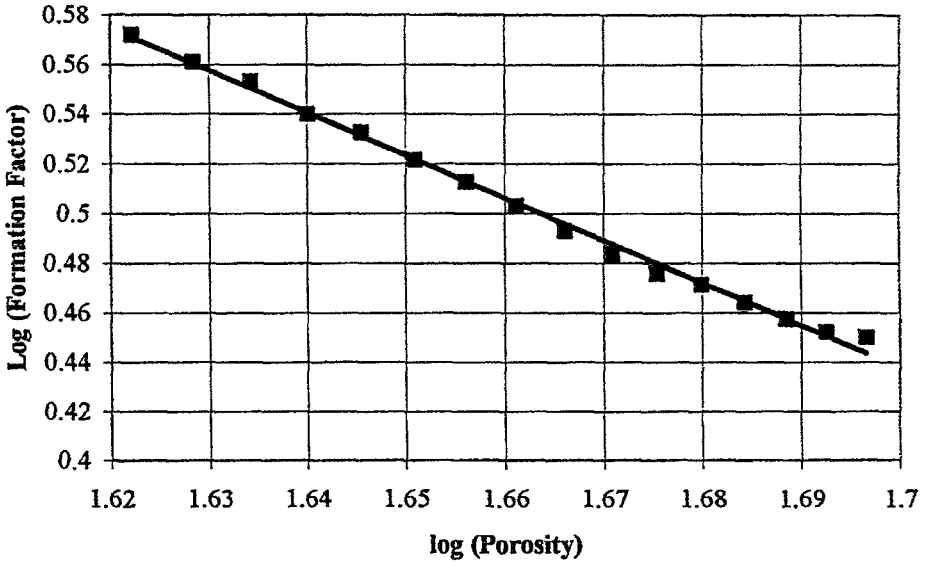

Figure 4 - Cell experiment formation factor data

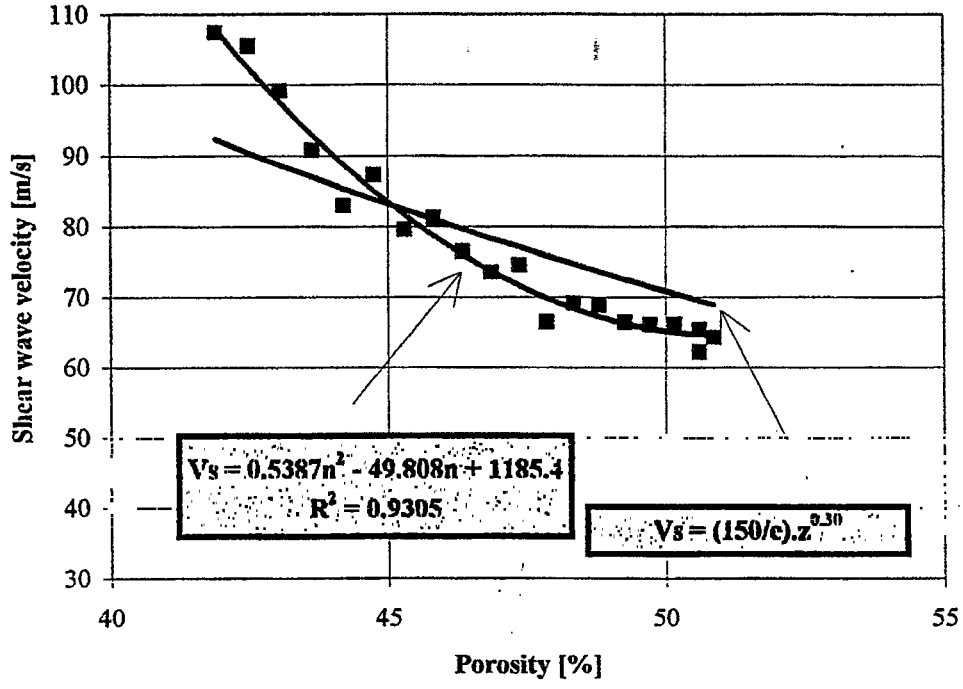

Figure 5 - Cell experiment shear wave velocity data

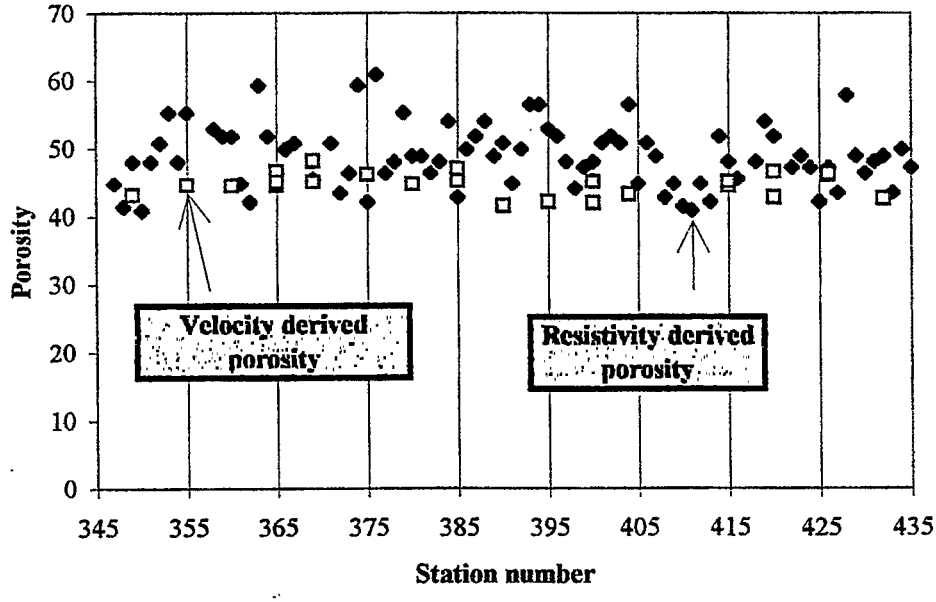

Figure 6 - Predicted porsosity along survey line

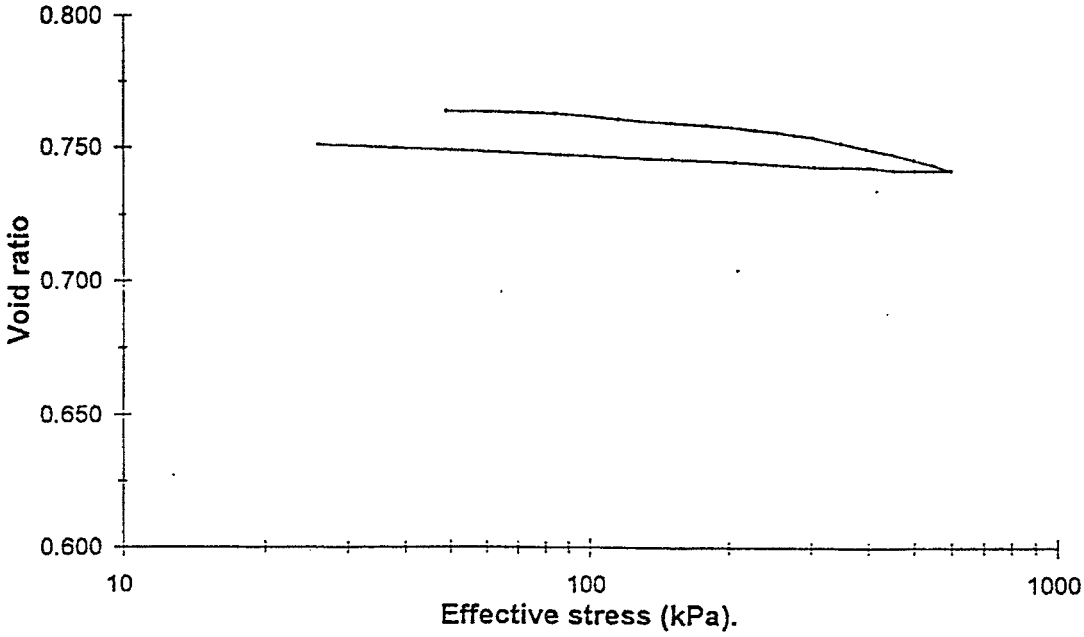

Figure 7 - Isotropic compression curve for sample

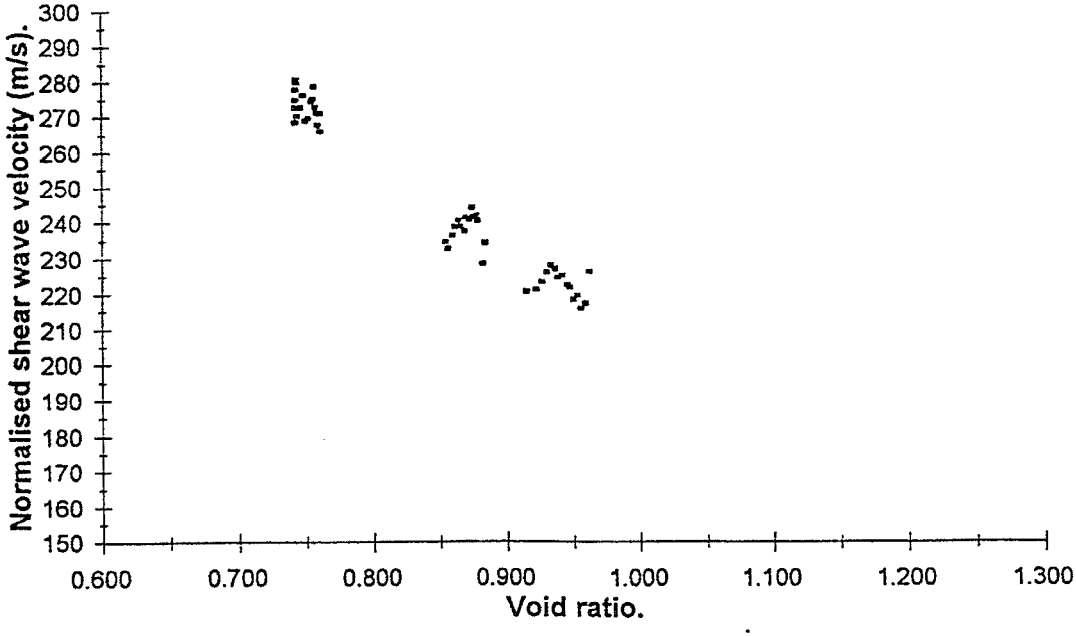

Figure 8 - Void ratio versus measured Vs for three compression tests

2.4 Holocene Paleoenvironmental Change at the Dry Tortugas and Marquesas Keys CBBL Localities (C.A. Brunner)

HOLOCENE PALEOENVIRONMENTAL CHANGE AT THE DRY TORTUGAS AND MARQUESAS KEYS CBBL LOCALITIES

Charlotte A. Brunner

Institute of Marine Sciences, University of Southern Mississippi, Stennis Space Center, MS 39529; e-mail, cbrunner@whale.st.usm.edu

Large vertical changes in paleoenvironment and lithologic facies belie the present-day surficial homogeneity of the Dry Tortugas and Marquesas Keys localities. Dramatic paleoenvironmental and facies changes occur with increasing depth in cores. Benthonic foraminifers in the sand fraction >150 μm were examined in long gravity cores (>2 m) from the two localities. Results from two representative cores are presented here, core KW-PE-GC-225 from ~30 m water depth at the Dry Tortugas site and core KW-PE-GC-235 from ~20 m water depth at the Marquesas Keys site. A census of foraminifer genera and species was made on 300 to 600 specimens per sample, and taxon frequencies compared to present-day distributions in order to interpret Holocene changes in paleoenvironment. Five end-member assemblages live in the present-day region: a marsh fauna found in shallow water exposed to large salinity extremes, a restricted-bay fauna typical of Florida Bay, an open-platform fauna found north of the study region, a back-reef fauna typical of Hawk Channel, and a reef fauna found amid actively growing reefs like those at the platform margin. Most assemblages appear as gradations between the five end-member assemblages.

Two assemblages appear in the Dry Tortugas core: a marshy to shallow back-reef fauna and a typical back-reef fauna. Samples from the basal silty clay from 243 to 200 cm below sea floor (bsf) contain the marshy fauna and are overlain by a coarser silt- and clay-rich sand with a diverse back-reef assemblage. The assemblage change is abrupt, occurring between 200 and 190 cm bsf with evidence of a slight transition between 190 to 170 cm bsf, where grain size also grades from fine to coarse. A disconformity may exist between the two assemblages and lithologies. The sand-rich unit appears to be prograding across the earlier Holocene marsh clay. The sand unit may be analogous to a contour deposit

accreting in the lee of the Dry Tortugas from sediment transported past the site by tidal and wind-driven currents flowing on the south and east sides of the Dry Tortugas site. This interpretation, although tentative, is supported by acoustic profiles (Don Walter, 1997, pers. comm.) and grain size distributions (Kevin Stephens?, 1997).

Two assemblages are recognized in the Marquesas core: a typical marsh assemblage and an open-platform assemblage. Basal samples from 244 to 200 cm bsf contain an open-platform assemblage with elements suggesting somewhat restricted circulation. Samples from 170 to 80 cm bsf contain a marsh assemblage dominated by *Ammonia* spp. The shallow samples from 40 cm bsf to the surface contain a typical open-platform assemblage. The shallowing and deepening succession of assemblages suggests migration of a mud shoal across the core site, although other interpretations are possible. Results from physical data sets must be explored to test this hypothesis.

The results show large vertical changes in paleoenvironments and lithologic facies, which are controlled by lateral dispersal of sediments by tidal and wind-driven currents in addition to rising sea level. The degree to which these large environmental changes produce changes in physical and acoustic properties will be explored by subsequent presentations at this workshop. The sedimentation models, to the degree that they are correct, may help predict the distribution of acoustically important materials, such as large shells.

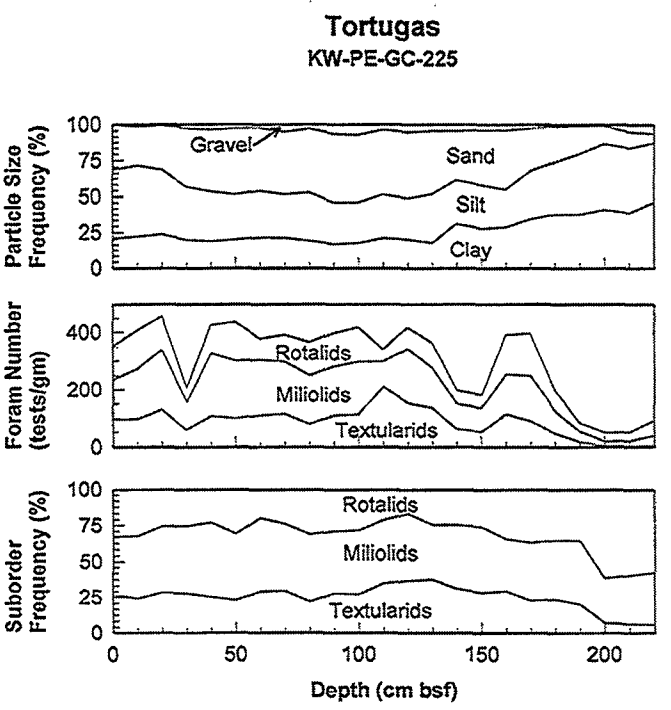
Tortugas
KW-PE-GC-225
Particle Size Frequency (%)
100
75
50
25
0
Gravel
Sand
Silt
Clay
Foram Number (tests/gm)
400
200
0
Rotalids
Miliolids
Textularids
Suborder Frequency (%)
100
75
50
25
0
Rotalids
Miliolids
Textularids
0
50
100
150
200
Depth (cm bsf)

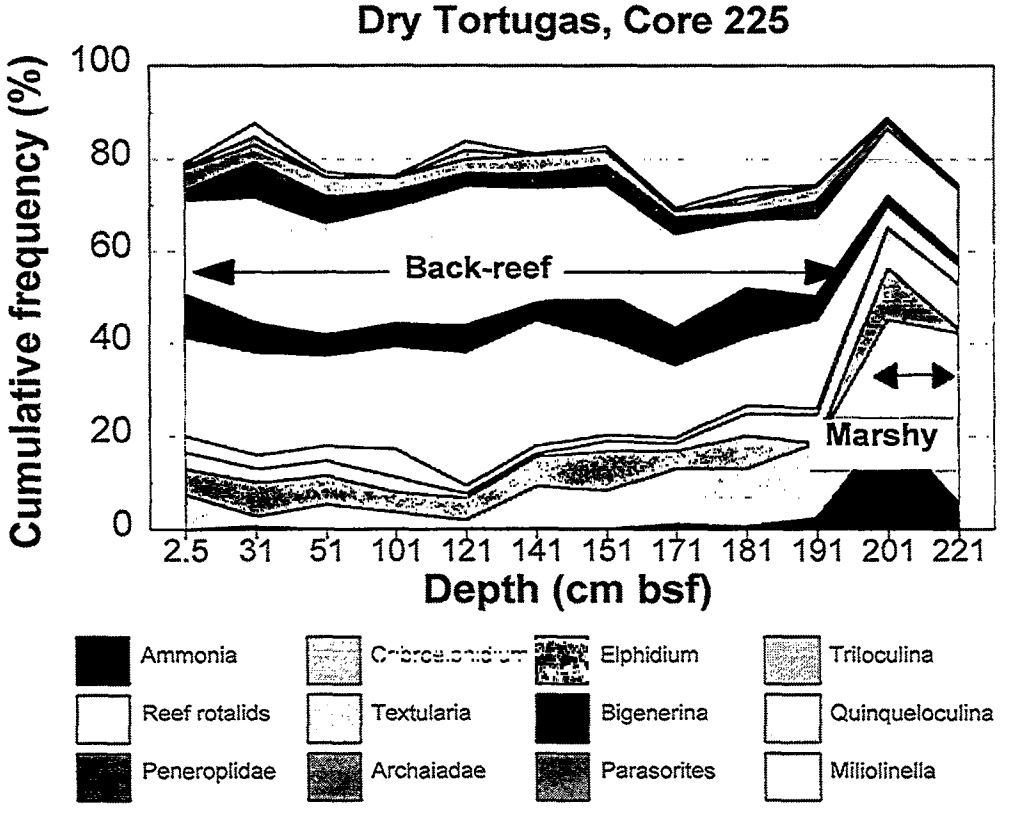
Dry Tortugas, Core 225
Cumulative frequency (%)
100
80
60
40
20
0
Back-reef
Marshy
2.5
31
51
101
121
141
151
171
181
191
201
221
Depth (cm bsf)
Ammonia
Reef rotalids
Peneroplidae
Cribroelphidium
Textularia
Archaiadae
Elphidium
Bigenerina
Parasorites
Triloculina
Quinqueloculina
Miliolinella

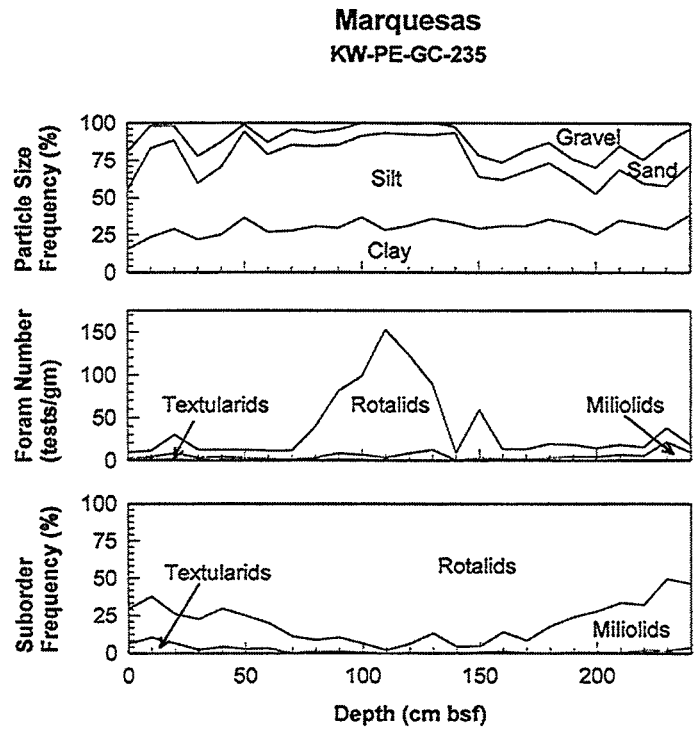
Marquesas
KW-PE-GC-235
Particle Size Frequency (%)
100
75
50
25
0
Gravel
Sand
Silt
Clay
Foram Number (tests/gm)
150
100
50
0
Textularids
Rotalids
Miliolids
Suborder Frequency (%)
100
75
50
25
0
Textularids
Rotalids
Miliolids
0
50
100
150
200
Depth (cm bsf)

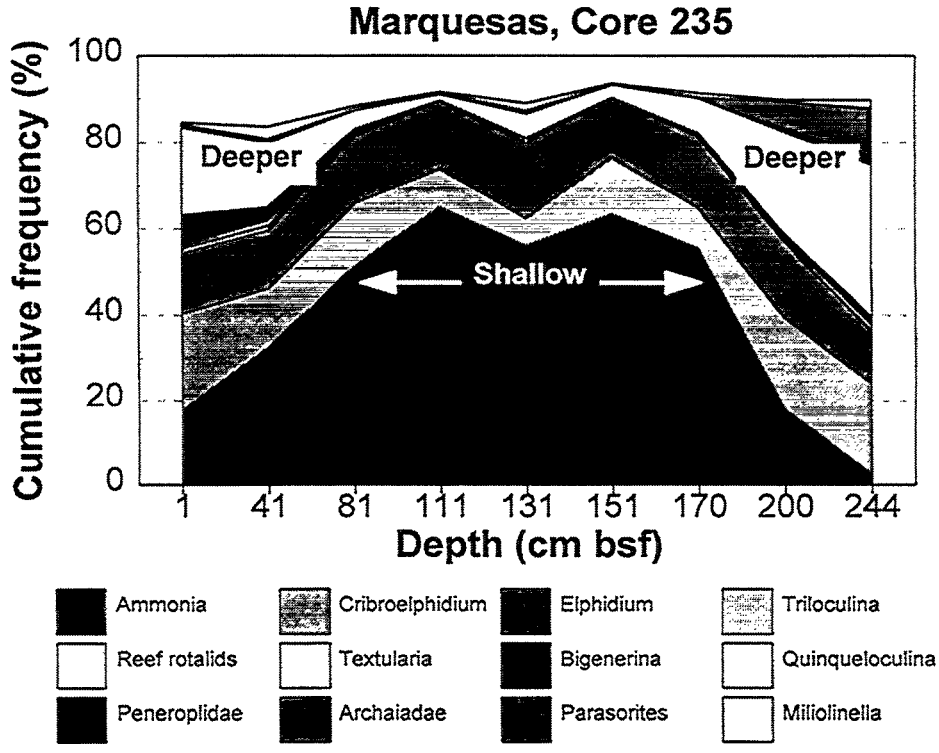
Marquesas, Core 235
Cumulative frequency (%)
100
80
60
40
20
0
Deeper
Deeper
Shallow
1
41
81
111
131
151
170
200
244
Depth (cm bsf)
Ammonia
Cribroelphidium
Elphidium
Triloculina
Reef rotalids
Textularia
Bigenerina
Quinqueloculina
Peneroplidae
Archaiadae
Parasorites
Miliolinella

3.0 Sediment Classification Systems

3.1 Southeast Channel, Dry Tortugas Geologic Setting and Comparison of Acoustically-predicted sediment properties with Laboratory-Measured Core Data (D. Walter, D. Lavoie, D.N. Lambert, D.C. Young and K. Stephens)

Southeast Channel,
Dry Tortugas

GEOLOGIC SETTING
&
Comparison of acoustically-predicted sediment properties
with laboratory-measured core data

Donald J. Walter, Dawn Lavoie, Douglas N. Lambert, David C. Young
and Kevin Stephens
Naval Research Laboratory/Code 7431
Stennis Space Center, MS 39571

ABSTRACT

High resolution 4-, 12-, and 15-kHz subbottom profiles have been collected in the Coastal Benthic Boundary Layer (CBBL) study site located in Southeast Channel near Garden Key in Dry Tortugas, FL (Figure 1) using the NRL Acoustic Seafloor Classification System (ASCS). Fifteen kilohertz data was collected by the German research vessel FWG *Planet* along north -- south trending tracklines with 130 m line spacing. Additional ASCS data was collected from the R/V *Seward Johnson* at 4- and 12-kHz in a grid with 1 km line spacings in both north - south and east - west directions over the same area. The 4- and 12-kHz surveys utilized the *Johnson's* hull mounted transducer arrays in conjunction with the standard ASCS electronics package. The 15-kHz survey on the *Planet* utilized an EDO model 6991 narrow beam transducer installed at hull depth in the ship's moon pool.

The ASCS uses 16 bit data acquisition and display in conjunction with narrow beam transducers to achieve excellent resolution with a dynamic range in excess of

92 dB. Raw bottom and subbottom signal intensities are displayed in real-time on a color monitor where 16 colors represent return signal intensity in programmable steps of dB per color.

Trackline maps generated in real-time during the acoustic surveys (Figures 2 and 3), provide a 2-D perspective of the surficial sediment type by displaying color coded sediment impedance predictions along track. Delineation of seafloor facies boundaries is possible with this technique. Figures 4 and 5 provide an expanded perspective of these tracks in the densely sampled CBBL study area at the NW corner of the surveyed area. Co-registered with the tracks on these maps are the locations of ground truth sampling points selected for the acoustic/core data comparisons.

The dominant sedimentary structure in the area is the Key Largo Limestone. This feature is graphically evident in the 4-kHz color acoustic records (Figure 6) illustrated as linear cross sections obtained along longitudinal lines. Holocene sediments are presently being deposited or ponded in the topographic lows of this limestone formation near the reefs to the south. These live coral reefs occur on topographic highs in a diagonal band across the southern portion of the study area. Sediment types within the surveyed area range from carbonate silts, to dense sands, to limestone rock and coral reefs. However, as depicted in Figures 2 and 3, the NW corner and CBBL study area consists mostly of a silty sand mixture with a layer of shell. This shell layer is evident about 1 m below the seafloor in the acoustic records provided in Figures 8 - 11. Also of note in the deeper sediments of the study area are the indication of zones which have little or no acoustic return (Figures 7-11). These zones occur at the same depths below seafloor where the sediment transitions into a finer, clay size fraction as well as changing in color from the tan/light carbonate color to a darker/gray clay-like color. Several karstic 'sink hole' features are evident on the limestone bedrock that indicate the probable presence of a paleo-stream-channel flows during a lower sea level stand. This

channel has a similar strike to that of the present reef structure, i. e. NE to SW. Exposed bedrock occurs at the NE corner of the surveyed area and transitions into the reef structures to the south. All geomorphic features in this area have a NE to SW trend indicating a possible dominant current pattern which flows around the platform to the north and west. This current regime may, in fact result in a retention of sediment within this region.

Sediment impedance and wet bulk density at selected sample sites was compared to acoustic predictions along both 12- and 15-kHz tracks which passed near the sites. Impedance data from core KW-PE-GC-167 was used to calibrate the acoustic data to one ground truth location (Table 1). The acoustic data set at each frequency was then re-processed using identical settings as determined during the calibration. Comparison of the impedance and bulk density data is provided in the form of a bargraph in Figure 13. As shown, the 15-kHz impedance values compare quite well with those of the cores (calculated from the product of sediment wet bulk density and measured sound speeds). The 12-kHz impedance predictions generated from the *Johnson* data, however, are higher. Fifteen kHz density values are lower than those from the core. A comparison of the core impedance vs. density values to other workers regressions in Figure 14 (Hamilton 1970 and Lambert 1988) indicates that the empirical relationships may be different for carbonate sediments than those of siliciclastics. The ASCS uses the Hamilton curve (the lower one) to develop the sediment property predictions from acoustic impedance. The (+) signs represent the core values from Southeast Channel used for this comparison. The second curve on this figure was constructed using core data obtained in Mississippi Sound (dots •), an area with a variety of sediment types (medium to coarse sands, fine and coarse silts, and combinations of these) which are nearly 100% of terrigenous origin and contain little or no carbonate fraction.

The main objectives for this presentation were to provide:

a) Views and perspectives of geologic setting
b) Identify geologic facies
c) Display sample sites relative to facies types
d) Identify core sites selected for comparing core data
e) Present initial data comparisons

OBSERVATIONS

The study site in Southeast Channel off Garden Key in the Dry Tortugas, is approximately 70 miles west of Key West Florida. The area lies at the outer, southwest boundary of the west Florida carbonate platform. It is bordered to the north by the Gulf of Mexico and to the south by the Straits of Florida. The site is well protected from seasonal storm activity, which generally approaches from the north and northwest, by the shallow carbonate platform that underlies the aerially exposed Tortugas Keys to the west and north. The protection afforded by this platform results in thick accumulations (approximately 2 to 5 m) of sediments in assorted combinations of silt, sand, and shell in several depositional zones of the study site.

Sediments in the region consist almost entirely of carbonate materials with $<10\%$ terrigenous content (Briggs et. al. 1996 and Stephens et. al. 1996). Portions of Southeast Channel are covered with accumulations of sediments which have either been eroded off the platform to the north and west and the reefs to the south, or were created nearby by the colonial calcareous benthic green-algae *Halimeda sp.*. Sediment types include combinations of carbonate silts, sands, and shell occurring in varying proportions within the sediment column. Exposures of limestone bedrock and living coral reef communities are apparent in several sections of the study area. The reefs occur on topographic highs formed by the rising bedrock in a NE to SW diagonal band across the southern portion of the study area. The dominant

geomorphic feature in the area is the limestone bedrock, identified as the Pleistocene surface in the 4-kHz color acoustic record shown in Figure 8. This structure underlies the entire CBBL study area, rising to an outcrop on the seafloor in the northeast as well as the southern sections of the study area. It lies either buried below the sediment cover, exposed where currents have kept sediments from accumulating, or forms the basement below the coral reef structures. The formation is Pleistocene in age as identified by Shinn, et.al. 1977, and appears to be of coralline origin (Shinn 1989). It extends over the entire southwest shelf portion of the west Florida carbonate platform and underlies a major portion of the Holocene shelf sediment sequence to the north and east.

Topographic lows in the bedrock further to the south, provide additional depocenters for sedimentary materials from the Tortugas platform. These "sediment ponds" are situated on the north and south flanks of the topographically high (2 - 5 meters relief) live coralgal reef structures. Up to 5 meters of Holocene sediments have been deposited in these bedrock lows. Thick sediment sequences are also prevalent at the northwest corner of the study area bordering the carbonate platform which surrounds Garden and Bush Keys. These sediments are presently being deposited along the base of the eastern escarpment of this platform, creating a sloping sedimentary sequence of mixed carbonate silt and sand, overlying a shell layer at about 1m below the sediment/water interface. Deeper sediments in the "sediment ponds", as well as other thick (> 3m) sediment sequences in the northwest corner of the study area, display a distinctly low acoustic signature and can be defined as "Acoustic Transparent Zones" (ATZ's), being ostensibly devoid of acoustic return below the sequence of carbonate sediments above them. These ATZ's coincide with the occurrence of darkening sediment colors (graying) and finer grain sizes (clayey silt) at core sample depths below approximately 2m within the CBBL study area (Stephens 1996). These zones may preserve, heretofore, unexplored geochronological records to assist in reconstructing the geologic history of this area. Stratigraphic studies of the "acoustically transparent" sediments

overlying the bedrock depressions may provide information on whether, and perhaps when, the bedrock mainland was subaerially exposed during glaciation and subsequently buried by post-glacial sea-level rise. Vertical accretion of finer sediments (clays and silts), soil zones, and possibly vegetative materials (peat, pollen) may be preserved in these sediment repositories, providing sedimentary evidence of a mainland exposed bedrock environment prior to flooding (Stone 1993).

Additional evidence of paleo-subaerial exposure is indicated by observing several karst features in the buried limestone bedrock in Figure 6. These features are indicative of the occurrence of previous erosional processes in the buried bedrock formation suggesting subaerial exposure during a period of lowered sea level. Initial evidence of a paleo-channel is provided in the acoustic record in Figure 6 along 82° 51.5′ W. Longitude (the second transect) and just to the north (right) of the yellow event mark highlighting Latitude 24° 35.0′ N. This feature appears as a sharp V in the Pleistocene bedrock formation. Visual inspection of the acoustic imagery from successive tracks to the east indicates that this feature continues to the east. A case can be made for the previous existence of a linear NE to SW trending channel by connecting a straightedge between the western and eastern lines. The dip in the bedrock just north of 24° 36.5′ N along the 82° 49.0′ W. transect accentuates this observation. This paleo-channel also has a similar strike to that of the present reef structure, i.e. SW to NE.

CONCLUSIONS

- The surveyed area has a variety of seafloor provinces ranging from hard corals in the southern portion to soft carbonate sandy silts in the topographic lows
- The NW corner (CBBL study area) has ≈ 1-3m of silty sand (with an inclusive shell layer at about 1 m depth) over limestone bedrock
- As the sediment thins over bedrock to the east, there is a transition to a coarser silty sand/shell mixture

- Carbonate bedrock underlies the surficial sediments in the entire area but rises to the seafloor and crops out in the NE corner of the study area
- These outcrop areas are devoid of significant sediment cover but may retain coarse sand and gravel size fractions
- This bedrock also outcrops at the southern portion and transitions into two separate carbonate reef structures which have a general SW to NE strike
- Topographic lows in the bedrock on the flanks of the reefs have resulted in a ponding of carbonate silts in thick sequences which exhibit a low acoustic response and can be defined as Acoustically Transparent Zones (ATZ's)
- The deepest sediments in thicker sequences in the northeast corner (CBBL study area) also have the ATZ's
- The ATZ's occur at approximately the same depth below seafloor as the graying/finer sediments in ground truth core samples
- Graphic evidence of a buried paleo channel in limestone bedrock is indicative of subaerial bedrock exposure during a time of lower sea-level stand
- The dominant morphologic seafloor characteristic, i. e. the SW to NE strike of all bottom features, provides evidence of present and paleo current flow in a NE to SW direction around the shallow platform
- Sediment transport out of this area is constrained by both the higher topography along the reefs to the south and the apparent presence of a dominant NE to SW current flow around the platform
- Acoustic impedance predictions match well with those calculated from core properties
- Acoustic predictions of wet bulk density, however, are somewhat low indicating a need to upgrade and modify previously defined empirical relationships between Impedance and Density with data from carbonate environments

LIST OF FIGURES

These averages are all posted over Stephens (1996) average wet bulk density vs. depth curve for all cores collected by the R/V *Pelican*

16. 2-D Impedance Contour Map with *Johnson* (12-kHz) tracklines and ground truth core locations posted.

Table 1. List of average (0-40 cm) core impedance and wet bulk density values with ASCS

REFERENCES

Hamilton EL (1980) Geoacoustic Modeling of the Sea Floor. Journal of the Acoustical Society of America 68/5, pp 1313-1340.

Lambert DN (1988) An Evaluation of the Honeywell ELAC Computerized Sediment Classification System. NORDA Report 169, Naval Research Laboratory, Stennis Space Center, MS.

Richardson MD Briggs KB 1993 On the Use of Acoustic Impedance Values to Determine Sediment Properties. Proceedings of the Institute of Acoustics, International Conference on the Acoustic Classification & Mapping of the Seabed, University of Bath, England, pp 15-24.

Shinn EA Hudson JH Halley RB Lidz BH (1977) Topographic control and accumulation rate of some Holocene coral reefs, South Florida and Dry Tortugas. In: Proceedings, Third International Coral Reef Symposium, Volume 2, Miami, FL, pp 1-7.

Shinn EA Lidz BH Halley RB Hudson JH Kindinger JL (1989) Reefs of Florida and the Dry Tortugas: Miami to Key west Florida. Field Trip Guidebook T176. American Geophysical Union, Washington , D. C.

Stephens KP Lavoie DL Fleischer P (1996) Scale Dependent Physical and Geoacoustic Property Variability of Recent, Shallow-Water Carbonate Sediments from the Dry Tortugas Keys, Florida, in press GeoMarine Letters.

Stone PA (1993) Dry Tortugas and South Florida Geological Development and Environmental Succession in the Human era. In: Murphy LE (ed) Dry Tortugas National Park, Submerged Cultural Resources Assessment, National Park Service, Santa Fe, NM, pp 5-26.

Walter DJ Lambert DN Young DC (1995) A 3-D acoustic View of the Seafloor Near Garden Key, Dry Tortugas FL. 1st SEPM Congress on Sedimentary Geology "Linked Earth Systems", St. Petersburg Beach FL.

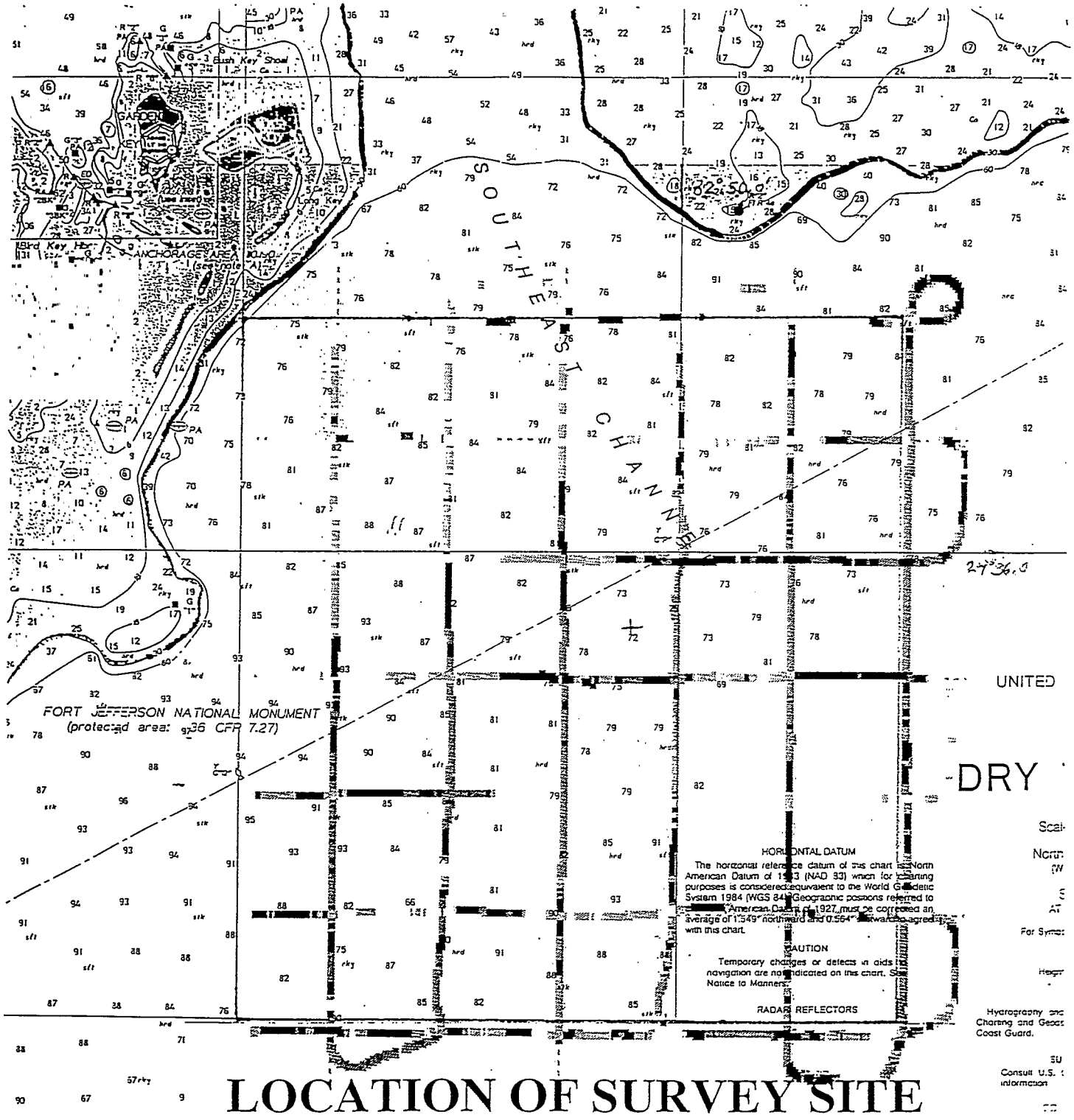

Figure 1. Superimposed 12-kHz tracklines covering the entire CBBL Southeast Channel study area (1:30,000 scale NOAA Chart # 11438). Survey conducted aboard R/V *Seward Johnson*, February 1995.
** Note platform shoals beyond NW and NE corners of survey grid (depth soundings are in feet).

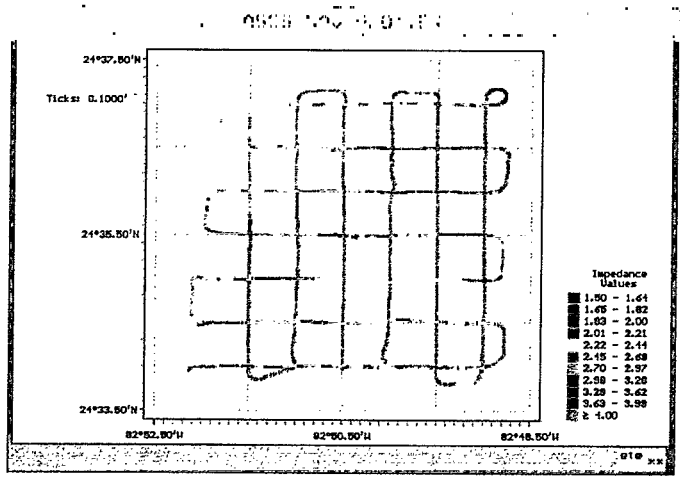

Figure 2. Color-coded trackplot of surficial (upper 0.4m) sediment acoustic impedance collected using NRL/ASCS with *R/V Johnson* 12-kHz transducer. Trackline spacing is 1 km.

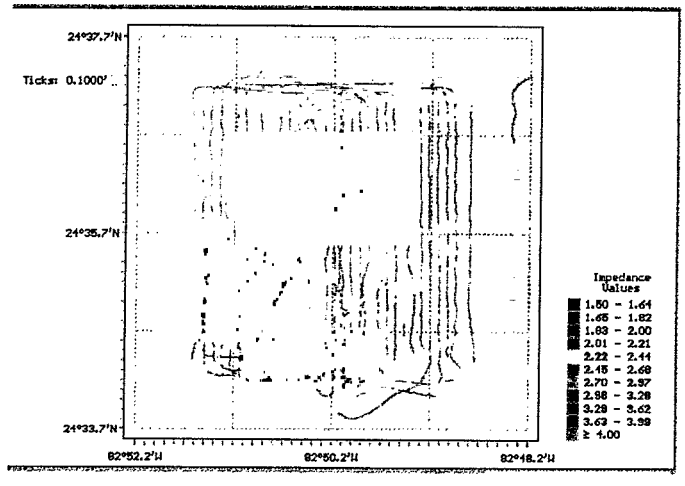

Figure 3. Color-coded trackplot of surficial (upper 0.4m) sediment acoustic impedance collected using NRL/ASCS @ 15-kHz aboard *WFS Planet*. Trackline spacing is approximately 150 m.

* Color Key: Interpretation of colorized tracklines using impedance/color scale on each figure above;

Yellow	Silt/sand mixture (probably includes shell)
Pink	Muddy or silty sand
Red	Carbonate Sand
Gray	Limestone rock (no distinction made between limestone rock and coral reef)
Blues/greens	Lower return signal due to effect of high slope angles near topographic features while using narrow beam transducer

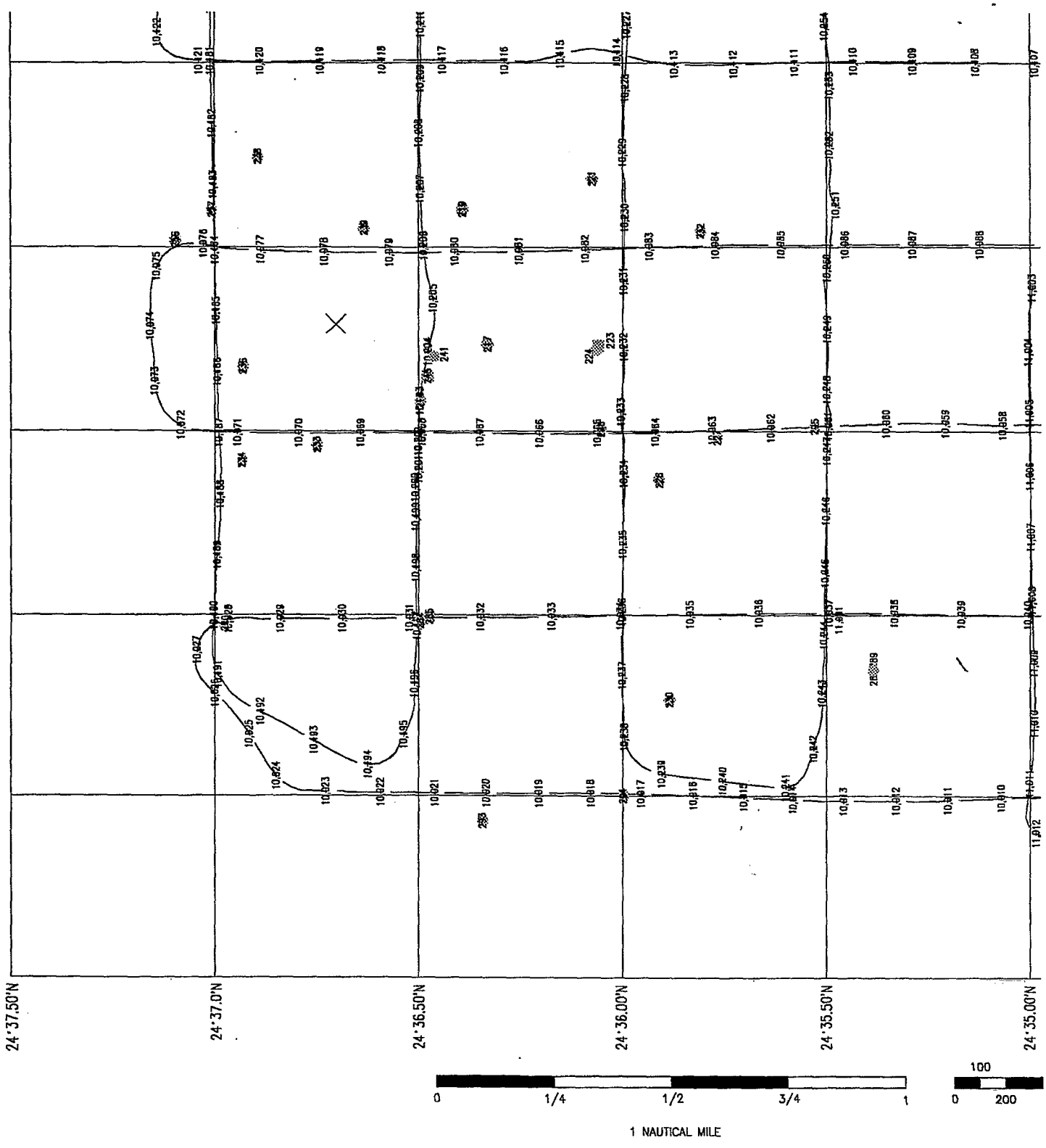

Figure 4. 12-kHz tracklines covering the NW corner of the CBBL Southeast Channel study area. Survey conducted aboard R/V *Seward Johnson*, February 1995. Labels along tracks designate ASCS data recording archival information. Dots and squares (with numbers) designate ground truth core sites sampled by *Seward Johnson*. The large X represents the location of the APL Tower site.

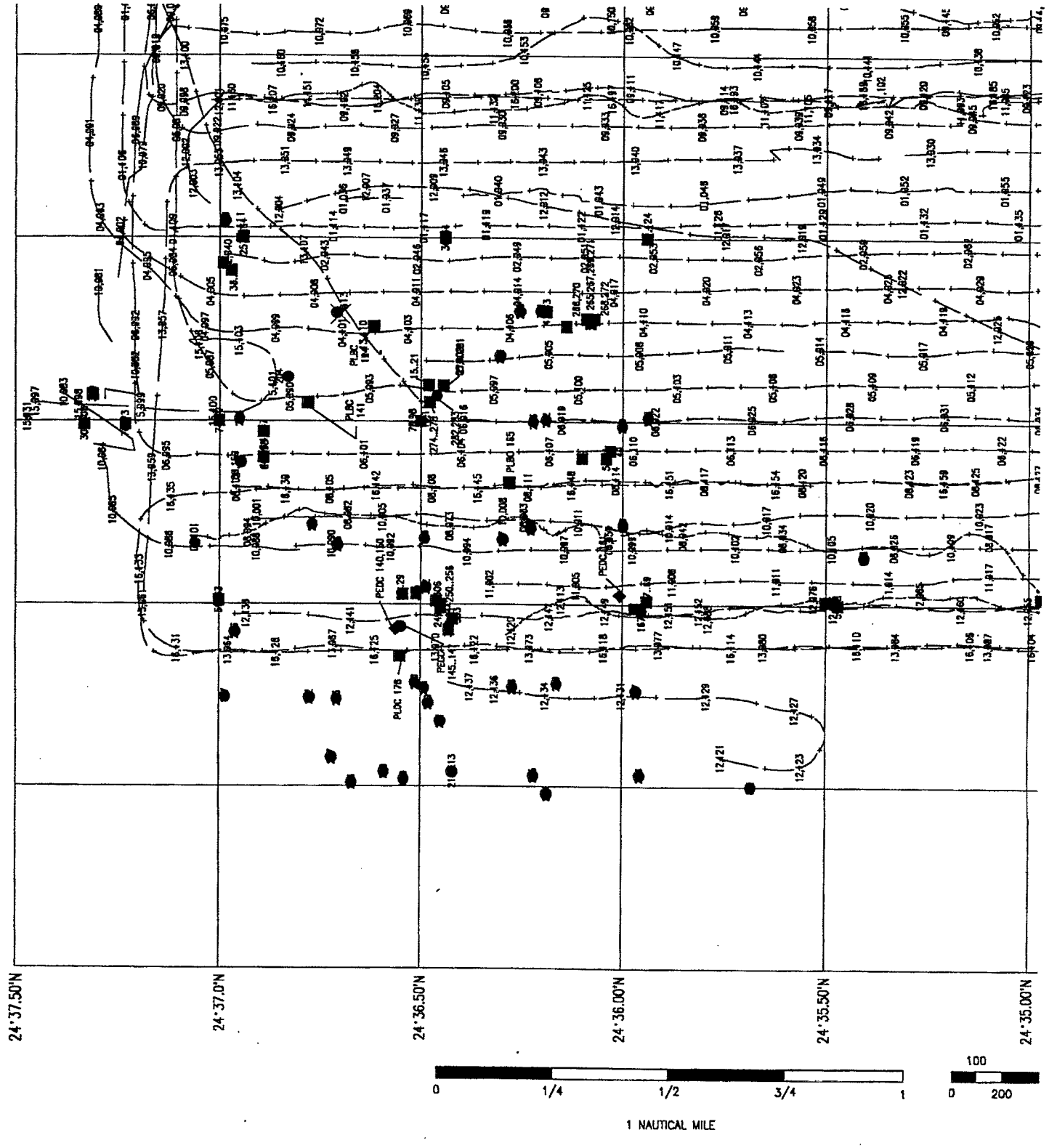

Figure 5. 15-kHz tracklines covering the NW corner of the CBBL Southeast Channel study area. Survey conducted aboard FWG *Planet*, February 1995. Labels along tracks designate ASCS data recording archival information. Dots, squares and diamonds (with numbers) designate ground truth core sites (gravity, box and diver , respectively) sampled by R/V *Pelican*.

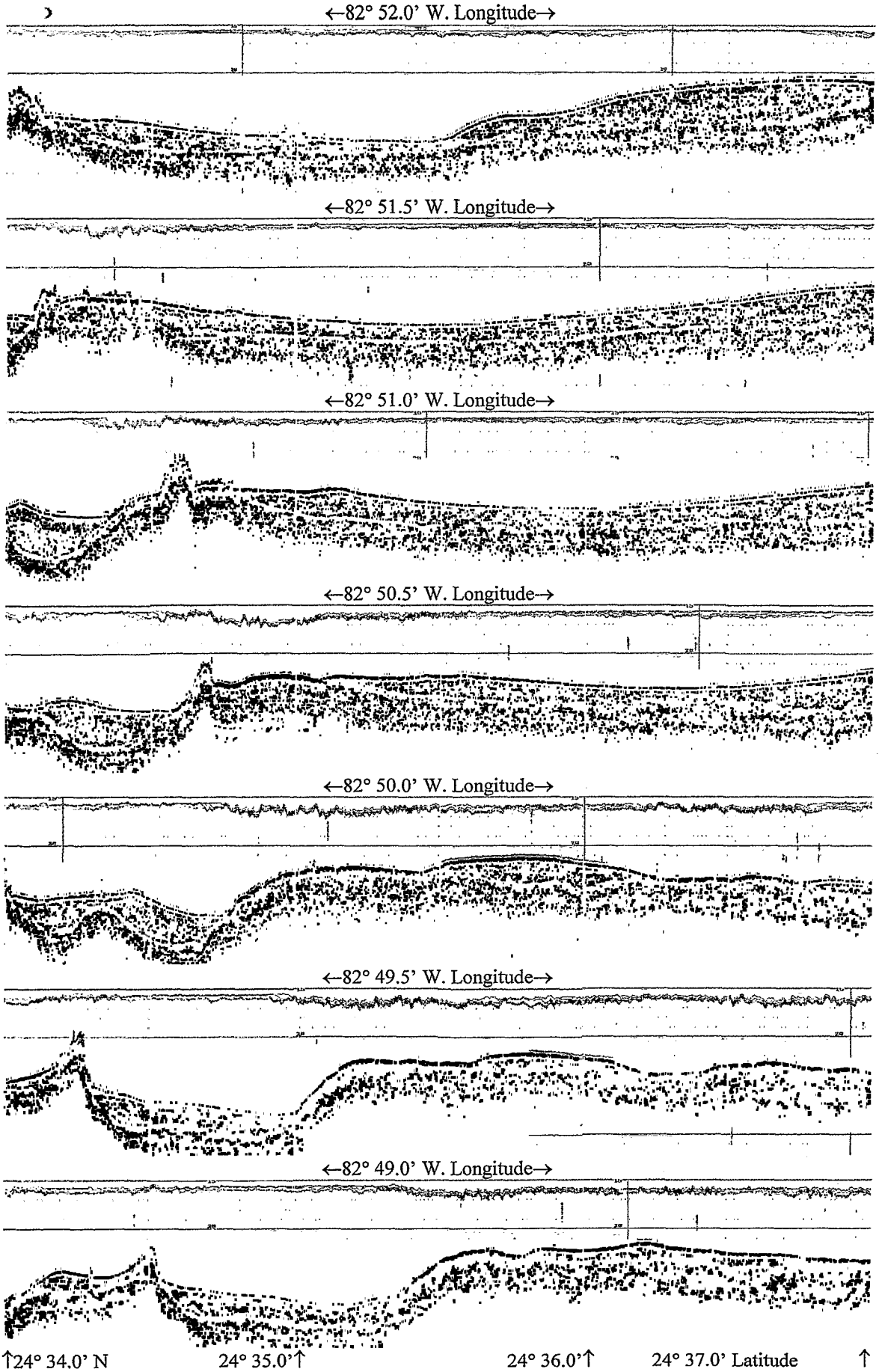

Figure 6. 4-kHz (south → north) acoustic imagery of CBBL Southeast Chanel survey grid. Top line = westermost track (82° 52.0 W). Sequential tracks @ 1km intervals to easternmost line = 82° 49.0 W.

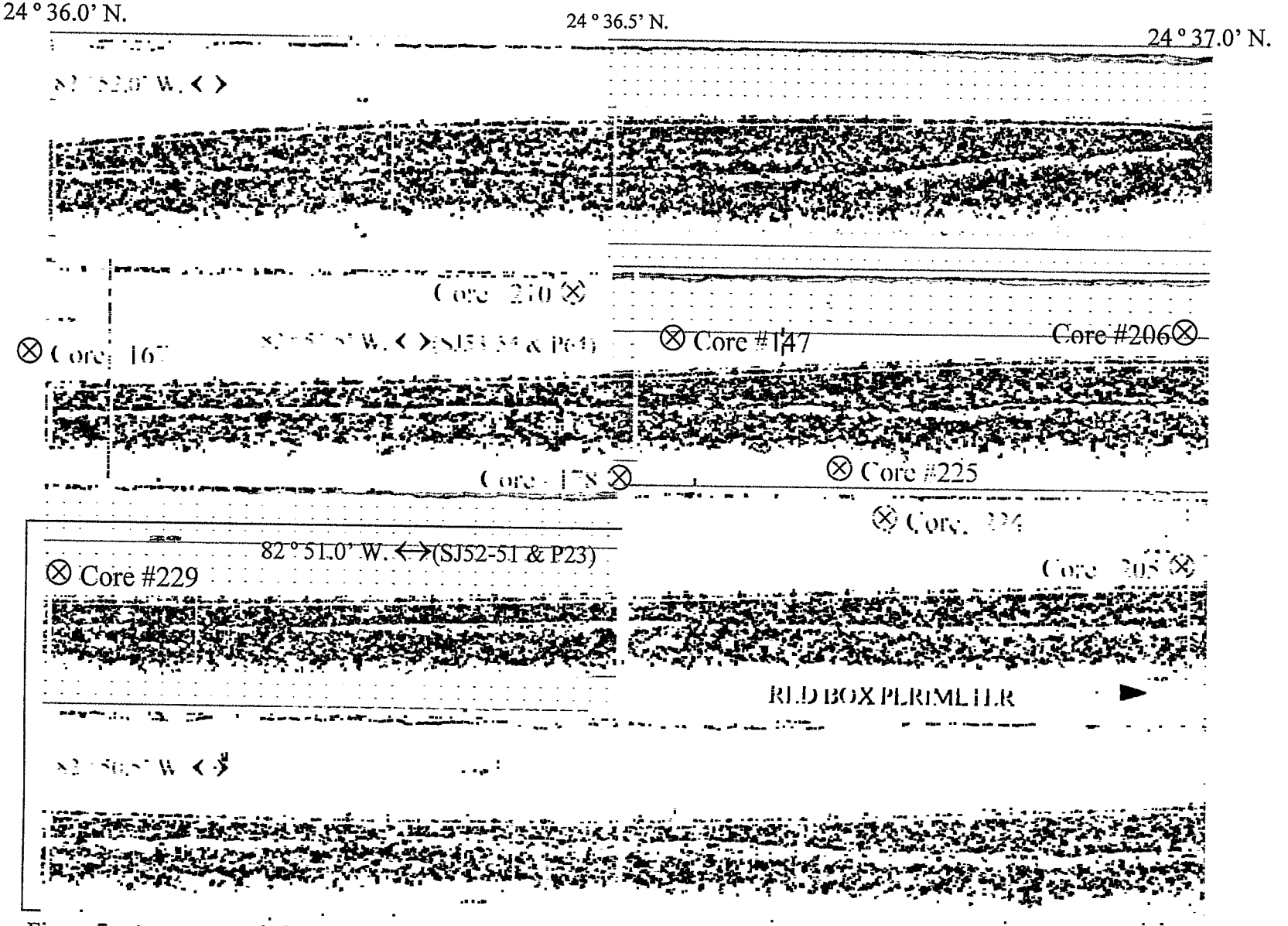

Figure 7. 4-kHz acoustic imagery through CBBL study area and "Red Box". Core locations approximate.

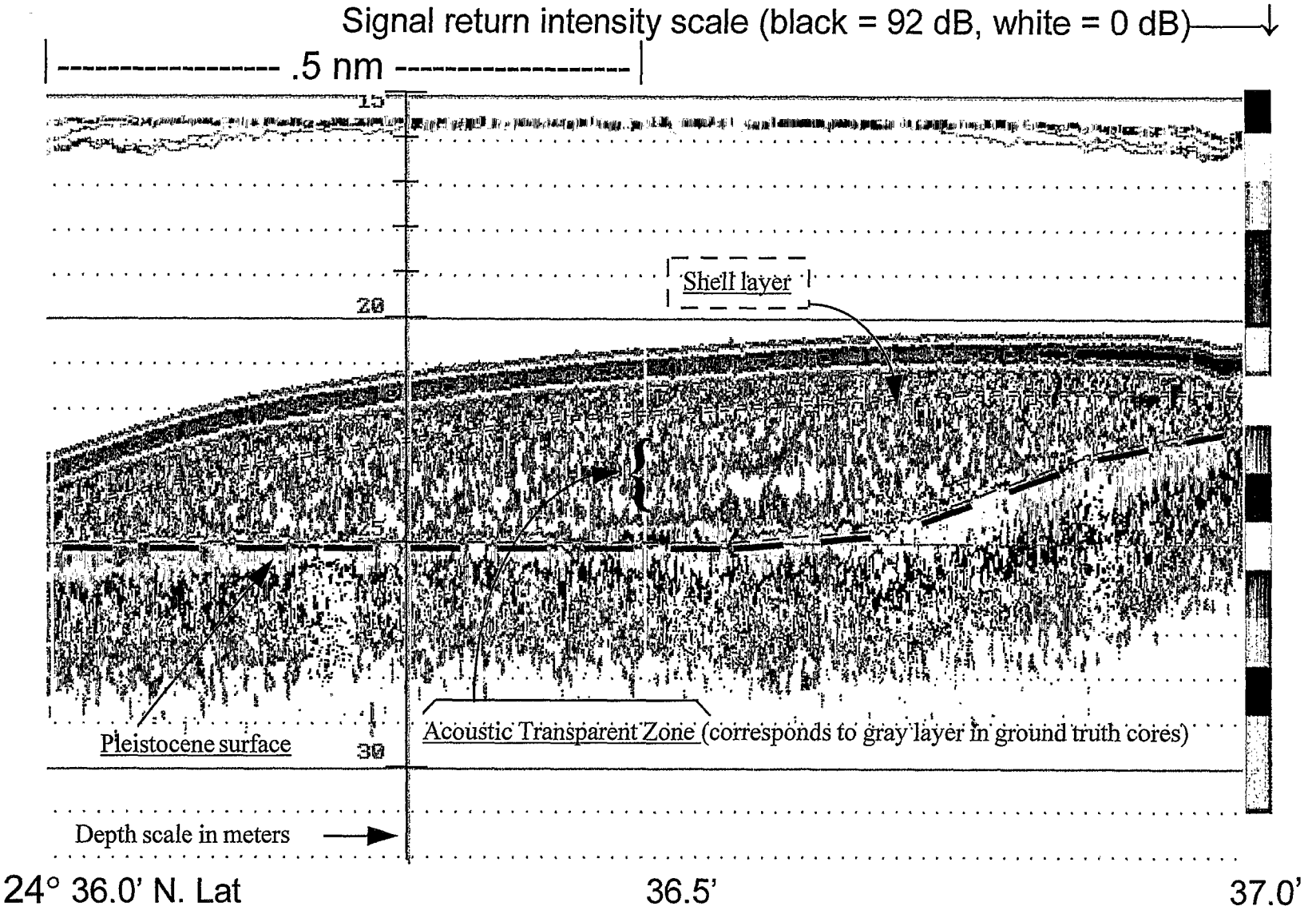

Figure 8. 4 kHz ASCS data collected along 82° 52.0' W. Longitude in the CBBL test area.

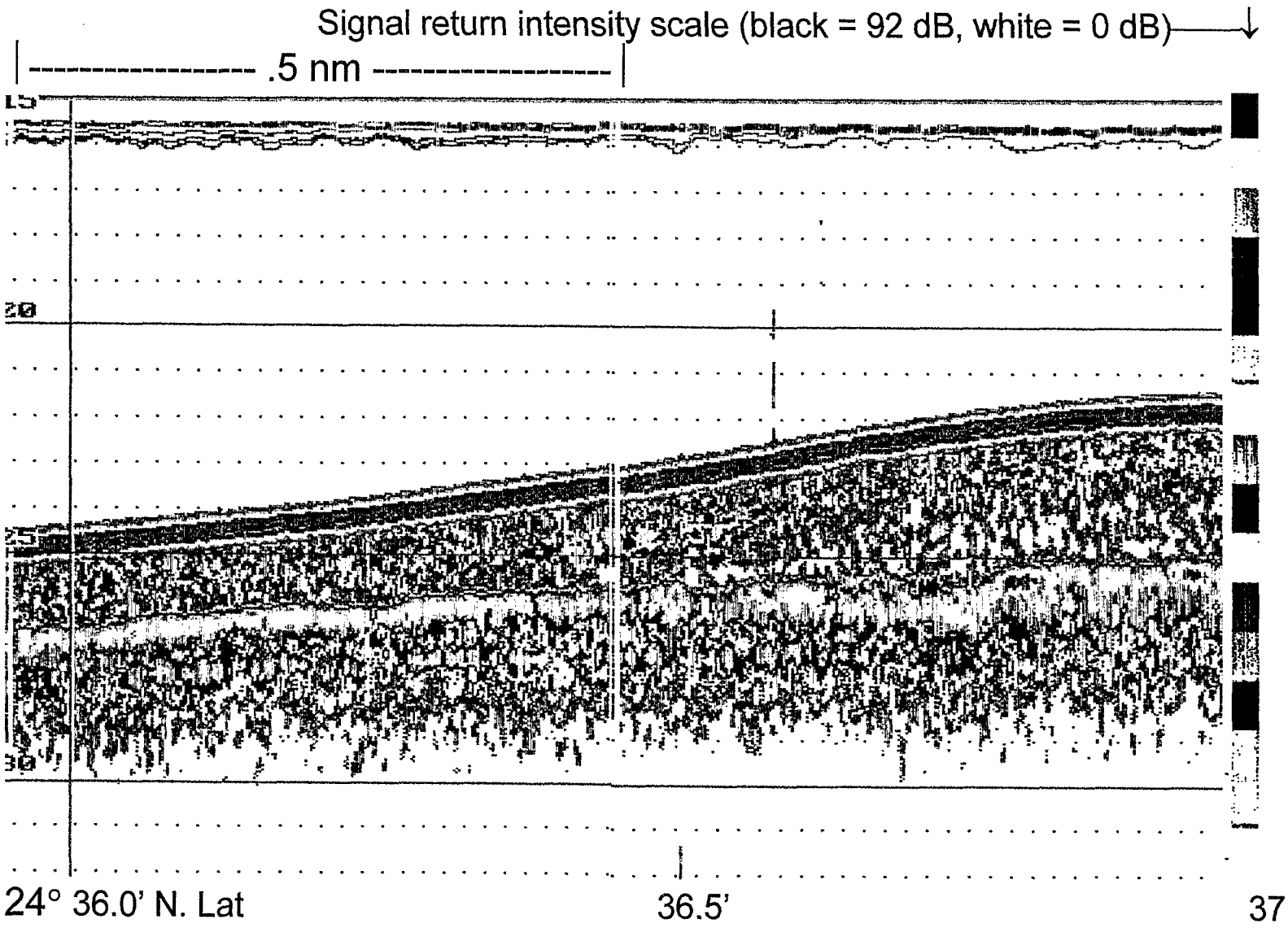

Figure 9. 4 kHz ASCS data collected along 82° 51.5' W. Longitude in the CBBL test area.

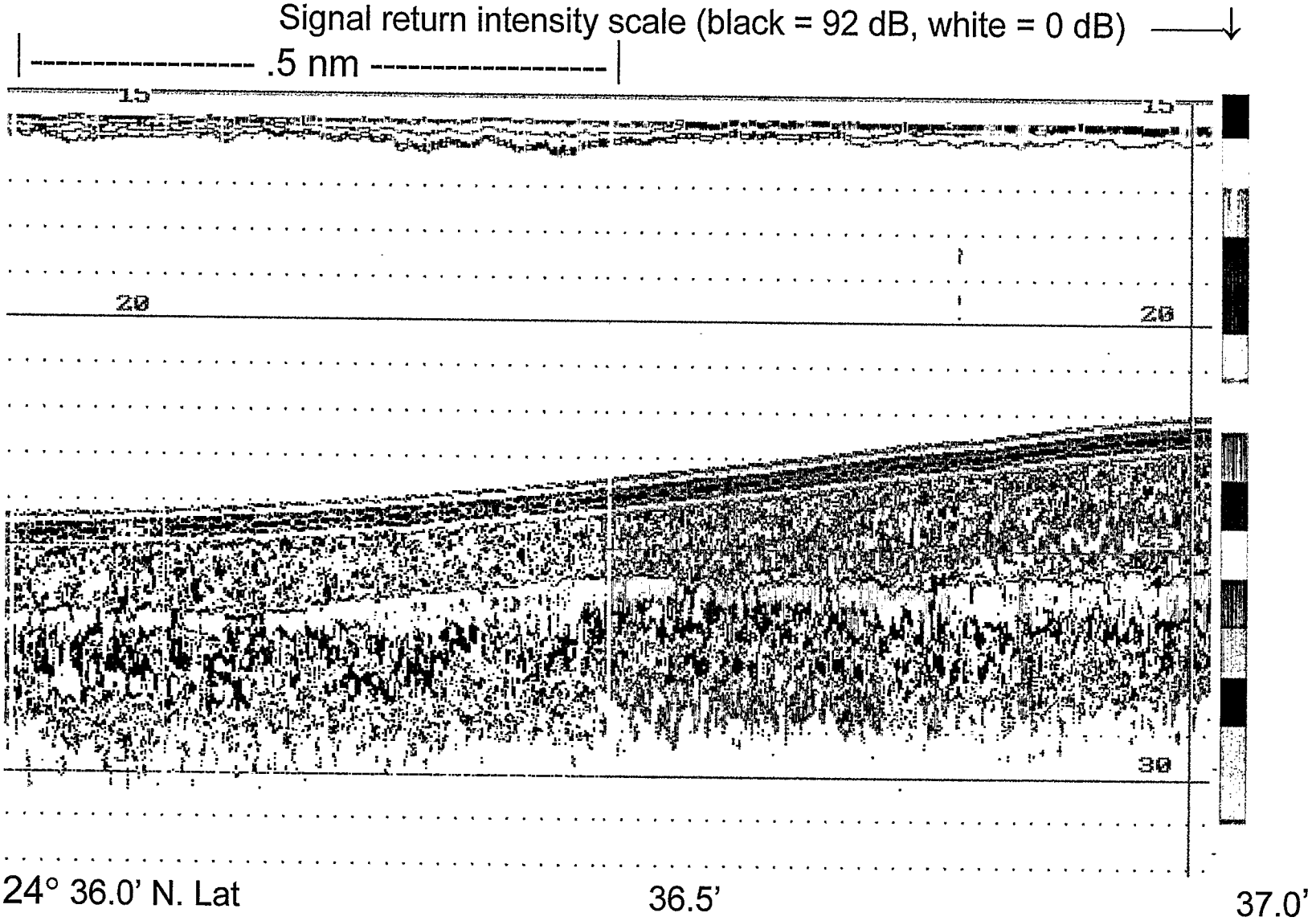

Figure 10. 4 kHz ASCS data collected along 82° 51.0' W. Longitude in the CBBL test area.

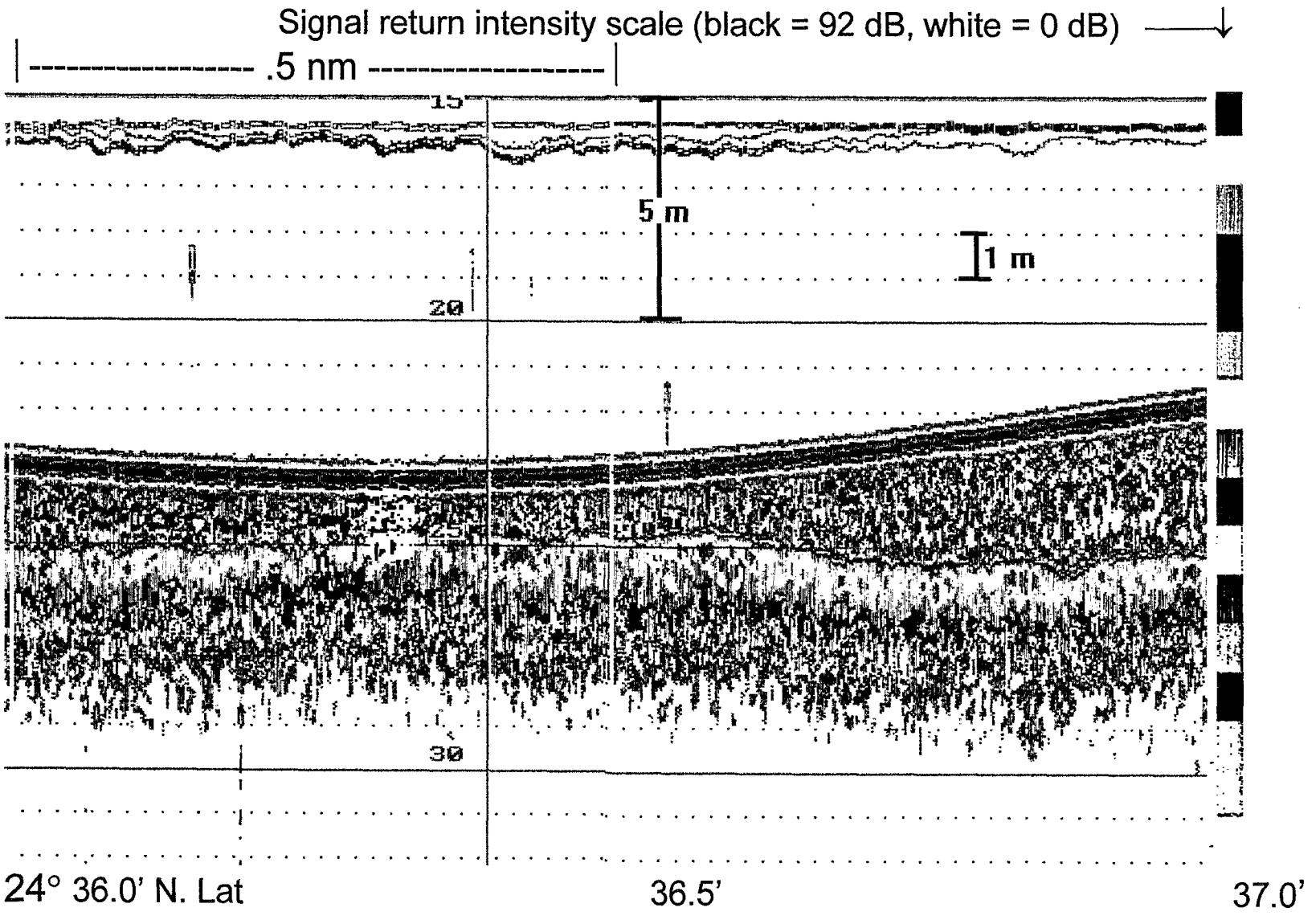

Figure 11. 4 kHz ASCS data collected along 82° 50.5' W. Longitude in the CBBL test area.

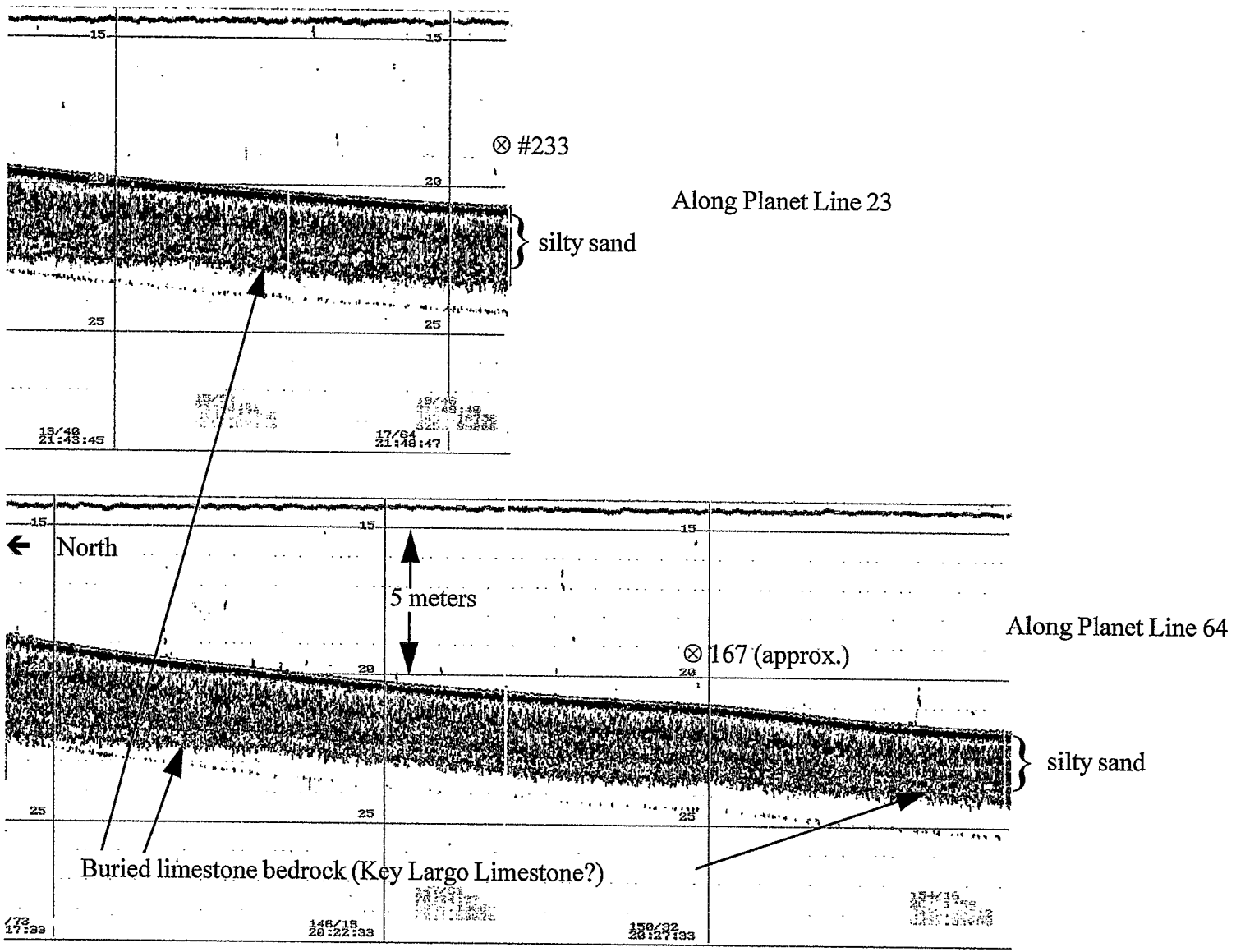

Figure 12. 15-kHz raw ASCS images taken near Pelican gravity core sites along tracklines identified.

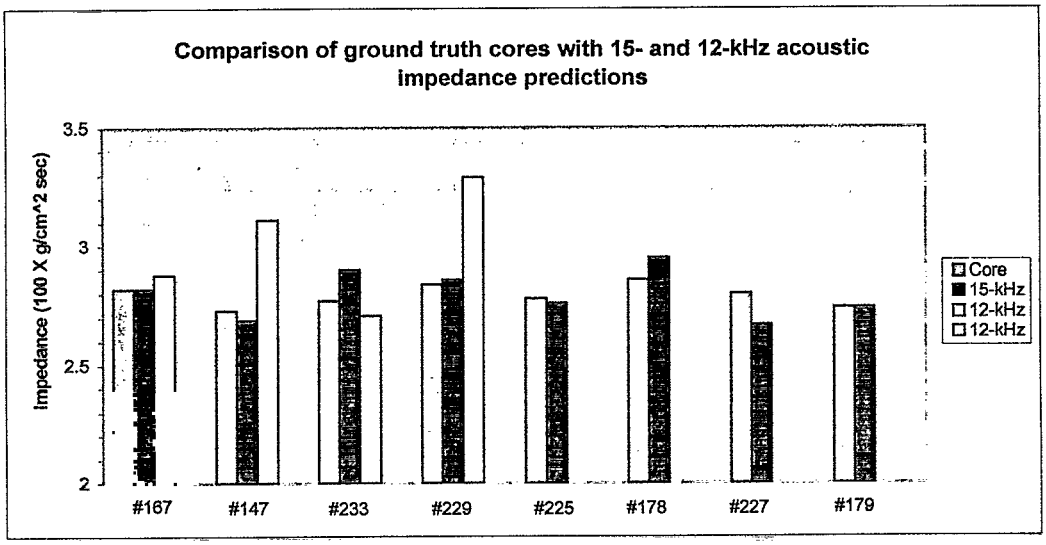

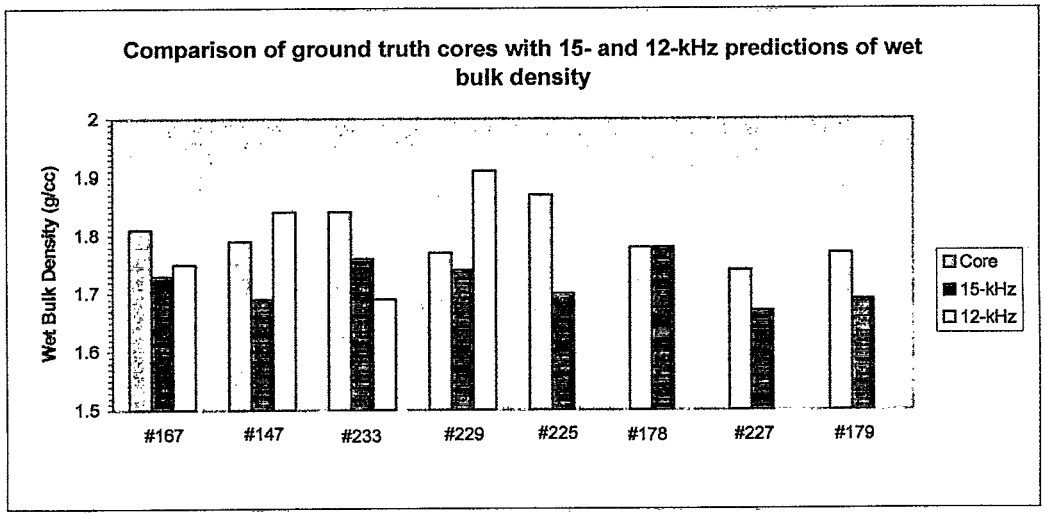

Figure 13. Bargraph comparing average (0-40 cm) core impedance and density measurements to ASCS predictions from the FWG *Planet* (15-kHz) and the R/V *Johnson* (12-kHz)

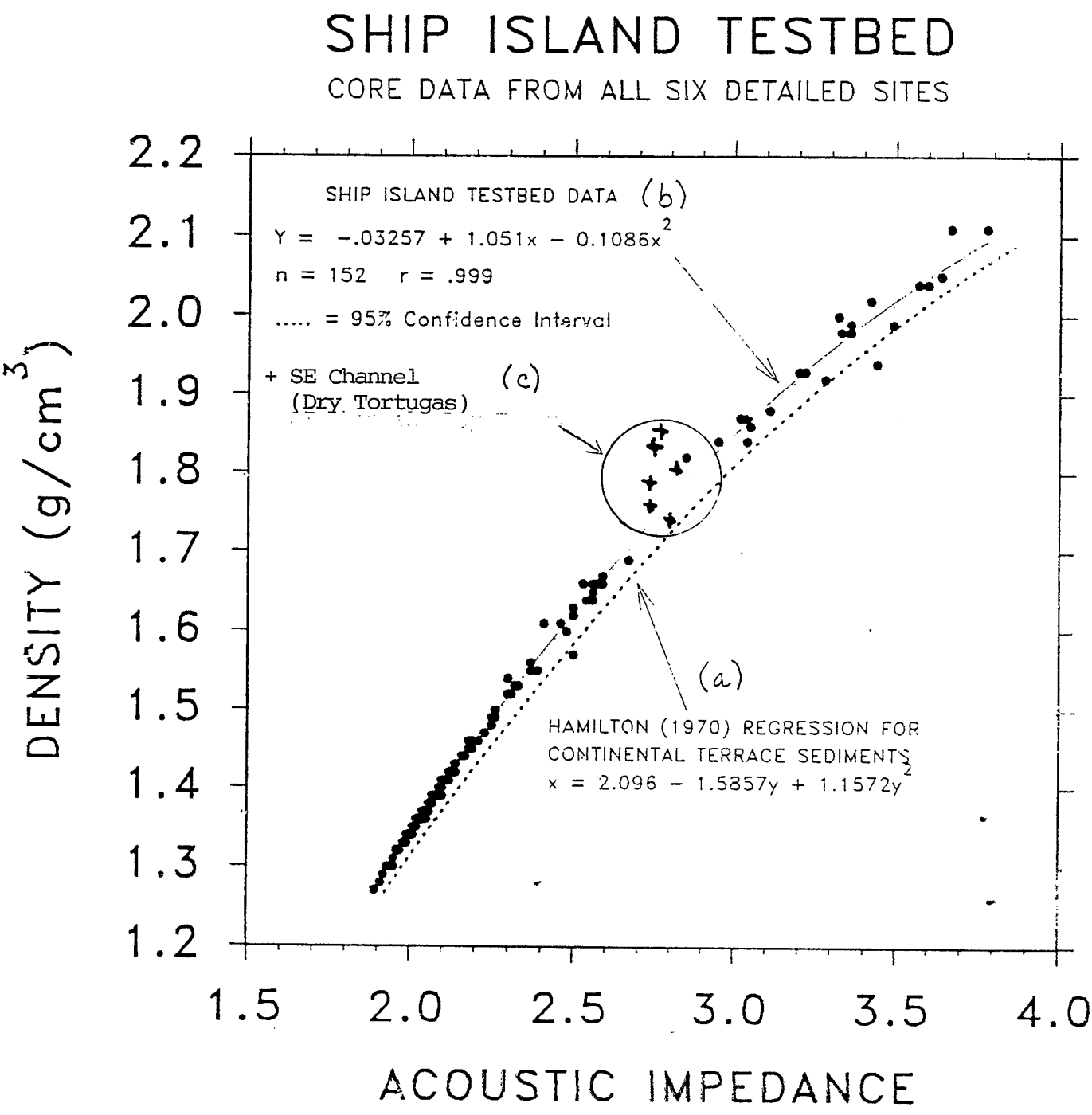

Figure 14. Acoustic impedance vs. Density regression curves from cores as reported by a) Hamilton (1970) - for Continental Terrace Sediments (------), b) Lambert, NRL internal documentation - for Mississippi Sound Sediments (●), and c) Walter (1997) new data from Southeast Channel/Dry Tortugas Sediments (+). Values for Southeast Channel (+) are averaged (0 - 40 cm depth below seafloor) from Stephens' (this workshop) core data at sites identified in Table 1.

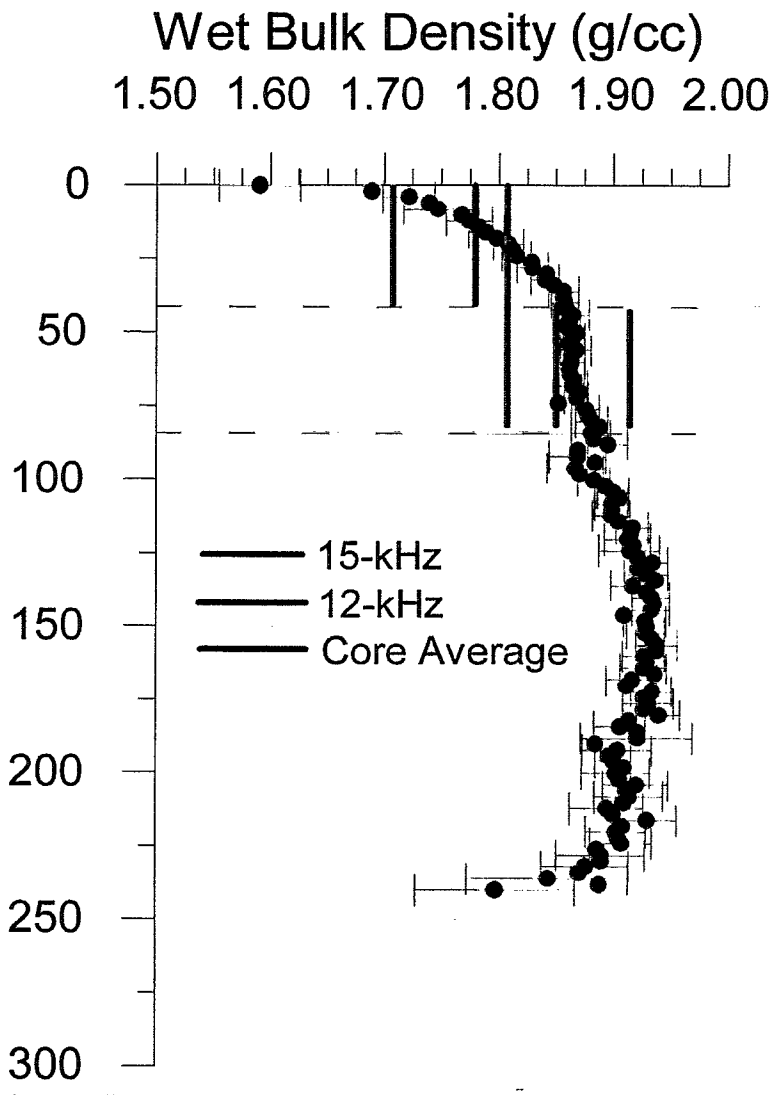

(Vertical scale = depth below seafloor in cm)

Figure 15. Graphic comparison of sediment wet bulk density profile to ASCS (12- and 15-kHz) density* predictions for 0-40 and 40-80 cm increments.

Average Wet bulk Density Profile of 14 Cores collected in northeast corner of Southeast Channel Study Site

Vertical lines are:

- average of 15-kHz predicted values near 7 core sites
- average of 12-kHz predicted values near 3 core sites
- average of core data from the same 7 sites only

* Acoustic predictions of density made after calibration of ASCS impedance prediction to average (0-40cm) impedance in core #167 (see highlighted area in Table 1).

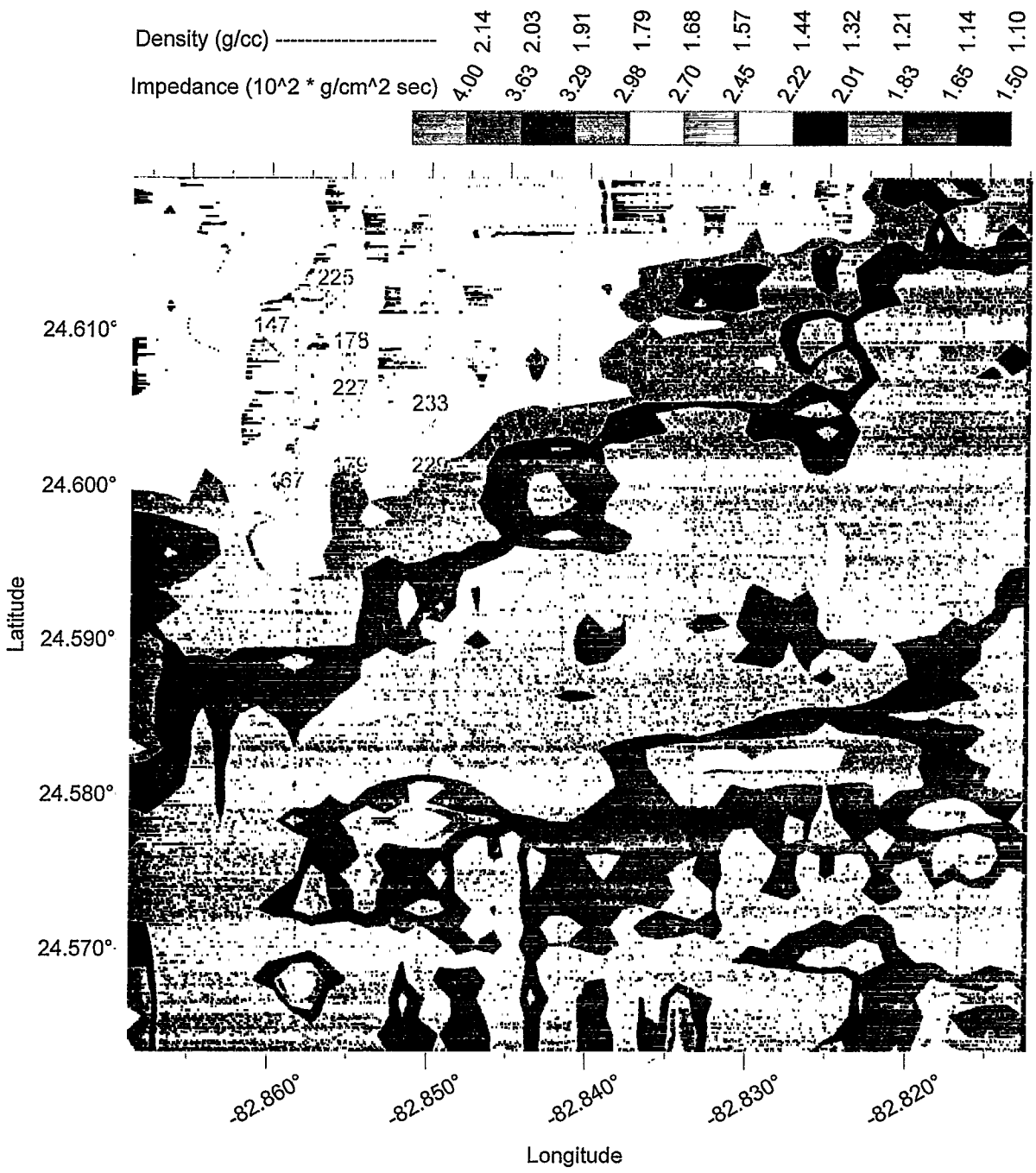

Figure 16. 12-kHz PREDICTED ACOUSTIC IMPEDANCE CONTOURS (0 - 40 cm)
SOUTHEAST CHANNEL, DRY TORTUGAS, FLORIDA
(Trackline spacing approx. 1km)

	IMPEDANCE					DENSITY				
	Core	15-kHz	Δ	12-kHz	Δ	Core	15-kHz	Δ	12-kHz	Δ
Core 167	(used for calibrating acoustic system)									
0-40 cm*	2.82	2.82	0.00	2.88	-0.06	1.81	1.73	0.08	1.75	0.06
40-80*	2.97	3.41	-0.44	2.88	0.09	1.9	1.95	-0.05	1.75	0.15
80-120*						1.97	1.95	0.02		
120-160*										
Core 147										
0-40 cm	2.73	2.69	0.04	3.11	-0.38	1.79	1.69	0.1	1.84	-0.05
40-80	2.85	3.11	-0.26	3.11	-0.26	1.88	1.87	0.01	1.84	0.04
80-120						1.94	1.87	0.07	1.31	0.63
120-160										
Core 233										
0-40 cm	2.77	2.9	-0.13	2.71	0.06	1.84	1.76	0.08	1.69	0.15
40-80	2.86	3.57	-0.71	2.71	0.15	1.9	2.01	-0.11	1.69	0.21
80-120				3.43		1.94	2.01	-0.07	1.96	-0.02
120-160				3.84		1.94			1.82	0.12
Core 229										
0-40 cm		2.86		3.29		1.77	1.74	0.03	1.91	-0.14
40-80	2.84	3.41	-0.57	3.29	-0.45	1.82	1.95	-0.13	1.91	-0.09
80-120						1.87	1.95	-0.08		
120-160										
Core 225										
0-40 cm	2.78	2.76	0.02			1.87	1.7	0.17		
40-80		3.2				1.91	1.88	0.03		
80-120						1.98	1.88	0.1		
120-160						2				
Core 178										
0-40 cm		2.95				1.78	1.78	0		
40-80	2.86	3.76	-0.90			1.82	2.06	-0.24		
80-120						1.87				
120-160						1.91				
Core 227										
0-40 cm	2.8	2.67	0.13			1.74	1.67	0.07		
40-80	2.85	3.03	-0.18			1.81	1.81	0		
80-120						1.89	1.81	0.08		
120-160						1.95				
Core 179										
0-40 cm	2.74	2.74	0.00			1.77	1.69	0.08		
40-80	2.83	3.18	-0.35			1.81	1.87	-0.06		
80-120							1.87			
120-160										

Table 1. Average of core impedance and density values (* averaged over listed depth window) and acoustically predicted values after calibration of ASCS impedance prediction to ground truth core impedance at site #167.

3.2 A comparison of chirp sonar and penetrometer measurements in the Dry Tortugas (S. Schock)

A comparison of chirp sonar and penetrometer measurements in the Dry Tortugas

Steven G. Schock
Dept of Ocean Engineering
Florida Atlantic University
Boca Raton, FL 33431

The capability of mapping the geotechnical properties of the seabed with a towed reflection profiler has many potential applications including 1) elevated causeway construction to support naval amphibious operations 2) pipeline route surveys 3) mooring and anchor capacity estimation and 4) coastal engineering. Currently, penetrometer, coring and boring surveys are used to obtain geotechnical properties; however, since these surveys provide only point measurements of seabed properties, the surveys have the potential of undersampling the seabed and missing sections of seabed containing geohazards. This paper describes an approach for using chirp sonar data and penetrometer data to map the shear strength of surficial sediments. The reflection coefficient of the sediment-water interface is compared with shear strength measurements estimated from penetrometer data to develop an empirical relationship between shear strength and the reflection coefficient. In the following it is shown that shear strength (psi) can be predicted from reflection coefficient data with an error of less than 50 % in a given depositional environment based on the Dry Tortugas data set..

During the 1995 CBBL and TTCP experiments in the Dry Tortugas, chirp sonar data and penetrometer data were collected by scientists from Florida Atlantic University (FAU) and Naval Facility Engineering Service Center, Port Hueneme, respectively. In February 1995, the chirp sonar was used to survey a 3 by 3 nm area off the Dry Tortugas. The survey grid consisted of E-W and N-S lines with a line spacing of 0.5 nm. The chirp sonar was calibrated at the pier in Key West before the survey. The

calibration was performed by inverting the tow vehicle and transmitting at the air-water interface which has a reflection coefficient of 0 dB. The system is calibrated by adjusting the sonar system constant until the measured reflection strength is identical to 0dB (+- 0.5 dB). During the survey, the chirp sonar transmitted 40 msec 1.5-7.5 kHz FM pulses at a rate of 8 pps. The reflection data was correlated with the transmission pulse , corrected for 1/r spreading losses and stored on 8mm tape with DGPS data. While surveying, the measured reflection coefficient was stored in memory with the DGPS data. After the survey a contour map of the reflection coefficient was used to determine the reflection coefficient at the penetrometer and piezocone measurement sites within the survey area; the penetrometer measurement sites usually fell between the survey lines, so the contour map was used to obtain the interpolated reflection coefficient at each site location.

NFESC scientists collected XDP (eXpendable Doppler Penetrometer) and piezocone measurements within the Dry Tortugas study area. The XDP was developed by the U.S Navy to measure the shear strength of cohesive soils. Recently, the work has been extended to estimation of the shear strength, undrained friction angle and relative density of non-cohesive sediments. (Ref 1) The XDP probe is shown in Figure 1. A transducer in the rear of the device transmits a CW acoustic signal. After the probe is dropped, the topside processor measures the frequency of the received signal. The velocity of the probe is calculated from the doppler shift of the received acoustic signal. The acceleration of the probe is the derivative of the acceleration. The bearing force F_{be} on the tip of the probe is calculated using Newton's second law

$$Mv\left(\frac{dv}{dz}\right) = W_b - F_{fr} - F_h - F_{be}$$

where M is mass of the penetrometer, v is velocity, z is depth, W_b is buoyant weight of penetrometer, F_{fr} is the side friction force and F_h is the hydrodynamic

drag force. The shear strength of the sediment is proportional to the bearing force on the tip of the probe and is calculated using empirical relationships given in Reference (1).

Piezocone measurements are performed by pushing a cone with an tip area of 0.775 in sq. into the seabed at a rate between 0.4 in/s and 0.8 in/s (ASTM D-3441). The instrument collects bearing force, sleeve friction, pore pressure changes, penetration and tilt.

A summary of effective shear strengths calculated from XDP and piezocone data, and reflection coefficient measurements made using normal incidence chirp data, are shown in Table 1.

TABLE 1 Comparison of shear strength and bottom loss

XDP Site #	Surficial Shear Strength (psi)	Bottom Loss (dB)
13	1.1	10.7
16	4.65	10.0
20	10.4	9.0
21	0.7	11.2
22	0.95	11.5
23	0.52	11
30	0.42	11.9
24	0.9	11
34	13.0	9.1
42	3.0	10.4
Piezocone site #		
3	0.9	11
4	13	9.2
5	8.0	9.1
7	2.5	10.4
8	0.5	11.4

As mentioned earlier, the reflection coefficient values in the table were interpolated from contour map of the reflection coefficient measurements made in the survey area using the chirp sonar. Note: BL=-RL. The shear strength values in Table 1 are the average shear strengths of the surficial sediments. The reported average shear strengths were calculated by averaging the shear strength data between 2 and 4

inches beneath the sediment-water interface. This interval was selected because the top 2 inches of penetrometer shear strength profile contains boundary effects. Since most of the energy of the processed reflection is at 4.5 kHz for a 1.5-7.5 kHz FM pulse, the amplitude of the processed reflection is mainly formed by the impedance contrast between the seawater and the sediments within a ¼ wavelength of the sediment-water interface which is about 4 inches at 4.5 kHz.

The bottom loss and shear strength data is plotted in Figure2. Note that the data falls on a line when plotted on a log-log scale. The figure shows that the worst case error in calculating shear strength from reflection coefficient data in this region is 50 %.

The results of the investigation show that it is possible to develop an accurate empirical relationship between the reflection coefficient and shear strength in a given depositional environment. One cannot expect to extend the BL-shear strength relationship developed in this study to other seabeds with different mineral compositions and grain shapes. A new empirical relationship will have to be developed for different seabeds. The development of the BL-shear strength relationship in a region allows one to conduct a subbottom survey with a small grid size to develop a detailed map of shear strength variations in surficial sediments.

Reference

Orenberg, P, True, D., Bowman, L., Hermann, H. and March, R., "Use of a dropped dynamic penetrometer in cohesionless soil." Offshore Technology Conference Proceedings, (OTC8027), May 1996, Houston, p.639-648.

Figure 1 Expendable Doppler Penetrometer (XDP)

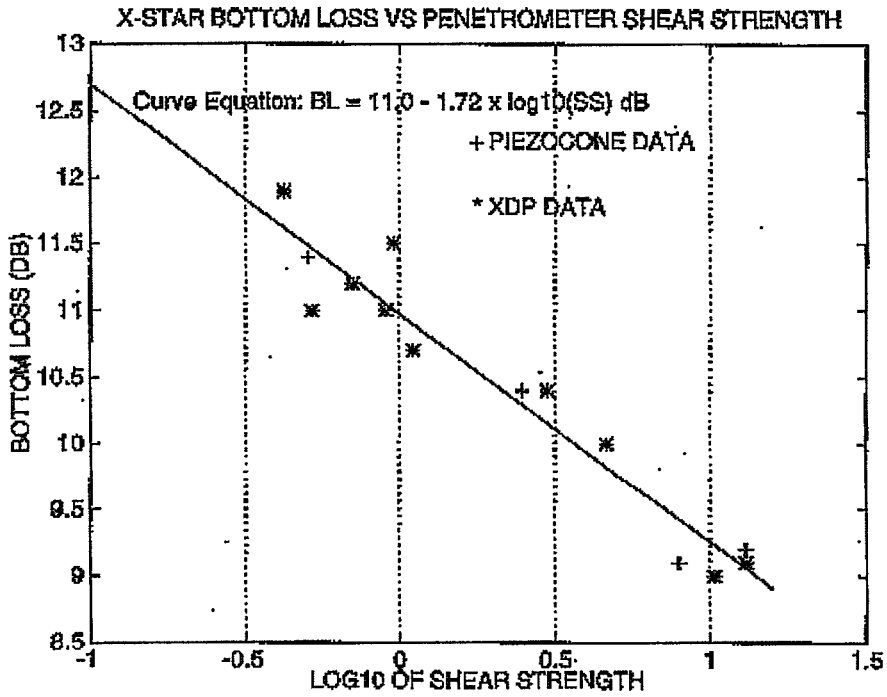

Figure 2 Bottom loss (dB) from chirp sonar data is plotted against the log of shear strength(psi) to obtain the empirical interrelationship shown above. Shear strength was calculated from XDP and piezocone profiles of shear strength using only the shear strength data in the interval of 2 to 4 inches under the sediment-water interface.

3.3 Environmental Estimation Using Navy Sensors (S.G. Tooma and N.P. Chotiros)

ENVIRONMENTAL ESTIMATION USING NAVY SENSORS

Samuel G. Tooma[1] and Nicholas Chotiros[2]

[1]Naval Research Laboratory, Stennis Space Center, MS 39529. [2]Applied Research Laboratory University of Texas, Austin, TX 78713

ABSTRACT

The Naval Research Laboratory (NRL) is investigating environmental monitoring using Navy combat systems. This concept's primary advantage is that acquired environmental data can be used to optimize performance of the very combat system used to collect the data.

Recent NRL programs in this area are the MCM Tactical Environmental Data System (MTEDS), Active Sonar Terrain Environmental Reconnaissance (ASTER), and Environmental Sensing using Tactical MCM Systems (or Through-The-Sensor (TTS)).

MTEDS demonstrated the capability to use AN/SQQ-32 mine hunting sonars to measure reverberation statistics and clutter density in real time to provide ping-to-ping real time sonar performance graphical displays. MTEDS also demonstrated the use of the ship's fathometer to provide bathymetry and sediment property profiles for use in providing mine burial estimates and mine burial probability maps.

ASTER utilized the multi-beam capability of hull-mounted AN/SQS-53B ASW sonars to provide acoustic reflection swath maps for use in quickly characterizing reverberation environments of unknown areas and for providing warning of approaching hazards to navigation.

TTS is addressing the environmental measuring capabilities of four MCM reconnaissance systems under development at the Naval Surface Warfare Center's Coastal Systems Station; these are the Torroidal Volume Search Sonar, the large aperture Side Looking Sonar, the Synthetic Aperture Sonar, and the Laser Line Scanner mine identification system.

INTRODUCTION AND SUMMARY

The Naval Research Laboratory (NRL) is investigating the concept of making environmental measurements using already-existing Navy combat systems installed on combat ships and using MCM reconnaissance systems presently in development. The advantages of this concept include: (1) dedicated environmental sensor development, and the need to incorporate these dedicated sensors on combat ships, is not required; (2) developed products are usually algorithms which are more easily incorporated into the involved combat and reconnaissance systems via pre-programmed product improvement funds; and (3) acquired environmental data can often be used in real time to optimize performance of the combat systems being used to collect the data. The latter is the fundamental foundation of future capabilities presently under consideration within the Navy for allowing sonar and other Navy systems to automatically adjust mode settings based on the existing environment as sensed by the system itself.

Recent NRL programs involved in monitoring the environment with Navy combat and reconnaissance systems include: (1) MCM Tactical Environmental Data System (MTEDS); (2) Active Sonar Terrain Environmental Reconnaissance (ASTER); and (3) Environmental Sensing using Tactical MCM Systems (short title is Through-the-Sensor).

The MTEDS program demonstrated the capability to use the primary combat system of the MCM ships, the AN/SQQ-32 mine hunting sonar, to measure reverberation statistics and clutter density. This information was used in real time to provide a ping-to-ping graphical display of sonar performance. The MTEDS program also demonstrated the use of the MCM ship's fathometer transducer to provide bathymetry and sediment classification/properties profiles along the ship's track. This information was used in real time to provide estimates of mine burial on impact and was used in near real time to produce maps of mine burial probability.

The ASTER program utilized the multi-beam capability of the hull-mounted AN/SQS-53B ASW sonar to provide acoustic reflection swath maps along the ship's track. This capability provides the potential for almost all combat ships to quickly characterize the reverberation environments of an unknown area and to provide warning of approaching hazards to navigation, including uncharted shoals and wrecks.

The Through-the-Sensor program is, essentially, a follow-on to the MTEDS program and is addressing the environmental measuring capabilities of four MCM reconnaissance systems presently under development at the Naval Surface Warfare Center, Coastal Systems Station in Panama City, Florida. These systems are: (1) Torroidal Volume Search Sonar (TVSS); (2) large aperture Side Looking Sonar (SLS); (3) Synthetic Aperture Sonar (SAS) system; and (4) Laser Line Scanner (LLS) mine identification system.

MCM TACTICAL ENVIRONMENTAL DATA SYSTEM (MTEDS)

The objective of the MTEDS program was to demonstrate a capability to make in situ measurements of critical environmental parameters for real time use by the MCM tactical action officer for optimum utilization of available MCM assets. The MTEDS program was essentially a 3-year program which started in August 1992

and was completed in September 1995 (Tooma, 1992). In March 1996, an opportunity arose to further demonstrate the MTEDS capabilities using an MCM-1 class ship during an international MCM exercise called PURPLE STAR. The results from the PURPLE STAR exercise were significant in that real time performance monitoring of the SQQ-32 sonar was achieved (Lott and Chotiros, 1996).

MTEDS was a demonstration program. As such, the major milestone of the effort was an at-sea demonstration involving all the selected environmental parameters. The objective of the demo was to measure the selected parameters from on-board sensors while the ship was underway at 4 to 5 knots, store the collected data in a commercial off-the-shelf (COTS) Geographical Information System (GIS) data base, display the data on the desktop workstation screen, and use the data to calculate MCM-significant information in real time (e.g., mine burial probability). This demo was conducted from the R/V SEWARD JOHNSON in the Key West, Florida area in February 1995 (Tooma and Richardson, 1995).

The environmental data collected and the systems used to collect the data were: (1) bathymetry using the ship's AN/UQN-4 fathometer's transducer; (2) current velocity profile using a COTS acoustic doppler current profiler; (3) sediment classification using the UQN-4 transducer and NRL's Acoustic Seafloor Sediment Classification (ASCS) system's processor (Lambert, Cranford, and Walter, 1993); (4) mine burial probability using the sediment classification data and a modified version (Hurst, 1992) of the impact burial prediction model initially developed at CSS (Arnone and Bowen, 1980); (5) reverberation statistics using pre-recorded SQQ-32 sonar signals provided by the Applied Research Laboratory:University of Texas (the SEWARD JOHNSON did not have an SQQ-32 sonar); and (6) sound speed profile using: (a) a COTS excursion-type profiler in which the vehicle is programmed to travel between two depth selected depths (Brown, Lott, and

Myrick, 1996); and (b) a COTS CTD system. All the above parameters were collected and were tied together using differential GPS navigation

During the PURPLE STAR exercise, fewer environmental parameters were measured because only on-board sensors organic to the MCM-1 class ship could be used. The same objectives, however, applied; i.e., collect data while underway, store in a GIS data base, display on the desktop workstation monitor, and use to provide information of interest to the MCM tactical action officer. During this test, the following information was collected and sensors used: (1) bathymetry using the UQN-4 fathometer transducer; (2) reflection loss using the UQN-4; (3) sediment classification using the UQN-4 and NRL's ASCS processor; (4) mine burial probability using ASCS sediment classification data and the impact burial prediction model; and (5) reverberation statistics using the SQQ-32 mine hunting sonar. Again, differential GPS navigation was used for geo-location of the collected data. The key achievement on the PURPLE STAR exercise was the use of the SQQ-32 itself rather than pre-recorded data as was done during the Key West test.

Figure 1 presents typical examples of surficial sediment impedance collected during the Key West demo. The bottom example depicts data from the tracklines used during the MTEDS test and the top example shows a more dense grid of the same area collected using the German ship WFS PLANET[1]. In both examples, trends in bottom impedance are clearly evident. The PLANET data set, of course, shows the value of closely-spaced track lines. With no extrapolation, the bottom impedance structure is clearly shown.

Figure 2 shows the SEWARD JOHNSON impedance data for two different depths into the sediments. The bottom example is a 2-D depiction of impedance for the

[1] WFS PLANET, involved in the Coastal Benthic Boundary Layer special research program (Tooma and Richardson, 1995), was using the same type sediment classification system as that used on R/V SEWARD JOHNSON. PLANET operations were done during the same time period as the MTEDS program.

Figure 1.

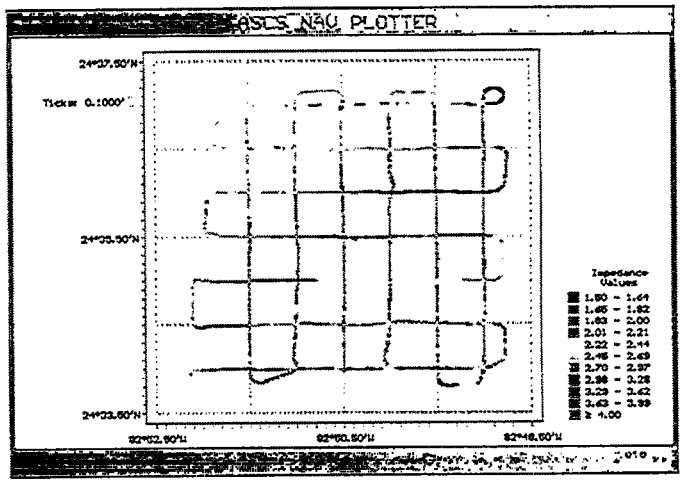

Color-coded trackplot of surficial (upper 0.4m) sediment acoustic impedance collected using NRL/ASCS with *R/V Johnson* 12-kHz transducer. Trackline spacing is 1 km.

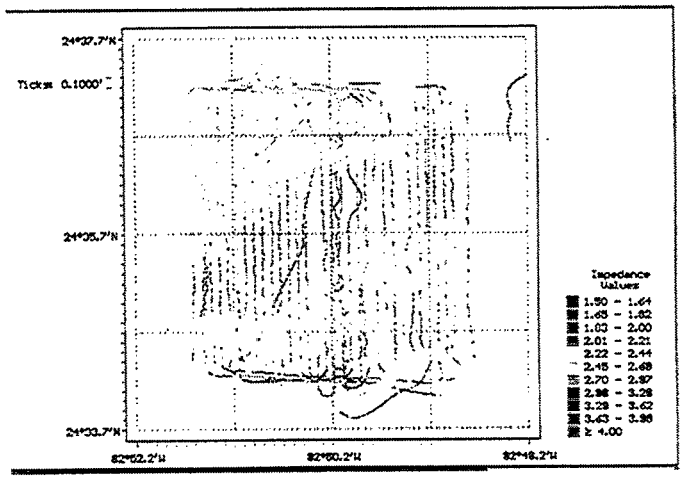

Color-coded trackplot of surficial (upper 0.4m) sediment acoustic impedance collected using NRL/ASCS @ 15-kHz aboard *WFS Planet*. Trackline spacing is approximately 150 m.

* Color Key: Interpretation of colorized tracklines using impedance/color scale on each figure above;

Yellow	Silt/sand mixture (probably includes shell)
Pink	Muddy or silty sand
Red	Carbonate Sand
Gray	Limestone rock (no distinction made between limestone rock and coral reef)
Blues/greens	Lower return signal due to effect of high slope angles near topographic features while using narrow beam transducer

3. 3-D CONTOUR MAPS

ASCS predicted impedance draped over transducer altitude with tracklines

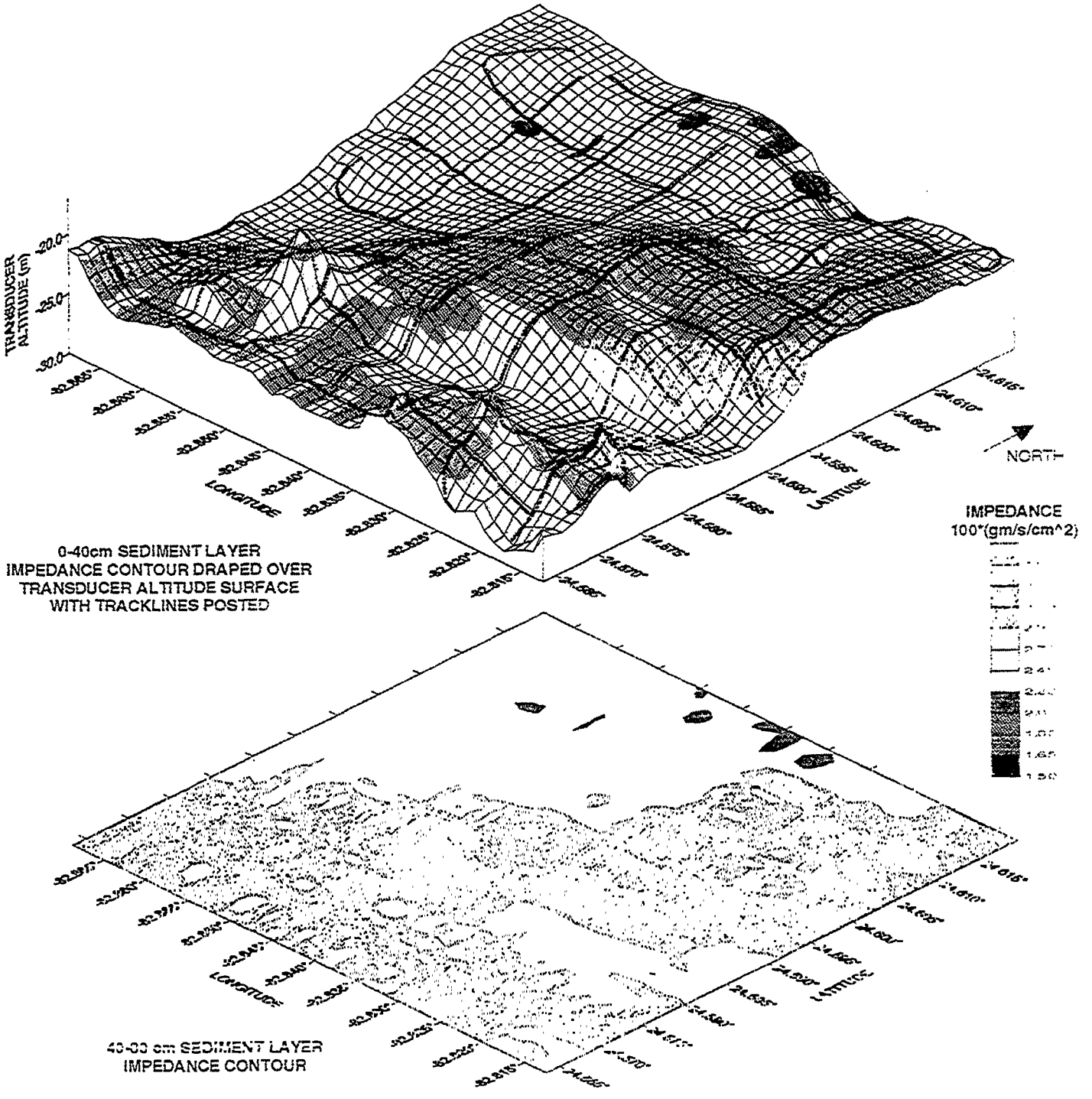

Figure 2. *Seward Johnson* 12-kHz ASCS acoustic impedance contours

40-80 cm sediment layer, and the top layer is for the 0-40 cm layer. In addition, the latter is draped over the bathymetry to provide a 3-D presentation of the data. The track lines are also shown to provide the location of the data coverage used in generating the maps. COTS interpolation software was used to create these images.

The basic impedance data was inverted to estimate sediment density and shear strength needed as inputs to the impact burial prediction model (Hurst, 1992). Figure 3 presents a 3-D map of the model results. The predicted percent of the mine exposed above the sediments is color coded using the color scheme presented in the figure. Clearly, for this area, the majority of the area does not present a mine burial problem. The northwest corner of the grid, depicted in yellows and reds, could pose a buried mine problem, and tactics can be used to address the problem.

Figure 4 presents a similar presentation as Figure 3 for bottom current vectors relative to bathymetry. This type of information can be extremely important in planning diver operations and for the launch, recovery, and operational use of the tethered remotely-piloted mine neutralization vehicle.

As mentioned above, during the PURPLE STAR exercise, the SQQ-32 mine hunting sonar was used to measure noise statistics. These noise statistics can be used for real time sonar performance monitoring and can be further processed to provide backscattering strengths and ambient noise for use as inputs to the sonar performance prediction model. During PURPLE STAR, only the real time monitoring of sonar performance was addressed on-scene. During normal MCM operations, a sound speed profile is generated (often using only an XBT), ray tracing is done, and expected sonar performance is determined. Tactics for use of the sonar, such as track line spacing, sonar depression/elevation (D/E) angle, and height above bottom are determined using this information. Changes to these mode settings are not usually made unless a determination is made to take another XBT or CTD. The

Impact burial predictions posted as percent volume exposed color contours

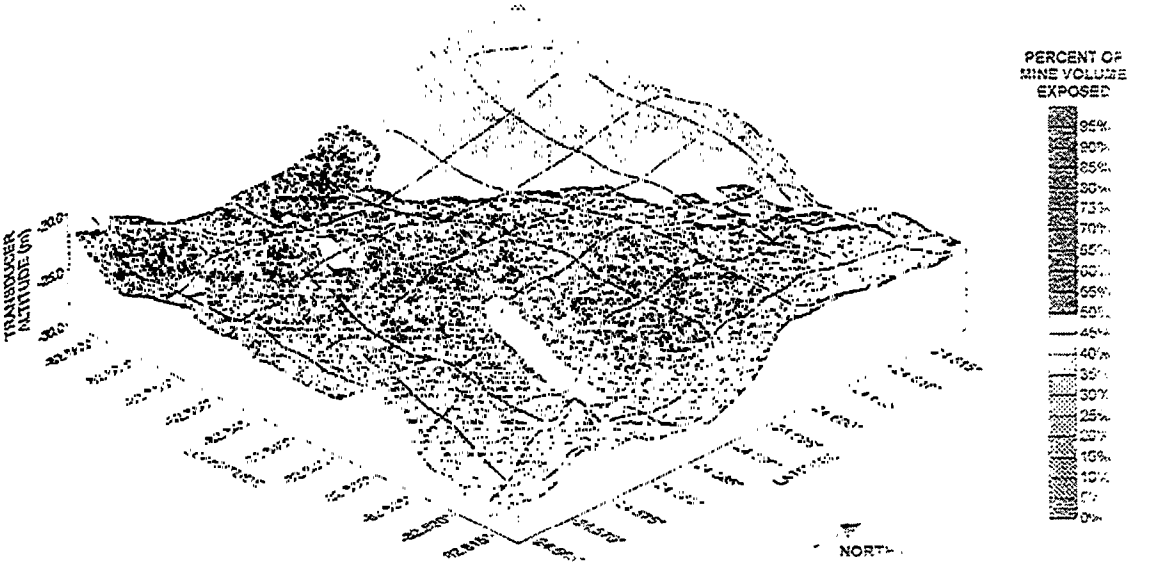

Figure 3 . Impact mine burial prediction map

- Percent of mine volume exposed color contour draped over transducer altitude above seafloor.
- Acoustic survey tracklines posted in black.

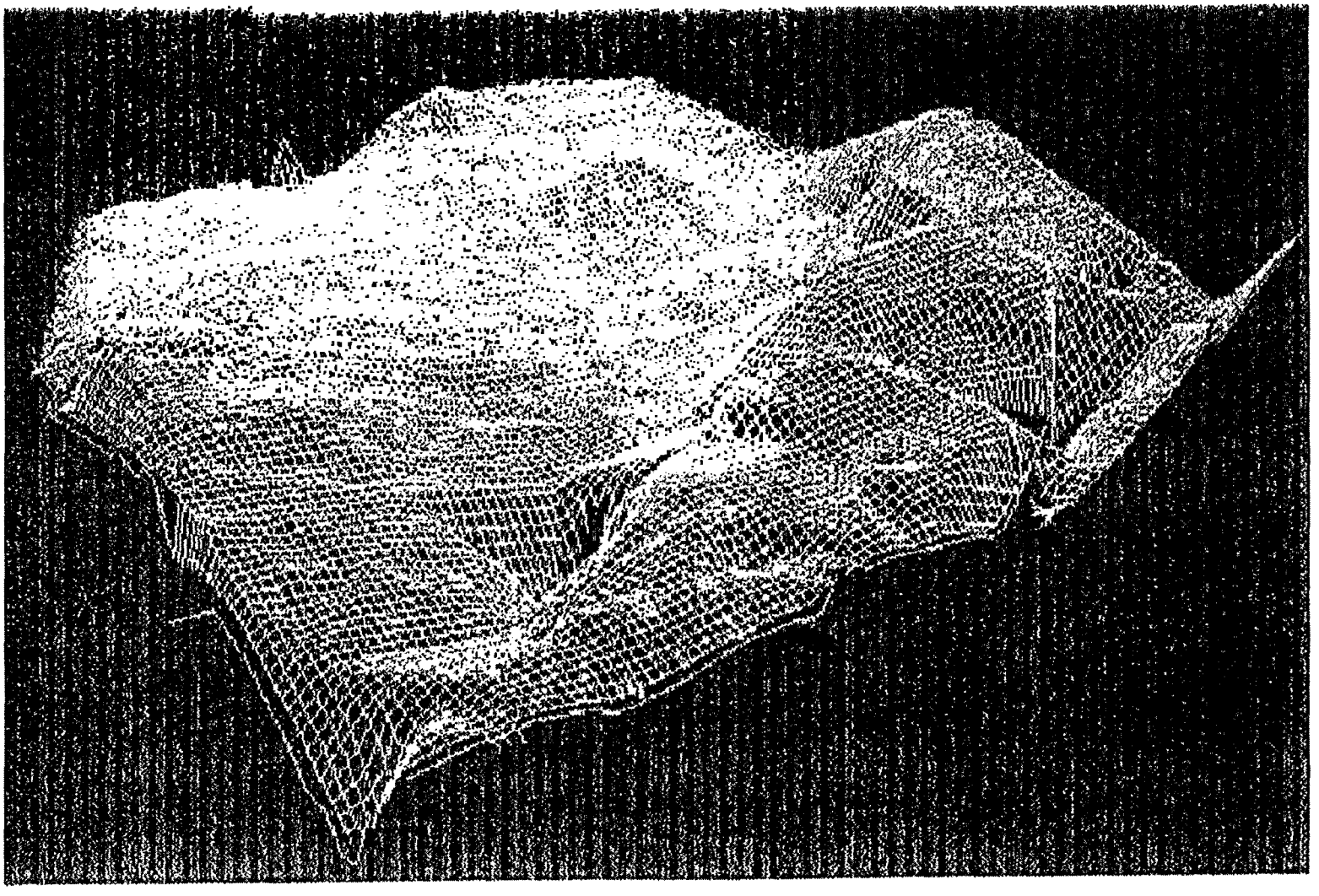

FIGURE 4 . Bottom Current Vectors Relative to Bathymetry

sonar data is displayed on a B-scope-type display using 2 selected beams, a so-called upper D/E and a lower D/E. The upper D/E "sees" out to farther ranges and the lower D/E sees ranges closer in. The sonarman must deal with a conglomeration of noise, false targets, and real targets. He has no way of determining where the sonar performance is optimum and where it may be degraded because of bottom morphology. This is a very tiring and stressful situation for the sonarman as he must deal with many potential targets. During the PURPLE STAR exercise, the sonar return data (measured raw reverberation) was used to calculate signal to background ratio (i.e., signal excess) for any particular ping.

The calculated signal to background ratio was color coded in 10 dB increments from 0 to 40 dB and overlain on the B-scope display. Figure 5 shows a typical example of this process for a single ping. Sonar performance is considered good in the green and hotter color areas and considered marginal or poor in the blue and darker areas. Effects of bottom features can be seen as incursions of blue into the green. In Figure 6, simulated mine-like targets are depicted on the same display as Figure 5. With this quantified color display, the sonarman can focus his evaluation of the targets falling in the areas where the sonar has the highest signal to background ratio (i.e., best performance). This could greatly reduce the fatigue factor associated with this activity.

A very revealing aspect of this monitoring of sonar performance is shown in Figure 7. Six sonar performance pings are depicted along a single 6 mile track during the PURPLE STAR exercise. Sonar performance is shown to vary from essentially no capability at the bottom of the track to relatively acceptable capability nearer the top of the track. Maintaining a data base of this performance capability for a gridded area can quickly reveal that in certain areas of the grid sonar performance can be good and in other areas poor. This type of information can be used to change tactics. Additional tracks in the poor area can be run, different mode

ARL:UT

NRL

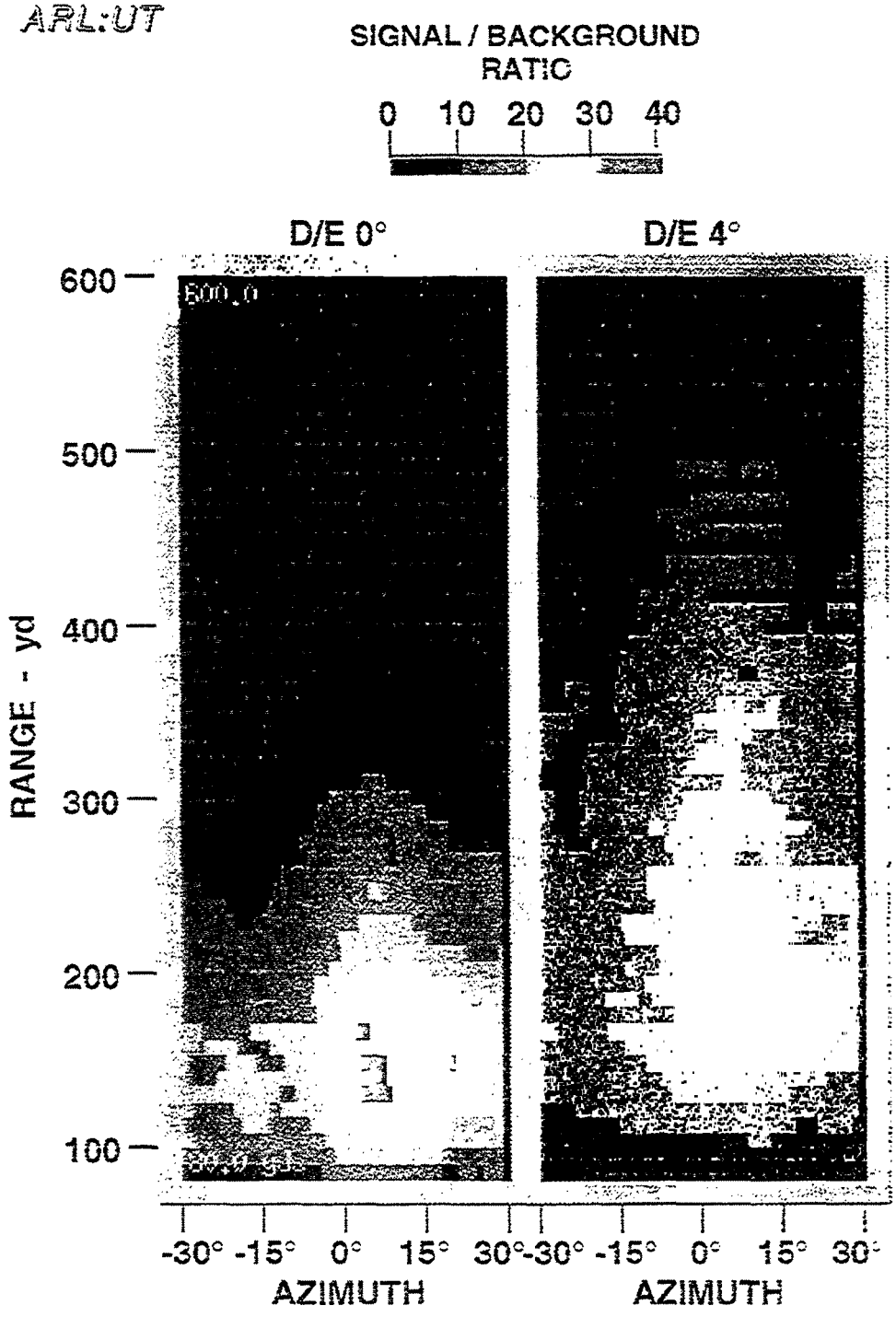

Lat. 34° 18.40' N Long. 77° 9.08' W
Heading 001 deg
Source Level: 221 dB, Pulse: 1 ms
Comment:

03:18:17 CST

Figure 5. Signal to background ratio in 10 dB increments.

8.03_18 17_oscan.canvas

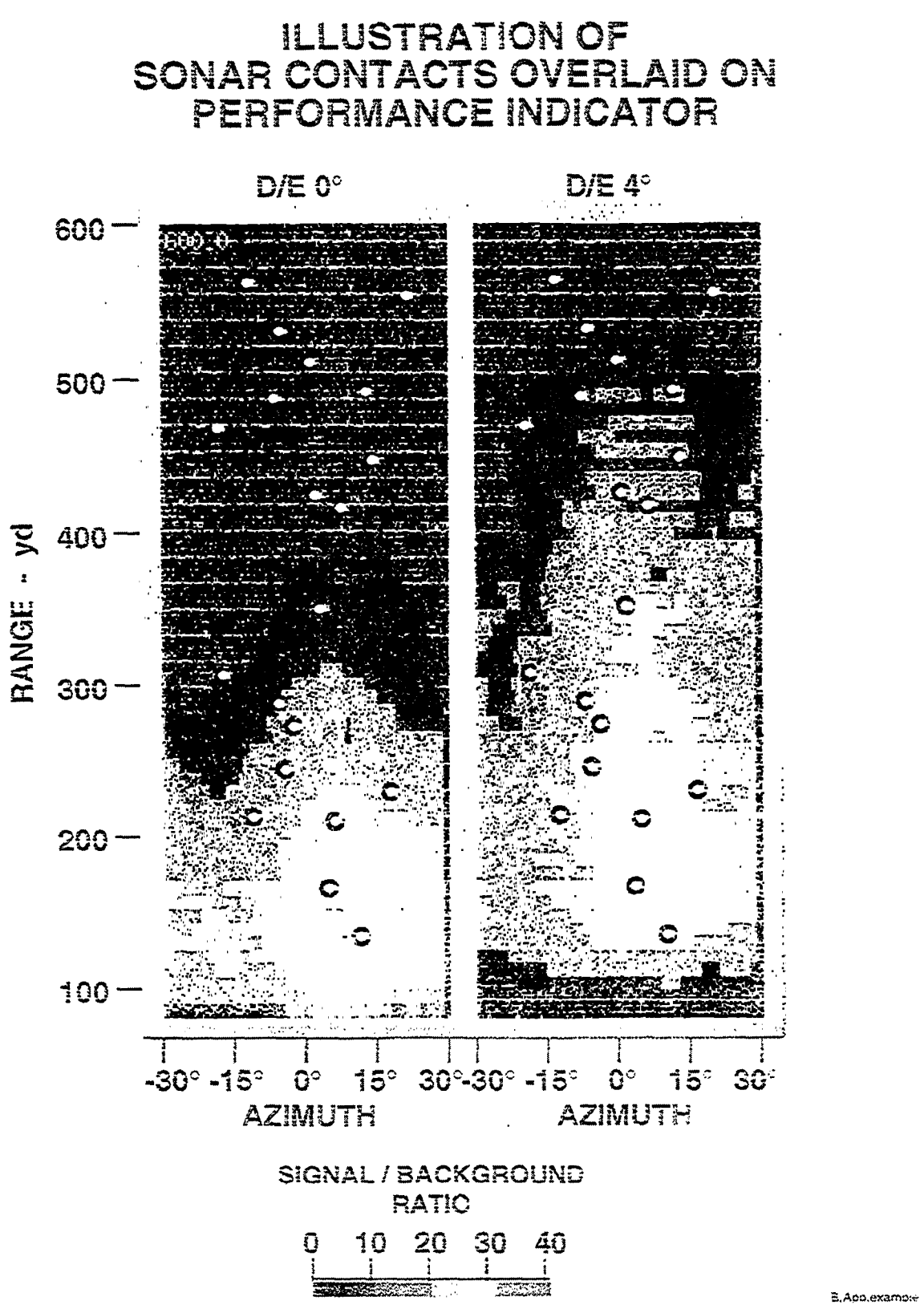

Figure 6. Simulated mine-like targets.

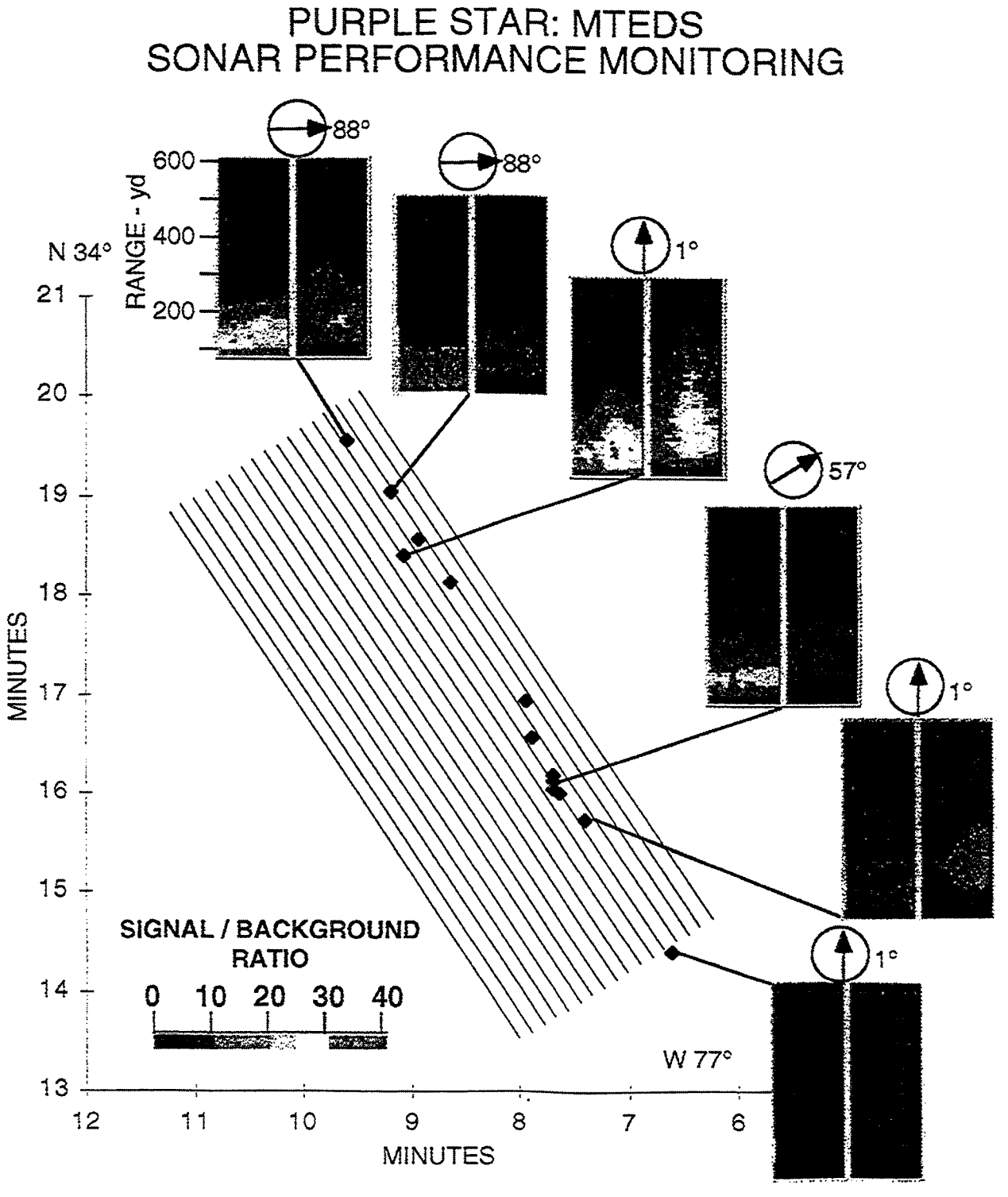

Figure 7. Sonar performance pings along a 6 mile track during Purple Star.

settings can be used, or acoustic mine hunting can be forsaken for influence mine sweeping[2]. In any event, considered decisions can be made based on the real time performance monitoring of the sonar. The information shown in Figure 7 also shows the folly of using a so-called "range-of-the-day" to determine sonar mode settings.

Tooma and Lott (1996) present recommendations relative to the transition of certain aspects of the MTEDS program to Navy ships, and Lott and Chotiros (1996) present results of the PURPLE STAR MTEDS demonstration.

ENVIRONMENTAL SENSING USING MCM TACTICAL SYSTEMS (Through-The-Sensor)

Following completion of the MTEDS program, NRL initiated a program designed to develop technology and techniques for exploiting the environmental measuring potential of MCM reconnaissance systems in development at the Coastal Systems Station (CSS) in Panama City, Florida. Extensive discussions were conducted with the system's engineers at CSS relative to the MCM reconnaissance systems under development as to their specifications, stage of development, future field tests, planned use, etc. Based on these discussions, four systems were selected for evaluation: (1) the Torroidal Volume Search Sonar (TVSS); (2) the real aperture Side Looking Sonar (SLS); (3) the Synthetic Aperture Sonar (SAS) system; and (4) the Laser Line Scanner (LLS) mine identification system.

Based on the capabilities of these systems, a list of possible environmental parameters that could possibly be inverted from their data as they operate in the

---

[2] Acoustic mine hunting is the location of individual mines using high frequency sonars. Once a target is classified as a mine, it is neutralized using other systems. Influence mine sweeping is the neutralization of mines by generating a magnetic and/or acoustic signal (i.e., influence) into the water volume to "fool" the mine into thinking a target is passing by. Once fooled, the mine explodes harmlessly.

MCM COASTAL SENSING

ENVIRONMENTAL PARAMETERS TARGETED

- **TORROIDAL VOLUME SONAR SYSTEM (TVSS)**
  - VOLUME REVERBERATION
  - ACOUSTIC MULTI-PATH ESTIMATION
  - SEA STATE
  - BATHYMETRY
  - SEDIMENT TYPE
  - SOUND SPEED FIELDS
- **LARGE APERTURE SIDE-LOOKING SONAR (SLS)**
  - BOTTOM BACKSCATTER ESTIMATES
  - SEDIMENT TYPE
- **SYNTHETIC APERTURE SONAR (SAS)**
  - SEDIMENT TYPE
  - BOTTOM BACKSCATTER ESTIMATES
  - BOTTOM MORPHOLOGY
- **LASER LINE SCANNER (LLS) MINE IDENTIFICATION SYSTEM**
  - OPTICAL SCATTERING FUNCTION
  - BOTTOM ALBEDO
  - TURBULENCE
  - ATTENUATION COEFFICIENT
  - BOTTOM TEXTURE

EXTERNAL REVIEW

Figure 8. MCM Coastal Sensing: Environment Parameters Targeted.

normal MCM reconnaissance mode was developed. Figure 8 presents this list. The list is extensive, but it does emphasize bottom characteristics. Some of the parameters, such as bathymetry from the TVSS, are considered as low risk, and others, such as turbulence from the LLS are considered as high risk. In structuring the technical program, the TVSS was selected as the initial system for evaluation. The primary reason for this selection was that the TVSS was the furthest along in the developmental cycle. It had been successfully tested at sea, and a large data set was available for analysis. CSS agreed to provide all data and information associated with the TVSS.

NRL realized that expertise outside of the laboratory was highly desirable for carrying out the objectives of the program. A series of workshops was held with representatives from CSS, Applied Research Laboratory:University of Texas, Applied Physics Laboratory:University of Washington, Scripps Institution of Oceanography, Woods Hole Oceanographic Institution, and the Defence Research Agency in the United Kingdom. During these workshops, technical issues were define, an integrated technical plan was developed, technical teams were selected, and a program white paper was outlined. This white paper was issued to the Office of Naval Research (ONR) for possible funding for the non-NRL participants. Funding was provided by ONR for the first year of the 4-year effort. The technical plan developed during the workshops outlined the first year's objectives associated with the TVSS. They are: (1) using vertical incidence sediment classification techniques; (2) applying established multi-beam swath bathymetry techniques; (3) applying established mapping segmentation techniques to produce province maps; and (4) using MTEDS-developed volume/bottom reverberation techniques to characterize the reverberation fields of an area.

ACTIVE SONAR TERRAIN ENVIRONMENTAL RECONNAISSANCE (ASTER)

The objective of the ASTER effort in 1995 was to demonstrate the use of the AN/SQS-53B hull-mounted ASW sonar to produce acoustic imagery of the seafloor for eventual population within the Master Seafloor Digital Data Base. Data collected for this effort was from aboard USS MONTEREY (CG-61) as it operated in the Red Sea in December 1995. An excellent data set was collected.

Due to the aspect angle dependence of acoustic backscatter from the seafloor, the initial imagery consisted of twelve azimuth-stabilized beams of the sonar. The acoustic backscatter records of these twelve beams were stacked to form composite backscatter maps which were overlain and compared to multibeam bathymetry data collected by the Naval Oceanographic Office during the same time period and area as the MONTEREY data. Also, shallow water acoustic imagery was developed in the same manner and compared to available bathymetric charts of the area (NAVOCEANO survey data was not collected in the shallow water areas).

Figure 9 shows ASTER data collected along a transit in the Red Sea. Bottom linear features are clearly depicted in this figure. This type of information can be used to determine optimum look directions for the ASW sonar by determining likely high bottom reverberation levels associated with the orientation of the bottom features. In other words, acoustic returns from energy normal to the lineations will most likely be more noisy than those which are generated by energy up-strike of the lineations.

Analysis of shallow water data compared to available bathymetric charts was very revealing. Figure 10 shows that acoustic reflection data associated with bathymetric features approaching an island in the Red Sea were clearly delineated with the MONTEREY about 4 kilometers from the island. Importantly, uncharted shoals were evident on the data. The obvious implication of these results in

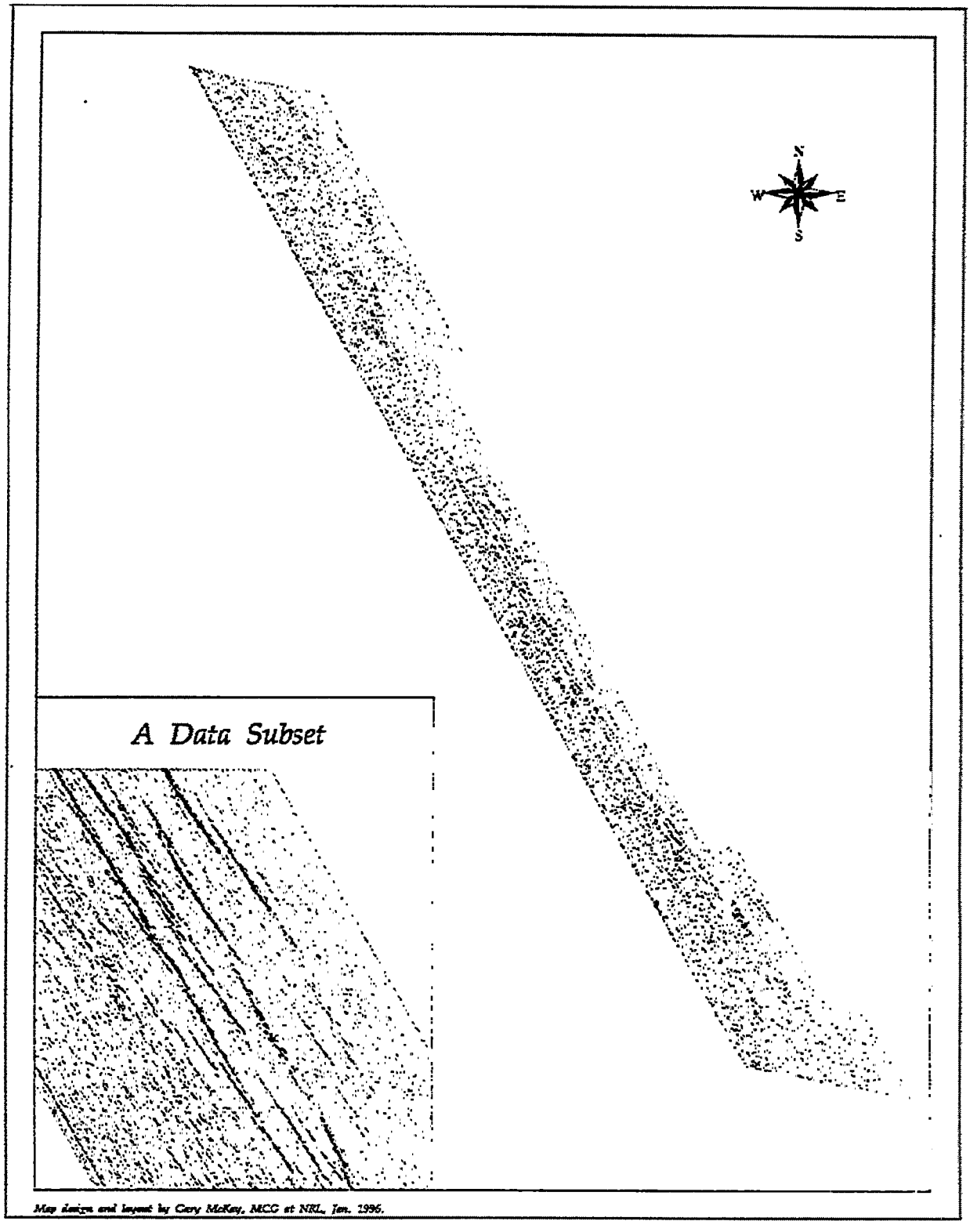

Figure 9. ASTER data from the Red Sea.

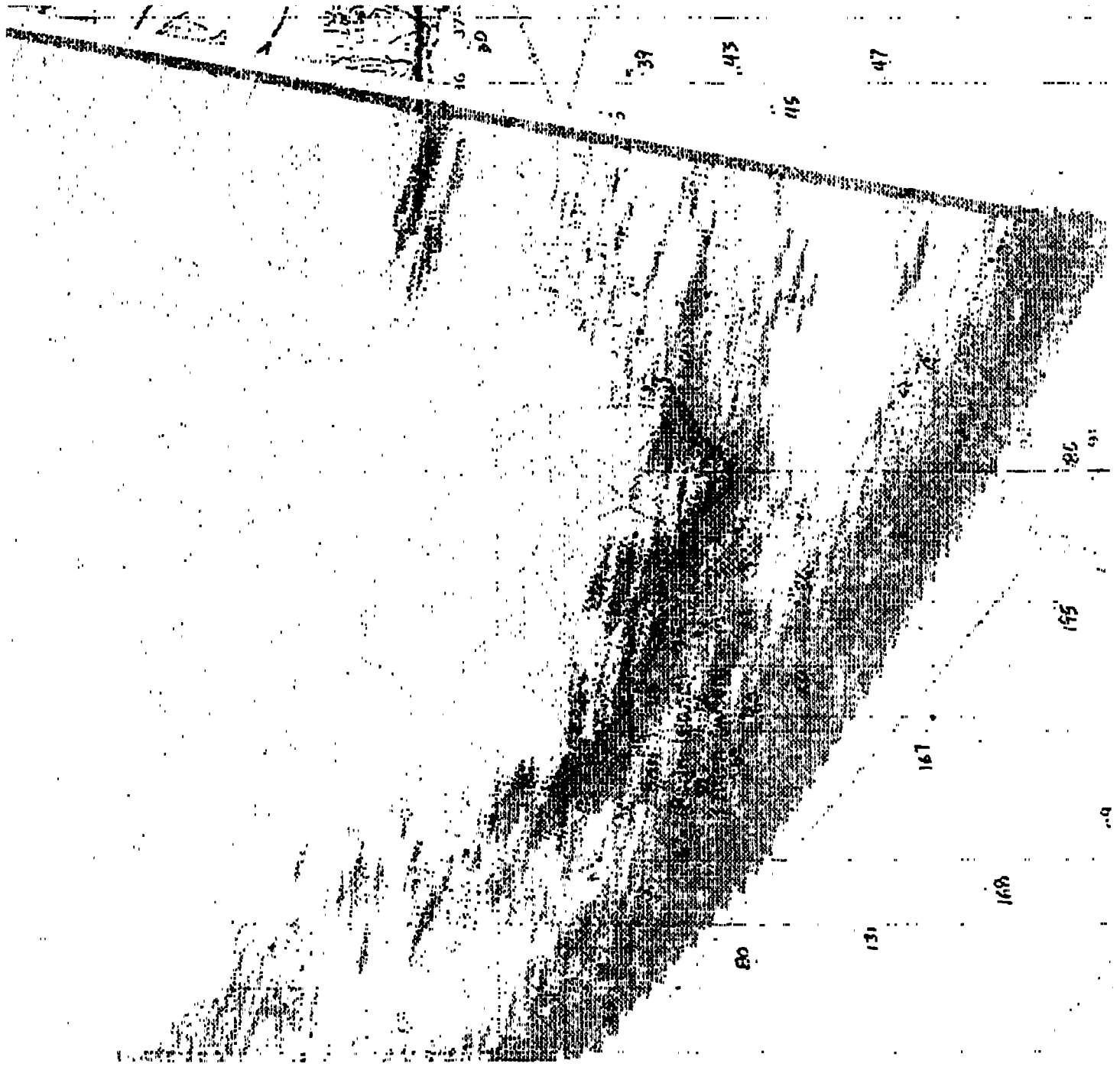

Figure 10. Acoustic returns shown in Figure 12a (but shown here as dark areas) superimposed on bathymetric chart of the area surrounding Perim Island.

shallow water is that U.S. combatants operating in unfamiliar or poorly charted areas have an on-board capability to detect shoals or other hazards to navigation well in front of the ship's track.

ACKNOWLEDGMENTS

The authors wish to acknowledge the efforts of Doug Lambert, Don Walter, and Dave Young, all of the Naval Research Laboratory, for the collection, processing, and analysis of the Acoustic Seafloor Classification System data used to generate figures presented in this report. We also wish to acknowledge the considerable efforts of the captains and crews of R/V SEWARD JOHNSON, WFS PLANET, and USS WARRIOR (MCM-10). The projects under which this work has been performed have been funded by the Office of Naval Research (ONR) through the Naval Research Laboratory under Program Element (P.E.) 0602435N. The at-sea demonstration conducted during the PURPLE STAR MCM exercise was funded by the Oceanographer of the Navy (N096) and managed by ONR Code 32 under P.E. 060375N, Mr. Eigoro Hashimoto, Program Manager. Funding for the ground truth data collection during the Key West demonstration was provided by ONR through the Coastal Benthic Boundary Layer research program under P.E. 0601153N, Dr. Michael Richardson, NRL, Chief Scientist.

REFERENCES

Arnone, R.A. and L.E. Bowen, 1980. "Prediction Model of the Time History Penetration of a Cylinder Throughout the Air-Water-Sediment Phases." Naval Coastal Systems Center, Panama City, FL. NCSC Letter Report 734-36.

Brown, R.A., D.F. Lott, and R.K. Myrick, 1996. "Mine Countermeasures Tactical Environmental Data System: Demonstration of Real-Time Measurements of Water Column Sound Speed and Clarity." Naval Research Laboratory, NRL/MR/7431—95-7712. May 1996. 21 pages.

Hurst, R.B., 1992. "Mine Impact Burial Prediction Model - Technical Description of Recent Changes and Developments." Defence Scientific Establishment, Auckland, NZ. DSE Report 149, February 1992.

Lambert, D.N., J.C. Cranford, and D.J. Walter, 1993. "Development of a High-Resolution Acoustic Seafloor Classification Survey System." Proceedings of the Institute of Acoustics, International Conference on the Acoustic Classification & Mapping of the Seabed, University of Bath, England. April 1993. pp 149-156.

Lott, D.F. and N.P. Chotiros, 1996. "Mine Countermeasures Tactical Environmental Data System: At Sea Demonstration During Exercise PURPLE STAR '96." Naval Research Laboratory, NRL/MR/7431-96-8021. 39 pages.

Tooma, S.G., 1992. "Development of an In Situ, Real Time Environmental Data Collection Capability to Support Mine Countermeasures Operations: MCM Tactical Environmental Data System (MTEDS) Program Master Plan." Naval Research Laboratory, NRL/AP/7430-92-0001. November 1992. 41 pages.

Tooma, S.G. and M.D. Richardson, 1995. "The Key West Campaign." Sea Technology, Vol. 36 (6) 1995. pp 17-25

Tooma, S.G. and D.F. Lott, 1996. "Transition and Research and Development Recommendations Resulting from the MCM Tactical Environmental Data System (MTEDS) Program." Naval Research Laboratory, NRL/MR/7430—96-8030. 9 pages.

4.0 Processes Which Affect Near-Surface Sediment Structure and Properties

4.1 Constraints on Rates of Sediment Accumulation and Mixing: Southeast Channel, Dry Tortugas Keys (S.J. Bentley and Charles Nittrouer)

Constraints on Rates of Sediment Accumulation and Mixing: Southeast Channel, Dry Tortugas Keys

Samuel J. Bentley and Charles A. Nittrouer

Marine Sciences Research Center
State University of New York
Stony Brook, NY 11794-5000

INTRODUCTION

Geochronological studies of cores from Southeast Channel, Dry Tortugas Keys, were undertaken to constrain rates and relevant length and time scales for sediment accumulation and mixing. Southeast Channel is a reentrant in the Dry Tortugas platform, and is characterized by accumulation of autochthonous skeletal-carbonate and allochthonous muddy-carbonate sediments derived from nearby shallow-water sources (Fig. 1) (Bentley and Nittrouer, in press; Wright et al., in press). Sediments in the study area are bioturbated by a tiered benthic community, characterized by a shallow tier of surface- and shallow-deposit feeding polychaetes, and a lower tier of deep-deposit feeding notomastid polychaetes and callianassid shrimp (D'Andrea and Lopez, in press). Physical sediment properties (i.e., porosity and grain-size gradients) and associated radiotracer distributions (excess ^{234}Th and ^{210}Pb) reflect the combined processes of accumulation and mixing in the shallow seabed of Southeast Channel.

METHODS

Data for this study were collected during two four-day cruises on the *R/V Pelican*, at the beginning and end of February 1995. Box-coring was conducted in

coordination with deployment and retrieval of an instrumented seabed tetrapod (Wright et al. 1996) and with studies of benthic biology (D'Andrea and Lopez 1996). Locations of cores discussed here are shown in Fig. 1.

Cores were examined through observations of X-radiographs, microfabric, grain size, ^{234}Th, ^{210}Pb, and porosity. Grain-size analyses were made with a Micromeritics ET-5100 Sedigraph following the methods of Coakley and Syvitski (1991). ^{234}Th activities ($t_{1/2}$ = 24 days) in the upper 10 cm were determined by γ-spectroscopy (63 keV peak: Buesseler et al. 1992). Samples for ^{210}Pb analysis were dried and sieved at 3 phi (125 μm) in order to remove large skeletal-carbonate particles. ^{210}Pb activities ($t_{1/2}$ = 22 years) were measured by wet chemical leaching of samples to extract the granddaughter ^{210}Pb, which was then analyzed by α-spectroscopy (Nittrouer et al. 1979). Excess activities of ^{210}Pb and ^{234}Th were determined by comparison with supported background activities. Porosity was determined by water loss overnight at 100° C.

ESTIMATING THE BIODIFFUSION COEFFICIENT AND SEDIMENT ACCUMULATION RATE

The radioisotopes ^{234}Th and ^{210}Pb are natural products of uranium-series decay, and are removed from seawater by adsorption onto settling particles (Cochran, 1992). If fluxes of sediment and of the radionuclide under study have remained constant, then the radioisotope activity, the accumulation rate, and the sediment biodiffusion coefficient (D_b) are related by the following solutions to the advection/diffusion equation. The equation and solutions are shown here in forms suitable for the study of particle reactive radionuclides in sediments (DeMaster and Cochran, 1982):

$$D_b \frac{d^2A}{dz^2} - S\frac{dA}{dz} - \lambda A = 0. \qquad (2)$$

where A is the activity of excess radiotracer (dpm/cm^3), z = depth in sediment (cm), D_b is the biodiffusion coefficient (cm^2/yr), S is the sediment accumulation rate (cm/yr), and λ is the decay constant for the radionuclide of interest (1/yr). For the boundary conditions

$$A = A_0 \quad at \quad z = 0$$
$$A \to 0 \quad at \quad z \to \infty$$

the general solution is

$$A_z = A_0 \exp\left\{\left[\frac{s - \left(s^2 + 4\lambda D_b\right)^{1/2}}{2D_b}\right] z\right\}. \tag{3}$$

Under conditions when $S^2 << 4D_b\lambda$, accumulation can be considered negligible and this equation can be solved for D_b:

$$D_b = \lambda\left(\frac{z}{\ln\left(A_0/A_z\right)}\right)^2. \tag{4}$$

If $S^2 >> 4D_b\lambda$, mixing can be ignored and the accumulation rate is calculated from :

$$S = \frac{-\lambda z}{\ln\left(A_z/A_0\right)}. \tag{5}$$

When $S^2 \approx 4D_b\lambda$, then neither accumulation nor mixing can be ignored.

RESULTS

Excess ^{234}Th was restricted to the upper 2 cm of the seabed for the cores analyzed. Porosity was determined for each profile, and the distribution of excess ^{234}Th closely tracks the thickness of the high-porosity surface layer (Fig 2). Sediment below this layer was shellier and more compact.

^{210}Pb activities have been determined for 9 cores from Southeast Channel, including replicates from two stations. The general shape of all profiles is similar (Fig. 3). The upper 12-20 cm is characterized by a steep gradient from surface values of 3

dpm/g to deeper activities of just over 2 dpm/g, with occasional spikes of higher activity. From ~15-35 cm, the gradients display uniform exponential decay to supported activities of 0.45 dpm/g, which characterizes deeper portions of the cores.

If we assume that bioturbation is the dominant mechanism producing the upper gradient, but is negligible in its influence on the lower, less steep gradient, then the following values for the mixing coefficient and accumulation rate can be calculated from solutions to the advection/diffusion equation (Table 1). The parameter L_b is the vertical length scale over which bioturbation appears to be the dominant process controlling activity gradients. These estimates of S, and L_b show very little variability. Variability for D_b is greater, but all estimates of D_b are sufficient to satisfy the scaling equation $S^2 << 4D_b\lambda$, indicating that the effects of accumulation on excess activity gradients are negligible in the upper zone.

Table 1. Accumulation rate, biodiffusion coefficient, and mixing depth estimates from $^{210}Pb_{xs}$ profiles of Southeast Channel cores.

Core	D_b , cm^2/yr (surface 12-17 cm)	S, cm/yr (measured below depth L_b)	L_b, cm
22	129.1	0.26	15
35	129.3	0.34	14
49	116.2	0.33	14
59	22.3	0.29	17
65		0.29	16
72	14.9	0.31	13
74	95.18	0.30	15
310	16.3	0.26	12
Mean	***74.8***	***0.30***	***14.5***
Standard Deviation	***54.5***	***0.029***	***1.6***

DISCUSSION

Distributions of excess ^{234}Th and ^{210}Pb reveal the presence of three distinct zones within the seabed, where sediment mixing and accumulation interact over differing time scales. These zones coincide with the distribution of invertebrate functional groups within the benthic community, and with the depth and intensity of observed physical mixing.

A thin surface layer (~2 cm) is characterized by high porosity, fine grain-size, and the presence of excess ^{234}Th (Fig 2). These properties are maintained by rapid biogenic and physical mixing over periods of less than three months, as well as by deposition of fine sediment transported to the sediment-water interface by both physical and biological processes (lateral advection in currents, and egestion of fines by particle-selective deep-deposit feeders, respectively) (Wright et al., in press; D'Andrea and Lopez, in press).

Below the surface layer, sediments to depths of 12-16 cm are bioturbated intensely by deep-deposit feeders over time scales of 10-20 years, based on observations of ^{210}Pb activities, biogenic sedimentary fabrics, and benthic community structure (Fig 3). Downward increases in mean grain size result from accumulation of coarse autochthonous skeletal debris (such as mollusk shells) and from the particle-selective feeding habits of dominant deep-deposit feeders.

Below ~15 cm depth, the gently sloping decay profiles of ^{210}Pb are probably controlled by sediment-accumulation rates (Fig 3), or by a combination of very slow mixing ($D_b < 1$ cm^2/yr) and accumulation. Deep, open burrows are observed, and biogenic structures observed in radiographs are consistent with deep mining of buried food sources, however, the uniform decay profiles and low variability of

accumulation rate among all cores analyzed are consistent with the dominance of accumulation over advective mixing.

CONCLUSIONS

Biological mixing is a major determinant of radiotracer distributions and physical sediment properties in the seabed of Southeast Channel. Vertical distributions of mixing depths and time scales correspond closely to the observed distributions of functional groups in the benthic community. Accumulation rates appear to be relatively high and laterally uniform (~0.3 cm/yr), however analyses of impulse tracers such as ^{137}Cs are necessary to confirm the presence or absence of deep mixing, and its effect on apparent accumulation rates.

REFERENCES

ALLER, R.C., and Cochran, J.K., 1976, ^{234}Th- ^{238}U disequilibrium and diagenetic time scales: Earth and Planetary Science Letters, v. 29, p. 37-50.

BENNINGER, L.K., Aller, R.C., Cochran, J.K., and Turekian, K.K., 1979, Effects of sediment mixing on the ^{210}Pb chronology and trace metal distribution in a Long Island Sound sediment core: Earth and Planetary Science Letters, v. 43, p. 241-259.

BENTLEY, S.J., and Nittrouer, C.A., submitted, Biogenic influences on the formation of sedimentary fabric in a fine-grained carbonate-shelf environment: Dry Tortugas, Florida Keys. Geo-Marine Letters.

BUESSELER, K.O., Cochran, J.K., Bacon, M.P., Livingston, H.D., Casso, S.A., Hirschberg, D., Hartman, M.C., and Fleer, A.P., 1992, Determination of thorium isotopes in seawater by non-destructive and radiochemical procedures: Deep-Sea Research, v. 39, p. 1103-1114.

COAKLEY, J.P., and Syvitski, J.P.M., 1991, Sedigraph technique: *in*, SYVITSKI, J.P.M., ed., Principles, Methods, and Application of Particle Size Analysis: Cambridge, Cambridge University Press, 368 p.

COCHRAN, J.K., 1992, The oceanic chemistry of uranium- and thorium-series nuclides: in Ivanovich, M., and Harmon, R.S., eds., Uranium-series Disequilibrium:

Applications to Earth, Marine, and Environmental Sciences, Oxford, Clarendon Press, p. 334-395.

D'ANDREA AF and Lopez GR (1996) Benthic macrofauna in a shallow water carbonate sediment: major bioturbators at the Dry Tortugas. Geo-Marine Letters in press

DEMASTER, D.J., and Cochran, J.K., 1982, Particle mixing rates in deep-sea sediments determined from excess ^{210}Pb and ^{32}Si profiles: Earth and Planetary Science Letters, v. 61, p. 257-271.

NITTROUER, C.A., DeMaster, D.J., Mckee, B.A., Cutshall, N.H., and Larsen, N.H., 1984, The effect of sediment mixing on ^{210}Pb accumulation rates for the Washington continental shelf: Marine Geology, v. 54, p. 201-221.

NITTROUER, C.A., Sternberg, R.W., Carpenter, R., and Bennett, J.T., 1979, The use of ^{210}Pb geochronology as a sedimentological tool: Application to the Washington continental shelf: Marine Geology v. 31, p. 297-316.

WRIGHT LD, Friedrichs CT, and Hepworth DA (1996) Effects of benthic biology on bottom boundary layer processes, Dry Tortugas Bank, Florida Keys. Geo-Marine Letters in press

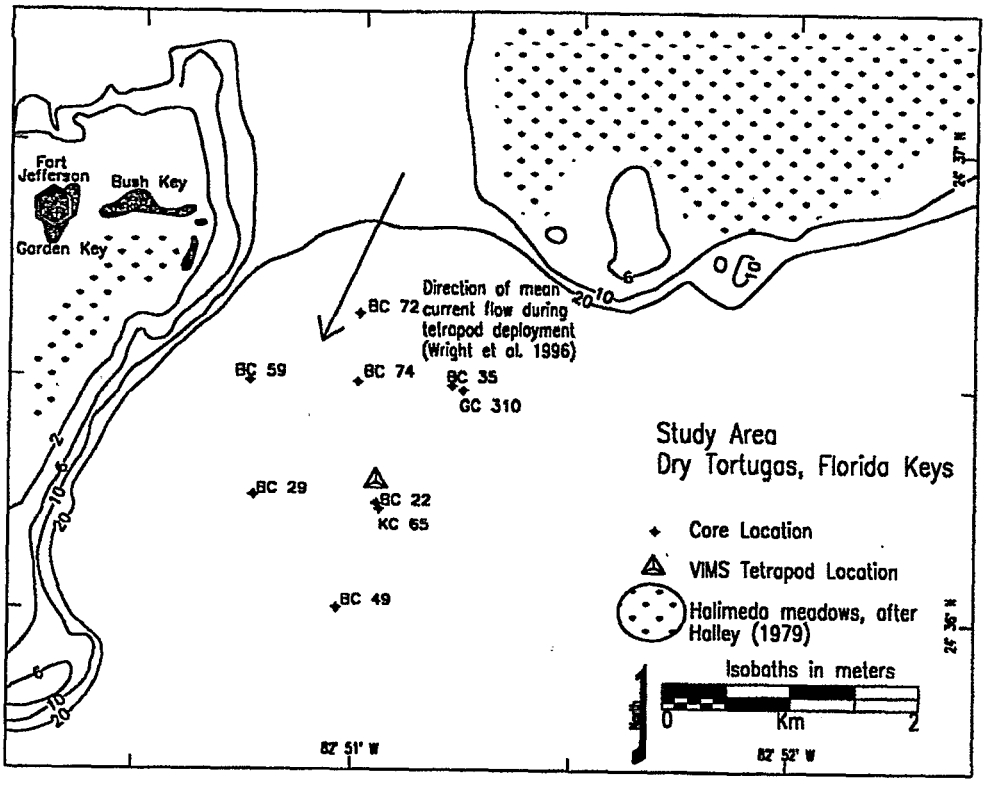

Figure 1 Map of study area, showing location of shallow-water *Halimeda* meadows (from Halley 1979) and direction of net current flow observed by Wright et al. (1996). The study area is down-current from a major source of carbonate particles.

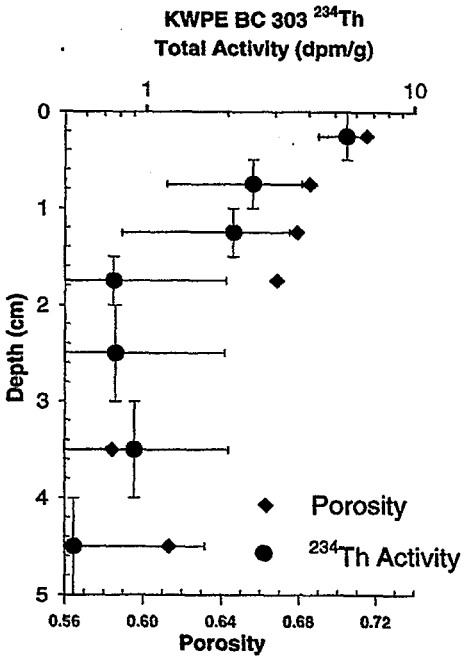

Figure 2 ^{234}Th activity and porosity profiles for KWPE BC303. Excess activity is restricted to the upper 2 cm, and the activity gradient is tracked by the porosity trend.

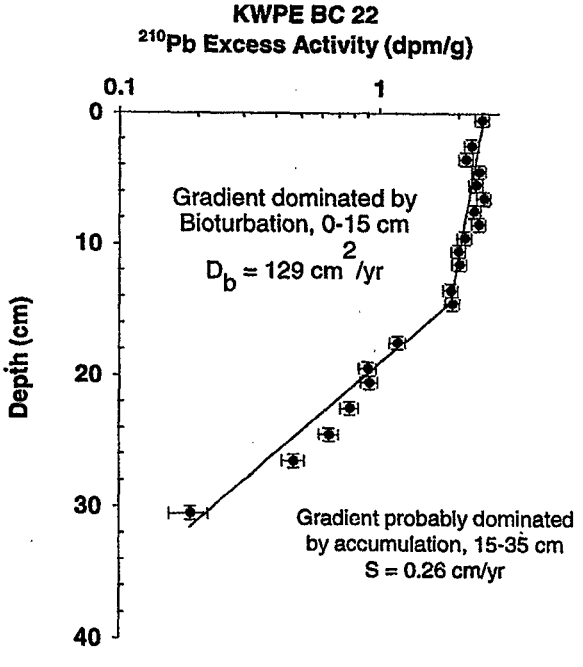

Figure 3 ^{210}Pb Excess Activity profile typical of Southeast Channel cores. The steep activity gradient in the surface layer is controlled by biological mixing, and the less steep gradient below 15 cm is probably controlled by the sediment accumulation rate.

4.2 Regional Comparison of Benthic Assemblages in the Lower Florida Keys (G.R. Lopez and A. D'Andrea)

Regional Comparison of Benthic Assemblages in the Lower Florida Keys

Glenn R. Lopez
Anthony D'Andrea

Marine Sciences Research Center
State University of New York
Stony Brook, NY 11794-5000

Benthic faunal samples were collected in three study areas of the lower Florida Keys for macrofauna abundance, functional-group composition, and bioturbation potential. The study areas included the Dry Tortugas, Marquesas, and stations between them. This report presents results from the Dry Tortugas and surrounding stations.

The benthic assemblage in the Dry Tortugas can be divided into two parts. The first is primarily a surface deposit feeding community dominated by the spionid polychaete *Prionospio cristata* and the oweniid polychaete *Myriochele oculata* (Table 1A). This community, dominated by surface deposit feeders and suspension feeders, is capable of mixing the top 1-4 cm of the sediment on short time scales (days to weeks) based on functional group and animal size. The second community is a deep-dwelling community dominated by large (>6 cm) *Notomastus* and *Callianassa* sp., a deep burrowing thallasinid shrimp (Table 2A). This deep community is dominated by carnivores/scavengers, deep deposit feeders, and head-down deposit feeders (Fig. 1B).

The benthic community at the intermediate stations has similar fauna to the Dry Tortugas community, but the animals tended to be much smaller (<1 cm). The

surface community was dominated by *M. oculata,* a surface deposit feeding polychaete (Table 1B) and abundances were an order of magnitude less than the Dry Tortugas (Fig 1A). Surface deposit feeders in the surface community were less important at the intermediate stations, and suspension feeders, shallow deposit feeders, and carnivores/scavengers were proportionally more important (Fig 1B). The deeper community at the intermediate stations were dominated by a small (<2 cm) sipunculan and capitellid polychaetes (Table 2B). The functional groups of the deep community at the intermediate stations were more evenly distributed in comparison to the Dry Tortugas with a noticeable absence of the large, deep deposit feeders common at depth in the Dry Tortugas.

The benthic assemblage at the Dry Tortugas includes a surface deposit-feeding community capable of mixing the top 2-4 cm on short time scales (days to weeks), and a deep community which can intensely bioturbate the deeper sediment layers. Both *Notomastus* and *Callianassa* have great potential for biogenic alterations of the deep layer. Fossil evidence indicates that this association may be geologically important. Benthic-boundary-layer processes suggest biological control of sediment structure in fair-weather conditions, and rapid removal of physical structure developed by storms. In contrast, the benthic community at the stations intermediate between the Dry Tortugas and Marquesas consists of a shallow (<10 cm) deposit-feeding community and should be important for shallow sediment structure on short time scales. However, the community may be dominated by physical processes, particularly during storm conditions, due to low abundances and small animal sizes at these stations.

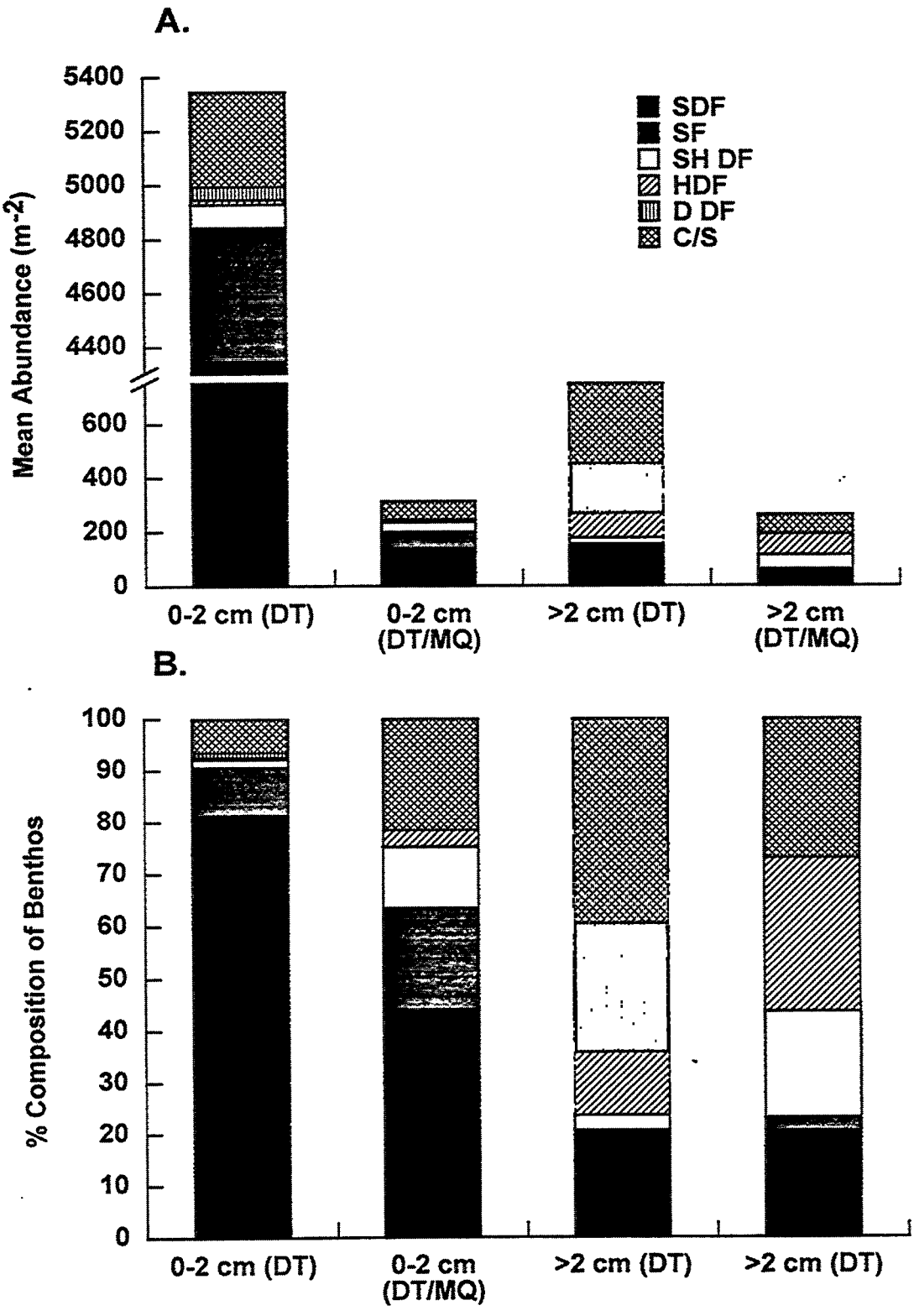

Figure 1 Mean abundances (A) and % composition (B) of functional groups at the Dry Tortugas tetrapod station (DT) and stations between the Dry Tortugas and Marquesas (DT/MQ). The results are divided into 0-2 cm and > 2 cm depth intervals. SDF = surface deposit feeders; SF = suspension feeders; SH DF = shallow deposit feeders; HDF = tubicolous head-down deposit feeders; D DF = deep-burrowing deposit feeders; C/S = carnivores, omnivores, and scavengers.

Table 1. Rank order, functional group, and mean abundances of major benthic fauna in the top 2 cm at the Dry Tortugas tetrapod site (A) and at stations intermediate between the Dry Tortugas and Marquesas. (B). SDF = surface deposit feeders; SF = suspension feeders; SH DF = shallow deposit feeders; HDF = tubicolous head-down deposit feeders; D DF = deep-burrowing deposit feeders; C/S = carnivores, omnivores, and scavengers.

A. Dry Tortugas

Species	Functional Group	Mean Abundance (m^{-2})
Prionospio cristata	SDF	3052.5
Myriochele oculata	SDF	539.0
Pseudocyrena sp.	SDF	466.5
Leptochelia sp.	SDF	389.5
Tellinid Bivalves (4 spp.)	SDF	217.4
Diplodonta sp.	SF	203.8
Lucina nassula	SF	176.6
Gammarid amphipods (3 spp.)	SDF	126.8
Penaeid shrimp (2 spp.)	S/C	117.8
Cyclaspis sp.	SDF	90.6
Caprellid amphipod	S/C	81.5
Sabellid sp.	SF	63.4
Corbula sp.	SF	54.4
Syllid sp.	S/C	54.4
Armandia maculata	Sh DF	54.4
	OVERALL ABUNDANCE:	**5344.2**

B. Intermediate Stations

Species	Functional Group	Mean Abundance (m^{-2})
Myriochele oculata	SDF	46.9
Holothurian	SH DF	26.8
Mulinia lateralis	SF	26.8
Corophiid amphipod	SDF	26.8
Polynoid sp.	C/S	23.5
Caprellid amphipod	C/S	16.8
Lima sp.	SF	13.4
Leptochelia sp.	SDF	13.4
Macoma tenta	SDF	13.4
Lucina nassula	SF	10.1
Amphiurid Brittlestar	SDF	10.1
Sipunculan	SH DF	6.7
Glycera sp.	C/S	6.7
Ampelisca sp.	SDF	6.7
Prionospio cristata	SDF	6.7
	OVERALL ABUNDANCE:	**312.1**

Table 2. Rank order, functional group, and mean abundances of major benthic fauna at depths > 2 cm at the Dry Tortugas tetrapod site (A) and at stations intermediate between the Dry Tortugas and Marquesas. (B). SDF = surface deposit feeders; SF = suspension feeders; SH DF = shallow deposit feeders; HDF = tubicolous head-down deposit feeders; D DF = deep-burrowing deposit feeders; C/S = carnivores, omnivores, and scavengers.

A. Dry Tortugas

Species	Functional Group	Mean Abundance (m^{-2})
Notomastus sp.	D DF	113.2
Caprellid amphipod	S/C	95.1
Lumbrineris verilli	S/C	72.5
Penaeid shrimp (2 spp.)	S/C	72.5
Prionospio cristata	SDF	58.9
Tellinid bivalves (4 spp.)	SDF	49.8
Callianassa sp.	D DF	40.8
Maldanid sp.	HDF	40.8
Capitellid sp.	HDF	31.7
Sipunculan worm (2 spp.)	D DF	31.7
	OVERALL ABUNDANCE:	**747.3**

B. Intermediate Stations

Species	Functional Group	Mean Abundance (m^{-2})
Sipunculan	SH DF	33.6
Capitellid sp.	HDF	30.2
Tubificid sp.	HDF	23.5
Corophiid amphipod	SDF	20.1
Syllid sp.	C/S	20.1
Prionospio cristata	SDF	13.4
Glycera sp.	C/S	13.4
Phyllodoce sp.	C/S	13.4
Capitella capitata	HDF	10.1
Mediomastus californiensis	HDF	10.1
	OVERALL ABUNDANCE:	**261.7**

5.0 Geochemistry

5.1 Pore Water Chemistry in Carbonate Sediments of the Dry Tortugas and Marquesas Keys—Implications for Sediment Structure (A. Shiller)

PORE WATER CHEMISTRY IN CARBONATE SEDIMENTS OF THE DRY TORTUGAS AND MARQUESAS KEYS--IMPLICATIONS FOR SEDIMENT STRUCTURE

Alan M. Shiller

Institute of Marine Sciences, University of Southern Mississippi, Stennis Space Center, MS 39529; ashiller@whale.st.usm.edu

Small diagenetic changes in sediments are often reflected in much larger changes in the composition of certain elements dissolved in interstitial waters. For the carbonate sediments of the Dry Tortugas and Marquesas Keys, it is expected that oxidation of organic matter will be a driving force for carbonate dissolution and precipitation. We examined the pore water chemistry in short cores from four locations in the Dry Tortugas and one location near the Marquesas Keys. Because major elements and the sulfate system were examined by others during this project, we focused on minor element chemistry.

A preliminary framework for examining pore water chemistry in this region can be drawn from the work of Rude and Aller, 1991 (Geochim. Cosmochim. Acta 55: 2491) who examined pore water chemistry in cores from Florida Bay (Bob Allen Key Bank near Plantation Key). They observed increases in dissolved Ca^{2+}, Sr^{2+}, and F^- in the upper few cm of their core, consistent with net carbonate dissolution driven oxic respiration and nitrate reduction. Deeper into their cores, SO_4^{2-} is greatly reduced and concomitant decreases in $Ca^{2+}$and Sr^{2+} indicate net carbonate precipitation. Because $SrCO_3$ is isostructural with aragonite, the Sr^{2+} decrease indicates the likelihood of aragonite precipitation. However, continued increase in pore water F^- with depth as well as undersaturation of high-magnesian carbonate,

suggests that the overall process is one of dissolution of high-magnesian carbonate and precipitation of aragonite.

In our cores, oxygen is depleted in the upper 1 cm but no evidence of SO_4^{2-} removal is observed down to 30 cm. Thus, these cores are suboxic. Pore water Mn^{2+} concentrations are low and show maxima near 5 cm, indicating removal of Mn^{2+} into carbonate below this. Sr^{2+} shows a slight increase in the upper 10 cm followed by a slight (<10%) decrease. This is similar to, though of lesser magnitude than, the changes observed by Rude and Aller. F^- shows a small minimum near 10 cm, suggested that with the reduced amount of carbonate dissolution (compared with Rude and Aller's cores) we are observing F^- incorporation into apatite. The slight increase in F^- below the minimum is compatible with continued dissolution of high-magnesian calcite. Several other minor elements were determined in the pore waters. Li and Rb show minimal change. U and Mo show sharp transitions below the Mn maximum which may be related to cycling of Fe.

There are several implications of this work for the CBBL program. First, the overall carbonate dissolution/precipitation process is likely to be one of high-magnesian calcite dissolution and aragonite precipitation. Net dissolution will occur in the upper oxic/suboxic core depths whereas net precipitation will occur in the more strongly suboxic and anoxic depths. In short cores from the Dry Tortugas and Marquesas Keys, the pore water data indicate that these processes are of minimal importance and thus likely to have minimal effect on sediment structure. Deeper into the sediments this may not be true. Comparing our results with those from Florida Bay suggests (in accord with previous work) that the extent of carbonate diagenesis and the depth at which it has an appreciable effect on sediment structure is likely controlled by input of organic matter to surface sediments. Other factors of relevance are likely to be bioturbation and physical mixing (which should increase the rates of oxic and suboxic organic matter oxidation) and long-term

environmental changes (which can lead to changes in the initial amount of deposited organic matter).

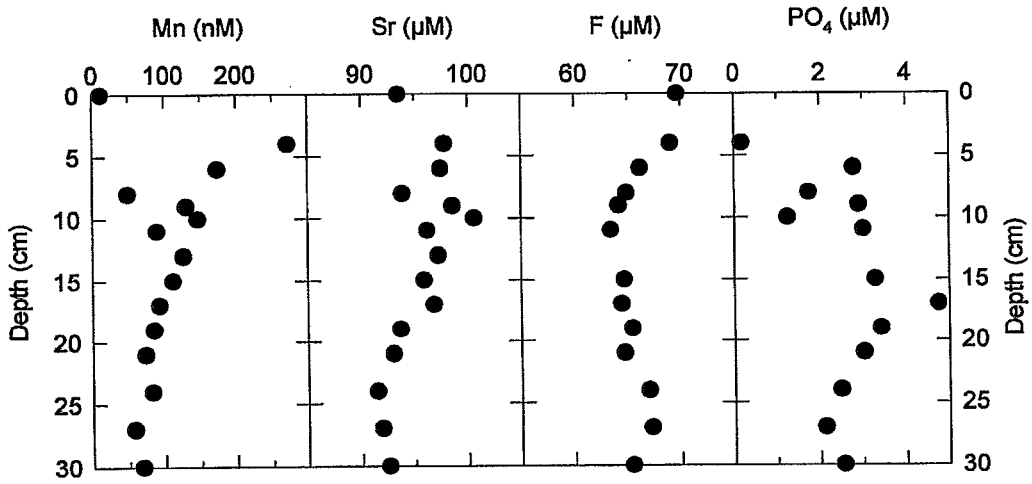

BC141
Dry Tortugas
Planet Site

5.2 A Geochemical Investigation of Early Diagenetic Effects on Sedimentary Structures (Y. Furukawa and D. Lavoie)

A Geochemical Investigation of Early Diagenetic Effects on Sedimentary Structures

Yoko Furukawa[1] and Dawn Lavoie[2]

[1]Institute of Marine Sciences, University of Southern Mississippi, Stennis Space Center, MS 39529(601) 688-5474, (601) 688-5752 (FAX), yokof@zephyr.nrlssc.navy.mil.

[2]Naval Research Laboratory, Code 7431, Stennis Space Center, MS 39529 (601) 688-4659, (601) 688-5752 (FAX), lavoie@zephyr.nrlssc.navy.mil

Early diagenesis affects the sediment fabric and structure in the Holocene carbonate sediments of Dry Tortugas test site. The most dominant processes are: (1) mechanical breakdown of biogenic carbonate grains into clay-sized matrix particles due to the sediment reworking caused by storms and bioturbation, and (2) subsequent change in the particle morphology among the matrix particles. The mechanical breakdown of skeletal carbonate grains, mostly fragments of *Halimeda* plates, is apparent as some *Halimeda* fragments show the features of partial breakdown (Figure 1) and as matrix is dominated by well-crystallized aragonite needles (Figure 2). The change in particle morphology is quantified by the decrease in the average aspect ratio: the matrix particles in older sediments are more rounded (Figures 3 and 4).

Geochemical models of early sedimentary diagenesis CANDI 1.2 (Boudreau, 1996, 1997) and STEADYSED1 (Van Cappellen and Gaillard, 1996; Van Cappellen and

Wang, 1996; Wang and Van Cappellen, 1996) have been used to model the amount of dissolution and precipitation within the upper 200 cm of the sediments. The preliminary modeling using CANDI 1.2 indicates that the volume of the sedimentary solids at 26 cmbsf may have increased by approximately 4 % due to calcite and aragonite precipitation since their deposition. Please note that this number is likely to be revised as this ongoing study progresses: the preliminary calculations used a rather small sedimentation rate (0.05 cm/a) and the models have not incorporated the simultaneous handling of the Ca^{2+} - CO_2 - H_2O system. See Bentley and Nittrour in this volume for the updated sedimentation rate.

The modeled solid volume change is not supported by the fabric change such as the production of cement, however. This may be due to the proton produced by the reoxidation of aqueous sulfide and bisulfide. Partial reduction and reoxidation of seawater sulfate have been shown to promote the dissolution of calcium carbonate phases using thermodynamic models (e.g., Stoessell, 1992). Once the simultaneous handling of the Ca^{2+} - CO_2 - H_2O system is included, the codes used in this study will be able to model the relationship between such recycling processes and the thermodynamics of calcium carbonate phases.

REFERENCES

Boudreau, B. P. (1996) A method-of-lines code for carbon and nutrient diagenesis in aquatic sediments. Computers & Geosciences 22, 479-496.

Boudreau, B. P. (1997) Diagenetic models and their implementation: modeling transport and reactions in aquatic sediments. Springer. New York.

Stoessell, R. K. (1992) Effects of sulfate reduction on CaCO3 dissolution and precipitation in mixing-zone fluids. Journal of Sedimentary Petrology 62, 873-880.

Van Cappellen, P. and Gaillard, J-F. (1996) Biogeochemical dynamics in aquatic sediments. In Reactive Transport in Porous Media (eds. Lichtner, P., Steefel, C. I., and Oelkers, E. H.), Chapter 8, Reviews in Mineralogy Volume 34.

Van Cappellen, P. and Wang, Y. (1996) Cycling of iron and manganese in surface sediments: A general theory for the coupled transport and reaction of carbon,

oxygen, nitrogen, sulfur, iron and manganese. American Journal of Science, 296, 197-243.

Wang, Y. and Van Cappellen, P. (1996) A multicomponent reactive transport model of early diagenesis: Application to redox cycling in coastal marine sediments. Geochimica et Cosmochimica Acta, 60, 2993-3014.

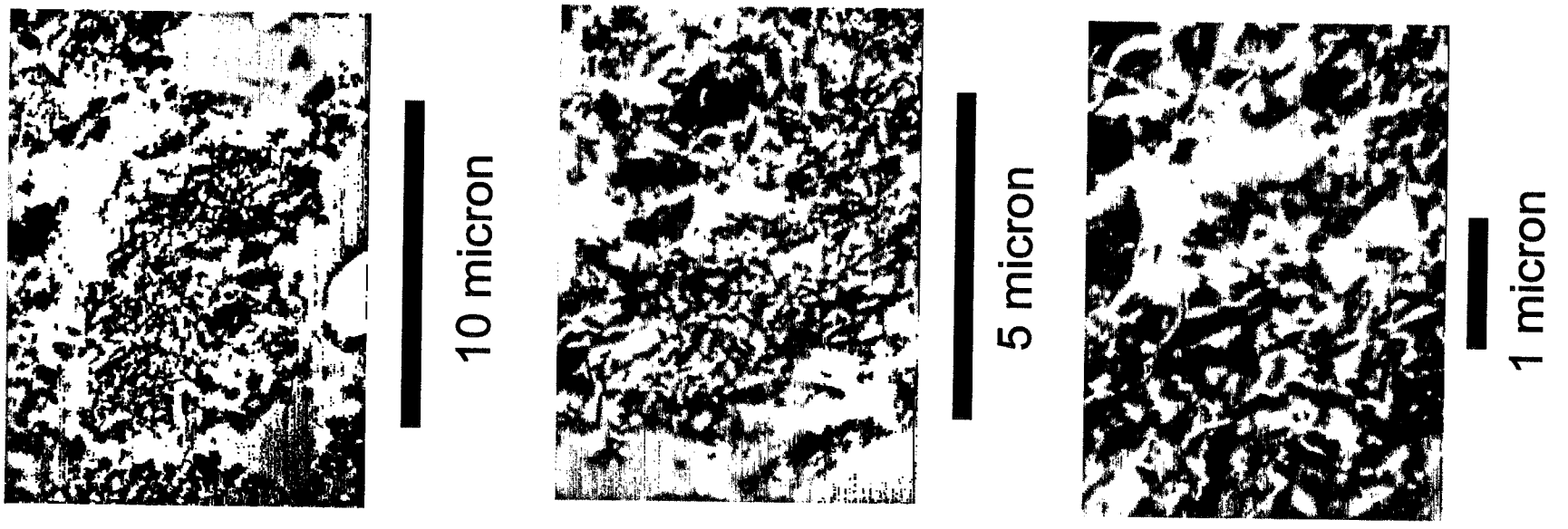

Figure 1. Transmission electron microscope (TEM) images of a fragment of Halimeda plates at various scales. Whereas the structure is dominated by the dense, random packing of aragonite needles, it is partially altered to exhibit the looser aggregation of particles with varied morphology.

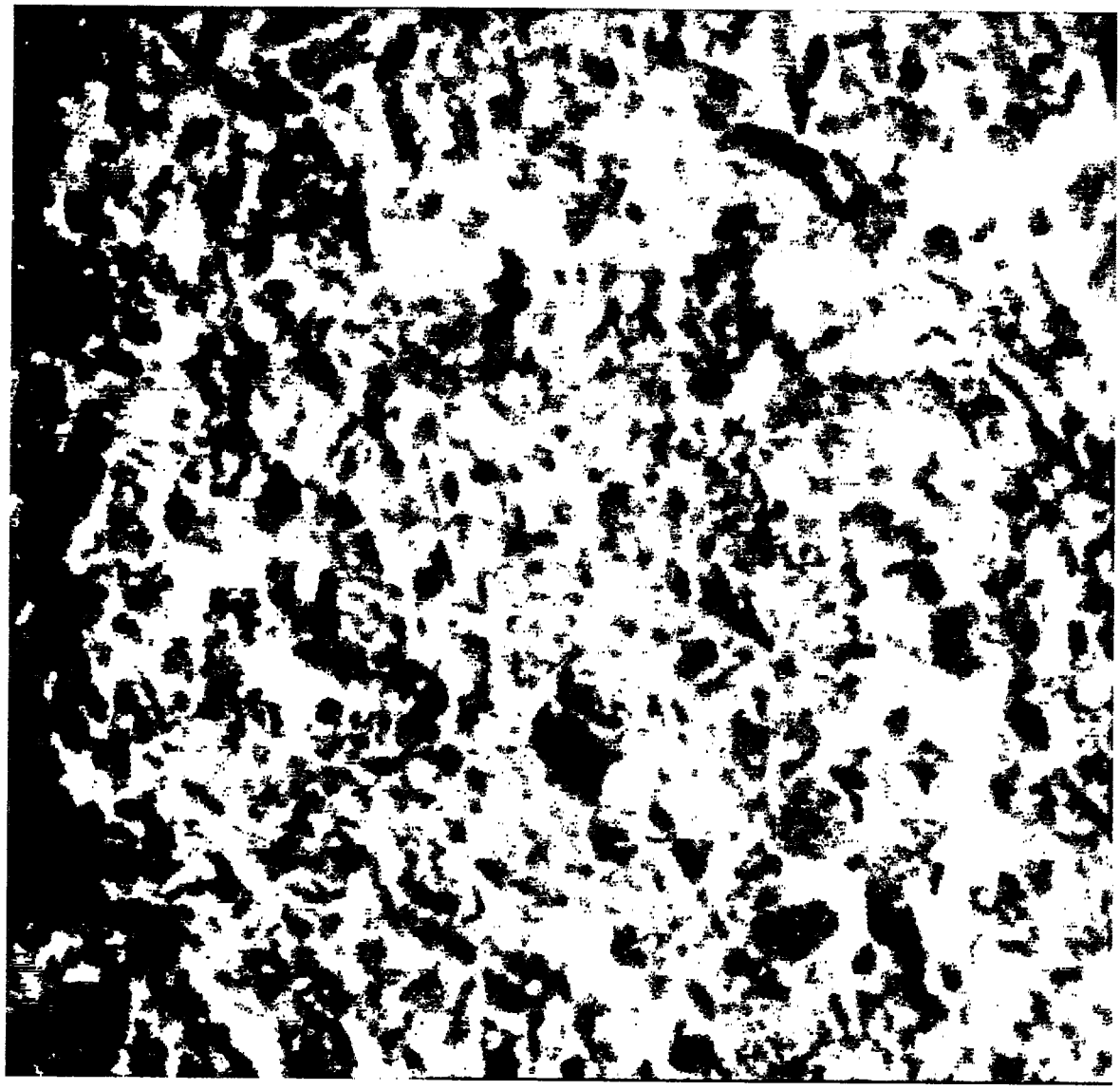

4 micron

Figure 2. A TEM image of the matrix fabric. The undisturbed sample was air-dried and impregnated in Spur's resin before ultra-thin sectioning. The most particles resemble the aragonite needles within the skeletal remains of Halimeda (see Figure 1).

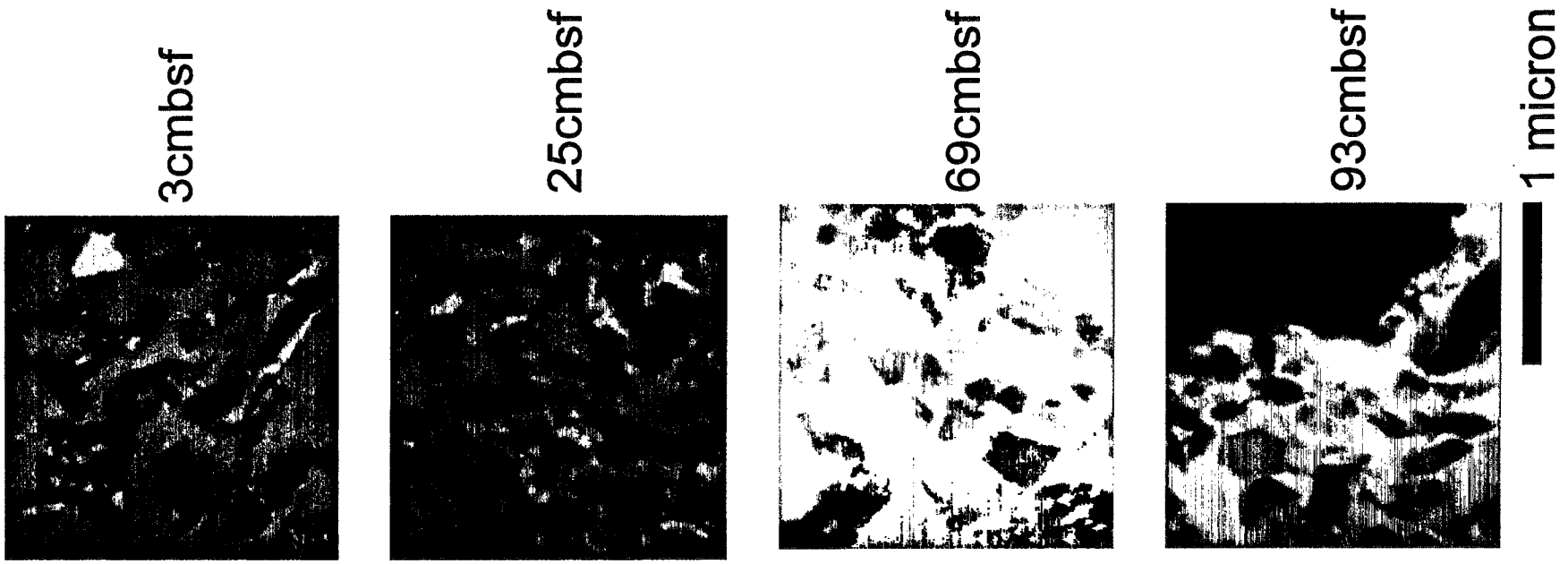

Figure 3. Transmission electron microscope (TEM) images of matrix fabric. The undisturbed samples were air-dried and impregnated with Spur's resin before ultra-thin sectioning. Matrix particles in recent sediments are angular and elongated whereas those in older sediments are rounded and more equi- dimensional.

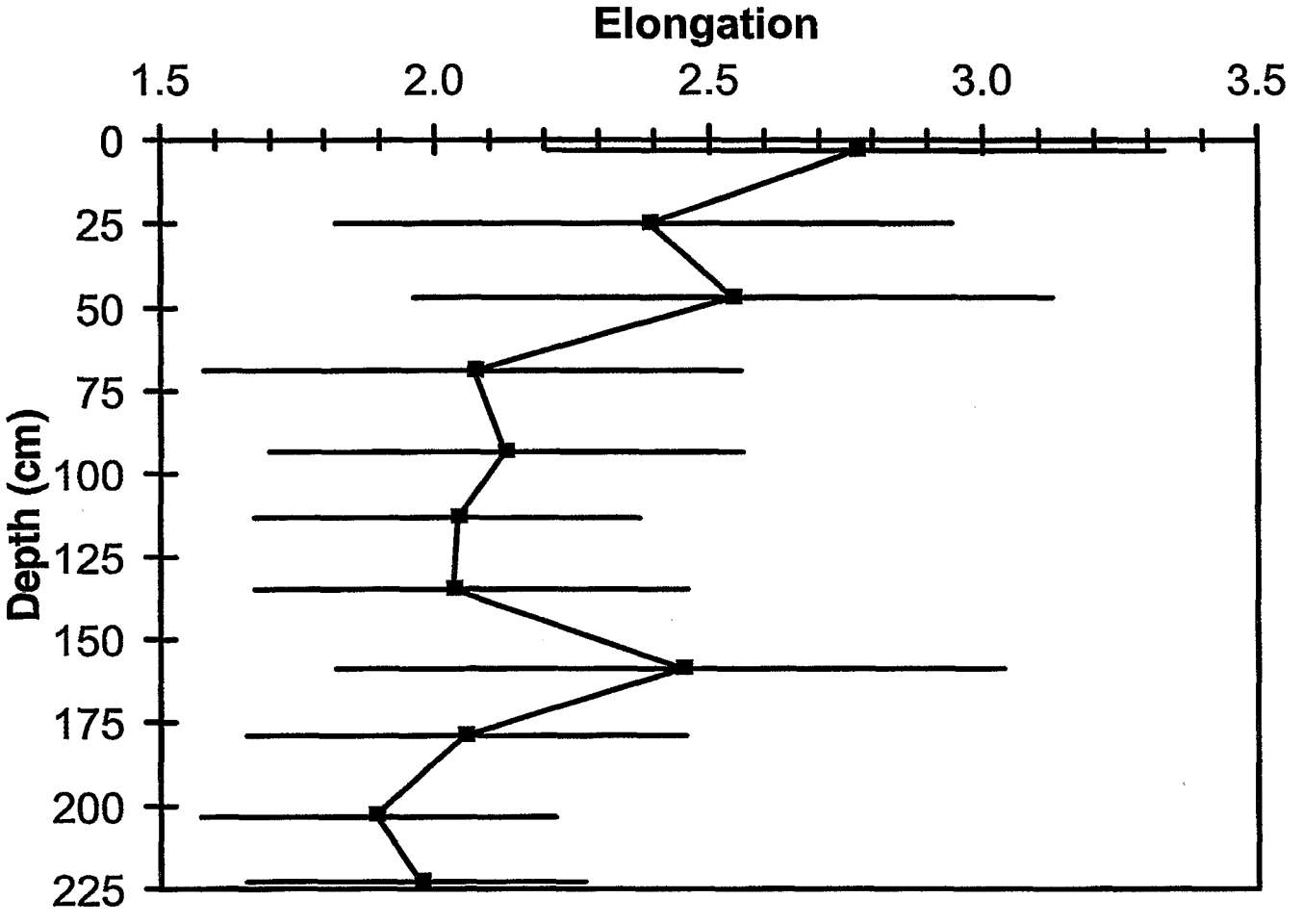

Figure 4. The depth profile of the average aspect ratio (the ratio of long axis to short axis). The averages are calculated from approximately 50 to 100 particles.

6.0 Sediment Structure

6.1 Geoacoustic and physical properties of carbonate sediments of the Lower Florida Keys. (M.D. Richardson, D.L. Lavoie, K.B. Briggs and K.P. Stephens)

Geoacoustic and physical properties of carbonate sediments of the Lower Florida Keys

M.D. Richardson, D.L. Lavoie, K.B. Briggs and K.P. Stephens

Marine Geosciences Division
Naval Research Laboratory
Stennis Space Center MS 39529-5004, USA

Abstract:

Near-surface sediment geoacoustic and physical properties were measured from a variety of unconsolidated carbonate sediments in the Florida Keys. Surficial values of compressional and shear speed correlate with sediment physical properties and near surface acoustic reflectivity. The highest speeds (shear 125-150 m s^{-1}; compressional 1670-1725 m s^{-1}) are from sandy sediments near Rebecca Shoal and the lowest (shear 40-65 m s^{-1}; compressional 1520-1570 m s^{-1}) are found in soft, silty sediments which collect in sediment ponds in the Southeast Channel of the Dry Tortugas. High compressional wave attenuation is attributed to scattering of acoustic waves from abundant shell material rather than high intrinsic attenuation. Compared to siliciclastic sediments, carbonate sediment compressional and shear wave speeds are high for comparable values of sediment physical properties. Sediment fabric, rather than changes due to the effects of biogeochemical processes, is responsible for these differences.

Introduction

Sediment structure is a direct result of the biological, geological, biogeochemical, and hydrodynamic processes which operate at the benthic boundary layer (Richardson 1994). This structure, in turn, determines sediment bulk properties (e.g., porosity, grain size distribution, density, permeability, etc.), sediment behavior (e.g., geoacoustic and rheologic) under various stress-strain conditions, and sediment acoustic properties such as propagation and scattering of high-frequency acoustic sound within or at the seafloor. Interrelationships among environmental processes, sediment structure, and sediment properties and behavior are being studied and modeled for a variety shallow-water environments by the Office of Naval Research's Coastal Benthic Boundary Layer (CBBL) program (Richardson 1994). This contribution is part of a special workshop dedicated to preliminary results of CBBL experiments in shallow-water, carbonate sedimentary environments of the lower Florida Keys.

In this paper, we present data on the spatial variations of surficial geoacoustic and physical properties from shallow-water carbonate sediments in the lower Florida Keys. Empirical predictive relationships among sediment geoacoustic and physical properties are compared to analogous relationships derived from siliciclastic sediments. The effects of the biogeochemical processes (dissolution, precipitation and cementation), sediment fabric (particle characteristics, spatial arrangements), dilution, and grain size distribution on sediment geoacoustic behavior are investigated.

Experimental Setting

Sediments in this study come from a low-to-moderate energy depositional basin (Dry Tortugas experimental site), a high energy shallow marine environment (Marquesas experimental site), and a highly mobile, biogenic sand shoal (Rebecca Shoal) all within the Lower Florida Keys (Fig. 1).

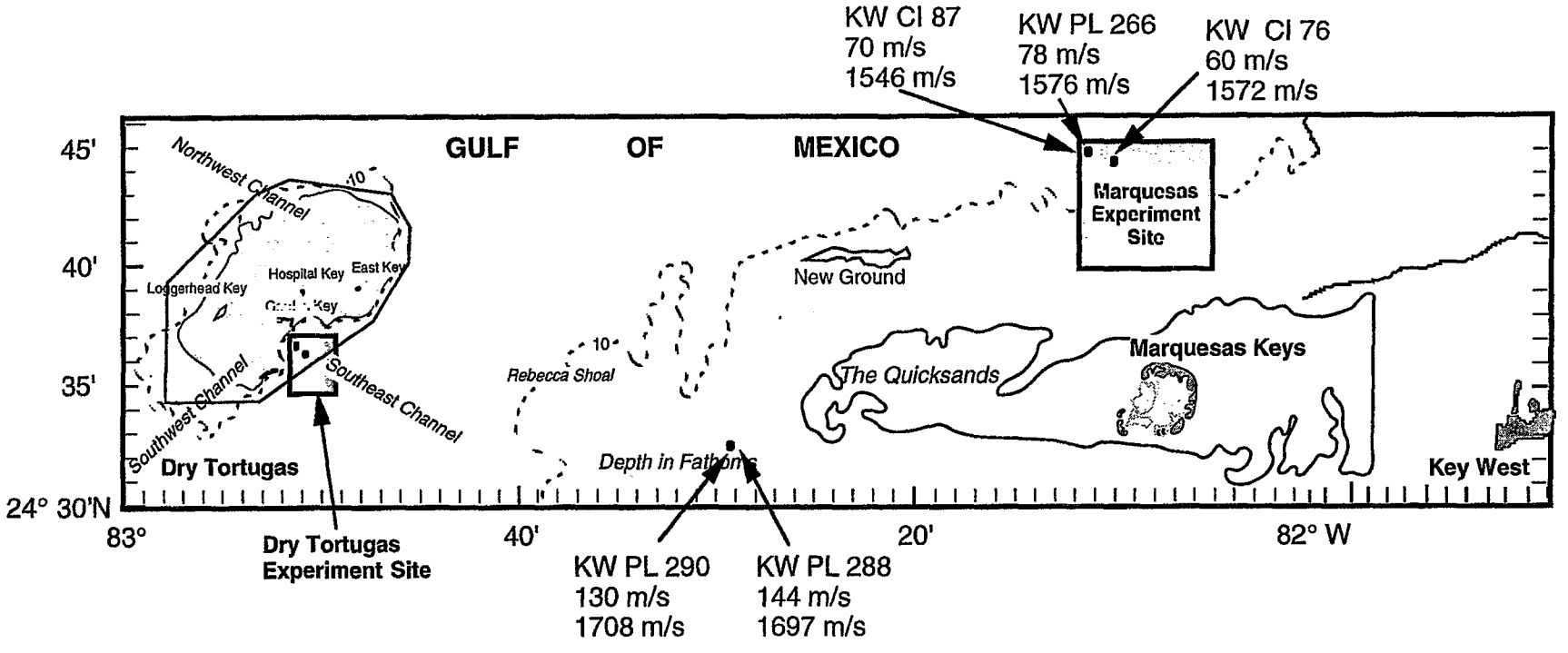

Figure 1. Experimental site locations with values of compressional and shear wave speeds for sites north of the Marquesas Keys and in Rebecca Shoal.

The Dry Tortugas experiment site, located in the Southeast Channel of the Dry Tortugas in waters depths of 18-25 meters, is approximately 130 km west of Key West and lies within the Fort Jefferson National Monument protected area. The site is well protected from both the prevailing weather and the local trawlers. Bed stresses, primarily due to tidal currents, only occasionally exceeds the threshold for sediment transport. Thus, the Dry Tortugas site is a low energy, sediment sink with most sediments presumably being derived from the Dry Tortugus Bank just to the north. The Holocene sediments of the Dry Tortugas are very poorly sorted sand-silt-clays with 85-95% carbonate. Holocene sediment thickness, 2-5 meters, thins southward to yield an outcropping of Key Largo Limestone and patch reefs. Surficial sediment becomes coarser because of the contribution of particles from the outcrop and patch reefs. Sediments primarily consist of aragonite plates and needles derived from the breakdown of aragonite green algae (*Halimeda*, *Penicillus*, and *Udeota)*, molluscan shells, benthic and planktonic foraminifera, echinoid spines, sponge and coral fragments, diatoms, and less than 5% particles of siliciclastic origin (quartz and clay minerals).

The Marquesas experiment site is located north of the Marquesas Keys in water depths ranging from 10-30 meters. This area is exposed to the prevailing weather conditions, such as winter storms and unpredictable hurricanes. Sediments in the Marquesas experiment area are derived from erosion of the Marquesas Keys, a circular accumulation of *Halimeda* sand spits and beaches approximately 30 km west of Key West, and become progressively finer in a northerly direction. Sediments, like those in the Dry Tortugas site, are very poorly sorted sand-silt-clays, but with a greater percentage gravel-size molluscan shells. Sediment particle types are similar to the Dry Tortugas site.

Between Rebecca and Half Moon Shoals, an area of highly mobile *Halimeda* sand forms east-west ridges up to 3-m high in response to strong tidal currents. Sediments are well-sorted, medium sand consisting primarily of fragments of

Halimeda and other algae plates which are abundant on the shallow Quicksands west of Halfmoon Shoal. The strong tidal currents probably winnow out any fine-grained material.

Methods

Values of near-surface sediment geoacoustic and physical properties were determined using in situ probes and from laboratory analysis of sediments collected with gravity, box and diver-collected cores (Figs. 1 and 2). Data were collected mostly during the February 1995 field season with stations 76, 87 and 121 occupied during presite surveys in February 1994.

In situ sediment geoacoustic properties were measured remotely using a hydraulically-operated platform that drives geoacoustic probes into sediments (Griffin et al. 1996) or a diver-deployed version of the same system (Barbagelata et al. 1991). Compressional wave speed and attenuation, and shear wave speed were measured over pathlengths ranging from of 30 to 100 cm at depths of 5–30 cm below the sediment-water interface. For compressional wave measurements, transmit pulses were driven utilizing 38-kHz pulsed sine waves and time delays and voltages were used to determine values of speed and attenuation between identical radial-poled ceramic cylinders. Actual values of compressional wave speed and attenuation were calculated by comparison of received signals transmitted through the sediment with those transmitted through seawater overlying the sediments. For comparison to other studies, compressional wave speed is also reported as compressional wave velocity ratio (ratio of in situ sediment sound speed to the sound speed of overlying water) and attenuation is expressed as k, in units of dB m^{-1} kHz^{-1} . Shear wave speed was measured as time-of-flight between bimorph bender elements mounted in flexible silicone rubber mounts and driven at 0.25 to 2.0 kHz.

After the cores were acoustically logged, sediments were subsampled at 2-cm intervals for grain size distribution, grain density, porosity, and wet bulk density. Where possible, sediment physical properties (Table 1) were derived from the diver-collected cores as surficial sediments are less disturbed during diver-collection than by gravity coring. Porosity was measured at 2-cm intervals on the sediment core samples by weight loss from samples kept in a drying oven at 105° C for 24 hours, or by weight-volume techniques using the Quantachrome multi-pycnometer helium gas pycnometers. Grain density was measured using a Quantachrome Penta-pycnometer. Sediment bulk density was either calculated from the measured values of grain density, porosity or directly determined from the weight-volume techniques. Sediment grain size distribution was determined by dry sieving for gravel- and sand-sized particles and with a Micromeritics sedigraph for silt- and clay-sized particles.

Results and discussion:

The highest wave speeds (shear 125-150 m s^{-1}; compressional 1670-1725 m s^{-1}) were measured in sandy sediments near Rebecca Shoal and the lowest (shear 40-65 m s^{-1}; compressional 1520-1570 m s^{-1}) measured from ponded, soft sediments near the Dry Tortugas (Figs. 1 and 2; Table 1). In the Dry Tortugas, where the majority of in-situ measurements were made, wave speeds decrease with depth of the ponded Holocene sediments and distance from underwater reefs and increase with acoustic reflectivity. The distribution of geoacoustic properties correlates with the areal distribution of surficial sediment physical properties including grain size, porosity and sediment bulk density which supports the proposed links between environmental process, sediment physical properties and sediment geoacoustic behavior. As a first order correlation, sediment physical and thus geoacoustic properties are controlled by depositional processes including proximity to the source of particles and to hydrodynamic processes which distribute particles. Higher compressional and shear speeds are associated with higher energy environments and shorter distances from particle source.

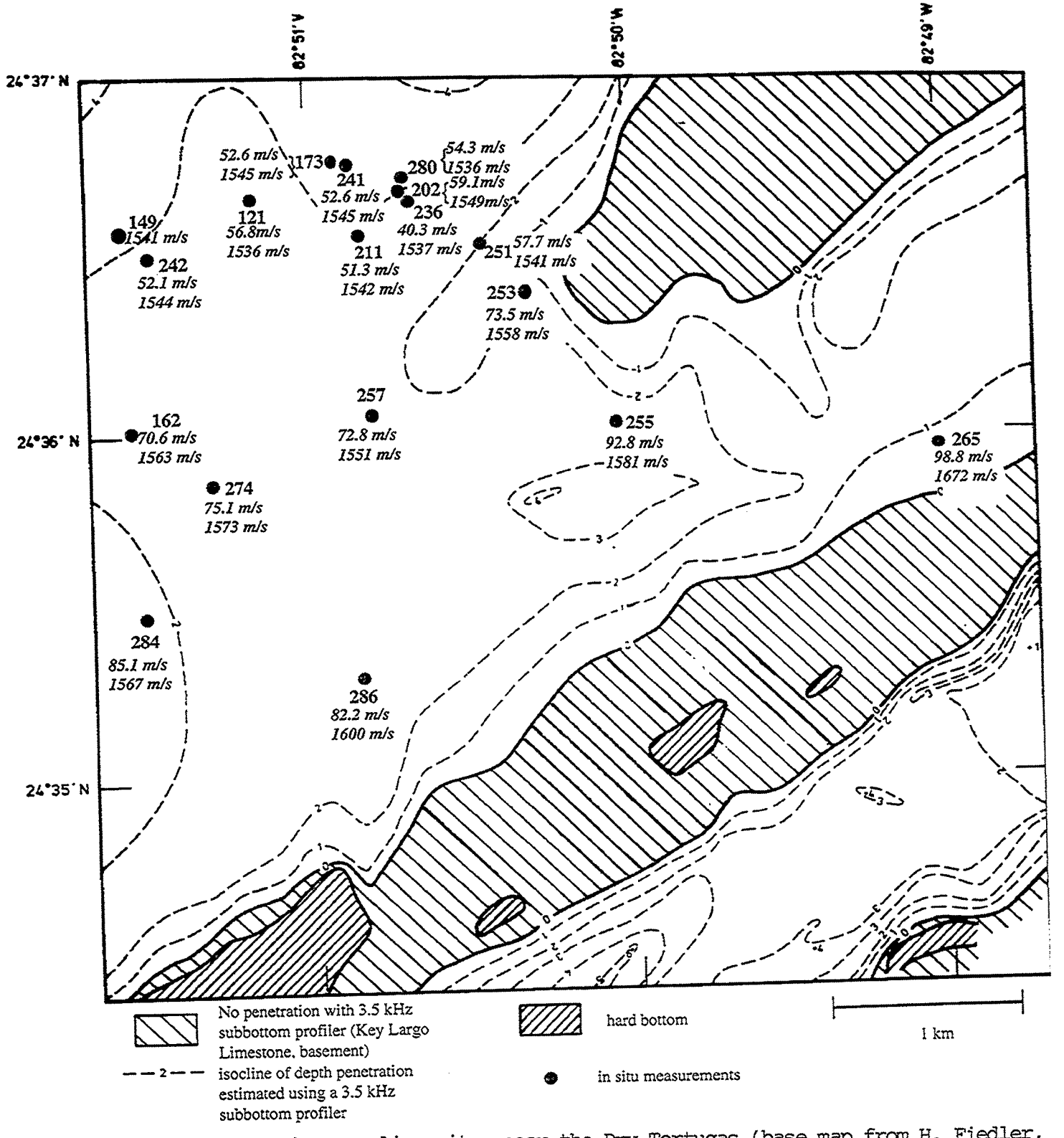

Figure 2. In situ sampling sites near the Dry Tortugas (base map from H. Fiedler, FWG) with values of shear and compressional speeds.

Table 1: Mean and Range of sediment physical and geoacoustic propertites for carbonate sediments in the lower Florida Keys.

Station	Vp (m/s)	Attenuation (dB/m)	Vs (m/s)	Wet Bulk Density (g/cm^3)	Porosity (%)	Mean Grain Size (Phi)
76	1571 (1557-1587)		59.8 (53-70)	1.73 (1.52-1.83)	59.3 (53.7-70.7)	5.3 (4.7-6.7)
87	1547 (1537-1561)		70.2 (70-71)	1.73 (1.57-1.86)	59.1 (52.0-67.6)	6.3 (4.6-8.4)
121	1532 (1506-1543)		56.8 (50-68)	1.73 (1.55-1.86)	56.8 (53.4-69.4)	6.5 (6.2-7.1)
149	1541 (1533-1547)	19.1 (18-20)		1.77 (1.68-1.84)	56.6 (52.7-61.3)	5.9 (6.2-5.6)
162	1563 (1562-1564)	23.7 (23-24)	70.6 (61-76)	1.79 (1.56-1.92)	55.9 (50.9-64.4)	5.0 (5.8-4.5)
173	1536 (1534-1537)	23.1 (19-27)	55.1 (50-64)	1.75 (1.48-1.85)	59.3 (54.3-73.9)	5.6 (5.9-5.2)
202	1549 (1546-1550)	19.9 (19-23)	59.1 (50-69)	1.78 (1.55-1.87)	63.1 (57.6-70.1)	6.6 (6.2-6.9)
211	1542 (1533-1547)	19.0 (14-29)	51.3 (47-60)	1.79 (1.66-1.86)	57.5 (53.4-64.5)	6.2 (4.9-7.8)
236	1537 (1524-1555)	12.9 (10-18)	40.2 (28-56)	1.77 (1.53-1.85)	57.9 (54.4-71.0)	6.8 (6.8-6.1)
241	1545 (1526-1563)	12.7 (9-18)	52.5 (38-66)	1.77 (1.53-1.85)	57.9 (54.4-71.0)	6.8 (6.8-6.1)
242	1544 (1532-1559)	12.3 (9-17)	52.1 (46-60)	1.78 (1.55-1.87)	63.1 (57.6-70.1)	6.6 (6.2-6.9)
251	1541 (1530-1555)	14.7 (6-23)	57.7 (49-63)			6.8
253	1558 (1544-1571)	13.9 (7-18)	73.5 (62-88)			5.9
255	1581 (1566-1592)	23.2 (19-27)	92.8 (83-110)			5.2
257	1551 (1537-1562)	14.3 (9-18)	72.8 (61-97)	1.75 (1.57-1.86)	58.1 (53.7-69.0)	6.1
265	1672 (1642-1697)	28.8 (21-43)	98.8 (75-116)	2 (1.99-2.01)	45.3 (44.7-46.9)	1.1 (1.4-1.0)
266	1576 (1546-1637)	19.9 (8-35)	78.2 (51-118)	1.76 (1.66-1.87)	57.8 (51.4-63.7)	6.5 (5.8-6.8)
274	1573 (1552-1602)	15.4 (7-24)	75.1 (52-91)	1.84 (1.56-1.92)	53.2 (50.9-64.4)	6.1
280	1536 (1518-1548)	10.8 (3-16)	54.3 (39-67)	1.75 (1.51-1.87)	59.0 (53.0-72.5)	6.9 (6.4-7.5)
284	1567 (1551-1589)	14.6 (8-23)	85.1 (74-91)	1.85 (1.77-1.81)	53.8 (52.8-58.1)	5.9
286	1600 (1589-1616)	23.2 (19-28)	82.2 (77-91)			3.4
288	1697 (1668-1725)	18.1 (12-25)	143.8 (129-154)	2.02 (2.00-2.05)	43.7 (42.1-45.1)	1.3 (1.1-1.5)
290	1708 (1684-1728)	25.5 (14-33)	129.6 (123-140)	2.06 (2.00-2.09)	41.5 (39.7-45.1)	1.2 (1.3-1.9)

Table 2: Linear regression equations and coefficients of determination for siliciclastic and carbonate sediments.

Relationship	Siliciclastic Sediments	R^2
Vs v. Porosity	$y = 0.0635x^2 - 9.940x + 399.006$	0.918
Vs v. Wet Bulk Density	$y = 225.910x^2 - 612.945x + 424.151$	0.933
Vs v. Mean Grain Size	$y = 0.0148x^2 - 9.965x + 118.546$	0.91
Vp-ratio v. Porosity	$y = 0.000138x^2 - 0.020x + 1.703$	0.947
Vp-ratio v. Wet Bulk Density	$y = 0.463x^2 - 1.327x + 1.917$	0.933
Vp-ratio v. Mean Grain Size	$y = 0.000233x^2 - 0.0188x + 1.144$	0.975
Attenuation v. Porosity	$y = 0.0244x^2 - 3.699x + 142.035$	0.766
Attenuation v. Wet Bulk Density	$y = 79.360x^2 - 218.433x + 151.68$	0.735
Attenuation v. Mean Grain Size	$y = -0.381x^2 + 1.019x + 29.071$	0.867
Relationship	**Carbonate Sediments**	**R^2**
Vs v. Porosity	$y = 0.149x^2 - 19.509x + 690.415$	0.829
Vs v. Wet Bulk Density	$y = 586.474x^2 - 1981.68x + 1731.49$	0.805
Vs v. Mean Grain Size	$y = 0.281x^2 - 13.847x + 138.22$	0.725
Vp-ratio v. Porosity	$y = 0.000304x^2 - 0.0372x + 2.150$	0.948
Vp-ratio v. Wet Bulk Density	$y = 1.0791x^2 - 3.741x + 4.257$	0.948
Vp-ratio v. Mean Grain Size	$y = 0.00212x^2 - 0.034x + 1.146$	0.931
Attenuation v. Porosity	$y = 0.000442x^2 - 0.0573x + 2.275$	0.289
Attenuation v. Wet Bulk Density	$y = 2.282x^2 - 7.954x + 7.370$	0.291
Attenuation v. Mean Grain Size	$y = -0.0162x^2 + 0.0798 + 0.565$	0.553

Acoustic wave speeds increase with decreasing porosity, and increasing bulk density and mean grain diameter following the general trends already reported by Hamilton and Bachman (1982), Bachman (1985, 1989) and Richardson and Briggs (1993) for other surficial, shallow-water sediments. However, detailed comparison of relationships between values of physical and geoacoustic properties for the carbonate sediments with the well-established empirical relationships developed for siliciclastic sediments suggest fundamental differences in structure of these two types of sediments (Fig. 3; Table 2). These structural differences should be traced

to differences in effects of biogeochemical, biological, hyrodynamic, and geological processes on sediment origin, deposition, and subsequent diagenetic changes in carbonate and siliciclastic sediments.

Shear wave speeds, a measure of the shear modulus or rigidity of sediments, are consistently higher in carbonate sediments than siliciclastic sediments for a given porosity or bulk density (Fig. 3a,b). Given the propensity for cementation to increase sediment rigidity in carbonate sediments, sediment microfabric was examined for evidence of cementation. Transmission Electron Microscope (TEM) micrographs of sediment microfabric from these carbonate sediments showed no evidence for inter- or intraparticle cementation up to depths of 1 meter below the seafloor. Most sediments in the study site consist of a large percentage of fragmented *Halimeda* plates in various stages of mechanical degradation. These plates are made up of aragonite needles (Fig. 4) which contain approximately 30% intraparticle porosity. This intraparticle porosity probably has little effect on sediment rigidity if grain-to-grain contact primarily controls sediment rigidity. Based on TEM examination of surficial sediments from ponded regions of the Dry Tortugas study site, 10-15% of the total porosity is tied up within Halimeda plates (Dennis Lavoie, personal communication). This reduction of average porosity (10-15%) is sufficient to eliminate the differences between siliciclastic and carbonate sediment without affecting the shear wave speed verses mean grain size relationships (Figure 3c). The reduction in effective porosity should also decrease expected shear wave velocity for a given sediment bulk density. The high standard deviation in empirical prediction of shear wave velocity from porosity and density may be a function of the variation in percentages of skeletal material and thus intra- and interparticle porosity.

Compressional wave speeds (Vp-ratio), primarily a measure of bulk modulus or incompressibility, are only slightly higher in carbonate sediments than siliciclastic sediments for a given porosity and nearly the same for a given bulk density (Figure 3 d,e). A reduction of 10-15% in porosity yields values of compressional wave

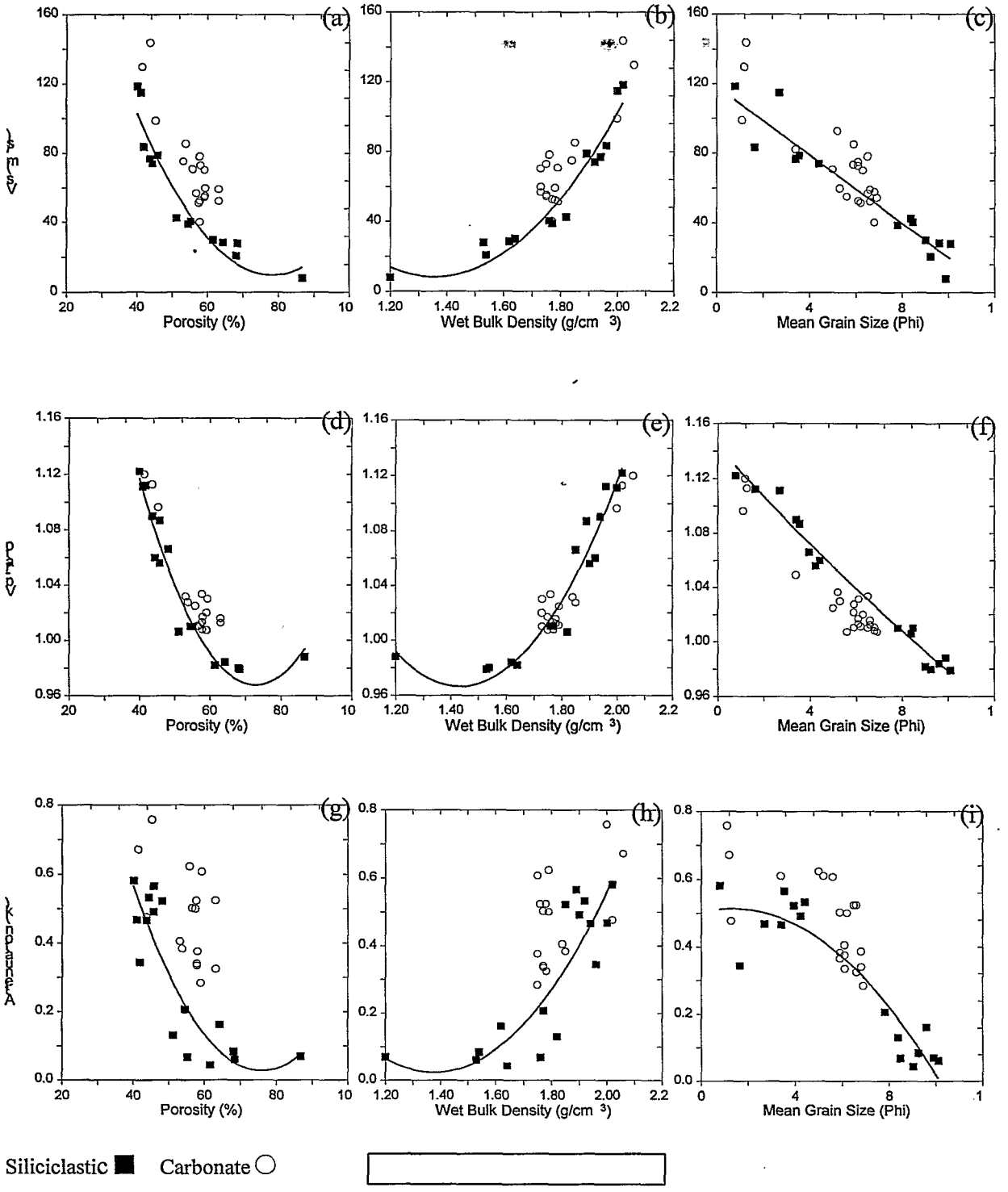

Figure 3. Relationships between sediment physical properties (porosity, bulk density, and mean grain size) and sediment geoacoustic properties (compressional wave velocity ratio, shear wave speed and compressional wave attenuation) for carbonate sediments in the lower Florida Keys. For comparison, regressions based on in situ data from siliciclastic sediments in included.

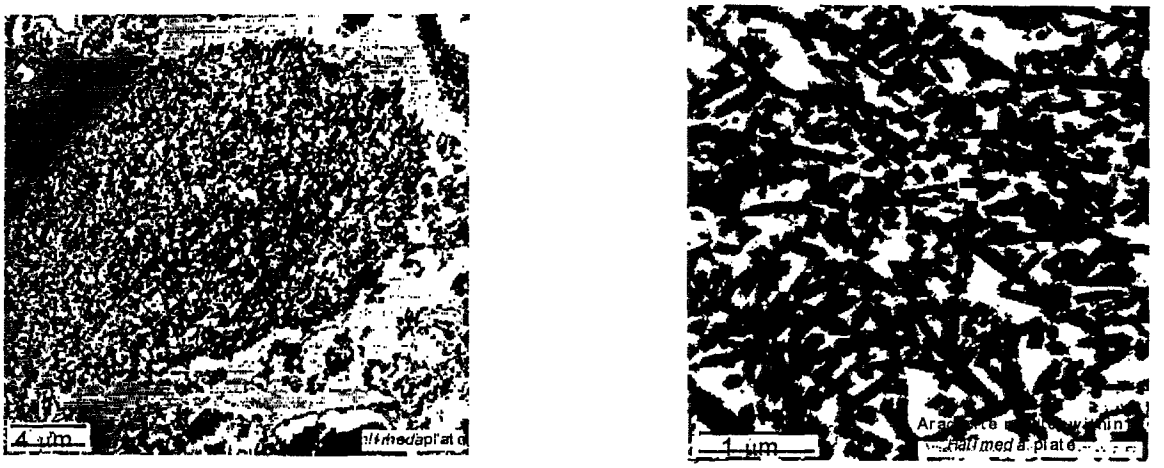

a b

Figure 4. (A) TEM micrograph of Halimeda plate. (B) At higher magnification,, TEM imagery reveals the porous nature of the aragonite needles which make up the Halimeda plate in (a).

speed lower than predicted for siliciclastic sediments. The higher compressional wave speeds probably result from the contribution of increased shear modulus (shear wave velocity) for a given porosity and the much higher bulk modulus of carbonate sediment grains (7.5×10^7 kPa) compared to silicliclastic sediment grains (3.6×10^7 kPa).

Compressional wave attenuation in carbonate sediments is higher than empirical predictions based on siliciclastic data for given porosity or bulk density (Figures 3 h,i). Attenuation, as measured by pulse techniques, is a sum of the intrinsic attenuation (due to internal pore fluid viscosity and internal friction) and loses due to scattering. The abundant coarse sand- and gravel-size shells found in most of these carbonate sediments scatter compressional waves and contribute to high, measured-attenuation values.

Most sediments in the study areas are very poorly sorted, sand-silt-clays (Standard Deviation = 3.5 to 4.5) consisting of a mixture of sand- and gravel-sized skeletal remains and silt- and clay-sized aragonite fragments and needles derived by

chemical and mechanical breakdown of larger coralline algae (*Halimeda*, *Penicillus*, and *Udeota)*. If the sediments are matrix supported (larger particles not in contact), sediment geoacoustic properties such as rigidity and compressibility should be controlled by properties of the matrix i.e., the larger carbonate particles contribute to mean grain size values but not compressional and shear wave speeds. It follows that mean grain size regressions based of siliclastic sediments would overestimate wave speeds in these carbonate sediments. In fact, this is the case for compressional wave speed but not shear wave speed where porosity effects cancel out the grain size effect (Fig. 3c,f).

Acknowledgments

Ships support was provided by the WFS PLANET from Forschungsantalt der Bundeswehr für Wasserschall- und Geophysik (FWG), RV COLUMBUS ISLIN from the University of Miami, and RV PELICAN from LUMCON. Special thanks is given to Sean Griffin for his support during in-situ measurements and for physical property data analysis. The research was supported by the Coastal Benthic Boundary Layer program, funded by the Office of Naval Research (Dr. Fred E. Saalfeld, technical director) and Naval Research Laboratory program element N0601153N (Dr. H. Eppert, program manager).

References

Barbagelata A, Richardson MD, Miaschi B, Muzi E, Guerrini P, Troiano L, and Akal T (1991) ISSAMS: An in situ sediment geoacoustic measurement system. In: Hovem JM, Richardson MD, Stoll RD (eds) Shear Waves in Marine Sediments, Kluwer Academic Publishers, Dordrecht, Netherlands, pp 305-312.

Bachman RT (1985) Acoustic and physical property relationships in marine sediments. Journal Acoustical Society of America 78:616-621.

Bachman RT (1989) Estimating velocity ratio in marine sediment. Journal Acoustical Society of America. 86:2029-2032.

Griffin SR, Grosz FB and Richardson MD (1996) ISSAMS: A remote *in situ* sediment acoustic .

Hamilton EL, Bachman RT, Berger WH, Johnson TC and Mayer LA (1982) Acoustic and related properties of calcareous deep-sea sediments, Journal of Sedimentary Petrology, vol. 52, no. 3, pp 733-753.

Hamilton EL and Bachman RT (1982) Sound velocity and related properties of marine sediments. Journal Acoustic Society of America 68:1891-1904.

Richardson MD (1994) Investigating the coastal benthic boundary layer. EOS 75: 201-206.

Richardson MD and Briggs KB (1993) On the use of acoustic impedance values to determine sediment properties. In: Pace NG, DN Langhorne DN (eds) Acoustic Classification and Mapping the Seabed. Institute of Acoustics, University of Bath, pp 15-25.

6.2 CT Analysis of Physical Property Variability in Carbonate Sediments (T.H. Orsi, K.B. Briggs, M.D. Richardson and A.L. Anderson)

CT Analysis of Physical Property Variability in Carbonate Sediments

Thomas H. Orsi

Planning Systems Incorporated, Slidell, LA

Kevin B. Briggs and Michael D. Richardson

Naval Research Laboratory, Stennis Space Center, MS

Aubrey L. Anderson

Texas A&M University, College Station, TX

Introduction

As part of the CBBL's 1995 Key West Campaign, we are using a density-calibrated X-ray computed tomography (CT) scanner to examine sediment cores collected by divers off Dry Tortugas. Our goals are to develop a better understanding of the relationship between macrostructure and physical property variability in these shallow-water carbonate sediments and to provide accurate and appropriately scaled input parameters for modeling high-frequency acoustic backscatter.

Core Locations

For this study, we collected five 12-cm-diameter sediment cores at the APL site off Dry Tortugas. Core 214-KW-PL was obtained from a "hot spot" in the field of view of the APL acoustic scans in the vicinity of their buoy farm. The "hot spot" was an asymmetrical pit with steep sides of stiff clay and a soft-sediment center. Finger-shaped sponges were observed in the pit's center where Core 214-KW-PL was inserted. Core 223-2-KW-PL was collected from a "cold spot" described by APL divers as being exceptionally "soft" sediment. Divers also observed scouring around bottom-moored objects suggesting that hydrodynamic processes are more active here than at the other ("hot spot") sample sites. The third, fourth, and fifth cores were collected from other "hot spot" regions: Core 228-2-KW-PL was taken near the APL calibrated

sphere; and Cores 238-1-KW-PL and 238-2-KW-PL were obtained from an area north of the APL tower.

Laboratory Procedures

CT images were made of the whole, intact cores using the Technicare 2060 CT scanner shown in Fig. 1. The cores were scanned every 2 mm, using a 2-mm-thick X-ray beam, to insure complete length coverage with no overlap of images.

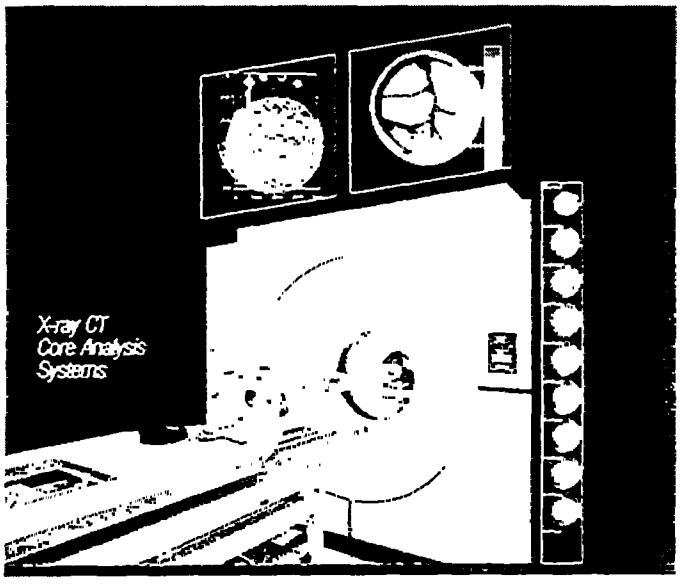

Figure 1—Technicare 2060 CT scanner at Texaco in Houston, TX. Note the positioning table and orientation of the sample. The X-ray scan (CT image) plane is parallel to horizontal bedding in the sediment core. Each scan produces a 512 x 512 voxel image, with each voxel assigned a value (a CT number) that is directed related to bulk density. The (x, y, z) dimensions of a voxel are 0.25 x 0.25 x 2 mm, representing a sediment volume of 0.125 mm^3. On average, 138 CT images were taken per core.

Variations in CT bulk density and standard deviation were determined using a fixed region-of-interest (ROI) centered within each CT image. The ROI is 150 x 150 (or 22,500) voxels in size, representing a sediment volume of 2812.5 mm^3. By incrementing the sample through the scan plane using a positioning table, contiguous sections can be obtained which, when compiled by imaging software, permit three-dimensional visualization of sedimentary structures. Equally important, quantitative analysis can be conducted on an image-by-image basis to develop downcore logs of selected CT statistical parameters; these profiles provide an excellent way to estimate the spatial variation in physical properties.

After scanning, the cores were slabbed longitudinally into 1-cm thicknesses for X-raying. Thereafter, the slabs were subsampled axially at 1-cm intervals to determine the vertical distribution of wet bulk density following standard geotechnical procedures. An empirical expression was developed for each core to convert CT numbers to equivalent sediment bulk density using the least-squares regression technique described in Orsi (1994) and Orsi et al. (1994). Correlations for the relationships were excellent with an overall mean r of 0.955 and a R^2 value of 0.912 (Figs. 2 and 3).

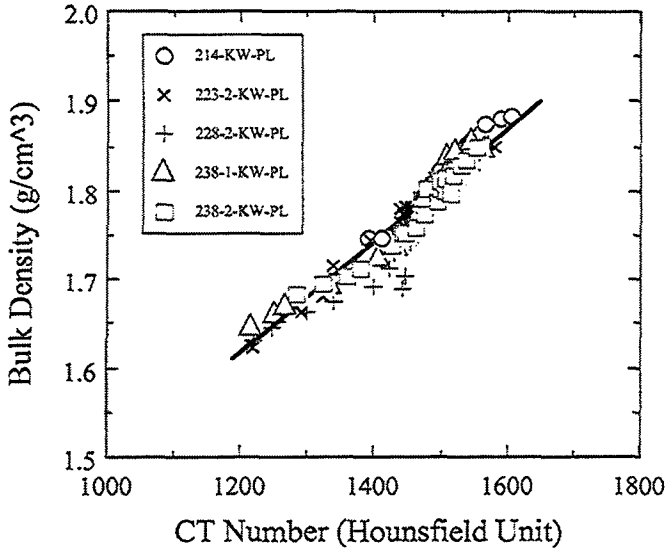

Figure 2—Scatterplot showing the correlation between CT number and laboratory bulk density measurements for the cores studied.

Physical Property Variability

Fig. 4 shows the downcore variation in CT density for the APL sediment cores. Overall, the profiles were similar, exhibiting a curvilinear increase in bulk density with increasing depth in the core. Surface densities vary between 1.55 g/cm^3 to slightly more than 1.60 g/cm^3 and approach a value of 1.725 g/cm^3 by about 5 cm depth. Thereafter, densities increase gradually to about 1.80-1.825 g/cm^3 at 25-30 cm depth. Although based on limited information, there does not appear to be any drastic difference between the "hot spot" profiles of Cores 228-2-KW-PL and 238-KW-PL and the "cold spot" profile of Core 223-2-KW-PL. Distinctly different, however, is the density profile of Core 214-KW-PL. Taken from a "hot spot" area, the overall densities of Core

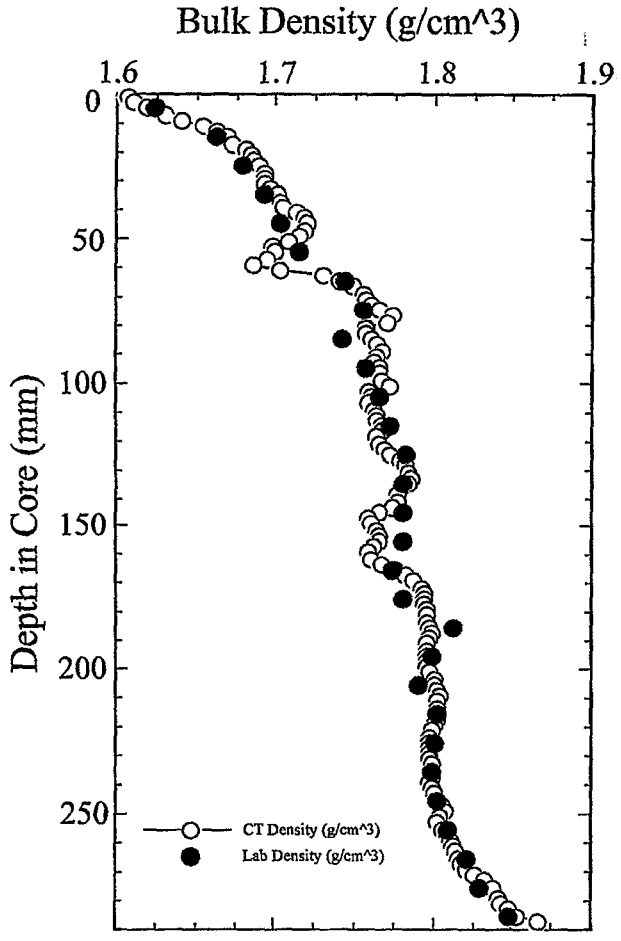

Figure 3—Correspondence between laboratory and CT bulk densities for Core 223-2-KW-PL.

214-KW-PL are higher throughout the entire length of the core. With surface densities of about 1.725 g/cm^3, values increase in a more-or-less linear fashion with increasing depth to a high of approximately 1.925 g/cm^3 by 23-24 cm depth. The reason for the discrepancy between profiles is presently being investigated.

Sediment Macrostructure

Our visual examination of the cores, the X-radiographs, and the CT imagery reveal no evidence of hydrodynamic structures. This is in agreement with Orsi et al. (submitted), who also found no evidence of hydrodynamic structures during a similar analysis of Dry Tortugas (and Marquesas Keys) cores taken the year before at the Key West Campaign's 1994 environmental preassessment. Instead, the dominant sources of macroscale variability in the studied APL sediments are biological in origin (Fig. 5).

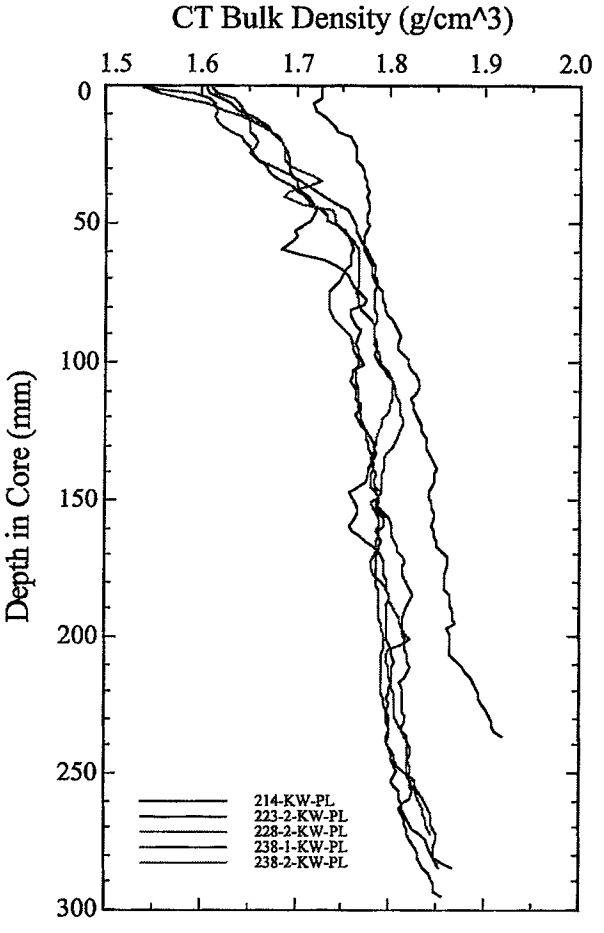

Figure 4—Vertical variation of CT (bulk) density for the CBBL cores.

Particularly prevalent are tubes and burrows, with walls composed of both low- and high-density material, which generate local variability and macrostructures that can be easily detected and quantified by CT. Also present, but much less common are shells and shell debris. As shown by Fig. 5, large intact gastropod shells are most common, whereas the shell fragments that we observed are probably from pelecypods. Most of the gastropod shells are sediment-filled, but several contain pockets of water (or slurry) which could result in considerable intratest porosity. The CT imagery also reveals several large feeding structures, possibly created by foraging urchins or some other type of large macrofauna.

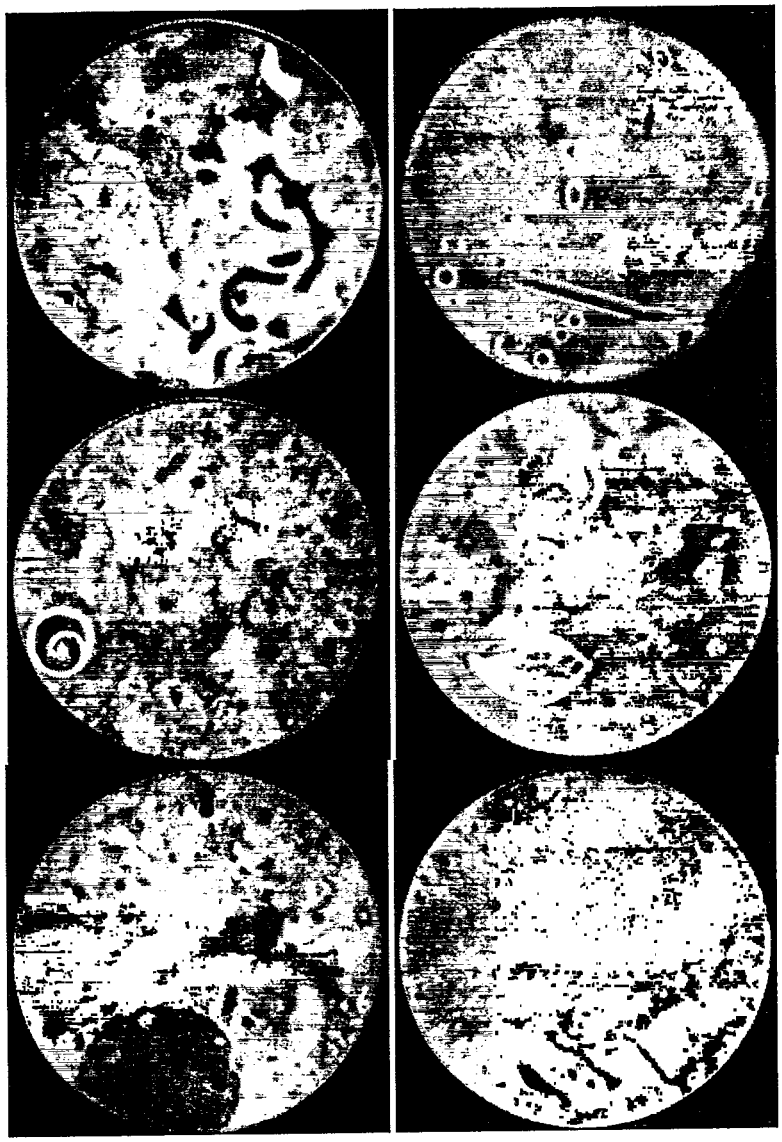

Figure 5—Biological macrostructures. Top images—(Burrows/Tubes): Left (low-density structures; Core 223-2-KW-PL; 87 mm depth). Right (high-density features; Core 214-KW-PL; 235 mm depth). Middle images—(Shells/Fragments): Left (shell; Core 228-2-KW-PL; 147 mm depth). Right (shell and fragment; Core 238-2-KW-PL; 191 mm depth). Lower images—(Miscellaneous): Left (urchin?; Core 223-2; 165 mm depth). Right (feeding structure; Core 238-1; 149 mm depth). The diameter of the core liner is 12 cm and each CT image is 12.5 cm per side.

Summary

(1) We have found CT to be a powerful analytical technique for characterizing sediment cores: it is nondestructive and quantitative, has a sub-millimeter resolution, and permits two- and three-dimensional visualization of sediment structure. The ability to quantify (without disturbing) the internal structure of shell-bearing sediments is particularly useful.

(2) We observed no evidence of hydrodynamic structures in the APL cores and the dominant sources of macroscale variability in the sediments studied are biologically created. Particularly prevalent are tubes and burrows; much less common are shells and shell debris; and rarer still are large feeding structures created by foraging macrofauna.

(3) Our future efforts will concentrate on a number of aspects relevant for modeling high-frequency acoustic backscatter. Included will be an examination of the utility of CT for determining scattering cross-sections of volume inhomogeneities; evaluation of the CT standard deviation statistic as a measure of physical property variability; calculation of correlation lengths using CT density profiles (2 mm lag); and implementation of three-dimensional visualization and movie sequencing to better examine the internal structures of these sediments.

References

Orsi, T. H. (1994) *Computed tomography of macrostructure and physical property variability of seafloor sediments*, Unpublished Ph.D. Thesis, Texas A&M University, College Station, TX, 184 pp.

Orsi, T. H., C. M. Edwards, and A. L. Anderson (1994) X-ray computed tomography: A non-destructive method for quantitative analysis of sediment cores. *Journal of Sedimentary Research*, A64, 690-694.

Orsi, T. H., A. L. Anderson, W. R. Bryant, K. S. Davis, and A. K. Rutledge (submitted) Computed tomography of carbonate sediment macrostructure: Marquesas Keys and Dry Tortugas (South Florida). *Geo-Marine Letters*.

6.3 Small-Scale Fluctuations in Acoustic and Physical Properties of Sediments from the Marquesas Keys and Dry Tortugas Sites (K.B. Briggs, P.D. Jackson and R.C. Flint)

Small-Scale Fluctuations in Acoustic and Physical Properties of Sediments from the Marquesas Keys and Dry Tortugas Sites

Kevin B. Briggs[1], Peter D. Jackson[2] and Robert C. Flint[2]

[1]Naval Research Laboratory, Marine Geosciences Division
Stennis Space Center, MS 39529-5004, USA

[2]British Geological Survey, Engineering Geology and Geophysics Group
Keyworth, Nottingham NG12 5GG, UK

INTRODUCTION

Characterization of sediment volume heterogeneity is necessary for modeling the acoustic backscattering from the sea floor, especially in the case of a muddy sea floor permitting substantial acoustic penetration (Hines 1990, Jackson and Briggs 1992, Lyons et al. 1994, Yamamoto 1996). Sound energy penetrating the sea floor is backscattered from fluctuations in sediment density and sound velocity according to the distribution and magnitude of the fluctuations (Briggs, 1994). Typically, any discontinuity in the sediment structure can cause fluctuations in density and sound velocity. Sediment inhomogeneity is most often created by buried shells, graded bedding, or bioturbation and is readily evident in systematic measurements of physical and acoustic properties from sediment cores, as well as direct measurements of electrical resistivity in sediment box cores (Jackson et al., 1996).

As part of the Coastal Benthic Boundary Layer project, we investigated the fluctuations of physical and acoustic properties of surficial sediments in the Marquesas Keys and Dry Tortugas, Florida Keys. These sites are characterized by a recent deposition of detrital algal, mollusk, and coral carbonate sediments that are extensively reworked by burrowing infauna and tidal- and wind-wave-induced currents. We examine surficial (top 20-30 cm) sediments with diver-collected cores, comparing the variation in compressional wave

velocity and attenuation, porosity, and mean grain size within and between the two sites. In addition, X-radiographs are used to examine the 2-dimensional sedimentary structure contributing to fluctuations in these properties. Lastly, box corer samples were investigated with an electrical resistivity array to examine the 3-dimensional tomographic distribution of sediment resistivity at the Dry Tortugas site.

METHODOLOGY

The upper 20-30 cm of surficial sediment was sampled by diver cores in order to obtain a relatively undisturbed sediment-water interface from two shallow-water carbonate environments. Within 24 h of collection, compressional wave velocity and attenuation at 400 kHz was measured at 1-cm increments with oil-filled rubber transducers on either side of the 6.1-cm-diameter diver cores (Richardson 1986, Briggs 1994). Porosity and grain size distributions were measured at 2-cm intervals on the sediment extruded from the diver cores and compared with the acoustic properties measured on the same cores. Percent water content was measured using weight loss from samples in a drying oven at 105°C for 24 hr and porosity was calculated with measured values of average grain density (Briggs 1994). Sediment grain size was measured from disaggregated samples by dry sieving with a sieve shaker for gravel- and sand-sized particles and by use of a Micromeritics Model 5000 sedigraph for silt- and clay-sized particles (Briggs et al. 1996).

Three-cm thick X-radiograph cores (36 cm wide x 44 cm long) were collected from the same areas to visually document the heterogeneity due to sedimentological and biological processes. Sediment slabs were X-rayed within a few hours of collection with a Kramex PX-20N portable X-ray unit.

Four freshly collected 0.25-m^2-area box cores were used to measure electrical resistivity with an 11-x-20-grid of electrodes evenly separated by 2 cm. The electrode grid was placed on the sediment surface after the overlying water was siphoned off with care not to disturb the sediment-water interface. Electrical resistivity data were inverted and a preliminary tomogram is presented here without complete processing.

RESULTS

Vertical profiles of sediment compressional wave velocity and attenuation, porosity and mean grain size measured on diver cores from the Marquesas Keys are displayed in Figure 1. Sediment compressional wave velocity (V_p) averages 1551 m/s with a standard deviation of 4.32 m/s in the 6 cores collected from this site. Sediment compressional wave attenuation averages 329 dB/m with a standard deviation of 57.9 dB/m. Sediment porosity averages 58.7 % with a standard deviation of 5.22 %. The sediment at the Marquesas Keys site is a sand-silt-clay with a mean grain size of 6.2 f (SD = 0.96 f). There are slight increases of compressional wave velocity and attenuation, and a large increase in variability in values of attenuation with depth in the sediment. Sediment porosity exhibits a pronounced decreasing gradient in the top 5 cm, wide variation in values from 5 to 9 cm and rather constant values centered around 56 % below 9 cm sediment depth. Mean grain size at the Marquesas Keys site varies from a fine-grained sediment (6.5-8.4 f) at the surface to a coarser sediment (lower phi values) with increasing depth in the sediment.

Sediment structure, as evidenced in X-radiographs, is characterized by fine laminations of fine particles in the upper 5-7 cm and a dramatic increase in proportion of gravel-size mollusk shell fragments with increasing depth immediately below this horizon. Indeed, the high concentration of shells and shell fragments impeded penetration of the cores at the Marquesas Keys site. There are little or no gravel-sized particles in the upper 2 cm, but percent gravel dramatically increases to as much as 17 % (by weight) deeper in the sediment.

Vertical profiles of sediment properties measured on diver cores from the Dry Tortugas site are displayed in Fig. 2. Average values of velocity, attenuation, porosity and mean grain size are not significantly different from the average values measured at the Marquesas

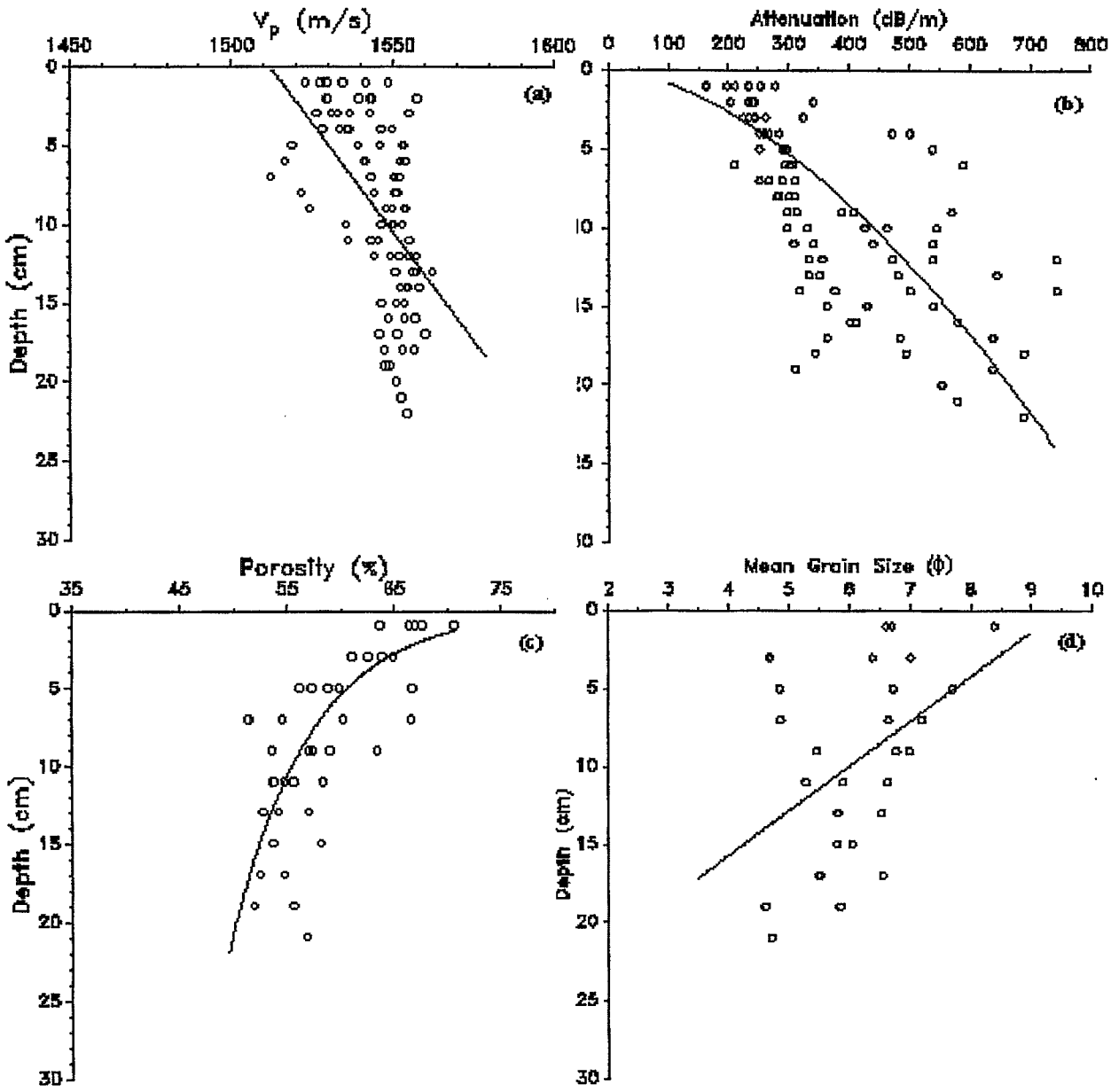

Figure 1. Vertical profiles of sediment (a) compressional wave velocity, (b) compressional wave attenuation, (c) porosity and (d) mean grain size at the Marquesas Keys site.

Keys site (V_p: 1552 m/s, attenuation: 331 dB/m, porosity: 58.4 %, mean grain size: 6.6 f). Variability is high for values of velocity (SD = 9.62 m/s), but comparatively low for attenuation (SD = 47.5 dB/m), porosity (SD = 4.47 %) and mean grain size (SD = 0.38 f).

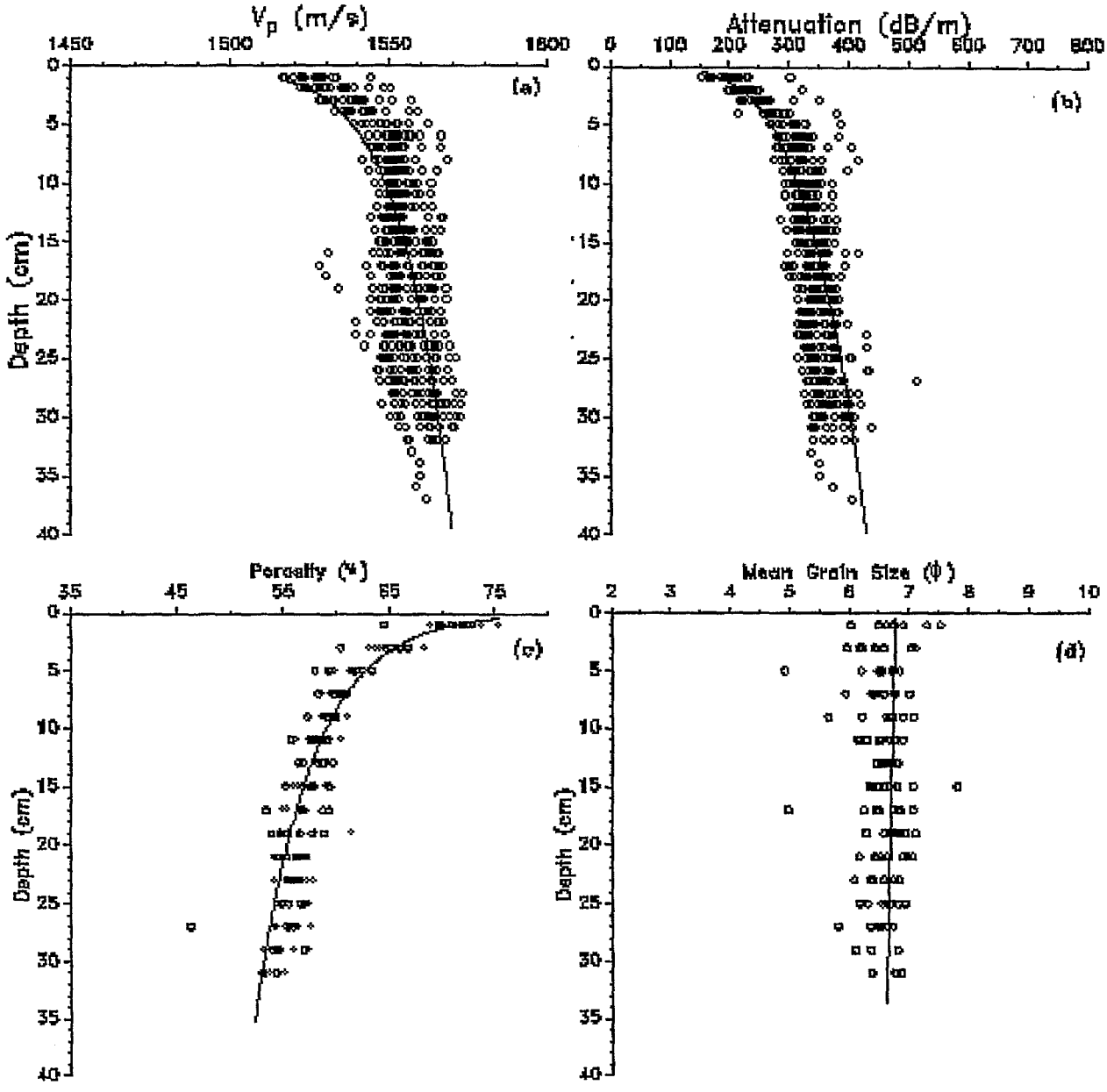

Figure 2. Vertical profiles of sediment (a) compressional wave velocity, (b) compressional wave attenuation, (c) porosity and (d) mean grain size from the Dry Tortugas site.

REFERENCES

Briggs K.B. (1994) High-frequency acoustic scattering from sediment interface roughness and volume inhomogeneities. PhD dissertation. University of Miami, Coral Gables, FL, 143 pp.

Briggs K.B., Lavoie D.L., Stephens K., Richardson M.D. and Furukawa Y. (1996) Physical and geoacoustic properties of sediments collected for the Key West Campaign, February 1995: A data report. Naval Research Laboratory Report NRL/MR/7431--96-8002.

Hines P.C. (1990) Theoretical model of acoustic backscatter from a smooth seabed. Journal of the Acoustical Society of America 88: 324-334.

Jackson D.R. and Briggs K.B. (1992) High-frequency bottom backscattering: roughness vs. sediment volume scattering. Journal of the Acoustical Society of America 92: 962-977.

Jackson, P.D., Briggs, K.B. and Flint, R.C. (1996) Evaluation of sediment heterogeneity using microresistivity imaging and X-radiography. Geo-Marine Letters 16: 219-225.

Lyons A.P., Anderson A.L. and Dwan F.S. (1994) Acoustic scattering from the seafloor: Modeling and data comparisons. Journal of the Acoustical Society of America 95: 2441-2451.

Richardson M.D. (1986) Spatial variability of surficial shallow water geoacoustic properties. In: Akal T and Berkson JM (Eds.), Ocean Seismo-Acoustics. New York: Plenum Press pp 527-536.

Richardson M.D. and Young D.K. (1980) Geoacoustic models and bioturbation. Marine Geology 38: 205-218.

Yamamoto T. (1996) Acoustic scattering in the ocean from velocity and density fluctuations in the sediments. Journal of the Acoustical Society of America 99: 866-879

6.4 Scale-Dependence of Sediment Property Variability of the Dry Tortugas, Florida (K.P. Stephens, P. Fleischer, D. Lavoie and C. Brunner)

Scale-dependence of Sediment Property Variability of the Dry Tortugas, Florida

Kevin P. Stephens[1,2], Peter Fleischer[1], Dawn Lavoie[1], Charlotte Brunner[2]

[1]Marine Geosciences Division, Naval Research Laboratory, Stennis Space Center, MS 39520-5004, USA. [2]Institute of Marine Sciences, University of Southern Mississippi, Stennis Space Center, MS 39520, USA

INTRODUCTION

When examining any attribute of a natural system, one must consider scale. Scales can range from the subatomic to the extent of the universe. However, scales of interest for an attribute of a natural system are often of limited range. In a geological system, such as a sedimentary depositional environment, vertical scale may be limited by the thickness and number of strata and lateral scale by the extent of the strata. Lateral scales are typically greater than vertical scales in sedimentary, depositional environments raising the question: how do sediment attributes measured laterally and vertically compare? Johannes Walther made the geologic observation "facies that occur in conformable vertical successions of strata also occur in laterally adjacent environments" (Prothero, 1990), which became known as Walther's Law. If sediment attributes at different vertical and lateral scales are consistent with Walther's Law, for a sedimentary, depositional system, then the sediment attributes are comparable.

When variability of an attribute is measured at different scales, the changes with scale are identified and inferences can be made as to why the attribute is changing. Variability with increasing scale can: 1) remain the same, 2) increase, or 3) increase and then level off. Variability can remain the same with increasing scale if the system is homogeneous with respect to the attribute. Variability of an attribute can

increase with increasing scale. Finally, variability can increase with increasing scale and then level off if all variations of the attribute have been accounted for. Variability versus scale, or scale-dependent variability, can be modeled by regression analysis with resulting equations comprising a scale-variability model. Vertical to lateral scale-variability ratios can be used to 1) quantify Walther's Law, 2) predict variability based on scale for similar depositional environments, and 3) quantify sediment property isotropy.

The objective of this study is to investigate sediment property variability of recent, shallow-water carbonate sediment to determine and model the scale-dependence of variability. Samples for this study are from gravity and diver cores collected aboard the R/V Pelican and WFS Planet from the Dry Tortugas, Florida in February, 1995 during the Coastal Benthic Boundary Layer Key West Campaign. Variability was computed for mean grain size, grain density, wet bulk density, porosity, and compressional wave velocity (Vp). The data (Stephens et al., in press) present a maximum 2.5-m vertical scale and 1750-m lateral scale.

METHODS

Compressional wave velocity and wet bulk density were measured with TAMU's GEOTEK Multisensor Core Logger. Compressional wave velocity was determined by picking first arrivals of wavelets. Wet bulk density was measured with a helium gas pycnometer on three gravity cores to check the accuracy of the core logger. Core logger wet bulk density values were consistently higher than pycnometer-measured values by 0.057 g/cm^3 due to calibration errors. Therefore, core-logged, wet-bulk density values were corrected by subtracting 0.057 g/cm^3 from core logger measured values. Grain density was measured with a helium gas pycnometer. Grain size was measured by sieve analysis for gravel- and sand-size particles and pipette analysis for silt- and clay-size particles after Folk (1974). Porosity was calculated. In all, 2244 Vp measurements, 3540 wet bulk density measurements, 1108 grain

density measurements, 403 grain size measurements, and 1251 porosity measurements were made.

Variability was measured with coefficients of variation (COV). Coefficients of variation are determined by dividing the sample standard deviation by the sample mean and multiplying the result by 100. Coefficients of variation, being measures of relative variation, are useful because direct comparisons of variability for different sediment properties can be made (Ostle, 1963). Vertical variability was determined by a one-dimensional approach by measuring variability at scales ranging from 20 cm to 240 cm in 10 cm increments. Lateral variability was measured at four scales: 0.1 m, 10 m, 850 m, and 1750 m. Lateral variability was determined by three two-dimensional approaches: stratigraphic, depth-integrated, and discrete-depth (Figures 1 a, b, and c). The approaches utilized in investigating lateral variability describe and interpret variability in three different applied situations. Stratigraphic lateral variability (Figure 1a) has not only geologic significance, but has an applied use for aiding in the interpretation and prediction of acoustic wave propagation in seismic reflection and refraction studies. Depth-integrated lateral variability (Figure 1b) is the method which determines the variability which probably affects vertical incidence acoustic systems. Discrete-

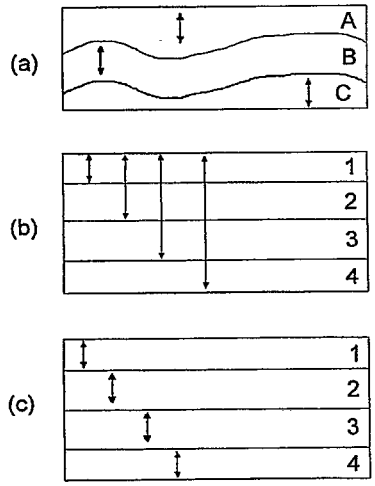

Figure 1: Conceptual model of three lateral variability approaches: a) stratigraphic, b) depth-integrated, and c) discrete-depth.

depth lateral variability (Figure 1c) was determined to aid in geoacoustic interpretations from *in situ* acoustic probes (Lavoie et al., 1996) deployed at specific, discrete intervals below the sea floor.

RESULTS AND DISCUSSION

By measuring variability at various lateral and vertical scales, variability trends with scale as well as relationships between vertical and lateral variability can be determined. Vertical variability increases with increasing scale for all properties analyzed (Figure 2). Mean grain size and porosity exhibit a high degree of variability (7 to 15 % and 4 to 6.5 % respectively) compared to wet bulk density (2 to 3 %), Vp (0.5 to 1.5 %), and grain density (0.5 to 1 %). Variability as determined by the three lateral approaches yielded similar results. Therefore, only discrete depth lateral variability will be discussed. It is most similar and comparable to vertical variability in the analytical approach. Lateral variability increases with increasing scale for all sediment properties analyzed with few exceptions (Figure 2). Porosity and wet bulk density variability did not increase with increasing scale between 0.1 and 10 m. Also, wet bulk density and grain density variability did not increase between 850 and 1750 m. The absence of an increase between 850 and 1750 m may indicate that grain density and wet-bulk density variability are leveling off, and that all variations of these properties has been taken into account.

Lateral variability of mean grain size and porosity are most variable (6 to 15 % and 2.5 to 5 % respectively) followed by wet bulk density (2 to 3 %), Vp (1 to 2 %), and grain density (0.5 to 0.8 %).

To gain some insight as to why the sediment properties vary, we need only to look at grain size and porosity variability. Compressional wave velocity is dependent on both porosity and wet bulk density. Grain density is dependent on mineralogy, which is controlled by such things as climate and water chemistry, which in turn

depend on large spatial-scale and long-temporal scale processes. Wet bulk density is dependent on grain density and porosity. Therefore, only grain size and porosity require discussion. For grain size, the types, percentages, and sizes of constituent particles determine grain size distributions and variability. The types, percentages, and sizes of particles are controlled by 1) transportation of silt- and clay-size

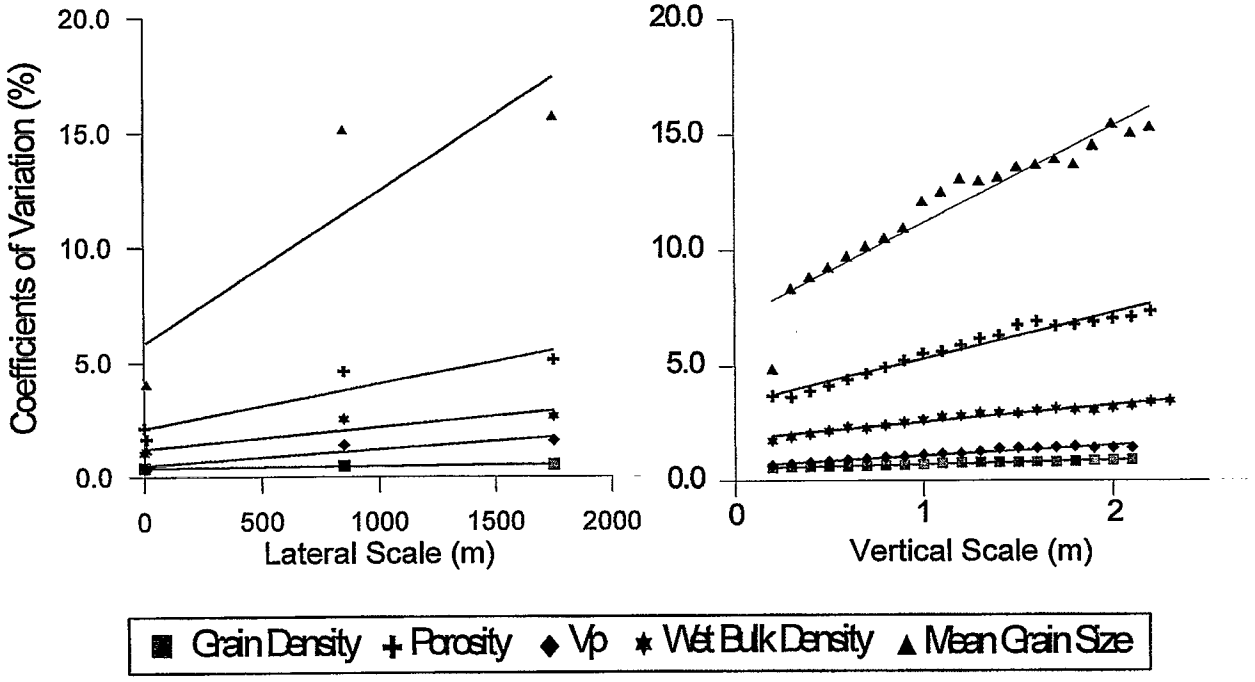

Figure 2: Data points represent average COV, or variability, of 12 to 44 values. There are four lateral scales and 20 to 22 vertical scales. Notice vertical and lateral variability generally increase with increasing scale, but vertical variability increases at a much greater rate than lateral variability. Vertical and lateral variability are nearly identical at a vertical scale of 2 m and lateral scale of 1750 m. Also, the order of sediment properties, based on the magnitude of variability, is the same vertically and laterally.

particles into and out of the experiment site (Mallinson et al., in press), 2) micritization of particles by tides and currents (Lavoie et al, this volume), bioturbation (Bentley et al., this volume), and tropical storm events, and 3) locations relative to reefs (sediment source) and/or channels. Consolidation is the most important process controlling porosity between 0 and 40 cm below the sea floor (bsf) while grain size is most important between 40 and 250 cm bsf (Lavoie et al., this volume). Relative percentages of particles such as *Halimeda*, which can

have high intraparticle porosity values, may also be important for controlling porosity variability if their percentages vary either vertically or laterally.

Vertical and lateral sediment property variabilities are consistent with Walther's Law, which states that "facies which occur in conformable vertical successions of strata also occur in laterally adjacent environments" (Prothero, 1990). The order of sediment properties, based on magnitude of variability, is the same for both the lateral and vertical variability versus scale plots (Figure 2). Vertical and lateral variability of the sediment properties are characteristics of the facies. Since these characteristics are the same both vertically and laterally, these sediments are consistent with Walther's Law. Walther's Law can be demonstrated graphically. A seen in the Acoustic Sediment Classification System profiles, facies that occur in a vertical succession of strata also occur in laterally adjacent environments (Walter et al., this volume).

Vertical and lateral variability versus scale were modeled by regression analysis. The resulting equations (Table 1) can be used to predict variability based on either vertical or lateral scale. The equations also quantify Walther's Law with respect to sediment properties. Predicted variability can be used to determine the degree of variability when extrapolating data to larger scales. Also, the degree of variability between acoustic tracklines can be determined. Since these cores were collected along acoustic tracklines, knowing the variability will enable more realistic ground truth for interpolated acoustic predictions between tracklines.

Finally, scale-variability ratios (ratio of vertical to lateral variability) can be determined as a way to characterize the spatial variability of some property of the sediments with a single number. From the regression equations, scale-variability ratios can be determined for the slopes and intercepts (Table 2). Scale variability ratios of the vertical and lateral intercepts are nearly a value of one, indicating the sediments are nearly isotropic with respect to the sediment properties at small

scales, i.e. centimeters. Scale-varaibility ratios of the slopes may give some information as to what processes are controlling variability or what properties are related. Mean grain size and Vp, for example, have similar scale-variability ratios for the slopes. If mean grain size is a first order control on Vp, then perhaps the 6.3:1 increase of mean grain size is controlling the 6.4:1 increase of Vp.

Table 1: Predictive equations for vertical and lateral variability

	Vertical Variability	R^2	Standard Error of Slope	Standard error of Intercept	Standard error of Prediction	n
Vp	y = 0.00463 * x + 0.616	0.942	0.000269	0.035	0.069	20
Porosity	y = 0.0198* x +3.328	0.962	0.000900	0.121	0.250	21
Grain Density	y = 0.00188 * x +0.521	0.978	0.000066	0.009	0.017	20
Wet Bulk Density	y = 0.00753 * x + 1.793	0.958	0.000353	0.050	0.105	22
Mean Grain Size	y = 0.0421 * x + 6.976	0.903	0.003150	0.424	0.876	21
	Lateral Variability	R^2	Standard Error of Slope	Standard error of Intercept	Standard error of Prediction	
***Vp	y = 0.000724 * x + 0.477	0.856	0.000296	0.333	0.365	4
Porosity	y =0.00196 * x +2.102	0.879	0.000516	0.503	0.745	4
Grain Density	y = 0.0000901 * x +0.387	0.977	0.000014	0.015	0.017	3
Wet Bulk Density	y = 0.000962 * x + 1.207	0.850	0.000286	0.278	0.413	4
***Mean Grain Size**	y = 0.00665 * x +5.807	0.773	0.003600	4.050	4.440	3

**The data used in the linear regression analysis of mean grain size is not within 90% confidence intervals necessary for the minimum number of samples for statistical significance. The accuracy of the regression equation is questionable.

***Should be used with caution since either the slope, y-intercept, or both may not be significantly different from zero.

y is the predicted coefficient and x is scale in meters.

Table 2: Scale-variability Ratios

	Slope	Intercept
Vp	6.4	1.3
Porosity	10.1	1.6
Grain Density	20.9	1.4
Wet Bulk Density	7.8	1.5
Mean Grain Size	6.3	1.2
Average	10.3	1.4

CONCLUSIONS

- Vertical and lateral sediment property variability depend on the types, percentages, and sizes of constituent particles, which in turn are controlled by facies changes. Facies changes, which occur within stratigraphic units and between stratigraphic units, are controlled by sediment transport and micritization by tides, currents, bioturbation, and storms as well as the proximity to sediment source(s).
- Vertical and lateral sediment property variability 1) generally increase with increasing scale, 2) are consistent with Walther's Law, and 3) can be modeled by regression analysis to predict variability from scale and quantify Walther's Law.
- Scale-variability ratios can be used to characterize sediment property variability of depositional environments and quantify sediment isotropy.

REFERENCES

Bentley, Samuel J. and Charles A. Nittrouer. 1997. Constraints on Rates of Sediment Accumulation and Mixing, Southeast Channel, Dry Tortugas. This volume.

Folk, R. L. 1974. Petrology of Sedimentary Rocks. Austin, Texas: Hemphill Publishing. 3-37.

Lavoie, Dawn L., Kevin P. Stephens, Yoko Furukawa, and Dennis Lavoie. 1997. Laboratory Measured Geotechnical Characteristics. This volume.

Lavoie, Dennis. Carbonate Microfabric. This volume.

Lavoie, Dawn L., Sean R. Griffin, and Francis B. Grosz. 1996. "DIAS - a Novel Technique for Measuring In Situ Shear Modulus." Geo-Marine Letters 16:254-260.

Mallinson, D., S. Locker, M. Hafen, D. Naar, A. Hine, D. Lavoie, and S. Schock. In press. "A High Resolution Geological and Geophysical Investigation of the Dry Tortugas Carbonate Depositional Environment." Geo-Marine Letters

Ostle, B. 1963. Statistics in Research: Basic Concepts and Techniques for Research Workers. Ames, Iowa: The Iowa State University Press. 64-65.

Prothero, Donald R. 1990. Interpreting the Stratigraphic Record. New York: W. H. Freeman and Company. 167-168.

Stephens, Kevin P., Dawn L. Lavoie, Kevin B. Briggs, Yoko Furukawa, and Michael D. Richardson. in press. Geotechnical and Geoacoustic Properties of Sediments off South Florida: Boca Raton, Indian Rocks Beach, Lower Tampa Bay, and The Lower Florida Keys. Naval Research Laboratory publication number NRL/MR/7431--97--?. Stennis Space Center, MS, GPO.

Walter, Donald, Dawn L. Lavoie, and Kevin P. Stephens. 1997. Geologic Setting, Southeast Channel, Dry Tortugas and a Comparison of Acoustically Predicted Sediment Properties with Lab-measured Core Data. This volume.

6.5 Acoustic Characteristics in Relation to Strength Behavior of Sediments from the Key West Campaign (G.F. Sykora, A.J. Silva and G.E. Veyera)

Acoustic Characteristics in Relation to Strength Behavior of Sediments from the Key West Campaign

Gabriella F. Sykora, Armand J. Silva, George E. Veyera

Marine Geomechanics Laboratory
University of Rhode Island
Narragansett, RI 02882

In conjunction with the Coastal Benthic Boundary Layer Special Research Program, the focus of this study is to investigate acoustic characteristics in relation to material properties and strength behavior of calcareous sediment from three study sites near Key West, Florida. To accomplish this task, a triaxial-compression cell specially modified for acoustic data acquisition has been implemented to determine shear and compressional wave velocity variation with increasing effective confining pressure and strain.

The majority of triaxial samples used for this research are subsampled from gravity cores retrieved from the Marquesas and Rebecca Shoals study sites. Sediment from these sites has been characterized as having a carbonate content greater than 85% and grain size ranging from clay size to shell fragments. Shear and compressional waves are generated within the triaxial cell by piezoceramic transducers located at the top and base of the sample. Wave velocities are calculated as sample length divided the difference in seconds between the start of the signal transmitted from the top of the sample and the start of the receive signal detected at the base of the sample. During consolidation and shearing phases of testing, acoustic wave velocities and corresponding effective confining pressures are recorded at select intervals.

Thus far, preliminary isotropically consolidated undrained triaxial tests incorporating compressional and shear wave speed measurements have been conducted on samples from the Marquesas and Rebecca Shoals study sites (Table 1). All tests were run using shear and compressional wave frequencies of 2.5 kHz and 150 kHz, respectively. Undisturbed tests from Marquesas core 188-GC at a depth of 98-112 cm indicate compressional wave speeds averaged between 1493 to 1618 m/s within an effective stress range of 0.30 to 14.1 kPa (Figure 1). Undisturbed tests from the same core at a slightly greater depth of 137-151 cm indicate compressional wave speeds averaged between 1507 to 1525 m/s within an effective stress range of 0 to 17.3 kPa. It was not possible to obtain shear wave velocities through these samples, most likely due to the effects of large shells as well as the sample length. As a result, shell fragments were removed from samples previously sheared using an 850μm sieve. Sediment reconstituted in this manner was remolded to the same void ratio and retested using the same techniques as the undisturbed samples. Test results on reconstituted material from core 188-GC at a depth of 98-112 cm indicate that compressional wave velocity results were comparable to the respective undisturbed sample at the same depth and location (Figure 2). In addition, shear wave speed measurements were detectable on this reconstituted sample, averaging 129 m/s during shear (Figure 3). To investigate the effect of sample length on acoustic wave propagation, the same reconstituted sample 188-GC (98-112 cm) was subsequently shortened 5 cm from its original length to 6.4 cm and retested. Compressional and shear wave speeds were slightly lower than the longer sample, averaging 1492 m/s and 82 m/s, respectively (Figures 3 and 4).

Acoustic measurements were also conducted on undisturbed samples (11.4 cm in length) from Rebecca Shoals core 326-GC at a depth of 102-116 cm. Results indicate compressional wave speeds averaged between 1475 and 1546 m/s and shear wave speeds averaged between 80 to 130 m/s within an effective stress

range of 2 to 29 kPa (Figures 5 and 6). Shear wave measurements for this sample were possible most likely due to the absence of large shells.

All results show a general increase in wave speed with an increase in effective stress. In addition, tests indicate that while material properties may not play a crucial role in compressional wave propagation, they seem to play a significant role in shear wave propagation. Therefore, current research is focusing on investigating and possibly improving shear wave propagation through shelly sediments from the Dry Tortugas and Marquesas sites. Recent improvements to shear wave signal quality include embedding shear wave transducers in a thin layer of Ottawa sand to improve acoustic coupling.

Table 1: Summary of Triaxial-Acoustic Strength Tests

Sample	*Sample Depth (cm)*	*Consolidation Stress (kPa)*	*Failure Effective Stress Ratio*	*Avg. P-Wave Speed (m/s)*	*Avg. S-Wave Speed (m/s)*
188-GC-U+	98-112	14.9	13.6	1565c	-
188-GC-U+	137-151	22	11	1518c / 1518s	-
188-GC-R+	98-112	28	4.2	1623c / 1633s	129s
188-GC-R+	102-108	29	-	1492c	82c
326-GC-U*	102-116	30	10	1517c / 1520s	112c / 128s

U= undisturbed R=reconstituted
c= consolidation s=shear
+= Marquesas site *=Rebecca Shoals site

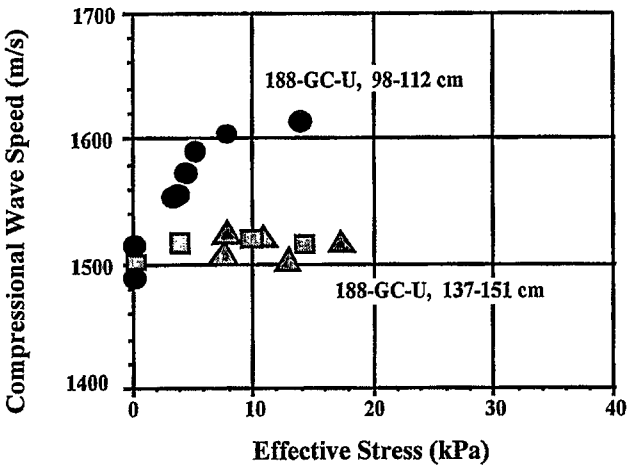

Figure 1: Undisturbed Compressional Wave Results (Marquesas Site)

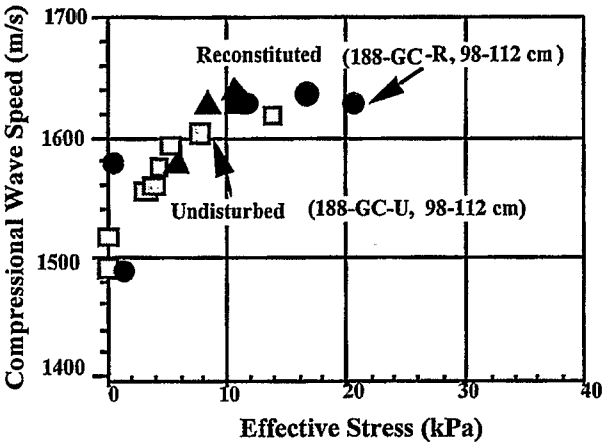

Figure 2: Undisturbed vs Reconstituted Compressional Wave Results (Marquesas Site)

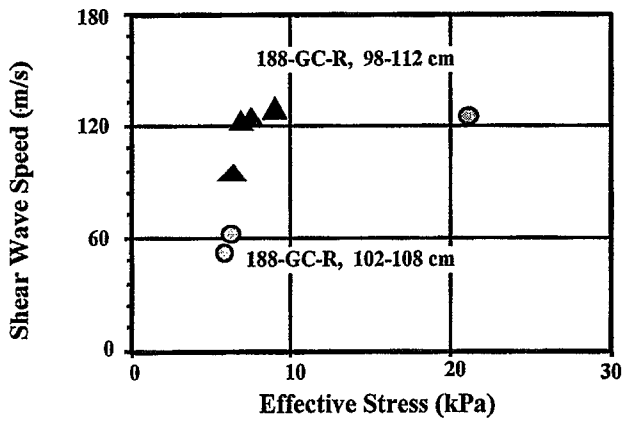

Figure 3: Reconstituted Shear Wave Results (Marquesas Site)

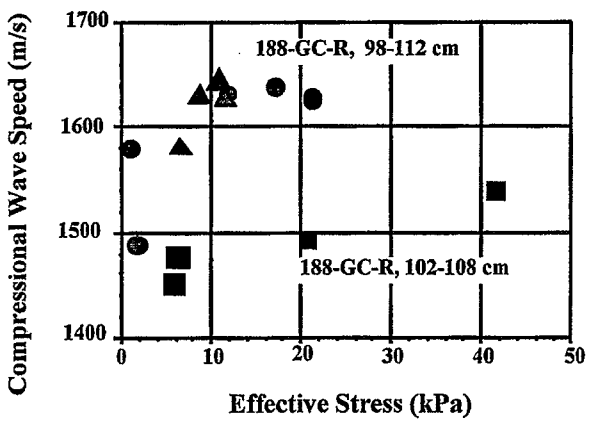

Figure 4: Reconstituted Compressional Wave Results (Marquesas Site)

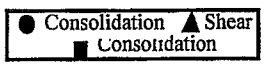

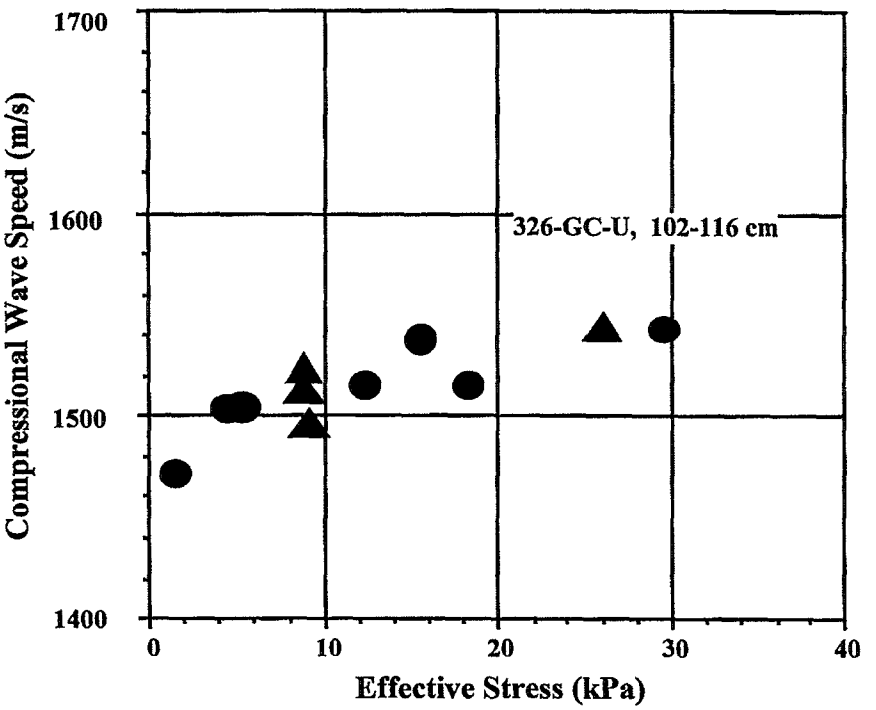

Figure 5: Undisturbed Compressional Wave Results (Rebecca Shoals Site)

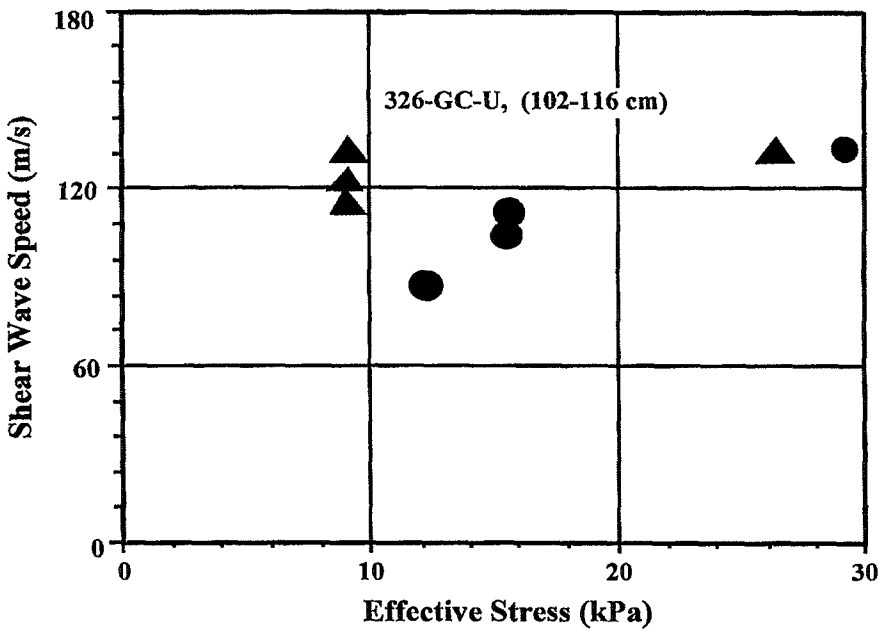

Figure 6: Undisturbed Shear Wave Results (Rebecca Shoals Site)

Consolidation ▲ Shear

6.6 Variability of Lower Florida Key Sediment Microstructure and Stress-Strain Behavior (D.R. Brogan, A.J. Silva and G.E. Veyera)

Variability of Lower Florida Key Sediment Microstructure and Stress-Strain Behavior

David R. Brogan, Armand J. Silva, George E. Veyera

Marine Geomechanics Laboratory
University of Rhode Island
Narragansett, RI 02882

Lower Florida Keys sediments from the Marquesas and Dry Tortugas study sites are a carbonate silty clayey fine sand composed primarily of angular particles. Calcium carbonate contents vary slightly between study sites ranging from about 85% to 93%. Measured specific gravities range from 2.73 to 2.90 averaging about 2.80. Liquid limits and plastic indices range from 33% to 53% and from 4 to 25, respectively, with many samples exhibiting non-plastic behavior. Little lateral variability of sediment physical properties is seen between and/or within the study sites. However, vertical variability is most evident within the upper 10 cm at both study sites.

Constant rate of deformation (CRD) compressibility tests and permeability tests were performed on eighteen samples from cores 178-GC, 313-GC and 326-GC at depths ranging from the upper 15 cm down to 230 cm from the Marquesas and Dry Tortugas study sites. The compression data show that the sediments have very low compression indices (0.15 to 0.50) and recompression indices (0.01 to 0.05). The low indices are representative of a relatively stiff sediment structure. The stress state ratio (preconsolidation stress normalized with effective overburden stress) for the samples ranges from about 1 to 63 reflecting the possibility of cementation and/or intraparticle bonding. In-situ permeabilities interpolated from measured permeabilities range from 0.6×10^{-6} cm/s to 6.0×10^{-6} cm/s showing a

linear relationship between void ratio and logarithm of permeability. In situ void ratios were determined from water content measurements of the samples and range from 1.0 to 1.8. A sample from core 313-GC at 147-151 cm depth was remolded to its original void ratio and retested. Remolding altered the sediment structure significantly as the compression index decreased from 0.21 to 0.14 and the permeability decreased from 4.6×10^{-6} cm/s to 0.6×10^{-6} cm/s. Remolding seems to create a stiffer and less permeable sediment structure probably due to a more even distribution of fine particles.

Isotropically consolidated undrained (CIU) strength tests were performed on a total of seventeen undisturbed and remolded sediments from cores 284-BC and 324-BC from the Dry Tortugas study site. The strength behavior of these sediments is typical of uncemented calcareous sediments and loose sands. During shear, the initial strength response is stiff while large excess pore pressures are developed as the sediment contracts. Dilative behavior sets in at about 5% axial strain as the sediment tends to expand forcing the excess pore pressures to decrease towards zero at large axial strains. Deviatoric stress responses continually increase with strain, flattening out only at large values of axial stain showing no signs of brittle behavior characteristic of cemented sediments. The maximum effective stress ratio was used as the failure criteria which occurred at large axial strains of about 10%. The resulting friction angles ranged from 37^{o} to 39^{o} for both undisturbed and remolded samples. Comparisons of undisturbed and remolded sediment deviatoric stress responses during shear point towards possible effects of particle interlocking. For remolded samples stress-strain behavior indicates a degree of particle rearrangement due to a looser fabric as stress relaxation is seen after the initial stiff response. Conversely, deviator stress responses of undisturbed samples suggest a restriction of particle movement (mobility) and a more rigid sediment structure as no stress relaxation is observed. Grain size analyses were performed on undisturbed and remolded samples before and after shear. Results show that there was no significant particle degradation (crushing) due to the remolding procedures

or shear stresses between particle contacts. Initial tangent moduli were calculated from deviatoric stress responses within the initial 2% of axial strain. Moduli range from 130 to 18,873 kPa and are exponentially dependent upon the initial effective stress suggesting that interlocking of the angular grains occurs to a higher degree with increasing effective stress.

In conclusion, lower Florida Keys sediments recovered from the Marquesas and Dry Tortugas study sites do not exhibit characteristics of cemented sediment and behave as a non-cemented calcareous sediment and a loose sand. The sediment physical properties are very similar between study sites yet do show vertical variations within the study sites, predominantly within the upper 10 cm. The sediment exhibits stiff deformation and stress responses and large axial strains at failure. Interlocking of the angular particles appears to be the controlling mechanism of the characteristic stiff non-cemented stress-strain behavior of these sediments.

Summary of Consolidation and Permeability Test Results for Lower Florida Keys Sediments

Sample[a]	Depth (cm)	Water Content (%)[b]	Compression Index, C_c	Recompression Index C_r	Preconsolidation Stress, σ'_c (kPa)	Overburden Stress, σ'_o (kPa)	SSR	Permeability k ($\times 10^{-6}$ cm/s)[c]
178-GC	11-16	44	0.22	0.02	4.3	1.0	4.3	-
	26-31	-	0.34	-	7.0	2.1	3.3	1.3
	54-59	63	0.40	0.02	10.0	4.1	2.5	0.7
	82-87	59	0.50	0.04	9.5	5.9	1.6	1.3
	181-186	53	0.26	0.01	11.0	13.0	0.9	-
	208-213	46	0.25	0.02	12.0	15.0	0.8	0.7
313-GC	5-9	49	0.25	0.01	30.0	0.5	62.5	5.5
	17-21	43	0.15	0.05	9.0	1.3	6.8	2.5
	45-49	42	0.23	0.01	72.0	3.6	20.3	6.0
	81-85	36	0.17	0.01	165.0	6.6	25.2	-
	147-151	35	0.21	0.01	64.0	12.3	5.2	4.6
R	147-151	35	0.14	0.01	-	-	-	0.6
	181-185	38	0.17	0.01	8.5	15.2	0.6	-
326-GC	10-14	41	0.16	0.02	6.0	0.8	7.5	5.5
	45-53	44	0.25	0.01	3.6	2.4	1.5	-
	79-83	53	0.38	0.01	8.6	6.4	1.4	3.9
	174-178	66	0.46	0.02	9.5	11.6	0.8	1.2
	229-233	48	0.39	0.02	28.0	17.2	1.6	-

Note:
R - Remolded
a - 178-GC - Marquesas Site; 313-GC and 326-GC - Dry Tortugas Site
b - corrected for 35 ppt salt content
c - at in-situ void ratio from e-log k plots

Summary of Box Core Triaxial Compression CIU Strength Tests of Lower Florida Keys Sediments, Dry Tortugas site

Core No.		Sample Depth[a] (cm)	Void Ratio	Failure Strain ε_f (%)	Failure Eff. Stress Ratio	Failure Deviator Stress (kPa)	Pore Pr. Parameter A_f	Initial Tangent Modulus[b] e_i (kPa)
284	2-13 U	1.2	31.7	11.6	3.9	51.4	0.27	-
284	2-15 R	1.0	34.0	11.8	4.3	58.0	0.33	18873
284	2-13 U	1.1	16.0	12.7	3.9	28.6	0.22	6077
284	2-17 R	1.3	13.9	11.6	4.0	13.9	0.50	6981
284	2-13 U	1.1	15.0	10.5	4.4	21.7	0.39	4444
284	2-13 R	1.1	16.5	11.4	4.4	32.3	0.23	-
284	3-14 U	1.2	2.4	6.9	5.9	9.2	0.05	2077
284	3-16 R	1.2	2.2	11.9	6.1	3.3	0.39	530
284	9-11 R	1.0	1.8	11.1	8.4	6.6	0.14	650
324	1-12 U	1.3	29.6	11.7	4.4	34.0	0.57	11125
324	1-14 R	1.2	28.2	13.0	3.9	25.5	0.75	12444
324	1-12 U	1.3	10.5	11.7	4.3	18.4	0.27	3988
324	0-15 R	1.2	10.0	11.0	4.8	20.0	0.24	3879
324	3-14 U	1.3	8.3	9.2	4.2	17.6	0.15	2397
324	3-17 R	1.2	6.2	17.2	4.1	11.7	0.21	-
324	2-13 U	1.4	1.5	14.0	5.8	3.7	0.19	130
3224	0-13 R	1.4	1.2	20.5	40.0	2.7	0.44	166

a - "U" and "R" denote undisturbed and remolded samples, respectively
b - Initial tangent modulus using Konders (1963) method

Undisturbed vs Remolded Shear Strength Behavior

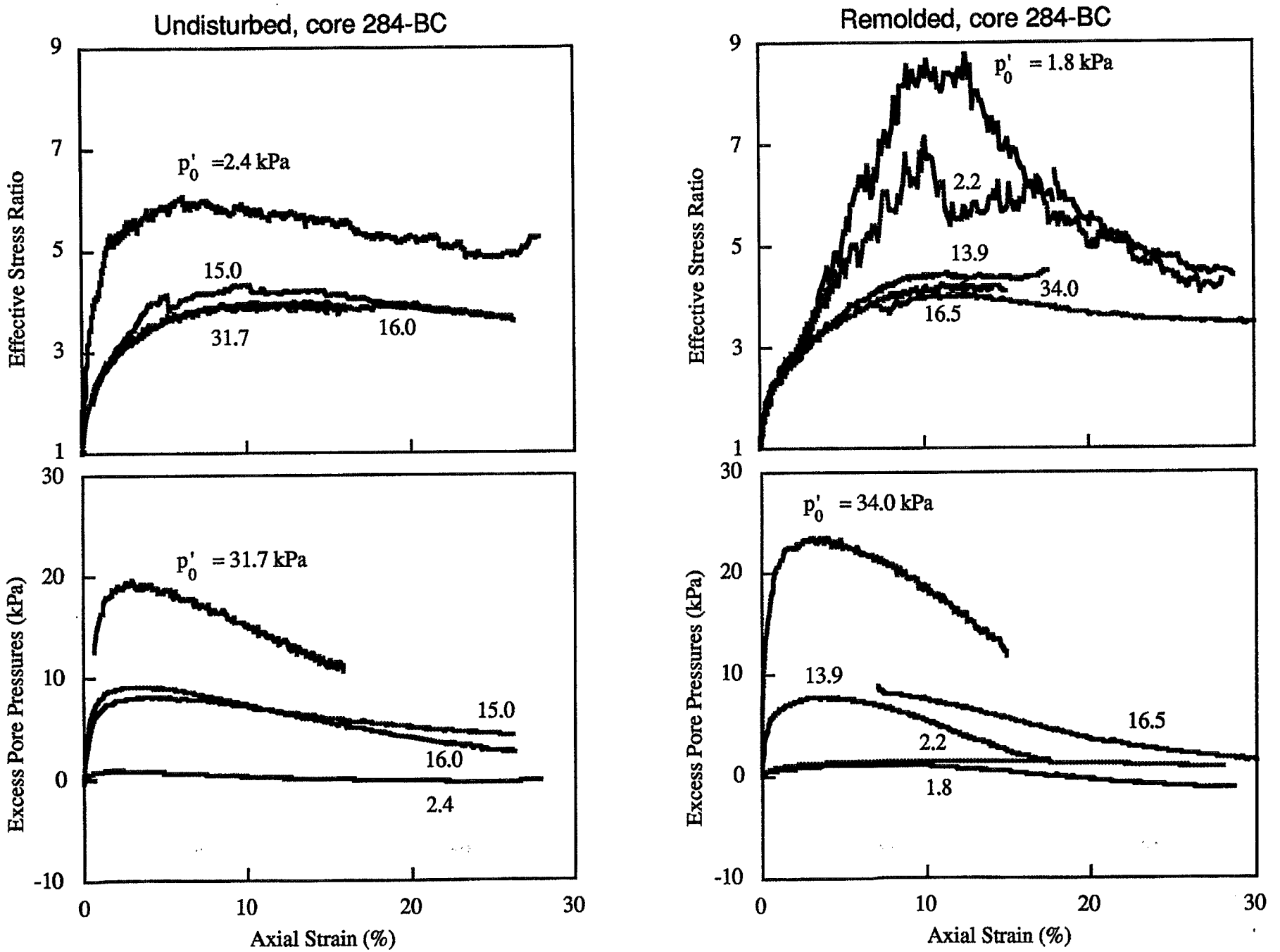

Undisturbed vs Remolded Deviatoric Stresses

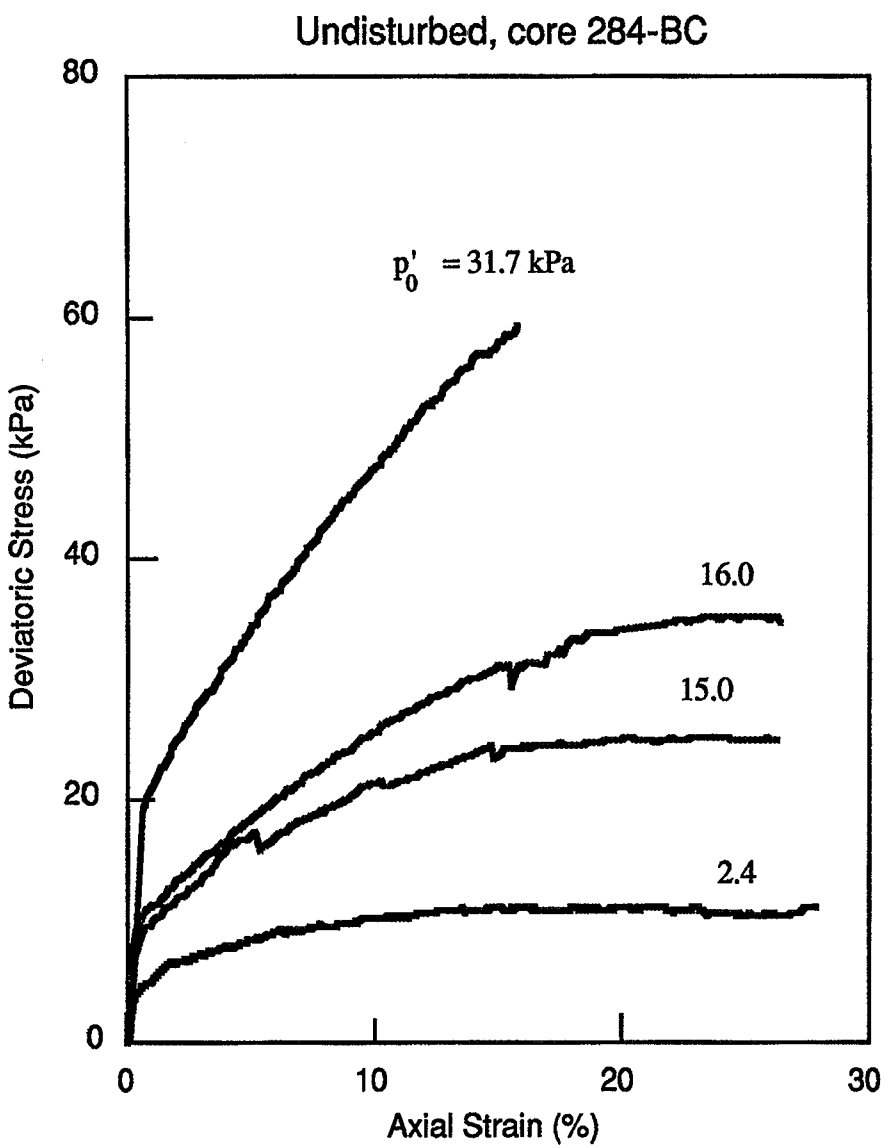

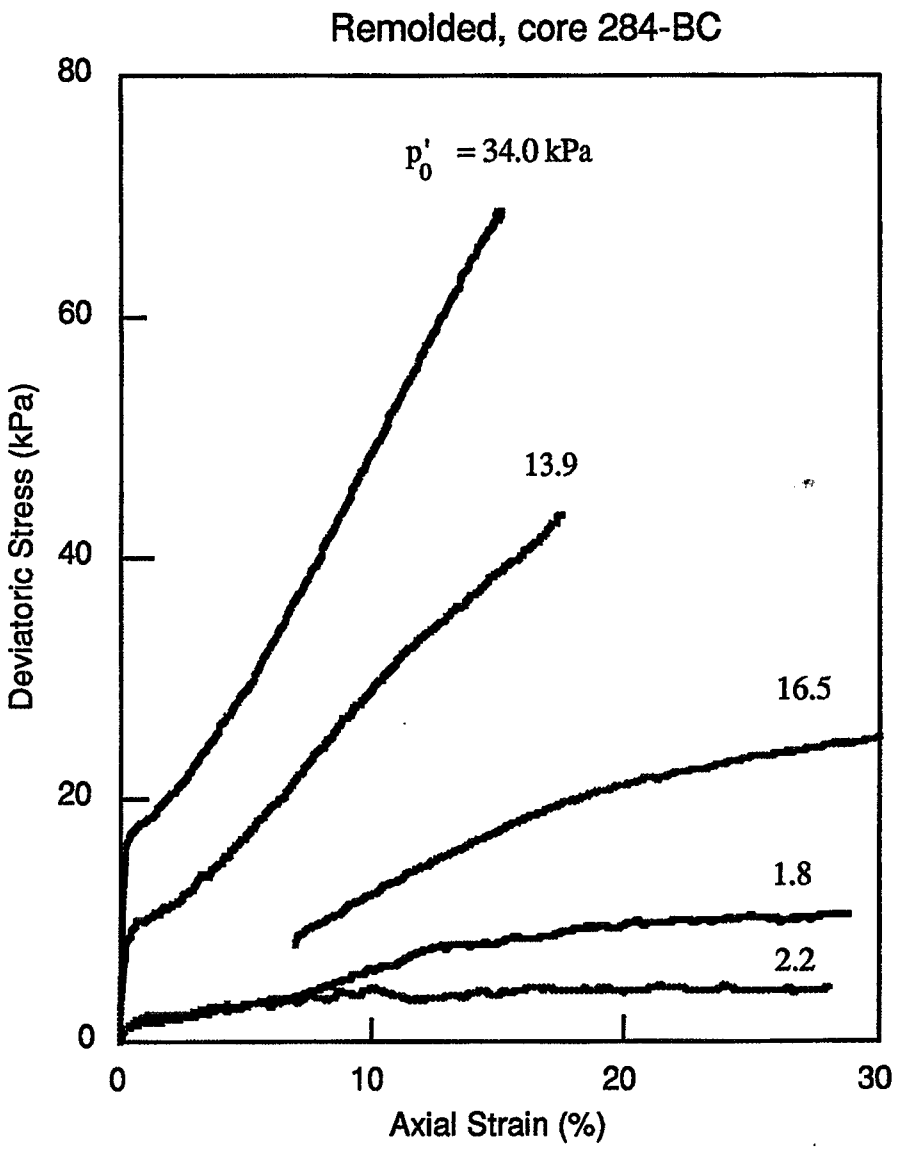

6.7 Geotechnical Characteristics of Dry Tortugas and Marquesas Sediments (D.L. Lavoie, K. Stephens, Y. Furukawa and D.M. Lavoie)

Geotechnical Characteristics of Dry Tortugas and Marquesas Sediments

***Dawn Lavoie, **Kevin Stephens,**
****Yoko Furukawa and *Dennis Lavoie**

*Naval Research Laboratory
Marine Geosciences Division
Stennis Space Center, MS 39529

**University of Southern Mississippi
Institute of Marine Science
Stennis Space Center, MS 39529

Introduction

Physical and acoustic properties depth profiles in marine sediments generally show a response to overburden loads, i.e., water content and porosity decrease, while density and velocity increase, with loading. We would like to extrapolate physical and acoustic property values measured during consolidation testing to the appropriate depths in situ. We assume when we consolidate sediments in the laboratory that: (1) we can relate laboratory-derived values to in situ values, (2) we can use these laboratory-derived values with confidence to model the seabed, and (3) that variables other than overburden have minimal effect in situ sediment properties. The purpose of this presentation is to examine these assumptions in the context of the shallow water carbonate sediments recovered from the Dry Tortugas and Marquesas Keys during the Key West Campaign.

Methods

Samples were analyzed for mass physical properties (water content, porosity, wet bulk density, grain density and void ratio) using a Quantachrome helium pycnometer. Grain size distribution was measured by sieving sand- and gravel-sized grains and pipetting silt- and clay- sized grains following Folk's (1974) methodology. Whole round sections of sediment (2.5 cm X 6.35 cm) were consolidated in a Soil Test consolidation frame with a modified cell instrumented with compressional and bender element shear wave transducers (Figure 1) . Compressional wave velocity is measured at ~190 kHz; shear wave velocity is measured at ~ 10 kHz. Standard testing procedures were followed for the loading and unloading sequence (Lambe, 1951; Lavoie, 1988).

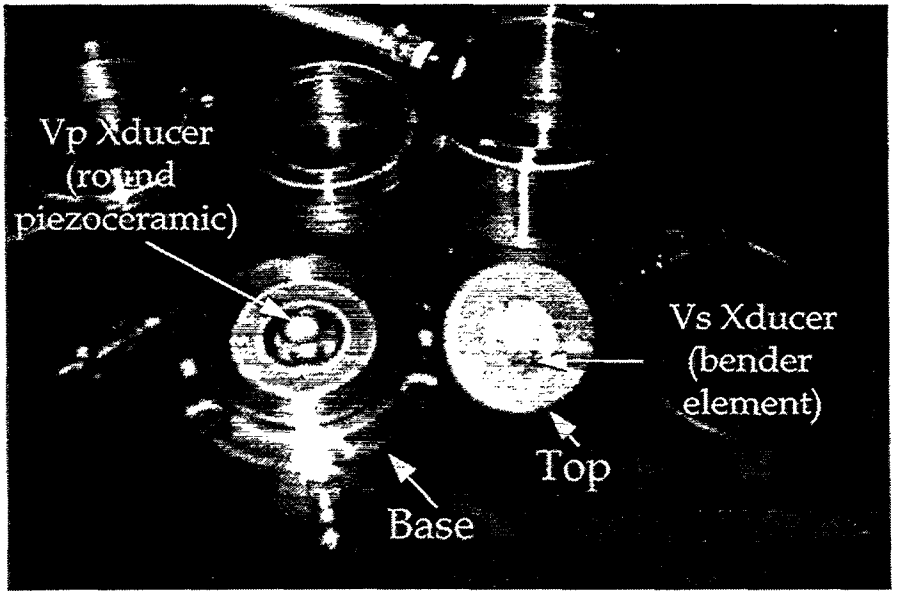

Figure 1. Consolidometer modified to accept compressional and shear wave transducers. Assembly mounts in a standard Soil Test Consolidometer frame and consolidation tests are loaded as usual with velocity measurements made at each load at the end of primary consolidaltion.

Results and Discussion

Consolidation results suggest that both the Dry Tortugas and Marquesas sediments are overconsolidated, by about 150-180 kPa and 40-55 kPa respectively (Figure 2).

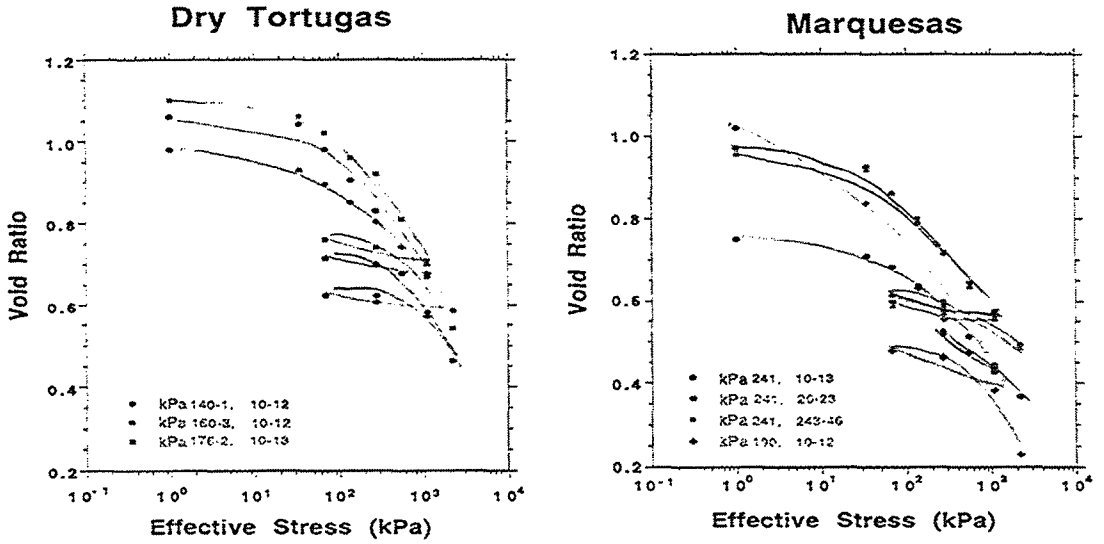

Figure 2. Consolidation testing was performed on Tortugas cores (KW-PE-DC-140-1 (10-13 cm), 160-3 (10-13 cm) and 176-2 (10-13 cm)) and Marquesas cores (KW-PE-DC-190-2(10-13 cm), KW-PE-GC-241 (10-13 cm), 241 (20-223 cm) and 241 (43-46 cm).

Compressional wave velocity, measured during consolidation testing in the laboratory, increases with increasing effective stress (converted to estimated depth in situ using measured bulk density) in both the Dry Tortugas and Marquesas sediments (Figure 3). In contrast, compressional wave velocity measured and corrected for in situ temperature, pressure and intraparticle porosity (Urmos and Wilkens, 1993) using transducers mounted in a Hamilton Frame in the laboratory on cores recovered from northern Little Bahama Bank (ODP Leg 101, Site 630) shows minimal increase with depth and significantly lower values of compressional wave velocity than those measured during laboratory testing (Lavoie 1986). Results from Site 630 suggest that the carbonate sediment (predominantly foraminifers and coccoliths) consolidate much less in situ than in the laboratory. Carbonate sediments in the Bahamas are probably undergoing early pressure solution and cementation, thus preventing significant consoliation with depth. Time and temperature conditions necessary for pressure solution and cementation in the laboratory cannot be adequately simulated, thus the Dry Torugas and Marquesas sediments are easily consolidated during laboratory testiing.

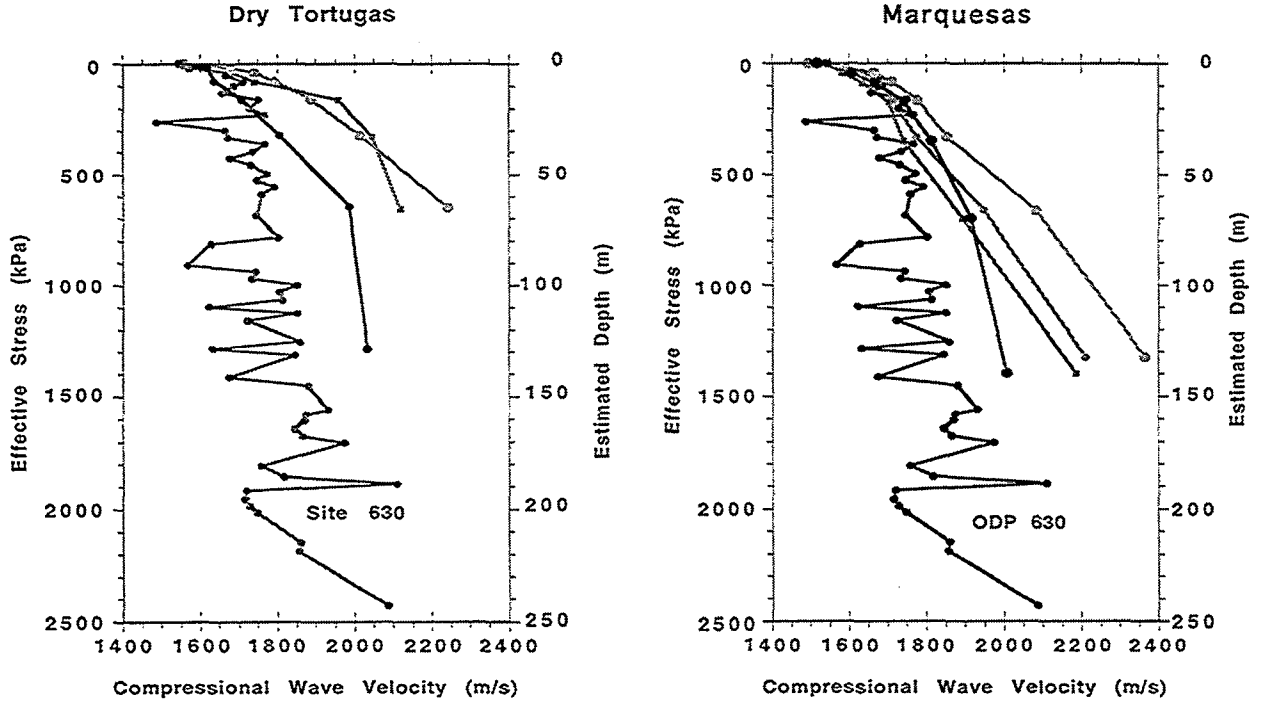

Figure 3. Compressional wave velocity measured in the laboratory during consolidation testing shows much higher values of velocity and a greater increase as a function of effectve stress than velocity measured on cores actually recovered from depth at ODP Site 630 after correcting for temperature, pressure and intraparticle porosity (after Urmos and Wilkens, 1993).

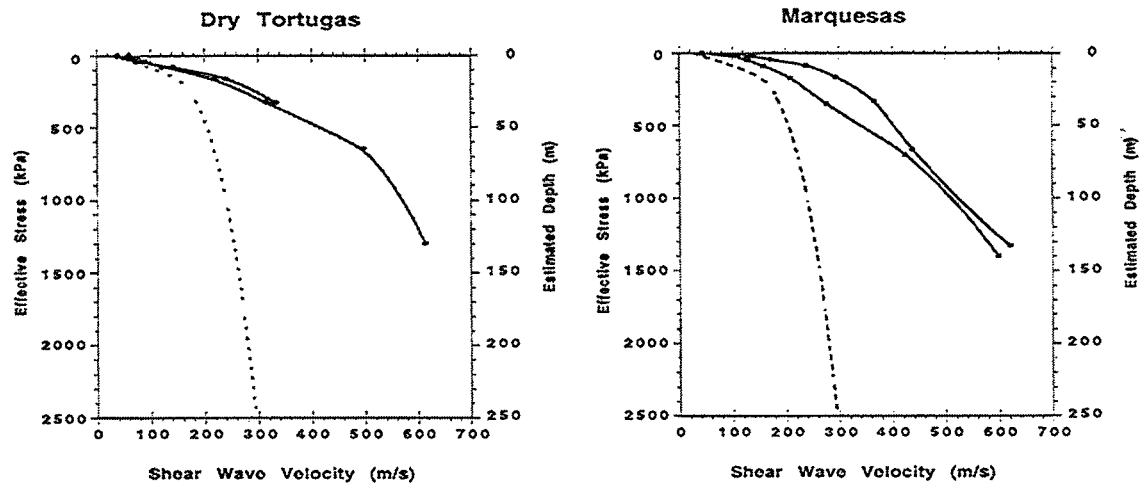

Figure 4. Shear wave velocity measured during consolidation testing and estimated from measured porosity using Bryan and Stoll's (1988) model. Solid lines represent values measured during consolidation testing. Dashed lines are predicted values of shear wave velocity (after Bryan and Stoll, 1988).

Meaured shear wave values, not available for Site 630, were estimated using Bryan and Stoll's model (1988) which uses void ratio and estimated effective stress as input parameters and calculates shear wave velocity. Shear wave velocity values measured during consolidation testing show much higher values and a greater rate of increase with estimated depth than the predicted values (Figure 4).

These results suggest that velocity values measured during consolidation testing cannot be extrapolated to estimated in situ depths because (1) in situ time- and temperature-related processes cannot be accounted for in laboratory consolidation testing and (2) shallow- water carbonate sediments are highly variable even in closely located sites. For example, measured properties from the Dry Tortugas and Marquesas sites show very different down- hole trends (Figures 5 and 6). Measured sediment properties from the Dry Tortugas show expected trends to about 2 m below sea floor (mbsf). Wet bulk density and compressional wave velocity increase; porosity decreases. The percentage of calcium carbonate stays the same, grain density increases very slightly. Mean grain size stays approximately the same until about 1.5 m, below which the mean grain size decreases. Below about 2 mbsf, a distinctly different layer of finer grain size, higher porosity and lower wet bulk density and compressional wave veloicty is present. In the Marquesas the pattern is very different. Wet bullk density and compressional wave velocity, after an initial increase, decrease and then increase again. Porosity trends mirror wet bullk den-

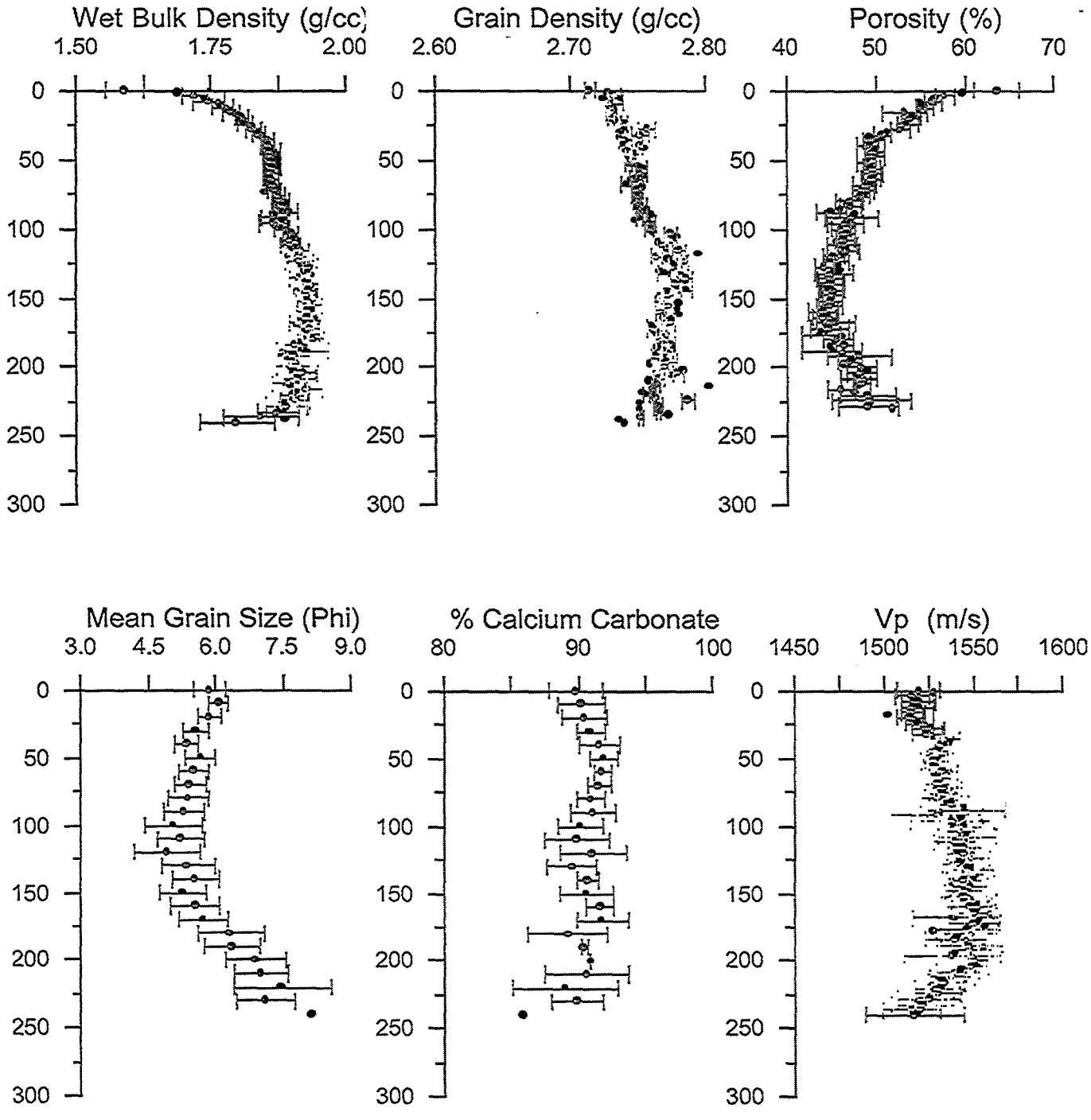

Figure 5. Measured sediment properties from the CBBL Dry Tortugas experiment site. Down hole values show the expected trends. Below 2 mbsf, a distinctly different layer of finer grain size, higher porosity and lower wet bulk density and compressional wave velocity is evident. Points are average values, error bars represent 90% confidence interval. Data are from between 12 to 44 gravity cores.

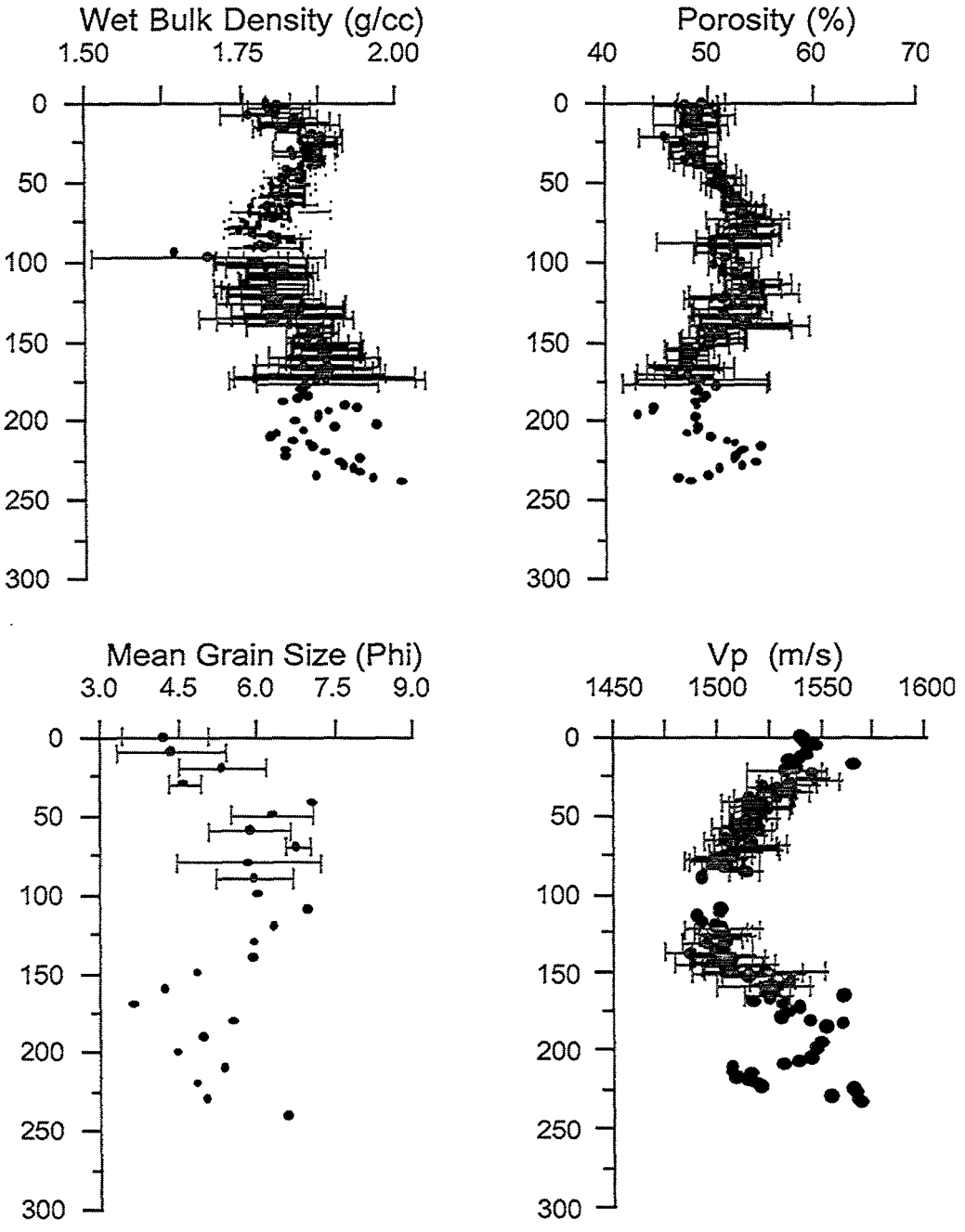

Figure 6. Sediment properties measured from the CBBL Marquesas experiment site. Variations reflect lithologic (indicated by mean grain size variations) changes rather than the effects of overburden pressure suggesting that time-dependent processes that tend to influence consolidation (not important over the short time span of laboratory testing) are operative in this site. Points are average values, error bars represent 90% confidence interval. Data are from between 12 to 44 gravity cores.

sity. Grain size increases and then decreases. It is apparent that mean grain size, which reflects fabric differences between the two sites, is a controlling variable.

Thin section views of the microfabric of the Marquesas Keys sediments explain why the expected trends (if the sediment column were consolidating normally) are not evident. Instead of decreasing porosity downhole, we see increasingly large void spaces held apart by large grains, particularly by 1.2 mbsf. No evidence of precipitation is apparent, thus cementation is not a factor. Pore fluid evidence (Furukawa and Lavoie, this volume) suggests that dissolution is a minor factor. Rather, bimodal grain size distribution (Stephens, personal comm.) and images (Figure 7a-f) suggest that the fabric is grain supported and the physical proximity of the grains is preventing any significant consolidation. Thus, the sediment property trends reflect mean grain size rather than respond to overburden pressure. In contrast, sediment fabric in the Dry Tortugas is generally matrix supported, and even the widespread shell layer at about 100 cm bsf has considerably more matrix material than the Dry Tortugas sedimentt (Figure 8a and b), allowing some consolidation which is reflected in the mass physical properties.

In conclusion, the measured sediment properties and microfabric suggest that in the shallow-water carbonate sediments of the Dry Tortugas and Marquesas Keys, overburden pressure is secondary to fabric in controlling sediment behavior.

REFERENCES

Bryan GM and Stoll RD (1988) The dynamic shear modulus of marine sediments. Journal of the Acoustical Society of America 83(6):2159-2164

Folk RL (1974) Petrology of Sedimentary Rocks. Hemphill Publishing Co., Austin, TX, 78703, 182 p

Furukawa, Y., and Lavoie D. (this volume) A geochemical investigationof early diagenetic effects of sedimentary structures.

Lambe, T.W., 1951. Soil Testing for Engineers. John Wiley and Sons, New York, 165 pp.

Lavoie, D.L. 1988. Geotechnical properties of sediments in a carbonate-slope environment; Ocean Drilling Program Site 630, Northern Little Bahama Bank. In: Austin, J.A, Schlager, W. and others (eds). Proceedings Ocean Drilling Program, Scientific Results, 101, College Station, TX, pp 315-326.

Lavoie, D.L. 1986. Physical properties, Site 629 and 630. Bahamas Vol 101, In: Austin, J.A, Schlager, W. and others (eds). Proceedings of the Ocean Drilling Program, Part A, Initial Report, College Station, TX pp282-294

Urmos, J. and R.H. Wilkens, 1993. In situ velocities in pelagic carbonates: new insights from Ocean Drilling Program Leg 130, Ontong Java Plateau. Journal of Geophysical Research, v 98. no. B5 pp 7903-7920.

Marquesas

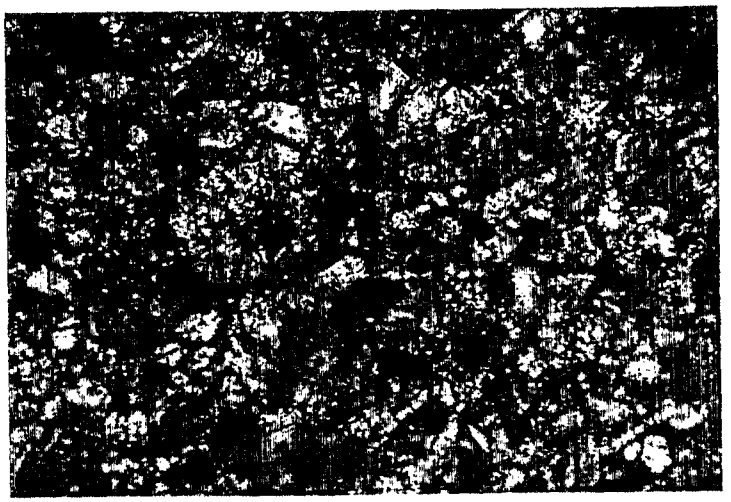

KW-PE-GC-203
(20-22 cm)

7a

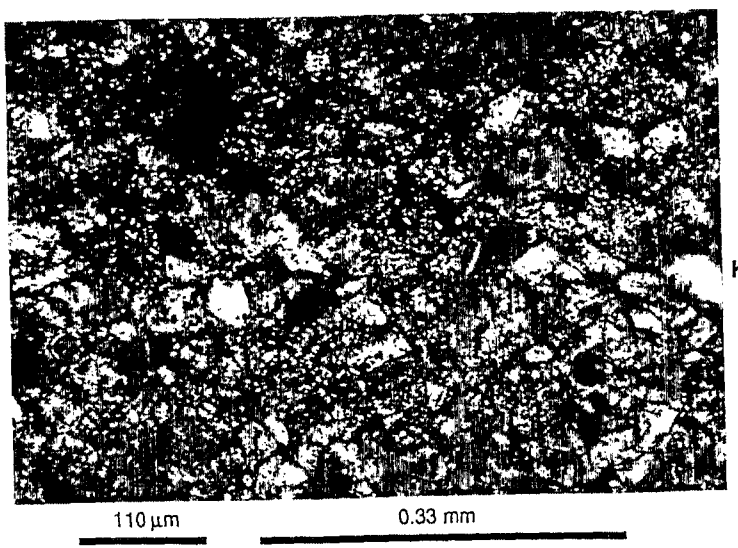

7b

KW-PE-GC-203
(60-62 cm)

Marquesas

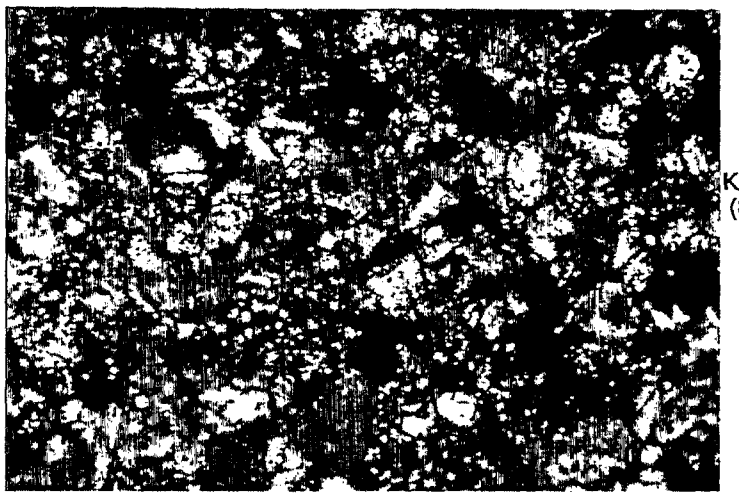

KW-PE-GC-203
(80-82 cm)

7c

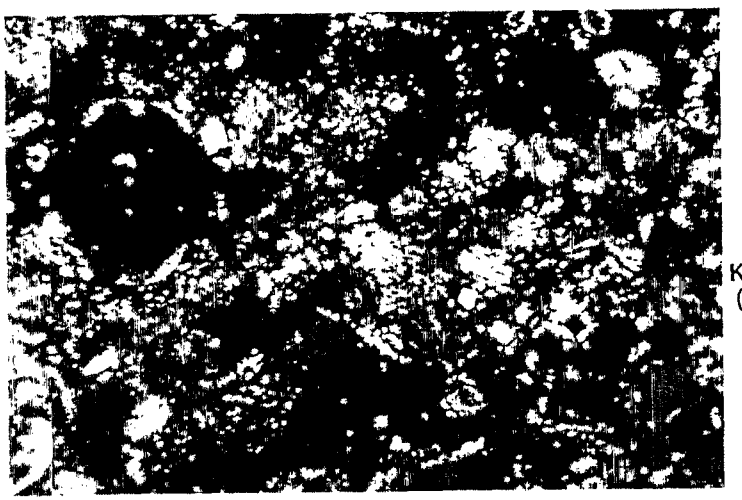

7d

KW-PE-GC-203
(100-102 cm)

Figure 7a-f. Thin section images of sediments recovered from the Marquesas Keys. Note the increasing void space and grain-supported nature of the fabric with depth.

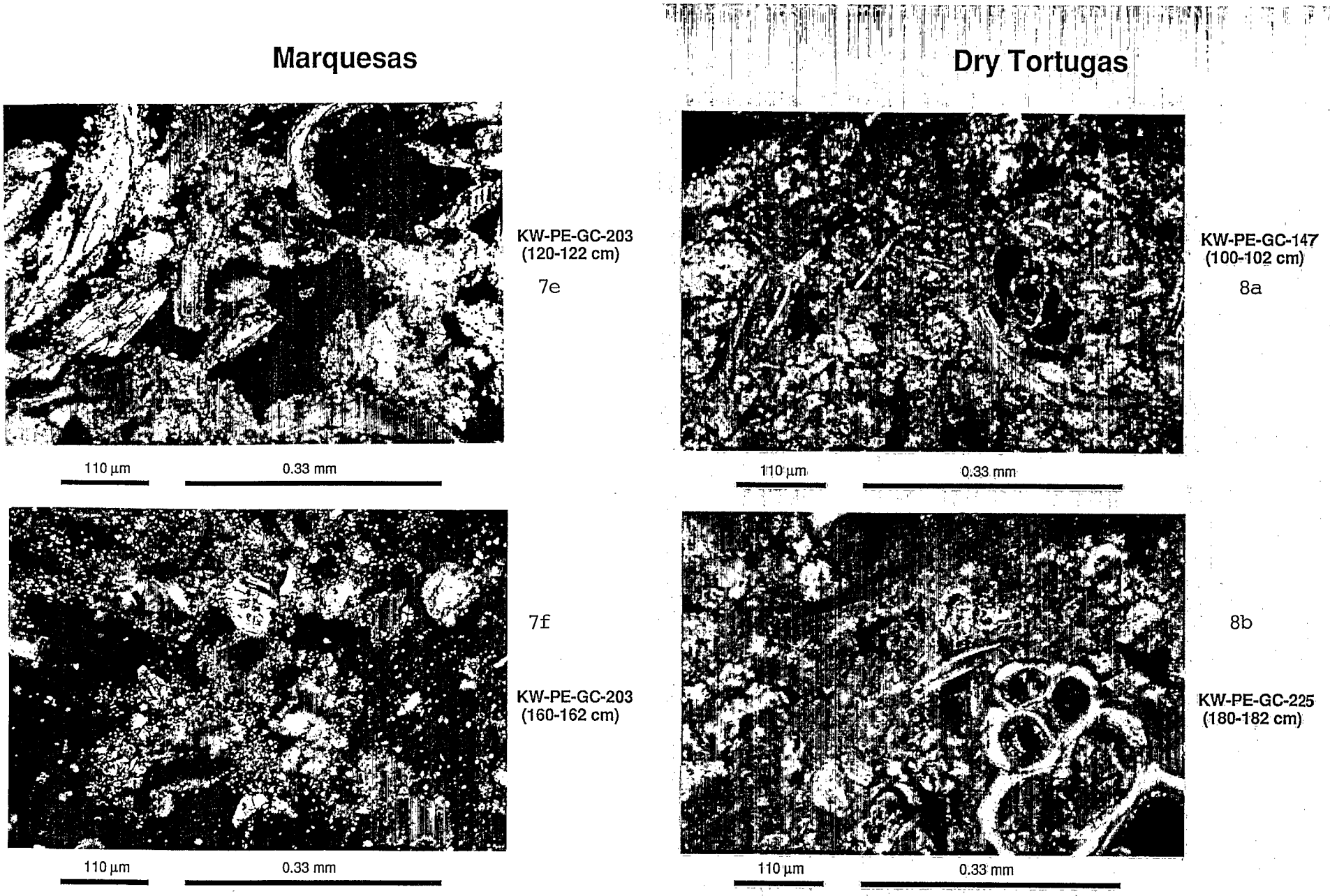

Figure 8a-b. Thin section images of sediment recovered from the Dry Tortugas. Note the amount of matrix material at 100 and 180 cm bsf.

6.8 Acoustic Imaging of Carbonate Sediments from the Lower Florida Keys (L.J. Pyrak-Nolte, D. Lavoie, K. Stephens, B.L. Mullenbach and A.S. Grader)

Acoustic Imaging of Carbonate Sediments from the Lower Florida Keys

L. J. Pyrak-Nolte[1], D. Lavoie[2], K. Stephens[2], B. L. Mullenbach[3], and A. S. Grader[4]

[1]Dept. of Civil Engineering & Geological Sciences Univ. of Notre Dame, Notre Dame, IN 46556-0767, Telephone: 219-631-8377; e-mail: pyrak-nolte@nd.edu. [2]Naval Research Laboratory, BLDG 1005, Stennis Space Center, MS 39529, Telephone: 601-688-5527; e-mail: dlavoie@zephyr.nrlssc.navy.mil. [3]Marine Sciences Research Center, SUNY-Stony Brook. [4]Department of Mineral Engineering, The Pennsylvania State University Park, PA 16802

Accurate interpretation of sediment strata from seismic data relies on a knowledge of the effect of sediment structure on acoustic wave propagation. In the laboratory, we performed acoustic imaging (360 kHz) on synthetic and natural marine sediments to determine the effect of grain size, density and layer thickness on acoustic wave propagation.

Synthetic unconsolidated saturated sediments (60 mm x 60 mm x 60 mm) were created from soda-lime silica beads with mean diameters of 127 microns (fine grain) and 570 microns (coarse grain). The fine grain layer exhibited a lower density, a higher velocity, more attenuation (Figure 1), and a lower frequency content than the coarse grain layer. The interface between two layers is a region of inter-mixing which produces a layer with a higher mass density and lower porosity than the individual half-spaces. These high-mass interfaces dominate the amplitude and frequency response of acoustic waves propagating parallel to the interface, but do not affect group velocity, which depends only on grain size and therefore is not sensitive to the interface.

The natural marine sediment cores were recovered from the sediment-water interface from the Southeast Channel of the Dry Tortugas, an area dominated by silt- and sand-size carbonate sediments. The Dry Tortugas experiment site is a low energy, lagoonal, coral reef environment near the Southeast Channel of the Dry

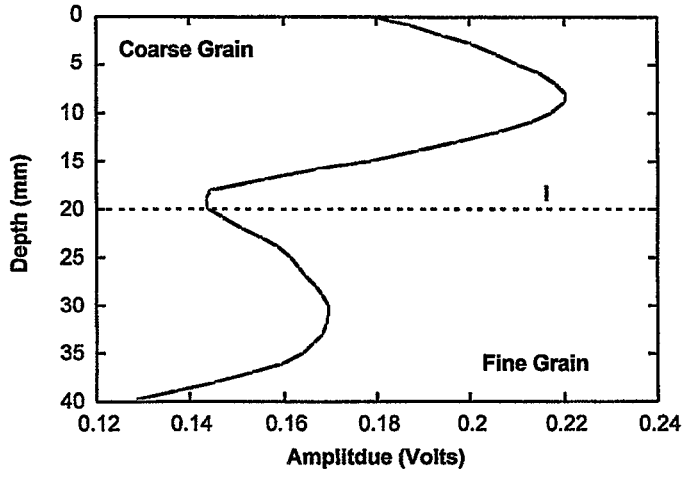

Figure 1. Variation in spectral amplitude as a function of depth in a synthetic sediment composed of a fine grain layer overlain by a coarse grain layer.

Tortugas. In the Key West cores, acoustic measurements (360 kHz) were made over a 95 mm length (1 mm increments) of the cores for several azimuthal angles. For core KW-160-2, alternating acoustic layers were marked by either (a) regions that exhibited high spectral amplitude, high group velocity, and high frequency; or by (b) regions that exhibited low spectral amplitude, low group velocity, and low frequency. The acoustically observed layers varied in thickness between 7 mm and 20 mm. Sediment analysis (in 0.5 cm intervals) indicated a monotonic increase and decrease in wet bulk density and porosity, respectively with depth but did not indicate the presence of distinct layers. However, the layers indicated by the variations in spectral amplitudes corresponded to changes in grain size (Figure 2). Regions of high spectral amplitude correlated with regions of high percent coarse grain sizes. Therefore, while the acoustic response of a sediment depends on density, porosity and grain size, sediment core analysis may not measure the other relevant physical properties that control the acoustic response, namely the spatial distribution of particles at a given depth, degree of cementation, the material between grain contacts, and intra-grain porosity.

LJPN acknowledges support of this research by the Office of Naval Research (N00014-94-1-0567) through a Young Investigator Award.

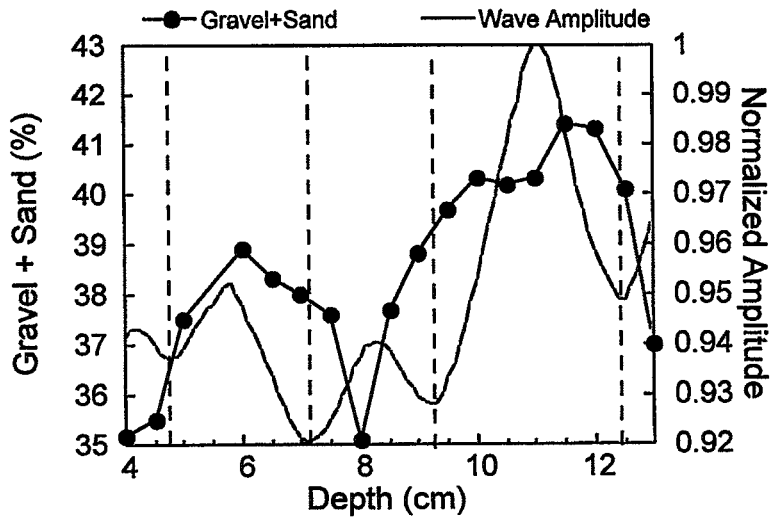

Figure 2. Percent coarse particles (gravel and sand sizes) and normalized spectral amplitude as a function depth in core KW-160-2. Dashes indicate layer interfaces based on acoustic data.

6.9 Microfabric of Dry Tortugas and Marquesas Carbonate Sediment (D.M. Lavoie) Modeling

MICROFABRIC OF DRY TORTUGAS AND MARQUESAS CARBONATE SEDIMENT

Dennis M. Lavoie

Ocean Sciences Division
Naval Research Laboratory
Stennis Space Center, MS 39529

EXTENDED ABSTRACT

Carbonate sediments of the Dry Tortugas site were studied primarily by embedding critical point-dried sediment subsamples in epoxy, polishing one surface, coating with a thin carbon conductive layer, and examining the sample with scanning electron microscopy (SEM) using the backscattered electron (BSE) signal. Images collected in this manner are virtually two-dimensional because the nanometer thickness of the image depth is orders of magnitude less than the x-y dimensions. Feature area and other measurements made on 2-D sections can be related quantitatively to volume parameters in the sample, according to the stereological principle of Delesse (Weibel, 1979). Eventually, we plan to collect a series of 2-D sections through this sediment to build a database that can be used to model the 3-D structure. Such a 3-D reconstruction is technically easier in a grain-dominated sediment compared to a siliciclastic mud because the grains are well defined, and the larger scale is more amenable to the precise positional registration needed between successive sections. Higher resolution images were collected using ultra-thin sectioned, embedded samples that were examined with transmission electron microscopy (TEM).

The typical appearance of sediment at the two sites is shown in Plate 1, which consists of a series of SEM micrographs at increasing magnification (not necessarily all of the same field). Except for varying amounts of molluscan shells and amounts and types of Foraminiferan shells, there was little obvious difference at the microscale among samples taken at different locations or at different depths. Larger (mm scale) shells and shell fragments, visible in Plate 1a, were often oriented vertically, for reasons unknown. Increasing magnification reveals the virtually complete biogenic composition of the sediment. Molluscan and Foraminiferan shell fragments of all sizes are frequent, but the most common particles sand-sized grains are fragments of the carbonate-secreting green macroalgae *Halimeda.* Many fragments of all types (and at all depths examined) appear to be perforated and eroded, possibly due to chemical dissolution or the action of boring algae (Charlotte Brunner, personal communication). At higher magnification (Plate 1b-d) , a darker gray layer of amorphous matrix can be seen associated with many fragments. At the nanometer resolution of the TEM, the matrix is revealed to be a loose mixture of what appears to be aragonite (a form a calcium carbonate) crystals admixed with particles of indeterminate origin (Plate 2, provided by Yoko Furukawa). Also by TEM, *Halimeda* fragments are seen to be composed solely of aragonite crystals (Plate 3). Mollusk shells are also composed of aragonite to a large extent, but the large volume of matrix material points to a *Halimeda* origin for most aragonite crystals in the matrix fraction. Matrix could have been incorporated into the sediment at time of deposition or could have been generated in situ by the breakdown of *Halimeda*-produced grains; however, few of the larger fragments of any type exhibit a gradation of particle sizes at the grain-matrix interface, indicating that matrix is not being produced in situ to an appreciable extent. Plate 4 shows one of the few grains undergoing degradation. Another observation is that very few grains (sand-sized particles of any composition) appear to be in direct contact. Most grains are separated by varying thicknesses of matrix material, despite the fact that this sediment would fall under Dunham's (1962) definition of grain supported carbonate sediment, and this fact

may have implications for micromechanical modeling. We shall undertake further studies of microfabric images to measure frequency and angles of grain contacts for input into micromechanical models of this sediment.

Interparticle porosity determined from images was in the range 20-40% (Figure 1). In order to test the hypothesis that sediment properties on the micrometer scale can be related to bulk properties, image porosity was compared to bulk porosity. Using an image analysis system that compared pixel areas of designated features, digital images were initially processed by correcting for uneven illumination (if necessary) by a multiple low-pass filter/background subtraction algorithm, then correcting for contrast and brightness. A single threshold was set by eye that best highlighted void space, and the program then automatically computed the percentage area covered by void. The threshold was then stepped 4 and 8 gray levels above and below the "best" threshold to measure variability in the technique (the 4 level step is arbitrary, chosen because it usually produces a slightly noticeable difference in the thresholded image). The amount of variability in area percentage induced by varying the threshold around a "best" gray level reflects both the choice of threshold (i.e., whether the operator has adequately separated the image features) and the contrast of the image (i.e., if all 256 levels of gray are represented and if contrast between void space and solids is sufficient). As an internal check on the thresholding procedure, the threshold was then visually set to measure the solids area without reference to the voids threshold. Generally, void + solid percentages were within a few points of 100%, indicating consistency in choice of the threshold. At least three different random micrographs of the same sediment sample were analyzed in this manner to determine sample variability. Dispersion about the mean was expressed as 95% confidence intervals calculated for small sets of numbers (Dean and Dixon, 1951). A composite confidence interval (technique error + sampling error) of 2 - 3% was typical.

Interparticle porosities measured by image analysis were significantly less than bulk porosities. Figure 1a plots image interparticle porosity alongside bulk porosities (provided by Dawn Lavoie, personal communication) for gravity core 147 from the Tortugas site and gravity core 203 from the Marquesas site. The missing porosity was believed to be intraparticle, i.e., in the matrix and Halimeda fragments. Intraparticle image porosity was determined on Plates 2 and 3, which were considered typical for matrix and *Halimeda* fragments respectively. Sampling variability was estimated by analyzing four quarters of each image and treating the measurements as separate samples. Porosity of *Halimeda* fragments was estimated to be 33% ± 3.9 and that of matrix 24% ± 11.3.

Next, the relative areas of *Halimeda* and matrix were determined in representative images. As seen in the Plates, *Halimeda* fragments tend to be bright while matrix tends to be darker. The theoretical basis for this effect is that electrons are backscattered proportionally to the average atomic weight of the particle. Shells and *Halimeda* fragments are dense, and thus bright, relative to matrix (void space, being filled with epoxy, backscatters few electrons and is thus darkest). Rather than setting a conventional binary threshold, proportional areas of fragments and matrix were separately measured by setting a double threshold, i.e., for each fraction, a threshold was set on either side of the range of gray levels representing that fraction (material obviously of shell origin — generally only a few percent of the total image area — was excluded from the count). (A total area was computed as an internal check on the technique and generally was within a few points of 100%.) Total porosity, F_t , was then determined by:

$$F_t = Fv + (Fh * Ah) + (Fm * Am)$$

where Fv = Void porosity (interparticle)
Fh = Halimeda fragment porosity
Ah = Proportional area of Halimeda fragments

Fm = matrix porosity

Am = Proportional area of matrix.

Porosity estimates were also made for a sample from the Marquesas site before (Plate 1c) and after (Plate 5) experimental consolidation in the laboratory. Confidence intervals about the mean were determined for sampling variability (threshold variability was not determined). As can be seen in Table 2, within experimental error, all the bulk porosity can be accounted for by analyzing the microfabric. Based on this result, it should be possible to use 2-D images of microfabric to estimate other volume properties of the sediment, such as grain contact angle frequency and area, degree of matrix buffering between grains, tortuosity, permeability, distributions of various solid constituents, etc. Also, assuming no significant variation in intraparticle porosities (an assumption that needs to be tested with further TEM work), the discrepancy between interparticle porosities can interpreted as variations in the amount of fragments and matrix with depth. This was done in Figure 1b, which indicates an increase in intraparticle porosity with depth in these two cores. More study will be necessary to determine which fraction is responsible for the increase. Furthermore, the distribution of each fraction down through the sediment column should help elucidate the depositional history and possible geochemical and mechanical factors at work in these areas, as well as enable multilayer refinements to micromechanical models of acoustic behavior.

References

Dean, R.B. and Dixon, W.J., 1951. Simplified statistics for small numbers of observations. Analytical Chemistry, vol. 23 no. 4, 4 April 1951, p. 636-638.

Weibel, E.R., 1979. *Stereological Methods. Vol. 1: Practical Methods for Biological Morphometry.* Academic Press, New York, NY. 412pp.

Dunham, R.J., 1962. Classification of carbonate rocks according to depositional texture. In: *Classification of Carbonate Rocks*, W.E. Ham (ed.). Memoirs of the American Association of Petroleum Geologists No. 1, p. 108-121.

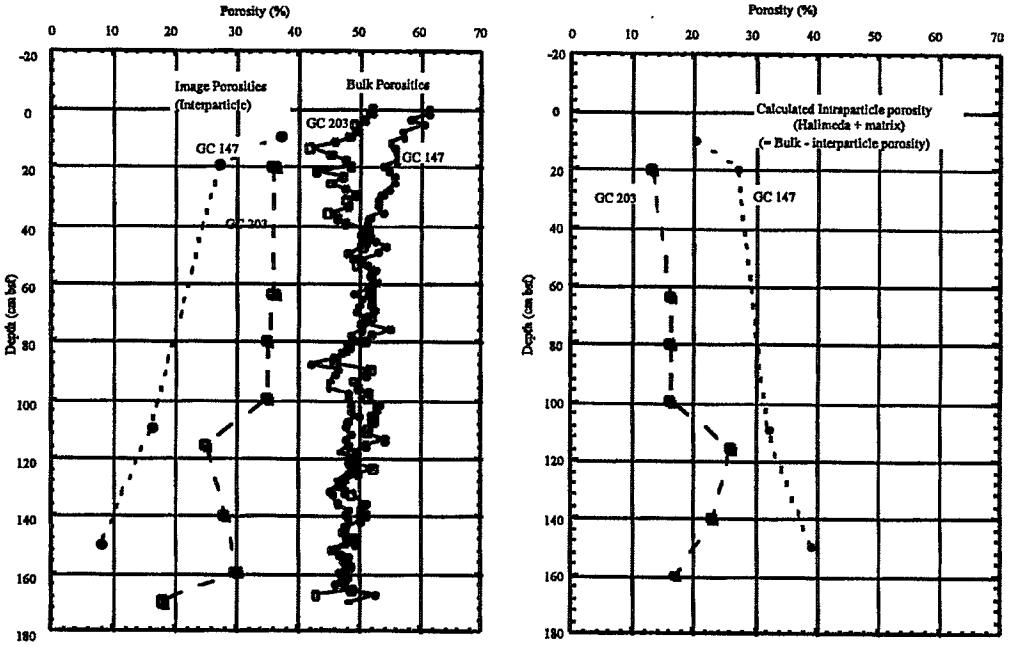

Figure 1: Porosities for gravity cores 147 (Tortugas site) and 203 (Marquesas site). Left: inter-particle porosity determined by image analysis and by bulk analysis (data provided by Dawn Lavoie). Right: Intraparticle porosity (i.e., *Halimeda* fragments and matrix together) estimated as the difference between image and bulk porosity.

Table 1: Core KW-PE-DC-160-2 before and after consolidation

	% Area			Porosity (%)	
	Before	After		Before	After
Voids	30	11		30	11
Halimeda *	38	36		11-14	10-13
Matrix**	26	48		3-9	6-17
			Totals	44-53	27-51
			Bulk Porosity	54	39

* Halimeda fragments: 33% ±3.9 (95% confidence interval)
** matrix: 24% ±11.3 (95% confidence interval)

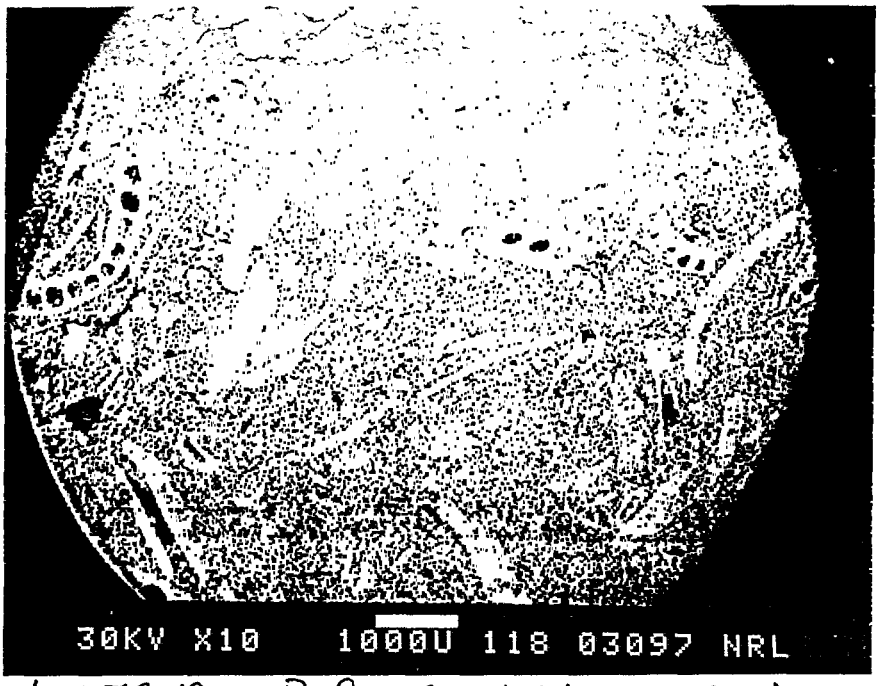

Plate 1a: First of a series of SEM micrographs of Florida Keys carbonate sediment, looking downcore. .Critical point-dried samples are embedded in epoxy resin, polished, coated with carbon for electrical conductance, and imaged in the scanning electron microscope using the backscattered electron signal. Note large shells oriented vertically. Magnification = 10x (minimum possible on SEM). Marker bar = 1000 μm .

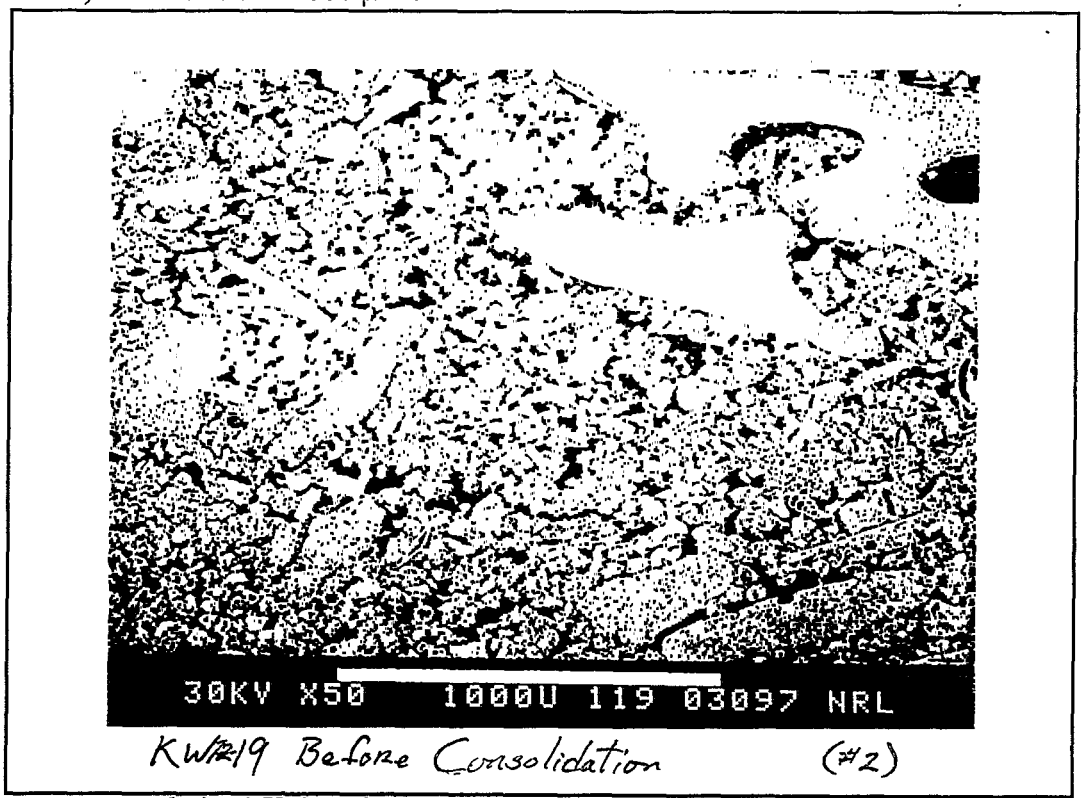

Plate 1b: Numerous sand-sized *Halimeda* fragments are visible among shell fragments. Magnification = 50x. Marker bar = 1000 μm.

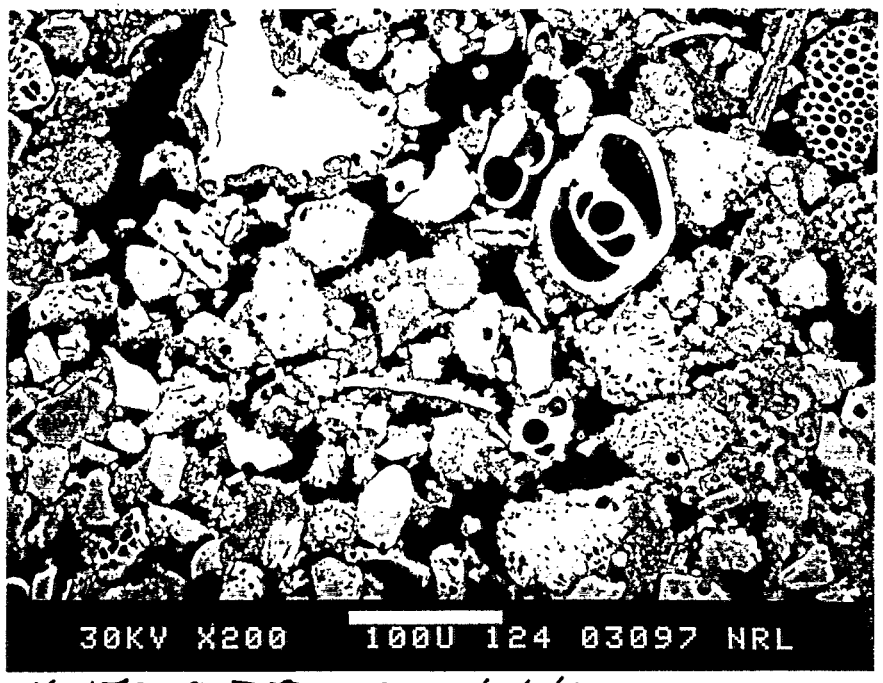

Plate 1c: Darker matrix (clay-sized particles) becomes visible between grains. *Halimeda* fragments are mostly subspherical features; linear and larger fragments are primarily molluskan shell origin; globular, enclosed features are Foramaniferan; lace-like features probably Bryozoan. Void space is black. Note holes in fragments caused by dissolution or boring algae.Magnification = 200x. Marker bar = 100 μm.

Plate 1d: Relationship of matrix and grains clearly shown. Note general lack of graded particle sizes at matrix/grain interface. Magnification = 500x. Marker bar = 100 μm.

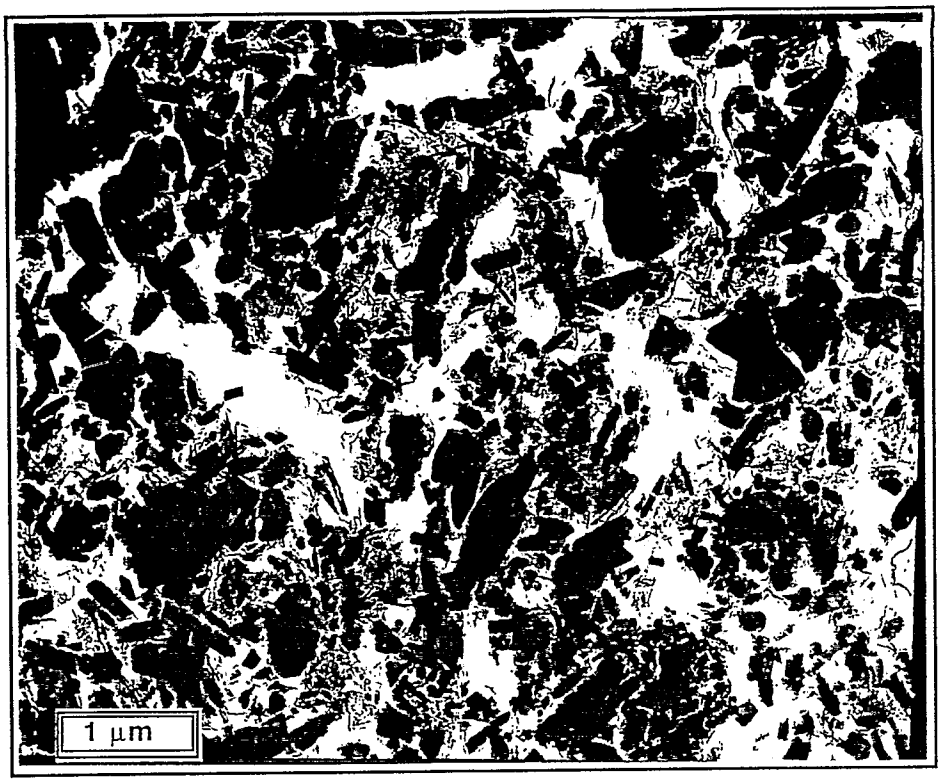

Plate 2: TEM micrograph (provided by Yoko Furukawa) of typical matrix material. Elongated, dark features appear to be aragonite crystals, while the rest are of indeterminate origin. Note variable void space among particles, reflected in porosity measurement using image analysis of 24% ± 11.3 (95% confidence limits)

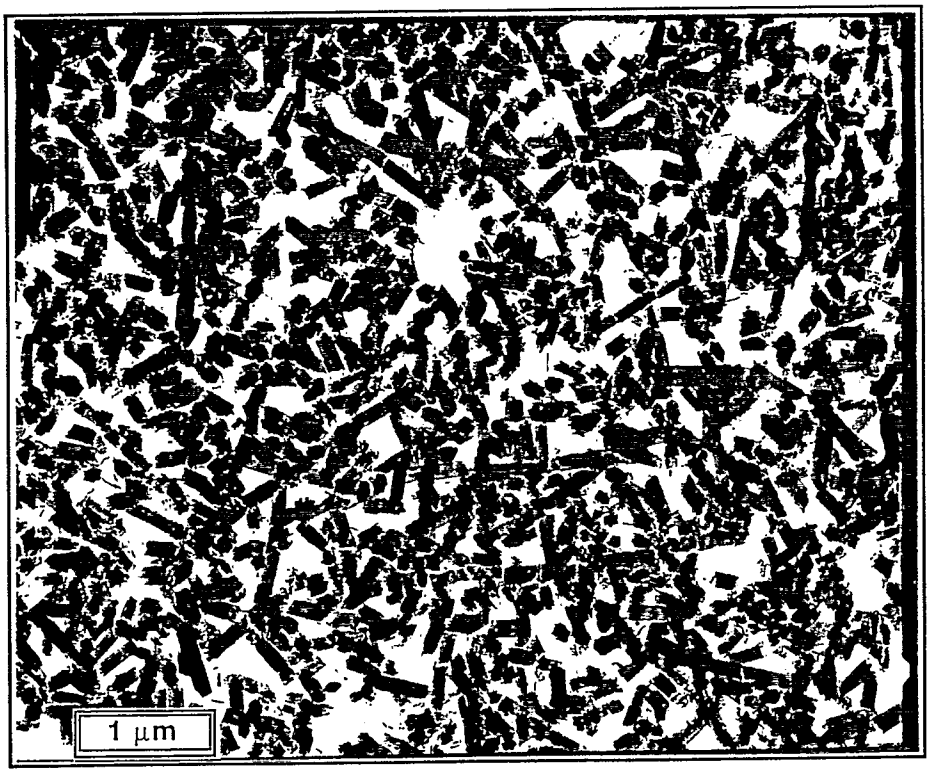

Plate 3: TEM micrograph (provided by Yoko Furukawa) of *Halimeda* fragment. Composition is entirely of aragonite needles; whether needles are cemented or held together by organics is unknown. Porosity measurement by image analysis of 33% ± 3.9 (95% confidence limits) indicates low variability in intraparticle porosity of these grains.

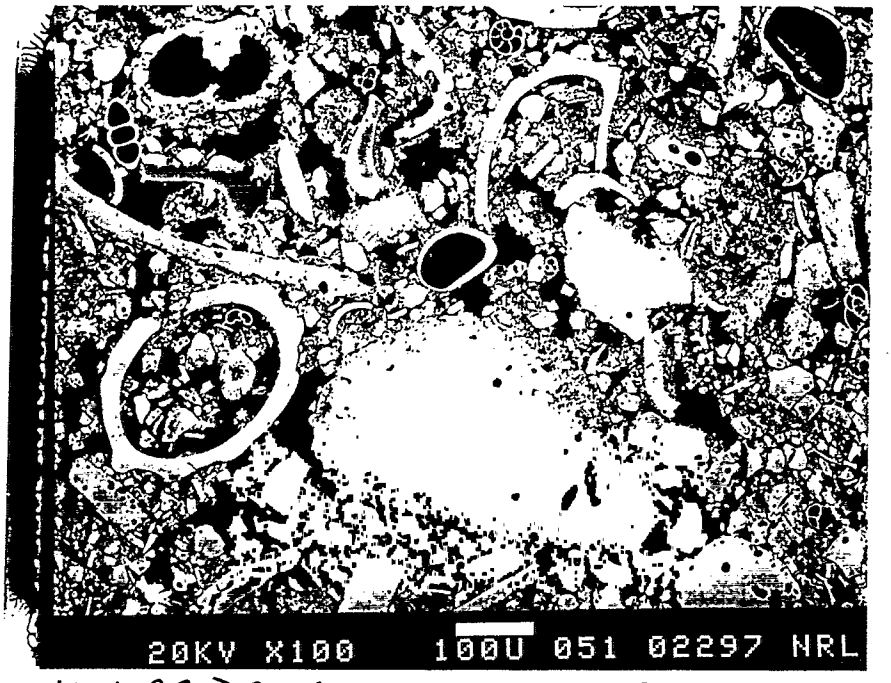

Plate 4: SEM micrograph of gravity core 160-2, 9 cm bsf (Tortugas). Note the degradion evident at the surface of the grain in the center of the field. Such gradation of particles was observed infrequently; most grains exhibited a sharp boundary between grain surfaces and matrix. Magnification = 100x. Marker bar = 100 μm.

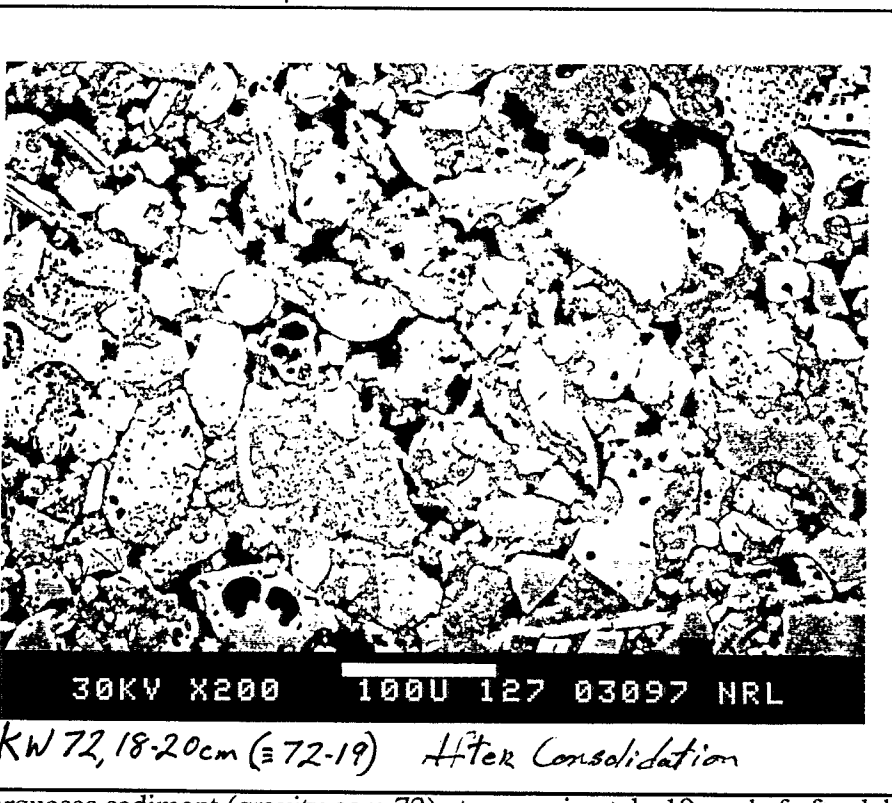

Plate 5: SEM of Marquesas sediment (gravity core 72) at approximately 19 cm bsf after laboratory consolidation. Compare to the same sediment before consolidation in Plate 1c. Magnification = 200x. Marker bar = 100 μm.

7.0 Modeling

7.1 Image Analysis of Dry Tortugas Carbonate Sediment Structure (R.J. Holyer, D.K. Young and J.C. Sandidge)

Image Analysis of Dry Tortugas Carbonate Sediment Structure

Ronald J. Holyer, David K. Young, and Juanita C. Sandidge

Naval Research Laboratory
Stennis Space Center
Mississippi 39529 USA

INTRODUCTION

The long term goal of our investigations is to derive new sediment textural classification methodologies based on image analysis and to use resulting variables directly as predictive model inputs or as proxy measures of and predictors for acoustic and physical properties of marine sediments. These image-based textural parameters are, by their very nature, readily automated for highly discriminating, rapid and reproducible results. As suggested from other applications of imaging science, these parameters could be particularly useful in quantifying inhomogeneities of sediment fabric patterns, including sediment contrast boundaries, gradients, interfaces, and anisotropy of component features (Young et al., 1994). Relationships between image-based values and sediment bulk density measurements have been demonstrated for X-radiographs of marine sediments from Eckernforde Bay (Holyer et al., 1995). Scales, orientations, and isotropy of density fluctuations imaged in cross-sectional X-radiographs of marine sediments have been analyzed by image-based methods (Holyer et al., 1996). Comparisons of sediment density heterogeneity, as interpreted from image-based analytical techniques of x-radiography and electrical resistivity measurements, have been made (Briggs et al., submitted).

KEY WEST SAMPLES

Sediment profile images collected during the February 1995 Key West Expedition were taken by two methods- sediment profile photography and x-radiography. SCUBA divers were used in sampling at several sites at the Dry Tortugas experimental area to

minimize disturbance of the sediment-water interface and surficial sediments. The x-radiographic cores used by divers were 36cm wide by 44cm high and 3 cm thick. The cores were stored in a container of sea water before they were photographed and x-radiographed using previously described methods. Subsequent to being imaged, the x-radiographic cores were analyzed by electrical resistivity methods by Peter Jackson and Robert Flint. Several of these cores were subsampled for electron microscopy of microfabric by Dennis Lavoie and for thin-sections by Dawn Lavoie. Diving could not be done at the Marquesas experimental area because of high sea state so an x-radiograph core was taken from a box core sample there. Therefore, cur data set was practically limited to the Dry Tortugas site off Fort Jefferson.

Visual inspection of sediment profile photographs exhibited homogeneous, cream-colored, fine-grained carbonate sediment showing no laminae or anisotropic features, except for bioturbated structure where the photograph plane intersected occasional mounds and burrows. X-radiographs of the diver-collected cores and box core subsamples showed extensive biogenic reworking fabric and buried shells throughout the cores (Fig. 1). Wallis filter transforms of the X-radiographs revealed a homogeneously mixed sediment column to depths of 15 cm (Fig. 2).

Whereas image processing analyses of x-radiographs from Eckernforde Bay revealed anisotropic features and subtle sediment structures which were not immediately obvious from visual examination, it is clear that similar analysis of the Dry Tortugas x-radiographs would serve little useful purpose. Therefore, it was decided that time would be more profitably spent in applying fractal analysis to the electron microscopic images collected by Dennis Lavoie and the images of thin-sections collected by Dawn Lavoie. Further, in discussions with Yoko Furukawa and Kevin Stephens, it became obvious that their TEM sections and thin-sections of sediments from gravity cores presented an opportunity to apply fractal analysis in quantifying geochemical changes occurring in sediments deeper than the surface biogenically mixed layer.

The following discussion presents the background which establishes, in part, the rationale for a fractal approach in analysis of diagenetic processes of marine sediments.

Also, some preliminary results are given which provide the basis for this approach being used for Dry Tortugas carbonate sediments.

BACKGROUND AND RATIONALE

Fractal aggregate models, which have been applied to aggregation phenomena in colloidal suspensions, were related successfully to suspended sediment aggregates (Kranenburg, 1994). Krone (1986) had previously shown experimentally that floc aggregate density, yield strength and viscosity depend on the order of aggregation which is more or less independent of scale. Kranenburg (1994) extended these experimental results to demonstrate that fractal aggregation models can also be applied to predict similar properties of cohesive sediments and suggested that such models could lead to the development of unifying concepts of sediment behavior. This application of fractal analysis was limited to sediment flocs and recently formed mud beds.

The fractal structure of pore space of sedimentary rocks has been experimentally verified from micro- to macro-structural scales (reviewed in Korvin, 1992). There has been intensive research by petroleum geologists over many years to describe the fractal relationships of sedimentary rocks and to predict their petrophysical properties based on fractal models (Thompson, 1991). Krohn (1988a) applied fractal analysis to digitally analyze thin sections of various sedimentary rocks in characterizing the amount of diagenetic alteration of pore-rock interfaces. Krohn (1988b) extended analysis of SEM images to quantify the fractal dimensions of diagenetic structures of sandstones, shales and carbonates.

A fractal approach has not yet been applied to quantify the diagenetic environment of unlithified carbonate sediments. Our rationale to extend a fractal approach to electron microscopic images and thin-section photographs of carbonate sediments from the Dry Tortugas site is the following. First, scale limits of fractal relationships, such as the fractal dimension, may help determine the scales where sediment properties are governed by certain defined processes. Thus, the fractal dimension could be used

heuristically to help guide analyses and provide interpretations of diagenetic phenomenology. Second, fractal parameters may be used to quantify processes only qualitatively interpreted or to independently verify measurements collected by other means. Third, the diagenetic environment may be predictively modeled by fractal models.

PRELIMINARY RESULTS

Fractal dimension is useful to quantify the complexity of grayscale texture within an image. A larger numerical value of fractal dimension indicates more complex grayscale structures. Mathematically pure fractal patterns are self-similar at all spatial scales. Fractals structures that occur in nature are usually self-similar over only a limited range of scales. Fractal dimension can, therefore, be a function of spatial scale, i.e., very simple, smooth texture (low fractal dimension) may exist at large scales and complex textures (high fractal dimension) may be present at fine scales. However, if the range of self-similarity isn't rather large, it is probably incorrect to describe the texture as being fractal.

Numerous algorithms exist for calculating fractal dimension of images. One of the more instructive methods utilizes the power spectrum of the image. If both the power and frequency axes of a power spectrum plot are in logarithmic units, a fractal structure results in a linear spectrum. Frequency (scale) ranges over which the spectrum is linear indicates the scale range over which the image is fractal in character. Slope of the linear spectral plot is related to fractal dimension. Further, if the x and y axes of the two-dimensional power spectrum are considered separately, indications of anisotropy in fractal textures are possible.

We have applied the power spectrum method to the fractal analysis of TEM and thin section photographs of Dry Tortugas sediments. To date we have considered only one core which was sampled at eleven depths ranging from 3 to 223 cm. Figures 3 and 4 show the TEM and thin section photographs, respectively, from a depth of 159 cm. Figures 5 and 6 are plots of power spectra from these images. The small number of

samples analyzed precludes conclusions at this time. However, indications are that both of these image types are fractal-like over scale ranges exceeding one order of magnitude. TEM images tend to be more fractal-like than thin section photographs. A trend of decreasing fractal dimension with depth was observed in TEM imagery but not in thin section photographs.

Future work will include analysis of many more Dry Tortugas sediment cores. SEM imagery will also be included in the analysis. We are presently optimistic that fractal characterization of these three types of imagery will result in quantification of the processes of early diagenesis of these sediments.

REFERENCES

Briggs, K. B., R. J. Holyer, P. D. Jackson, J. C. Sandidge and D. K. Young (1997) Two-dimensional variability in sediment porosity , density, and electrical resistivity in Eckernforde Bay sediment. Submitted. Continental Shelf Research.

Holyer, R. J., D. K. Young and J. C. Sandidge (1995) Density structure of Eckernforde Bay sediments derived from image analysis: Relationships with sediment properties. Workshop on Modeling Methane Rich Sediments of Eckernforde Bay, Eckernforde, Germany, 26-30 June 1995.

Holyer, R. J., D. K. Young, J. C. Sandidge, and K. B. Briggs (1996) Sediment density structure derived from textural analysis of cross-sectional x-radiographs. GeoMarine Letters 16:204-211.

Korvin, G. (1992) Fractal Models in the Earth Sciences. Elsevier Press, Netherlands, 396p

Kranenburg, C. (1996) The fractal structure of cohesive sediment aggregates. Estuarine, Coastal and Shelf Science 39:451-460.

Krohn, C. E. (1988a) Sandstone fractal and Euclidean pore volume distributions. J. Geophysical Research 94 (B4):3286-3296.

Krohn, C. E. (1988b) Fractal measurements of sandstones, shales, and carbonates. J. Geophysical Research 94 (B4):3297-3305.

Krone, R. B. (1986) The significance of aggregate properties to transport processes. In Estuarine Cohesive Sediment Dynamics, A. J. Mehta, ed., Springer-Verlag, Berlin, pp. 66-84.

Thompson, A. H. (1991) Fractals in rock physics. In Annual Review of Earth and Planetary Sciences, G. W. Wetherill, ed., Annual Reviews Inc., Palo Alto, 19: 237-262.

Young, D. K., R. J. Holyer, and J. C. Sandidge (1994) Texture of sediments from Eckernforde Bay: An image analysis approach. Gassy Mud Workshop, FWG, 11-12 July 1994.

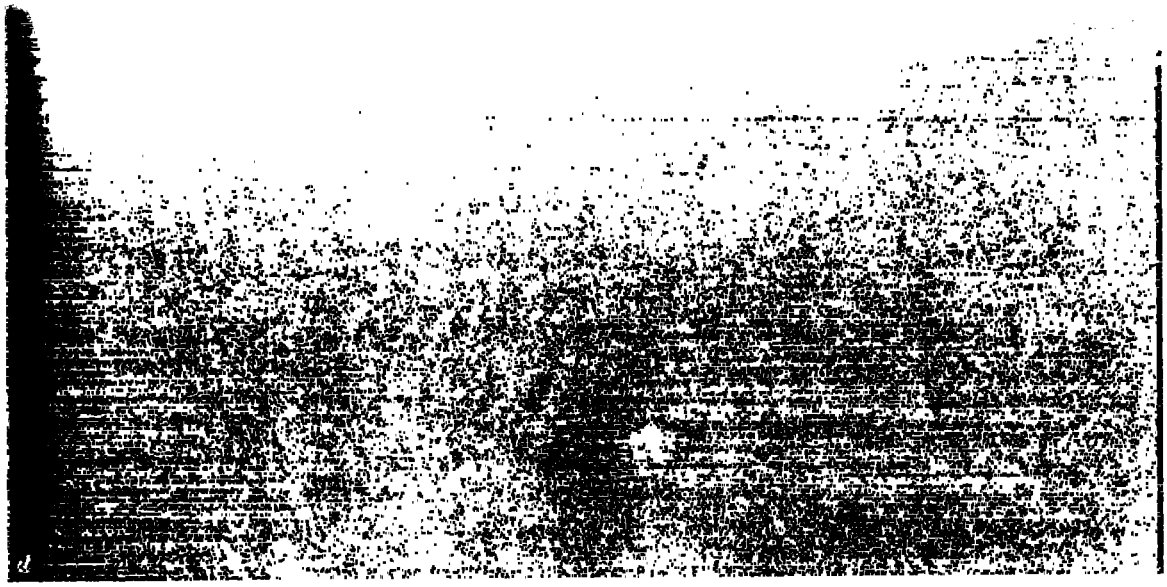

Figure 1 X-radiograph of core 197.

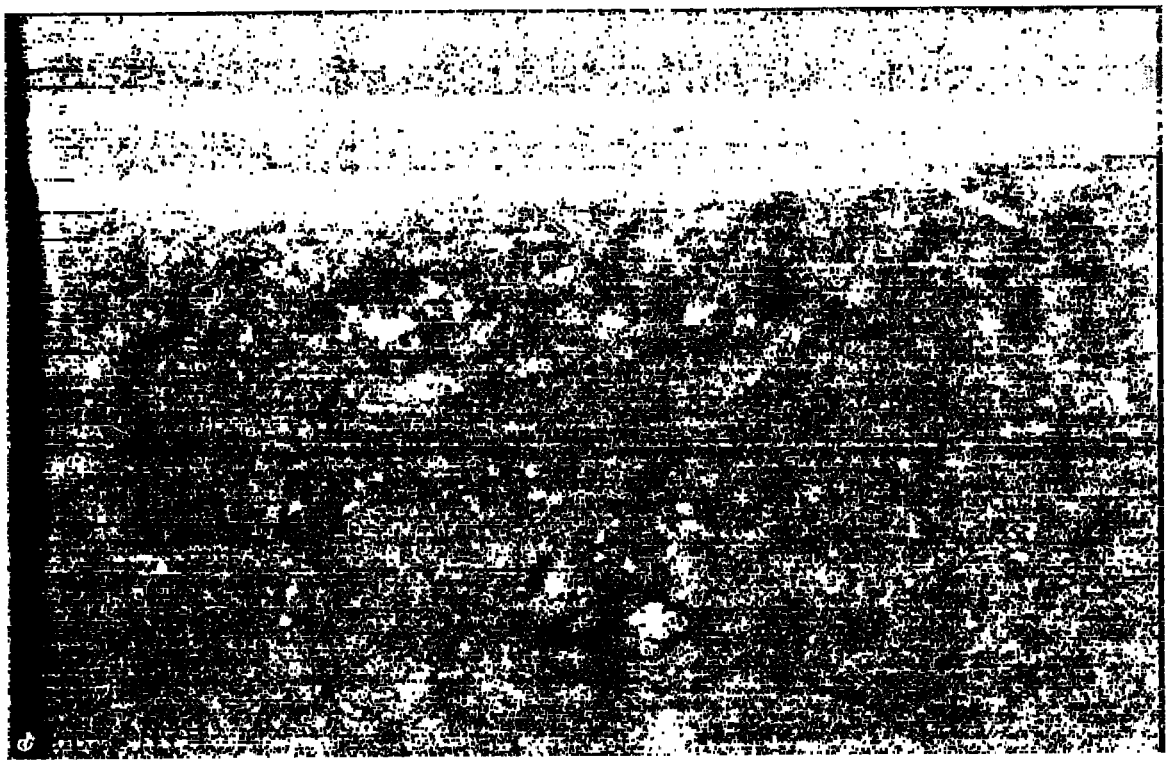

Figure 2 Enhanced version of Figure 1.

Figure 3 TEM image at 159 cm depth.

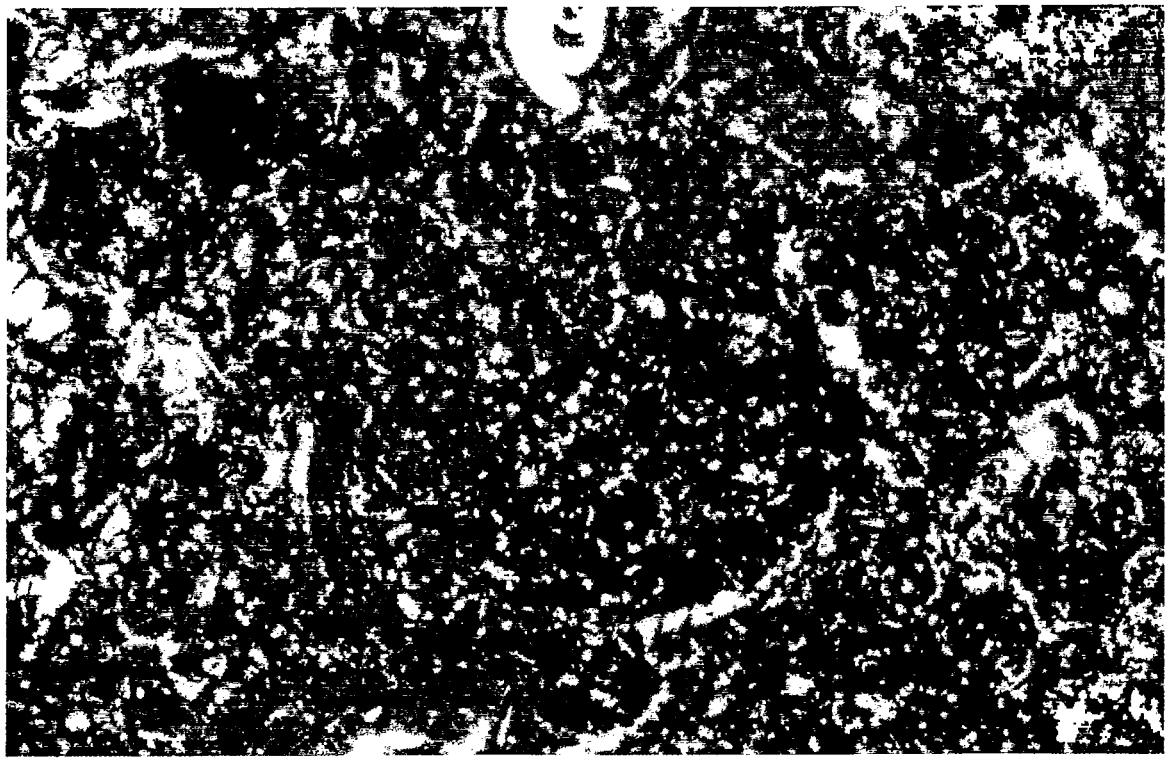

Figure 4 Thin section photograph at 159 cm depth.

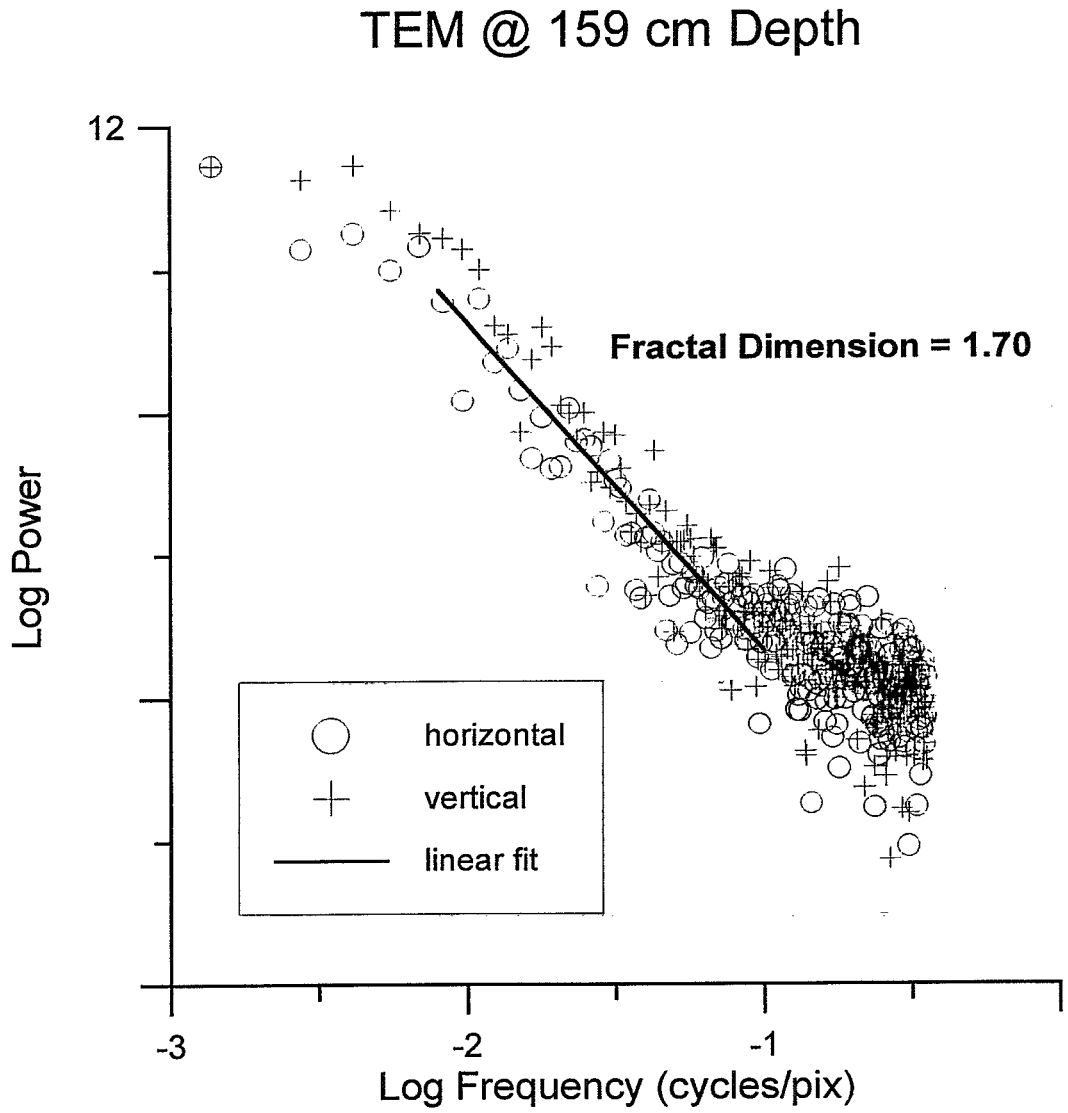

Figure 5 Power spectrum of TEM image.

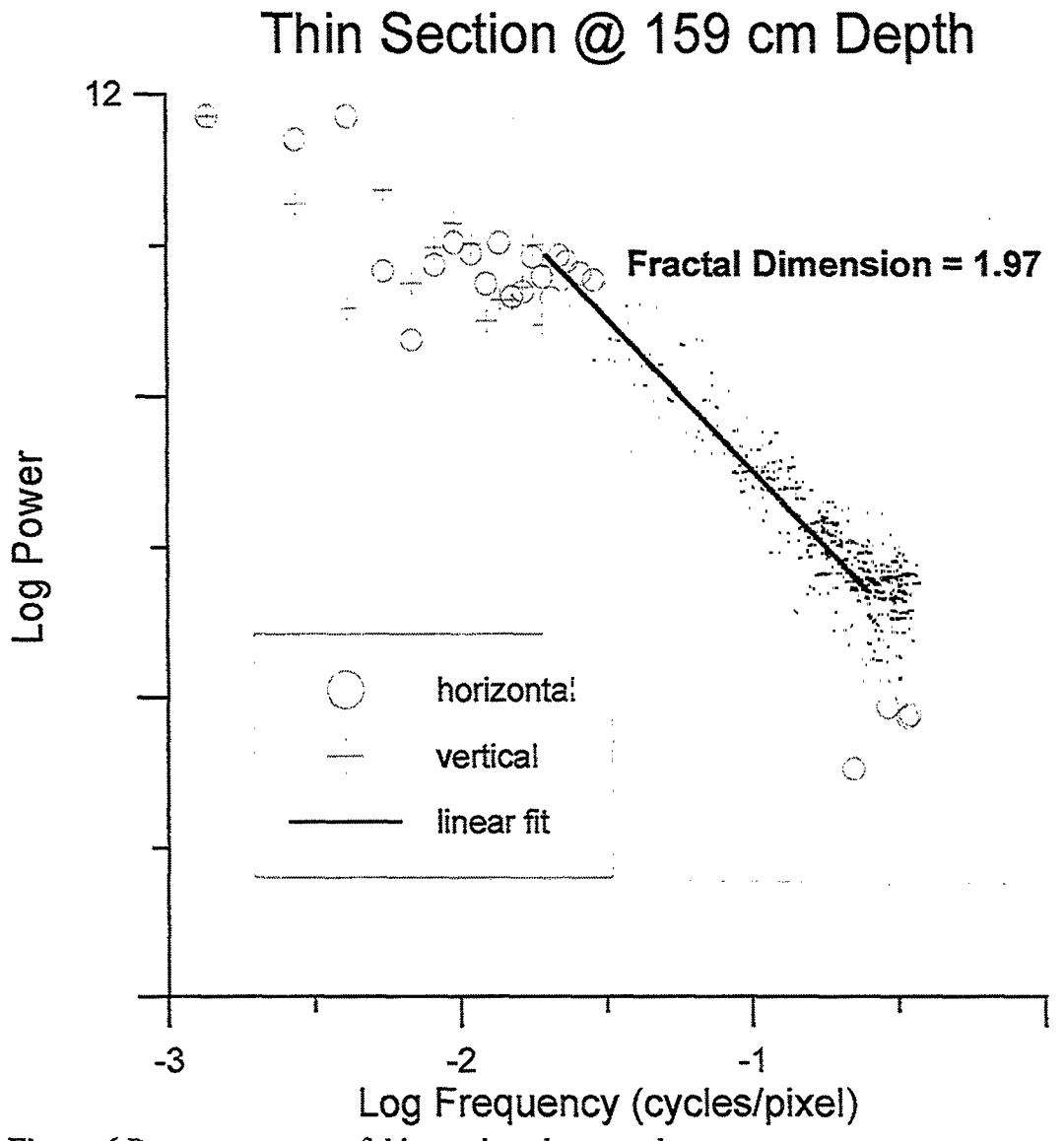

Figure 6 Power spectrum of thin section photograph.

7.2 Contact Microstructure for Constitutive Acoustic Modeling of Particulate marine Sediments (M.H. Sadd and J. Dvorkin)

Contact Micromechanics for Constitutive Acoustic Modeling of Particulate Marine Sediments

Martin H. Sadd
Mechanical Engineering & Applied Mechanics
University of Rhode Island

Jack Dvorkin
Department of Geophysics
Standford University

NRL/CBBL Workshop
Key West Evaluation
Stennis Space Center, MS
February 1997

Abstract

The research program is to create new geoacoustic constitutive models of coarse-grained, particulate and cemented particulate seafloor sediments as found in CBBL sites at Panama City and Key West. The modeling will include particulate, cementation and pore fluid microstructures (see Figure 1) that strongly affect the acoustic properties of such sediments. One specific behavior is energy transfer through *interparticle contact cement or matrix material*. Such material may be elastic (e.g., calcite), or viscoelastic (e.g., clay, silt). The other phenomenon of interest is *squirt flow* (fluid squirting from the contacts during wave propagation). As shown in Figure 2, both contact mechanisms are explicitly considered at the particulate scale through the analytical development of new particle contact law relations, and the resulting solutions have been incorporated into a numerical *discrete element method* (DEM)modeling scheme.

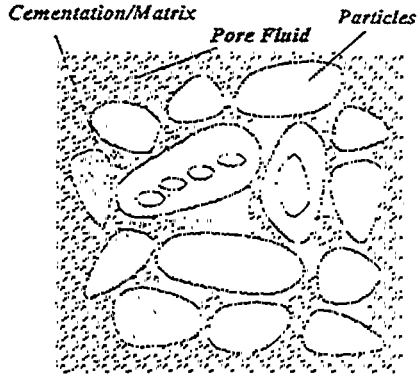

Figure 1. Sediment Microstructures

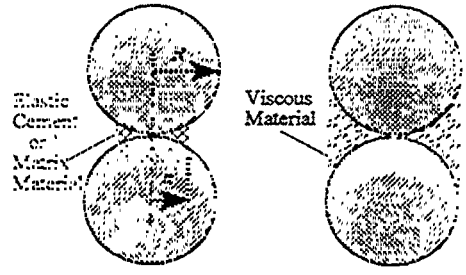

Figure 2. Basic Contact Models

The DEM technique analyzes model particulate assemblies by considering the basic mechanics of each particle in model systems, see Figure 3.

Although our stage of development is still preliminary, several DEM simulations have been carried out for one- and two-dimensional assemblies of spherical particles including cementation and pore fluid. Cementation models considered the cases of identical particles of 2mm diameter, and the density and elastic moduli parameters for the grains and cement were chosen to correspond to the case of glass particles cemented by either glass or epoxy material. Acoustic input was modeled as an applied particle loading of triangular time dependence corresponding to an approximate 0.5MPa pressure input with a 500kHz primary frequency. Our preliminary DEM simulations focused primarily on the effect of variations of the cementation parameter α = cement radius/particle radius.

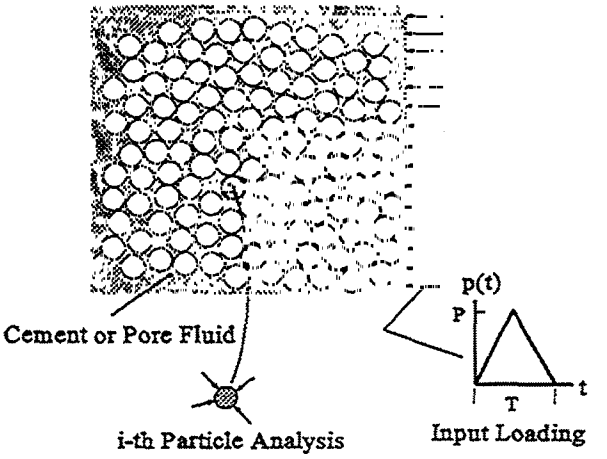

Figure 3. DEM Modeling Procedure

One example is shown in Figure 4, consists of a hexagonal close packing (HCP) of a cemented spherical particulate system. An acoustic input is applied to the top of the assembly model as shown and propagation and attenuation behavior is studied as the mechanical excitation is propagated vertically through the model. The sediment model has been constructed with a variety of cementation microstructures including cases with uniform ($\alpha_1 = \alpha_2$ = constant), layered ($\alpha_1 \neq \alpha_2$), and anisotropic ($\alpha_{vertical} \neq \alpha_{horizontal}$) distributions. Discrete element simulations have been conducted on various cases as summarized in Table1. It is observed that cementation will significantly increase the wave speed while producing only small effects on wave attenuation (interpreted as interparticle load transmission ratio from top to bottom). The wave speed effects of anisotropic cementation are very pronounced for this assembly model.

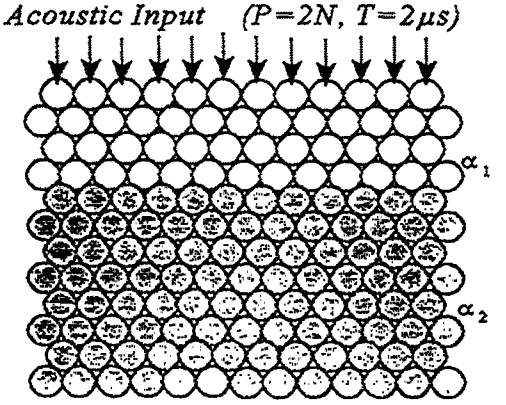

Figure 4. HCP Assembly Model

Table 1. HCP Assembly Results

Model	α_1	α_2	α_{horz}	α_{ver}	Trans.Ratio	Wave Speed
A-1	0.00	0.60			0.252	3123
A-2	0.60	0.00			0.215	1780
A-3	0.02	0.60			0.300	3664
A-4			0.60	0.00	0.426	1376
A-5			0.00	0.00	0.426	1376
A-6			0.05	0.05	0.472	2268
A-7			0.20	0.20	0.405	4142

Additional DEM simulations were conducted on random sediment models (see Figure 5) with biased cementation distributions. For these cases, model sediment fabric was characterized by the distributions of branch vectors (drawn between adjacent contacting particles) and the polar distribution is shown in Figure 5, indicating a near-vertical preferential direction for energy transfer. The cementation for this material model was biasly distributed by the following relations:

$$\textit{Vertical Distribution}: \quad \alpha = \begin{cases} 0.4\,, & |\theta_v| \le 50^\circ \\ 0.0\,, & \textit{otherwise} \end{cases}$$

$$\textit{Horizontal Distribution}: \quad \alpha = \begin{cases} 0.4\,, & |\theta_h| \le 50^\circ \\ 0.0\,, & \textit{otherwise} \end{cases}$$

where θ_v and θ_h are the angles measured from the vertical and horizontal. Using this type of biased cementation, a *cementation branch vector* can be defined as the product $\alpha \boldsymbol{b}$. Distribution plots of this new fabric variable for vertical and horizontal cementation distributions are shown in Figure 6. DEM simulation results for this random assembly indicated that preferred cementation produced significant differences in wave speed with vertical cementation leading to a speed of approximately 3km/s while horizontal cementation produced a speed of about 1km/s.

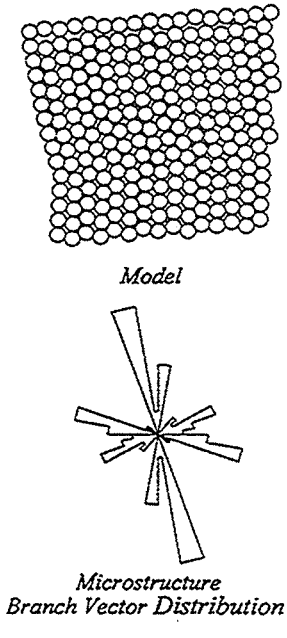

Figure 5. Random Model

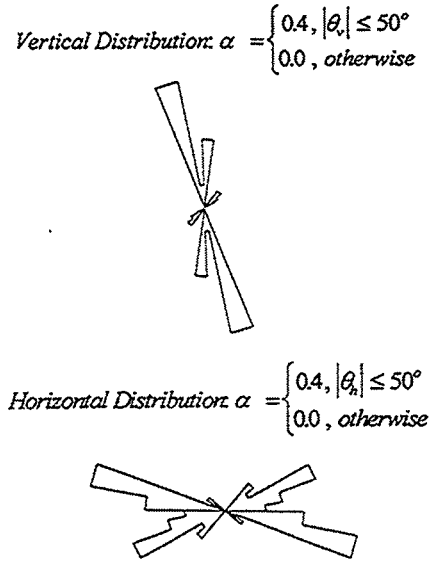

Figure 6. Cementation Branch Vector

The preliminary fluid particulate contact model is described by the following equation

$$F_C = \frac{8G\sqrt{R}}{3(1-\nu)}\delta\sqrt{\delta} + \frac{3}{2}\pi\mu R^2\frac{\dot{\delta}}{\delta},$$

where R = the particle radius, G = particle shear modulus, ν = particle Poission's ratio, μ = pore fluid viscosity, δ = contact deformation. This model accounts for the local Hertzian contact and radial viscous flow (see Figure 7). In order to use this contact law, the model particulate system had to have some small initial compression to avoid having a zero local strain value in the demoninator of the second term in the contact law. Preliminary DEM simulations for one-dimensional particulate chains have been conducted. These results indicated increasing wave speed with consolidation stress, and wave speed values below 1km/s were obtained. Thus it would indicate that additional load transfer mechanisms would be needed in this model to predict realistic wave speeds.

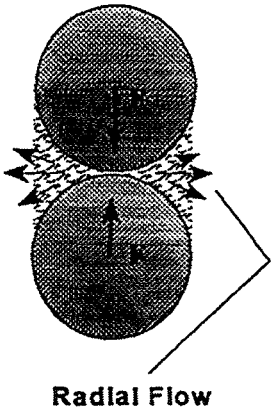

Figure 7. Pore Fluid Model

The simple contact models incorporated into the DEM codes give qualitatively reasonable predictions, but specific and realistic microstructures including particulate and matrix or cementation fabric are now to be incorporated for further model refinement and testing. New contact models are currently under development to look at porous particle and matrix material and viscous cements with more general behaviors. Finally, a Stoll/Biot wave propagation code will also be used to simulate these materials and comparisons are to be made with the micromechanical model results.

7.3 High Frequency Scattering from Dry Tortugas Sediment: Model/Date Comparison (K.L. Williams and D.R. Jackson)

High Frequency Scattering from Dry Tortugas Sediment: Model/Date Comparison

Kevin L. Williams and Darrell R. Jackson

Applied Physics Laboratory
University of Washington
Seattle, WA 98105

During the Key West experiment three different sonar systems were deployed as part of the APL effort. The BAMS tower was deployed to examine both spatial and temporal variations in backscattering. The BAMS tower was also operated in conjunction with a mobile, ship-deployed, steerable "bistatic" array to examine bistatic scattering. Finally, the bistatic array was also used in conjunction with omnidirectional sources deployed via spar buoy to examine the spatial coherence of the near forward scattered energy. The data from these three different systsm along with the environmental measurements of the Naval Research Laboratory allow three separate tests of scattering models.

Figure 1 shows backscattering of data acquired using the BAMS tower. The top panel compares this data with the bistatic model of Jackson (with angles set to calculate backscattering) using the environmental parameters measured by Briggs and Richardson. Core averages for the sediment density and sound speed are used. The resulting model curve overpredicts the backscattering. In the bottom panel the surficial values for density and sound speed are used resulting in much better agreement.

In Figure 2 the bistatic data acquired using BAMS and the bistatic array are compared to the Jackson model. Each panel in the figure plots the azimuthal dependence of data for all data with both incident and scattered grazing angles

between the values given at the bottom of the panel. The model curves were calculated with both grazing angles set to the lowest value and then both set to the highest one. The surficial values for density and sound speed were used. The model/data comparison is good.

Figure 3 shows spatial coherence data, taken with the bistatic array and the spar-deployed sources, for receiver separations out to 6 wavelengths. This data was acquired by Dr. Peter Dahl at APL. The curves in each panel are calculated using the bistatic model. The top panel shows the model prediction using the parameters of Briggs and Richardson. Agreement is again good. However, in the lower panel there are three curves. The lowest one was calculated with the measured environmental parameters. The highest two are for different surface roughness spectra designed to maintain agreement with the bistatic data of Figure 2 for all azimuths except near forward scattering (phi = 0). The reason for the disagreement between data and model, when the measured environmental parameters are used in the bottom panel, is unknown at present. However, there is some reason to believe that it is because the bottom vertical layering has not been taken into account in the present model.

The environmental processes of the region are known to have resulted in a layer of lower density and sound speed sediment about 5 cm thick above a denser, higher sound speed, one. A model taking this layering into account may resolve the model/data disparity in the spatial coherence results. Indeed, reexamination of both Figure 1 and 2 show room for improvement in the model/data comparisons also. In the bottom panel of Figure 1 the data lies above the model at high grazing angles and below at low grazing angles. The bottom left panel of Figure 2 also shows some indication that the data is above the model predictions. Furthermore, the top right panel of Figure 2 indicates an oscillation in bistatic scattering strength data with azimuthal angle that is not seen in the model. Overall, the data sets shown will offer a variety of checks on any alternate bistatic models put forth for the region.

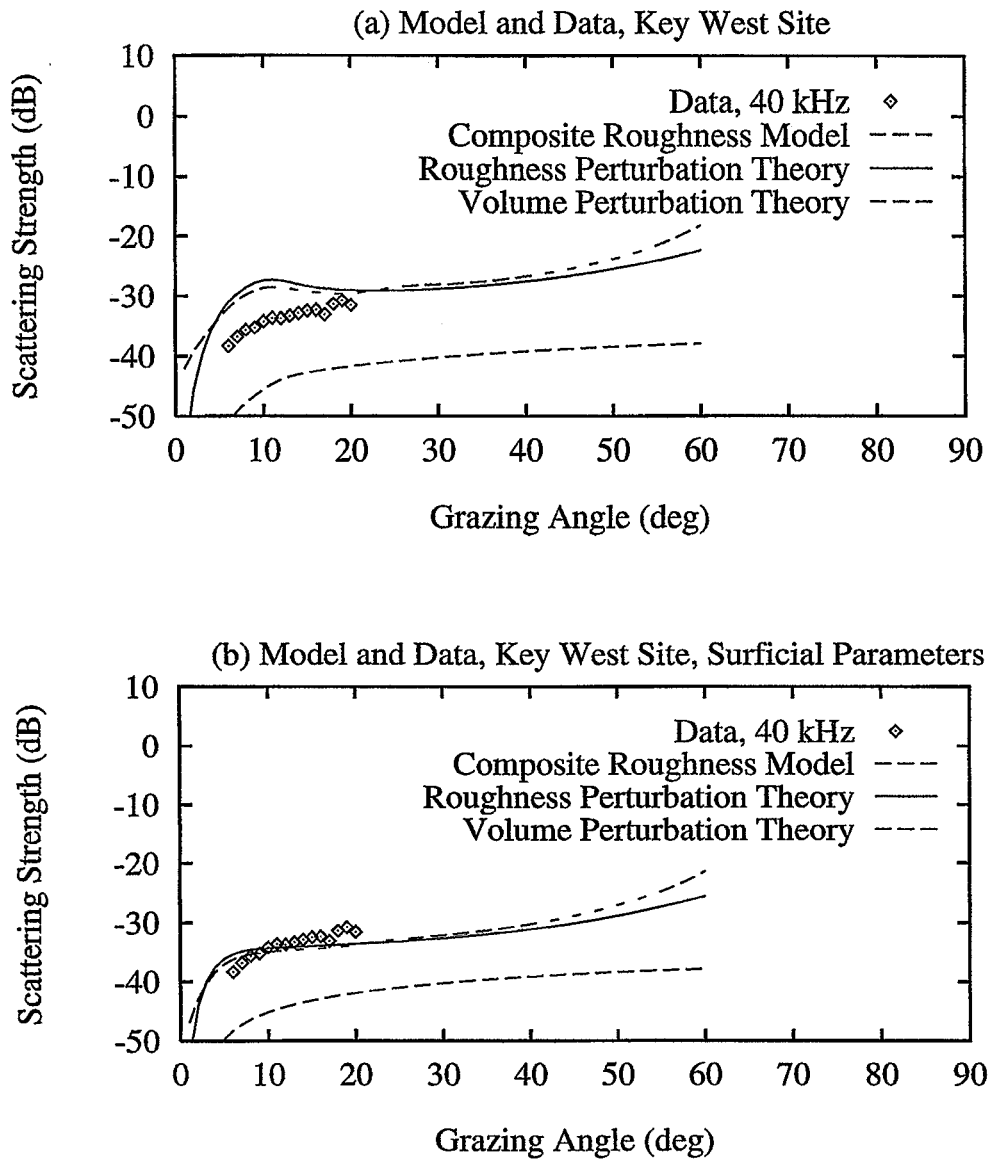

FIGURE 1. Backscattering strength data and model predictions for the Key West site using (a) parameters averaged over core depth, (b) surficial parameters.

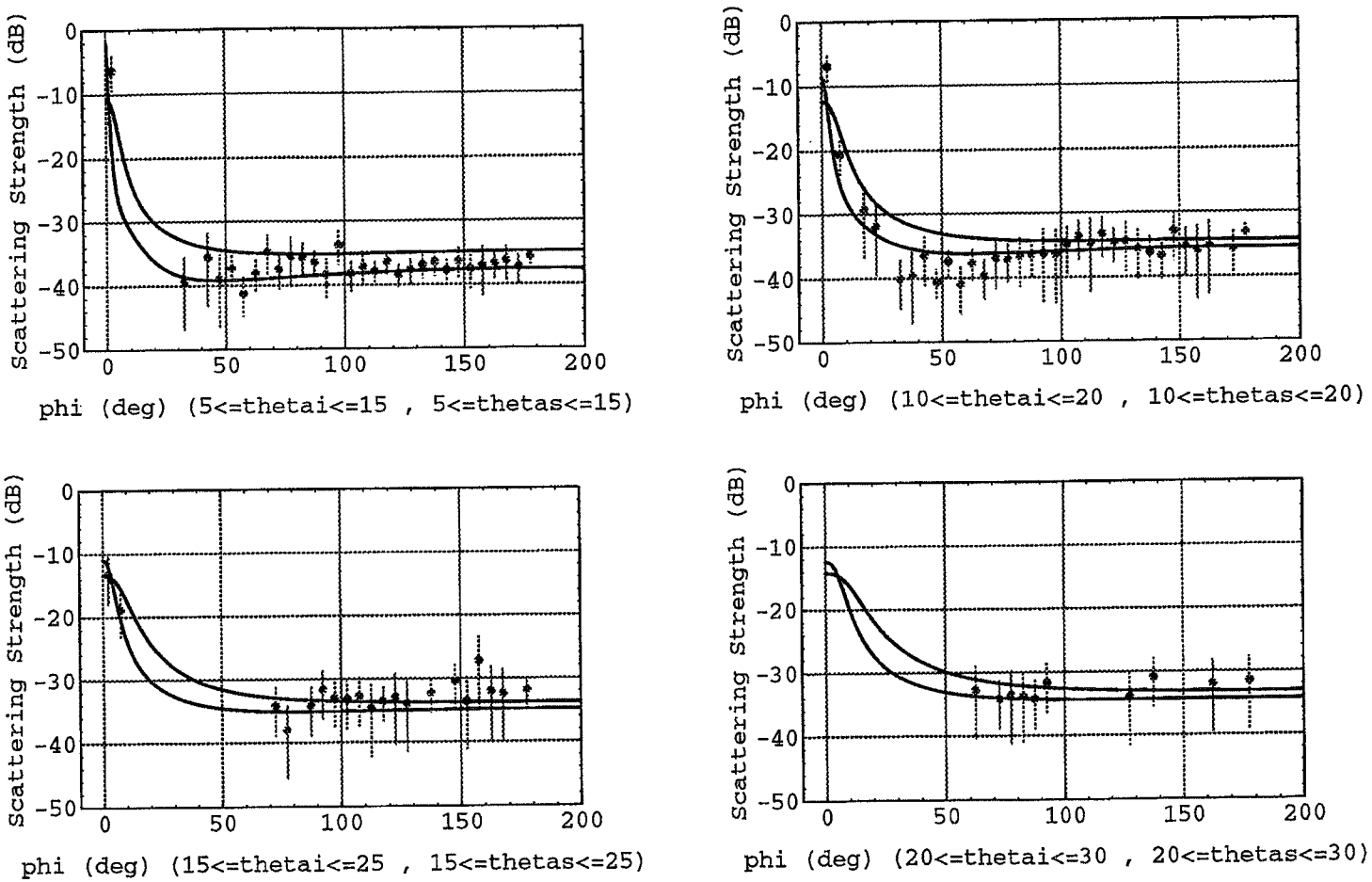

FIGURE 2. The azimuthal angle dependence for the bistatic scattering data is compared with model predictions. Model predictions, shown as curves, are for the upper and lower values of the grazing angles given at the bottom of each panel. The model was run using environmental parameters measured by Briggs and Richardson.

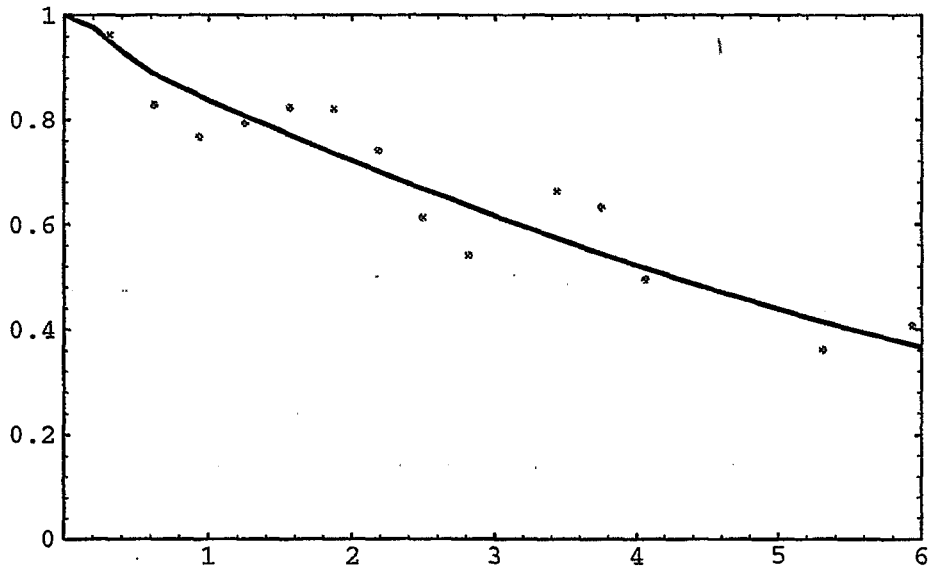

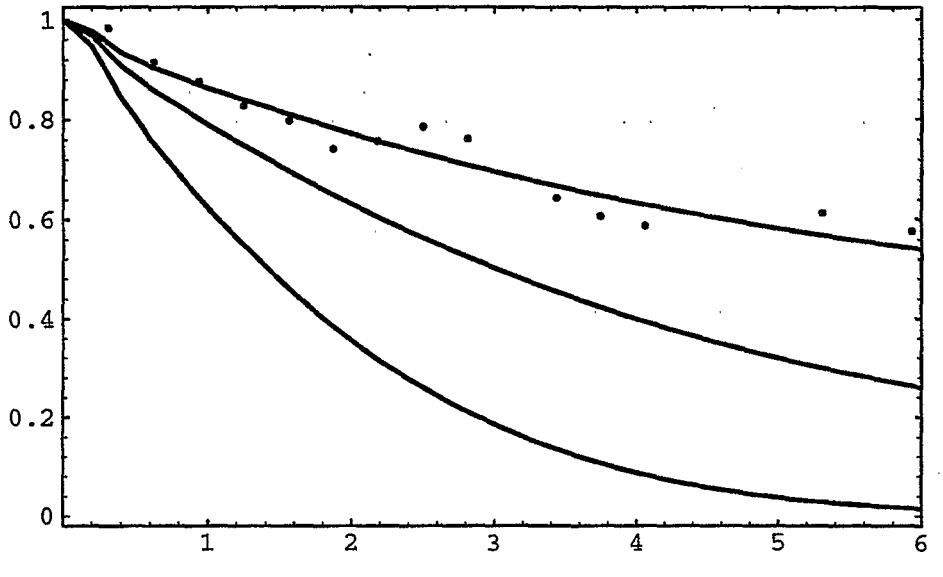

FIGURE 3. Horizontal coherence data points compared to predictions based on the bistatic scattering model. In the top panel the model used the environmental parameters measured by Briggs and Richardson. (The "specular reflection" angle for this case was 21 degrees). The bottom panel shows three different model results compared to another set of spatial coherence data.(The "specular reflection" angle for this case was 25.7 degrees).The lowest line is the model prediction using the measured environmental parameters. The highest two are for different spectra of surface roughness designed to maintain the agreement with the bistatic data of figure 2 for all azimuths except near forward scattering (phi=0). The reason for the disagreement between data and model, when the measured environmental parameters are used in the bottom panel, is unknown at present.

Appendices:

A. Workshop Itinerary

B. Attendees Names and Addresses

Appendix A Workshop Itinerary

KEY WEST WORKSHOP

AGENDA
February 4-7, 1997

Tuesday Schedule:

8:30 9:00 **Continental Breakfast,** Rouchon House

9:00 - 9:10	Herb Eppert	Welcoming Remarks
9:10 - 9:20	Dawn Lavoie	Introductory Remarks
9:20 - 9:30	Mike Richardson	Objectives

Geologic Background

9:30 - 9:50 Dave Mallinson. An overview of the shallow subsurface geology of the Dry Tortugas area

9:50 - 10:10 Charlotte Brunner. Holocene paleoenvironmental changes at the Marquesas and Dry Tortugas Keys

10:10 - 10:30 **Break**

Sediment Classification

10:30 - 10:50 Thomas Wever. Backscatter characteristics of the seafloor within the Dry Tortugas research area

10:50 - 11:10 Don Walter and others. A comparison of acoustically-predicted sediment properties with laboratory-measured core data

11:10 - 11:30 Dei Hews/Angela Davis. Geophysical seafloor sensing in a carbonate sediment regime

11:30 - 11:50 Ed Mozley. Electrical properties of carbonate sediments

Steve Schock. Variability of acoustic sediment properties in the Dry Tortugas. Will be given at 2:20 PM Wednesday

11:50 - 1:00 **Lunch**

1:00 - 1:30 Dan Lott/Sam Tooma. Seafloor Classification Systems Comparison

1:30 - 2:00 Sam Tooma/Dan Lott. MTEDS demonstration results from Key West

Processes which Affect Near-surface Sediment Structure and Properties

2:00 - 2:20 Chuck Nittrouer. Comparison of benthic communities in the Dry Tortugas and surrounding regions

2:20 - 2:40 **Break**

2:40 - 3:00 Glen Lopez. Regional comparison of benthic assemblages in the Lower Florida Keys

3:00 - 3:20 Sam Bentley. Constraints on rates of sediment accumulation and mixing, Southeast Channel, Dry Tortugas Keys

Geochemistry

3:20 - 3:40 Alan Shiller. Pore water chemistry in carbonate sediments from the Marquesas and Dry Tortugas keys

3:40 - 4:00 Yoko Furukawa. A geochemical investigation of early diagenetic effects on sediment structures

4:00 - 4:20 Ron Holyer/Dave Young/Juanita Sandidge. Image analysis applications

Wednesday Schedule

8:30 - 9:00 **Continental Breakfast**

Sediment Structure and Properties

9:00 - 9:20 Mike Richardson/Dawn Lavoie. In situ geoacoustic properties prediction from sediment characteristics

9:20 - 9:40 Tim Orsi/Kevin Briggs. CT Analysis of Physical Property Variability in Carbonate Sediments

9:40 - 10:00 Kevin Briggs - Small-scale fluctuations in acoustic and physical properties of sediments from the Marquesas Keys and Dry Tortugas sites

10:00 - 10:20 Kevin Stephens and others. Scale-dependent variability of the Dry Tortugas sediments

10:20 - 10:40 Break

10:40 - 11:00 Bill Bryant/Niall Slowey. Geoacoustic and geotechnical characteristics of Key West sediments

11:00 - 11:20 Gabriella Sykora - Acoustic characteristics in relation to strength behavior of calcareous sand from the Key West Campaign

11:20 - 11:40 Dave Brogan. Variability of Lower Florida Keys sediment microstructure and stress-strain behavior

11:40 - 12:00 Dawn Lavoie and others. Laboratory-measured geotechnical characteristics of the Dry Tortugas and Marquesas sediments

12:00 - 1:00 Lunch

1:00 - 1:20 Laura Pyrak-Nolte and others. Acoustic imaging of carbonate sediments from the Lower Florida Keys

1:20 - 1:40 Dennis Lavoie/P.J. Burkett. Carbonate microfabric

High-frequency Acoustic Scattering and Propagation

1:40 - 2:00 Kevin Williams and Darrell Jackson, "High frequency scattering from Dry Tortugas sediment: Model/Data comparisons "

Modeling

2:00 - 2:20 Marty Sadd/Jack Dvorkin. Contact Micromechanics for Constitutive Acoustic Modeling of Particulate Marine Sediments

Jack Dvorkin, Marty Sadd Part 2: Contact Micromechanics for Constitutive Acoustic Modeling of Particulate Marine Sediements. Will be given Thursday 9:00 AM

2:20 - 2:40 Steve Schock. Variability of acoustic sediment properties in the Dry Tortugas

2:40 - 3:40 **Break**

3:40 - ? Mike Richardson. Summary of what we know

Wednesday Evening: Dinner at the Diamondhead Yacht club

Thursday Schedule

8:30 - 9:00 **Continental Breakfast**

9:00 - 9:20 Jack Dvorkin, Marty Sadd "Contact Micromechanics for Constitutive Acoustic Modeling of Particulate Marine Sediments

9:20 - 10:20 Jack Dvorkin, Effective Medium Modeling

10:20 10:40 Towards integrated models of carbonate sediment properties and behavior

10:40 - 12:00 Working subgroups

12:00 - 1:00 **Lunch**

1:00 - 1:30 Subgroup reports/summary

1:30 - ? Mike Richardson. Integrated models (cont.)

Friday Schedule

8:30 - 9:00 **Continental Breakfast**

9:00 - Future Publications

Research Plan/recommendations

11:30 - 12:00 **Wrap-up**

Appendix B Names and addresses of attendees

Sam Bentley Marine Sciences Research Center State University of New York Stony Brook, NY 11794-5000	Kevin Briggs Code 7431 Naval Research Laboratory Stennis Space Center, MS 39529-5004
David Brogan Marine Geomechanics Laboratory University of Rhode Island Narragansett, RI 02882	Charlotte A. Brunner Center for Marine Science University of Southern Mississippi Stennis Space Center 39529
William Bryant Department of Oceanography College of Geosciences and Maritime Studies Texas A&M University College Station, TX 77843-3146	P.J. Burkett Code 7431 Naval Research Laboratory Stennis Space Center, MS 39529-5004
Jack Dvorkin Department of Geophysics Stanford University Stanford, CA 94305-2215	Yoko Furukawa Code 7431 Naval Research Laboratory Stennis Space Center, MS 39529-5004
Sean Griffin Omni Technologies, Inc. 450 31st Street, Suite A Kenner, LA 70065	Mark H. Hafen Department of Marine Science - MSL 119 University of South Florida 140 7th Avenue South St. Petersburg, FL 33701-5016
Ron Holyer Code 7241 Naval Research Laboratory Stennis Space Center, MS 39529-5004	Dei Huws School of Ocean Sciences Menai Bridge Ggqynedd LL59 5EY United Kingdom
Darrell Jackson Applied Physics Laboratory University of Washington 1013 NE 40th Seattle, WA 98105	Douglas Lambert Code 7431 Naval Research Laboratory Stennis Space Center, MS 39529-5004
Dawn L. Lavoie Code 7431 Naval Research Laboratory Stennis Space Center, MS 39529-5004	Dennis M. Lavoie Code 7333 Naval Research Laboratory Stennis Space Center, MS 39529-5004
David Mallinson Department of Marine Science - MSL 119 University of South Florida 140 7th Avenue South St. Petersburg, FL 33701-5016	Edward C. Mozley Code 7442 Naval Research Laboratory Stennis Space Center, MS 39529-5004

Charles A. Nittrouer Marine Sciences Research Center State University of New York Stony Brook, NY 11794-5000	Tim Orsi Planning Systems, Inc. 115 Christian Lane Slidell, LA 70458
Laura Pyrak-Nolte Department of Civil Engineering and Geological Sciences Unviersity of Notre Dame Notre Dame, IN 46556-0767	Michael D. Richardson Code 7431 Naval Research Laboratory Stennis Space Center, MS 39529-5004
Martin Sadd Narragansett Bay Campus, OE-2 University of Rhode Island Narragansett, RI 02882-1197	Juanita Sandidge Code 7241 Naval Research Laboratory Stennis Space Center, MS 39529-5004
Alan Shiller Center for Marine Science University of Southern Mississippi Stennis Space Center, MS 39529	Kevin Stephens Code 7431 Naval Research Laboratory Stennis Space Center, MS 39529-5004
Gabriella Sykora Marine Geomechanics Laboratory University of Rhode Island Narragansett, RI 02882	Samuel G. Tooma Code 7430 Naval Research Laboratory Stennis Space Center, MS 39529-5004
Joseph Urmos Code 7432 Naval Research Laboratory Stennis Space Center, MS 39529-5004	Donald J. Walter Code 7431 Naval Research Laboratory Stennis Space Center, MS 39529-5004
Thomas Wever Forschungsanstalt der Bundeswehr Fur Wasserschall- U. Geophysik (FWG) Klausdorfer WEG 2/24 2300 Kiel 14 Germany	Kevin Williams Applied Physics Laboratory University of Washington 1013 NE 40th Seattle, WA 98105
David K. Young Code 7331 Naval Research Laboratory Stennis Space Center, MS 39529-5004	